

ACTIVE CONTROL OF V/STOL AIRCRAFT

BY

DAVID JOHN FREDERICK HOPPER

A THESIS SUBMITTED FOR THE DEGREE OF

DOCTOR OF PHILOSOPHY

OF THE

DEPARTMENT OF AERONAUTICAL AND MECHANICAL ENGINEERING

THE UNIVERSITY OF SALFORD

APRIL 1990

To Jesus, the author and finisher of life, for helping to carry the load,
for making it worthwhile and for putting it all in the right perspective.

" What good will it be for a man if he gains the whole world,
yet forfeits his soul ? "

Matthew: Ch 16, vs 26

CONTENTS

List of Figures	viii
List of Tables	xiii
Acknowledgments	xiv
Summary	xv
1 INTRODUCTION	1
1.1 Introduction	2
1.2 The VAAC Programme	5
1.3 Outline of the Report	7
2 REVIEW OF PERTINENT CONTROL THEORY	13
2.1 Introduction	14
2.2 Classical Controller Design Techniques: Strengths and Weaknesses	14
2.3 Modern Controller Design Techniques: A Critical Appraisal	17
2.4 The High-Gain Technique	28
3 THE HIGH-GAIN CONTROLLER DESIGN METHOD	35
3.1 Introduction	36
3.2 Overview of Design Method and Comparison to Requirements	38
3.2.1 Overview of the Basic High-Gain Technique	38
3.2.2 Overview of the New Developments	44
3.2.3 Reasons for Using the High-Gain Method	48

3.3	Mathematical Definition of the Basic High-Gain Theory	52
3.3.1	General Definition of the Closed-Loop System Incorporating Extra Measurement Feedback	52
3.3.2	Definition of the Closed-Loop Asymptotic Structure	55
3.3.3	Definition of the Controller Matrices	57
3.3.4	Definition of the Resultant Zeros and the Asymptotic Closed-Loop Transfer Function	59
3.4	Mathematical Description of the "New Developments" and their Roots	61
3.4.1	Review of the Effects of Relatively Fast Parasitic Dynamics on Systems with High-Gain Controllers	61
3.4.2	Review of Relevant Results from Multivariable Root-Locus Theory	63
3.4.3	Description of the "New Developments"	75
3.5	Assessing Actuator Compatability	87
3.6	Tuning Criteria for the High-Gain Method	91
3.7	The High-Gain Method - A Step-By-Step Procedure	96
4	THE GVAM87 AND THE DESIGN/ANALYSIS/SIMULATION ENVIRONMENT	110
4.1	Introduction	111
4.2	The Aircraft Configuration	113
4.2.1	Primary Control Inputs	113
4.2.2	Secondary Control Inputs	115
4.3	The Rigid Body Aircraft Dynamics and SESAME	118
4.4	The Structure of the GVAM87	123
4.5	The Aircraft Aerodynamics	127

4.6	The Actuator Modelling	129
4.6.1	Aerodynamic Surfaces and Reaction Controls	130
4.6.2	Flaps	130
4.6.3	Undercarraige	131
4.6.4	Air Brake	131
4.6.5	Nozzles	132
4.6.6	Engine	132
4.7	Engineering Constraints and Non-Linearities	137
4.8	The "Flight" Environment	142
4.9	The Design/Analysis/Simulation Environment	144
4.9.1	Description of the Package TSIM	144
4.9.2	Description of the Package Pro-Matlab	147
4.9.3	Description of the DAS Environmment	149
5	APPLICATION OF THE HIGH-GAIN METHOD TO V/STOL AIRCRAFT - CASE STUDIES	159
5.1	Introduction	160
5.2	Flight Case Definition	162
5.3	Derivation of the Basic Plant Dynamics	165
5.4	Application of the Design Method to the Basic Plant Dynamics (Plant-1)	171
5.4.1	Case 1	171
5.4.2	Case 2	181
5.5	Controller Design with Engine Dynamics Included - Case 3	194
5.5.1	Analysis of the Asymptotic Root-Locus Structure for the Plant-2 System	195
5.5.2	Investigation of the Closed-Loop Performance and Tuning	202

5.6	Controller Design with the Full Actuator System Included - Case 4	210
5.6.1	Analysis of the Asymptotic Root-Locus Structure for the Plant-3 System	211
5.6.2	Investigation of the Closed-Loop Performance and Tuning	217
5.7	Analysis of Controller Robustness to Plant Changes - Case 5	228
5.8	Design of Dynamic Compensators for High-Gain MIMO Systems - Case 6	232
5.9	Working Backwards	241
6	THE DESIGN BRIEF	273
6.1	Introduction	274
6.2	Task Tailored Control	275
6.2.1	The Considerations	276
6.2.2	The Requirements	286
6.3	Aircraft Handling Qualities	290
6.3.1	The Considerations	291
6.3.2	The Requirements	299
7	THE CONTROLLER DESIGN	310
7.1	Introduction	311
7.2	Overview of the Controller Structure	312
7.3	Interfacing the Controller to the GVAM87	314
7.4	The Basic Control-Laws and Gain Scheduling	316
7.5	Integrator Wind-Up Protection	321

7.6	Controller Management	325
7.6.1	Controller Initialisation	325
7.6.2	Task Tailored Control Mode Sensing	326
7.6.3	Task Tailored Control Mode Changing	328
8	DEMONSTRATION OF THE CONTROLLER DESIGN	337
8.1	Introduction	228
8.2	Demonstration of Standard Control Modes	343
8.2.1	Low Speed Transition - The Hover	343
8.2.2	High Speed Transition - 80 Kts (135 Ft/s)	345
8.2.3	High Speed Transition - 120 Kts (\approx 200 Ft/s)	346
8.2.4	High Speed Flight (Wing-Borne) - 250 Kts	348
8.3	Accelerating Transition to Wing-Borne Flight - Task 1	350
8.4	Low Speed Manoeuvring - Task 2	352
8.5	Decelerating transition from Wing-Borne Flight - Task 3	354
8.6	Decelerating Transition from Jet-Borne Flight - Task 4	356
8.7	Demonstration of Integrator Wind-Up Protection	357
8.8	Demonstration of Disturbance Rejection	358
8.8.1	Wind-Gust Disturbance Rejection	358
8.8.2	Turbulent Air Disturbance Rejection	359
8.9	Automatic Ship Landing System's - A Demonstration of the Possibilities	362
8.10	Handling Qualities of the Controller	364

9	CONCLUSIONS AND RECOMMENDATIONS	380
9.1	Conclusions	381
9.1.1	Development of a Suitable Controller Design Method	381
9.1.2	Design of an Active Flight Controller for a V/STOL Aircraft	384
9.1.3	The Specification of Task Tailored Control Modes and Handling Qualities for V/STOL Aircraft	386
9.2	Recommendations	388
9.2.1	The Controller Design Method	388
9.2.2	The Controller Design	390
9.2.3	The Design Environment	391
9.2.4	Design Trade-Offs	392
	REFERENCES	393
	APPENDIX A	414
	Block Diagonalisation of a Singularly Perturbed System	
	APPENDIX B	422
	Example 3.2	
	APPENDIX C	438
	Header Listings of the Pro-Matlab Functions	
	APPENDIX D	447
	Glossary of terms for Handling Qualities	

LIST OF FIGURES

Figure (3.1)	Block Diagram of Controller Plus Plant	100
Figure (3.2)	Block Diagram of the Equivalent Feedback System for High-Gain Method Root-Locus Studies	101
Figure (3.3)	Asymptotic Structure for Example (3.1)	102
Figure (3.4)	Pattern A Asymptotes for Root-Loci	103
Figure (3.5)	Pattern B Asymptotes for Root-Loci	104
Figure (3.6)	Block Diagram of the Control System for Example (3.2)	105
Figure (3.7)	Asymptotic Structure for Example (3.2)	106
Figure (3.8)	Frequency Response of a Second-Order Dominant Mode	107
Figure (3.9)	Relationships Between Key Performance Parameters and the Damping	108
Figure (3.10)	Example of Tuning to a Constant Damping Line	109
Figure (4.1)	The Default Configuration for GVAM87	151
Figure (4.2)	Typical Layout for GVAM87-Type Engine	152
Figure (4.3)	Block Diagram of Translational Equations from SESAME Report	153
Figure (4.4)	Block Diagram of Rotational Equations from SESAME Report	154
Figure (4.5)	Illustration of the Euler Angles	155
Figure (4.6)	Illustration of the Relative Wind Angle	156
Figure (4.7)	Subroutine Calling Structure for the GVAM87	157
Figure (4.8)	Throttle to Thrust Relationship	158
Figure (4.9)	Engine Dynamic Changes Caused By the Engine Governor System	158

Figure (5.1)	Case 1: Root-Locus of Plant-1 System	246
Figure (5.2)	Case 1: Frequency Response for Plant-1 System	247
Figure (5.3)	Case 1: Step Response for Plant-1 System	247
Figure (5.4)	Case 1: Frequency Response for Plant-1 System	248
Figure (5.5)	Case 1: Step Response for Plant-1 System	248
Figure (5.6)	Case 1: Root-Locus of Plant-1 System for $RH01 = RH02 = 5$	249
Figure (5.7)	Case 2: Root-Locus of plant-2 System	250
Figure (5.8)	Case 2: Frequency Response for Plant-1 System	251
Figure (5.9)	Case 2: Step Response for plant-1 System	251
Figure (5.10)	Case 2: Frequency Response for Plant-1 System	252
Figure (5.11)	Case 2: Step Response for Plant-1 System	252
Figure (5.12)	Case 2: Root-Locus of Plant-1 system for $m1 = 0.2$	253
Figure (5.13)	Case 3: Root-Locus for Plant-2 System	254
Figure (5.14)	Case 3: Root-Locus for Plant-2 System	254
Figure (5.15)	Case 3: Root-Locus for Plant-2 System	255
Figure (5.16)	Case 3: Frequency Response for Plant-2 System	256
Figure (5.17)	Case 3: Step Response for Plant-2 System	256
Figure (5.18)	Case 3: Frequency Response for Plant-2 System	257
Figure (5.19)	Case 3: Step Response for Plant-2 System	257
Figure (5.20)	Case 3: Root-Locus for Plant-2 System	258
Figure (5.21)	Case 3: Root-Locus for Plant-2 System - Tuning with Sigma	258
Figure (5.22)	Case 3: Frequency Response for Plant-2 System	259

Figure (5.23)	Case 3: Frequency Response for Plant-2 System	259
Figure (5.24)	Case 3: Step Response for Plant-2 System	260
Figure (5.25)	Case 3: Step Response for PLant-2 System	260
Figure (5.26)	Case 4: Root-Locus for Plant-3 System	261
Figure (5.27)	Case 4: Root-Locus for Plant-3 System	261
Figure (5.28)	Case 4: Root-Locus for Plant-3 System	262
Figure (5.29) (a and b)	Case 4: Frequency Response for Plant-3 System	263
Figure (5.30)	Case 4: Root-Locus for Plant-3 System	264
Figure (5.31)	Case 4: Frequency Response for Plant-3 System	265
Figure (5.32)	Case 4: Frequency Response for Plant-3 System	266
Figure (5.33)	Case 4: Step Response for Plant-3 System	266
Figure (5.34)	Case 4: Frequency Response for Plant-3 System	267
Figure (5.35)	Case 4: Step Response for Plant-3 System	267
Figure (5.36)	Case 5: Root-Locus for Plant-4 System	268
Figure (5.37)	Case 5: Frequency Response for Plant-4 System	269
Figure (5.38)	Case 5: Step Response for Plant-4 System	269
Figure (5.39)	Case 6: Root-Locus for Plant-5 System	270
Figure (5.40)	Case 6: Root-Locus for Plant-5 System	270
Figure (5.41)	Case 6: Root-Locus for Plant-6 System	271
Figure (5.42)	Case 7: Frequency Response for Plant-6 System	271
Figure (5.43)	Case 7: Root-Locus for Plant-7 System	272
Figure (5.44)	Case 7: Frequency Response for Plant-7 System	272

Figure (6.1)	Illustration of Stick Breakout Force	303
Figure (6.2)	Schematic Diagram of the Control Scheme	304
Figure (6.3)	Pitch Response to an Abrupt Input	305
Figure (6.4)	Handling Qualities Bandwidth Definition	306
Figure (6.5)	Bandwidth HQ Criteria (for Up and Away Flight)	307
Figure (6.6)	Bandwidth HQ Criteria (for Approach and Landing)	307
Figure (6.7)	Time Response Boundary	308
Figure (6.8)	Time Response Boundary	308
Figure (6.9)	Effective Time Delay and Time Constant	309
Figure (7.1)	Block Diagram of Controller Structure	334
Figure (7.2)	Diagram of Scheduled Throttle Lower Limit	335
Figure (7.3)	Illustration of 2D Gain Scheduling	336
Figure (8.1)	Cubic Ramp Pilot Input Shaping	367
Figure (8.2)	Basic Manoeuvre at the Hover	368
Figure (8.3)	Basic Manoeuvres at 80 Kts	369
Figure (8.4)	Basic Manoeuvre at 120 Kts	370
Figure (8.5)	Basic Manoeuvres at 250 Kts	371
Figure (8.6)	Task 1 - Forwards Accelerating Transition	372
Figure (8.7)	Task 2 - Low Speed Manoeuvres	373
Figure (8.8)	Task 3 - Forwards Decelerating Transition	374
Figure (8.9)	Task 4 - Low Speed End of Transition	375
Figure (8.10)	Demonstration of Wind-Up Protection	376
Figure (8.11)	Demonstration of Gust Rejection	377

Figure (8.12) Demonstration of Turbulence Rejection	378
Figure (8.13) Demonstration of Ship Landing Potential	379

LIST OF TABLES

Table (2.1)	29	Table (5.19)	215
Table (3.1)	-	Table (5.20)	219
Table (3.2)	74	Table (5.21)	219
Table (3.3)	82	Table (5.22)	220
Table (4.1)	117	Table (5.23)	221
Table (4.2)	122	Table (5.24)	223
Table (4.3)	136	Table (5.25)	224
Table (5.1)	162	Table (5.26)	225
Table (5.2)	163	Table (5.27)	226
Table (5.3)	166	Table (5.28)	229
Table (5.4)	175	Table (5.29)	234
Table (5.5)	177	Table (5.30)	235
Table (5.6)	190	Table (5.31)	236
Table (5.7)	192	Table (5.32)	237
Table (5.8)	196	Table (5.33)	240
Table (5.9)	197	Table (5.34)	243
Table (5.10)	198	Table (7.1)	319
Table (5.11)	199	Table (7.2)	324
Table (5.12)	201	Table (8.1)	342
Table (5.13)	203		
Table (5.14)	205		
Table (5.15)	209		
Table (5.16)	212		
Table (5.17)	213		
Table (5.18)	214		

ACKNOWLEDGMENTS

I would like to thank my supervisor, Professor Alan Bradshaw, for his continuous guidance and many helpful comments throughout the course of this project. Similarly, I would like to thank the Royal Aerospace Establishment (Bedford), Flight Systems Department, for their financial and technical support; in particular Phil Smith and later Gerry Shanks, Ian Muir and Martin Kellett.

Thanks are also due to various members of the Department who have helped and encouraged me, especially Paul Brand, Ann Clutton and Dr Mike Woodhead. Furthermore, a great debt of gratitude is owed to Mrs Jean Evason for turning my raw manuscript into this neatly typed volume, after much trouble and no extra pay !

Pennultimately, I would like to thank my parents for starting me out on this long educational journey by giving me the necessary encouragement. Last, but by no means least, I would like to thank my wife Angela for helping me in every way to complete this journey and for suffering me during the completion of this report.

SUMMARY

Vertical/Short Take-Off and Landing (V/STOL) fighter aircraft are characterised by increased control complexity caused by the extra degree of freedom. This can result in a high pilot workload which may be alleviated with the careful application of active flight control. However, the advent of control configured vehicles demands that the controller design must be part of a fully integrated and iterative aircraft design; hence it must allow the two-way flow of design information.

In this thesis a suitable controller design method is developed to solve this two-fold problem.

The method is based upon a singular perturbation analysis which is used to expose the underlying dynamics of a closed-loop state-space system. New developments are described which allow high-order, dynamically complex parasitics, such as actuators, to be included in the design. Furthermore, the method gives the designer insight into the problem allowing tuning and engineering trade-offs to be performed intelligently with a two-way flow of design information. The end result is a robust high-gain multivariable controller.

In order fully to develop and analyse the method it has been applied to a representative non-linear time-varying aircraft simulation model. This was supplied by the Royal Aerospace Establishment, Bedford. The necessary

state-space matrices are obtained by linearising the model at several different flight cases. This occurs over a wide flight envelope, from hover to 300 Kts, and consequently the multivariable control laws are implemented using gain scheduling.

Finally, task tailored control and handling qualities requirements are derived for a V/STOL aircraft in the form of a design brief. This design brief is then fulfilled by designing a controller which alleviates pilot workload during transitions from jet-borne to fully wing-borne flight (and vice versa).

CHAPTER 1

INTRODUCTION

INTRODUCTION

1.1 Introduction

The days of "seat of the pants" combat flying are long gone. The wires that once braced the biplanes wings now hum to the tune of digital computers. The single glass windscreen has now developed into several glass TV screens which barrage the pilot with a multitude of information. Today's modern fighter aircraft can be unstable, supersonic and packed with sophisticated electronics; today's modern fighter pilot is being stretched to the limit using hands, feet, eyes and even voice to perform the mission. The addition of Vertical/Short Take-Off and Landing (V/STOL) capability will stretch the aircraft and pilot still further. Indeed, for V/STOL aircraft it has already been shown [Franklin & Anderson] that the increase in control complexity and the additional degree of freedom can result in a high pilot workload.

The next generation of V/STOL aircraft will have to overcome all of these problems in order to be effective, but fortunately many of the solutions can be found in the emerging new technologies. The use of digital computers for active flight control is a typical example which is already being proven in the air. However, within the field of active flight control there is a need to develop a Multi-Input Multi-Output (MIMO) control law design method which interacts with, and gives insight to, the control engineer. Furthermore, to be properly effective the control law design method must be part of a fully integrated design programme and therefore able to interact with

the other design disciplines. This requires that the design method is capable of working two ways; from the planned hardware to a performance specification, or, from the planned performance to a hardware specification.

In this report a robust high-gain* error-actuated MIMO control law design technique is developed into a new design method which satisfies the need described above. It is then used to design a controller for a representative V/STOL aircraft model in order to alleviate pilot workload during the transition from jet-borne to fully wing-borne flight (and vice versa), and to provide enhanced manoeuvres in otherwise conventional flight phases. The controller design achieves this by: decoupling the flight variables that are relevant to the piloting task in each flight mode, reducing the number of pilot control inputs and providing some "carefree handling" characteristics ("carefree handling" means the aircraft is automatically restricted to a safe flight envelope, thereby relieving the pilot of this responsibility).

Hence there are two main objectives which permeate this report. Firstly, the development of a controller design method which fulfils the criteria described. Secondly, the design of a controller that reduces the workload which is characteristic of V/STOL aircraft.

* The term "high gain" refers to the fact that a high gain is used in the theoretical analysis, however, practical gains are used for implementation. Furthermore, the original high-gain technique has been developed further here and the new derivative is referred to as the high-gain method.

These two themes are interwoven through this report as they are complementary and interdependent. It would be impossible fully to evaluate a design method without applying it to a problem that is as realistic as possible. Similarly, it would be impossible to design a realistic controller without a suitable method. In the conclusions though, the two themes are discussed separately for clarity.

It should also be noted that current Handling Qualities (HQ) criteria and Task Tailored Control (TTC) ideas are reviewed and included in the controller design specification where possible. However, the available data is very limited, especially with respect to MIMO systems and transition flight phases. Accordingly, general criteria are suggested in this thesis which may be used with other MIMO techniques to help specify the HQ and TTC modes for V/STOL aircraft. This may be considered as a secondary objective.

This brief introduction (section 1.1) is developed further in the next two sections. In section 1.2 this report is put into perspective by describing the wider research programme of which it is a part. Section 1.3 contains an outline of the rest of the report, and describes the conventions that have been used throughout. It should be noted that the outline contains more than just a list of chapters, as it is intended to give an overview of the whole report. These two sections together explain the reasons for the project being necessary and describe the way in which it was carried out.

1.2 The VAAC Programme

VAAC represents Vectored-thrust Aircraft Advanced flight Control. The VAAC research programme is being conducted by the Flight Systems Department of the Royal Aerospace Establishment (RAE) Bedford [Flight International^{a,b}, Walker, Owen], who are also the sponsors of this project. The VAAC group consists of staff from RAE Bedford, British Aerospace, Smiths Industries, GEC Avionics, Rolls Royce, Cranfield Institute of Technology, Salford University and occasionally other contributing parties. It has been confirmed by RAE Bedford [Flight International^b, Walker] that results from the VAAC programme could be relevant to the joint US/UK technology programme which is assessing the full potential of V/STOL. This memorandum of understanding between NASA, the US Department of Defence, and the UK Ministry of Defence should lead to a "proof of concept" aircraft after a design specification is agreed upon.

The design specification will probably call for an Advanced Short Take-Off and Vertical Landing (ASTOVL) aircraft with supersonic capability, an unstable airframe and redundant control surfaces to enable decoupled or enhanced manoeuvres and reconfiguration. The aircraft would necessarily be a Control Configured Vehicle (CCV) meaning that the design of the control surfaces and the MIMO control laws becomes an integral and essential part of the aircraft design and not an "afterthought". The controller must be designed carefully to prevent there being a high pilot workload, and as a primary flight system it must be of high integrity. In view of these requirements it is doubtful that the current design techniques in use would be adequate for the task (this is discussed in greater detail in

Chapter 2).

Consequently the RAE VAAC programme was initiated with the primary objectives of developing new concepts and design assessment techniques for the controls and displays of future ASTOVL aircraft. Expertise from various industries and universities are drawn together in the VAAC programme for cross fertilisation. In addition to performing original research, the RAE also provides an organisations base, extensive flight simulation facilities and a test aircraft, the VAAC Harrier. This allows work from all group members to progress from mathematical studies to non-real-time simulation studies, real-time piloted simulation studies and ultimately flight trials.

As part of this programme, the RAE have developed a Generic V/STOL Aircraft Model (GVAM87) for use by group members and other outside research groups. It is a non-linear time varying representative V/STOL model which can "fly" within an extensive flight envelope, unrestricted by small perturbation limits. This model is described more fully in chapter 4. It is intended to be used for development of ASTOVL controller design techniques, investigations into reconfigurable control, fault detection and optimisation techniques. The RAE support this model on their Advanced Flight Simulator (AFS) allowing the ideas to be assessed in real-time possibly leading to piloted simulation trials. This facility is of course a great benefit to university based studies, allowing them to gain a practical evaluation of their research work.

The research into robust high-gain error actuated multivariable controller design techniques at Salford was chosen as a useful area

of collaboration by the RAE. The RAE have subsequently sponsored this project at Salford and more recently another project applying the same technique to the reconfigurable controls problem, now based at Lancaster University. The RAE have not only financed this research but also provided the GVAM87 and considerable practical input. This has resulted in two main results for the VAAC programme: firstly the development and assessment of a multivariable design technique, secondly the design of a controller for the GVAM87 which addresses many of the practical and implementation problems that current MIMO controller design techniques face.

This is not the place to review all of the VAAC programme or to describe its future work plan. However, it is relevant to mention that the RAE have sponsored one year of further research, on this project, starting from October 1988. This has taken the controller design to a greater level of maturity and the controller has undergone piloted flight simulation trials at the RAE. This work is contained in a separate report [Hopper] and the conclusions from this work will help to decide whether this work will be taken forward to flight trials. This concludes the description of the VAAC programme.

1.3 Outline of the report

This report consists of nine chapters and four appendices. This first chapter introduces the whole report and gives the objectives of the work. The problem of high pilot workload that is characteristic of V/STOL aircraft is described before a solution using multivariable control is proposed. This in turn defines the requirement for a suitable multivariable controller design method. The whole report is

then put into perspective by describing the VAAC programme which spawned this Project. The chapter concludes with this section, by giving an overview of the report and by highlighting the new work.

Chapter 2 contains a review of the pertinent work. Classical and modern control theory is reviewed to bring out the features that a suitable design method should have. The features which fall short of the requirement are also described. The evolution of the high-gain technique is then given from its conception to its current form. Areas where development has taken place and areas which need further development are described with reference to past research. The chapter concludes with a summary of the developments that have already been made to show the status of the technique up to 1985. This is followed by a summary of past "recommendations for further work" which have been fulfilled in this report.

A detailed description of the new high-gain method is contained within chapter 3. First, an overview of the old high-gain technique and its main features are given followed by an overview of the new developments. Then the strengths and weaknesses are assessed and reasons for favouring the new high-gain method are given in view of the requirements made at the start of this report. The main body of this chapter contains the mathematical derivation of the high-gain theory and the new developments. The theory is then put together into a step by step method, listed at the end of the chapter.

The aircraft model (GVAM87) which was supplied by the RAE is described in chapter 4. The rigid body dynamics, the actuators and the "flight" environment are all discussed. The nature of the

non-linearities and practical constraints are described in detail as they form the real constraints which compromise the design. Several features are described with the aid of figures. Finally, the design environment which is used is discussed and the software which forms the environment is described.

Case studies are worked through in chapter 5 in order to illustrate particular features of the new high-gain method, and to show how it may be applied to a problem. A linear model is extracted from the non-linear GVAM87 at a transition flight case, and it is used as the basis for the case studies. Initially only the rigid body dynamics are used with no parasitic dynamics (actuators, sensors etc) so that the most basic features of the design method may be shown clearly. The step by step method is then applied and the design progresses with the model becoming increasingly complex at each stage. In this way the designer can build up his knowledge of the problem gradually as the design progresses, whilst being aware of the effects of his decisions at each stage. Thus the effect of adding complex, relatively slow actuators is demonstrated and the effect this has on the closed-loop system is clearly seen.

Chapter 5 also contains a simple robustness test which is performed by simulating a controller at an off-design flight condition. Next, a method for designing dynamic compensation is shown which is identical to the root-locus method used with SISO systems. This example also shows the effect that the engine non-linearities can have on the closed-loop response. Finally, a very important and useful characteristic of the high-gain method is demonstrated, namely the ability to "work backwards". It is shown how the poor closed-loop

performance of a particular system can be improved by discovering the actuator responsible and taking appropriate action. This feature makes the method suitable for use in a fully integrated aircraft design programme because it offers "design feedback". It is this feature which is lacking in many other methods and it is one of the main requirements listed at the start of this report.

In order to show that the method is capable of working to a realistic design brief, one must first be defined. This is the purpose of chapter 6. Current ideas on task tailored control are reviewed and the needs specific to V/STOL aircraft are discussed. The handling qualities criteria that exist are also reviewed and the features that are relevant to this application are extracted. In order to ensure that the controller is realisable, several practical considerations are examined resulting in extra constraints to be considered. Finally, information from each of these three areas is drawn together to form the basis for the design brief. Where there is insufficient information or lack of continuity in the existing data, new criteria have been defined.

The design brief of chapter 6 is used as a basis for designing a controller for the GVAM87, utilising the method described in chapters 3 and 5. The structure and function of the resulting controller are described with the aid of figures in chapter 7.

The controller which is described in chapter 7 is demonstrated in chapter 8 with a series of flight simulations. After demonstrating the basic controller features four realistic flying tasks are performed followed by two specific tasks. Finally, the possibilities

of automatic ship landing systems are described before the handling qualities of the controller are discussed.

The last chapter, chapter 9, contains the conclusions and recommendations drawn from this work. The conclusions are divided between the two main objectives and the secondary objective. The recommendations are listed in four subject groups: the controller design method, the actual controller design, the design environment and the design trade-offs.

The last chapter is followed by the list of references and then the appendices. Appendix A contains the mathematical derivation of the block diagonal closed-loop system which is referred to in section 3.3. Appendix B contains the bulk of a worked example from section 3.4. Appendix C contains a listing of the help banners for some of the Pro-Matlab functions that have been used and which are referred to in section 4. Lastly, Appendix D contains a glossary of terms for handling qualities criteria, referred to in section 6.

All references are listed by first author's name at the back of this report, and where different authors have the same surname an initial is also given. If an author appears more than once, a superfix is attached to the name (i.e. Smith^a, Smith^b...). Occasionally an author is mentioned by name in the text but mostly it is the work which is mentioned, the authors name appearing in brackets nearby, e.g. [Smith]. Where more than two authors have written one paper, only the first author is given e.g. [Smith et al]. All abbreviations and notation is defined when it is first used.

All figures appear at the end of each chapter. The figures and tables

are numbered as they are mentioned in the text, beginning with the chapter number and equations are numbered as they are defined in a similar way e.g. (2.4) for figure, table, or equation 4 of chapter 2. There is also a list of tables and a list of figures at the front of this report, giving the page number on which the figure or table appears.

CHAPTER 2

REVIEW OF PERTINENT WORK

REVIEW OF PERTINENT CONTROL THEORY

2.1 Introduction

This review is divided into three sections. Firstly, section 2.2 contains a discussion on the use of classical design techniques and highlights their strengths and weaknesses, especially with regard to MIMO control problems. Secondly, section 2.3 contains a review of several MIMO controller design techniques and a discussion of reasons why they were not considered suitable for this project. Finally, the third section (section 2.4) contains a description of the evolution of the high-gain technique up to the start of the project. Its roots and its development are described, but no comment is made about its suitability or operation at this stage as this is contained within chapter 3.

2.2 Classical Controller Design Techniques : Strengths and Weaknesses.

The classical design techniques referred to here are the frequency domain techniques of Bode (1945) and Nyquist (1932) and the root-locus technique of Evans (1948). These techniques were developed separately and also used separately for a while, but

eventually it became apparent that the root-locus and frequency domain techniques were complementary. Designs could be performed more readily using the techniques together. Studying the root-locus of a system quickly shows the effects of adding actuator, sensor and compensator dynamics to the basic plant under feedback control. It is also possible to study the effects of varying parameters other than the feedback gain. This combines to give the designer insight into the design problem, its limitations and the possible cause of poor closed-loop dynamics. The system may then be studied using Bode's technique to assess the frequency response. This will indicate bandwidth, possible resonance problems and the stability robustness to plant changes or noise (through the phase and gain margins). There are other techniques based in the frequency domain which can also be used effectively depending on the nature of the problem and the usual practice of the design group/individual. Finally, the designer can generate time responses to check the closed-loop behaviour and to perform fine-tuning of the control parameters.

Methods such as these have been used successfully for many years as can be shown by the following case studies: the Fly By Wire (FBW) Jaguar [Nelson & Smith, Smith et al] and the F-18 Hornet [Moran, Harschburger & Moomaw] are two examples of current operational aircraft with classically designed control laws, the space shuttle [Powers] is an example of an aerospace vehicle and the EAP [Kaul et al] is an example of a modern unstable supersonic aircraft. Classical techniques were also used on an F-8 [Butler et al] to test a variable gain controller to alleviate sensor noise effects on the actuators.

Classical techniques have also been used in conjunction with more complex methods. For example, the Quiet Short-haul Research Aircraft (QSRA) [Franklin & Hynes] which had Single-Input Single-Output (SISO) control loops around the non-linear system inverse which was the core of the controller (discussed further in the next section). Furthermore, multi-objective optimisation was used [Grübel & Kreisselmeier] to design a SISO controller for an F-4C aircraft which used parameters from classical analysis as bounds for the design. Lastly, a modern controller design technique was combined with classical design and analysis techniques [Moomaw & Lowry] to design a controller for the Short Take-Off and Landing (STOL) F-15 technology demonstrator.

Despite all of this, there are drawbacks to the classical SISO techniques when applied to MIMO problems. Having to design each loop separately for an m input m output system requires m^2 loops to be studied. The effects of tuning one loop may "upset" one already tuned, and if it is important that the loops do not interact (i.e. the system is to be decoupled) the problem can become intractable. Furthermore, the robustness measures of phase and gain margins may no longer be applicable in the MIMO case as they do not give an indication of simultaneous gain or phase changes on more than one channel.

This section has highlighted the advantages of the classical design techniques and some significant examples of their use have been referred to. The three extensions of the classical techniques mentioned shows that engineers still desire the simplicity and insight of these techniques. However, it has also been shown that classical techniques are inadequate for many MIMO problems. Clearly

a MIMO design technique which encapsulates the benefits of the classical techniques whilst overcoming their deficiencies is required.

2.3 Modern Controller Design Techniques : A Critical Appraisal

Here, modern control or multivariable control is taken to mean those techniques developed since the late 1950's which were originally inspired by aerospace servo problems, and the advent of digital computers. The field of modern control is very broad and consequently it is not possible to review every technique in detail here, so only those features most relevant to the current problem are discussed below. The strengths and weaknesses of each technique are pointed out, and the relative merits are assessed with regard to the comment at the end of the preceding section.

The broad field of modern control may be divided into two schools of thought. One is based on time-domain state-space descriptions of the physical plant and the other on frequency-domain descriptions of the physical plant. The control objectives and sensitivity properties are described in a compatible way for each branch. Although engineers have tended to use one or the other, there are precise mathematical relationships between the two domains. This is beginning to be exploited by some techniques, as will be mentioned, but first three techniques based in the frequency domain are discussed.

The Inverse Nyquist Array (INA) [Rosenbrock^{a,b}] was intended as a design technique rather than a synthesis technique. Consequently, graphical methods are used so that there can be rapid communication of information between the computerised technique, and the designer. It is intended that stability, sensitivity, speed of response etc. are presented so that the designer can make the necessary decisions to progress towards the "best" solution. However the technique also has less attractive features. In order for the stability results to be applied easily the compensator-plus-plant must be made diagonally dominant. Various means of achieving this are suggested, but they can lead to complexity and an unnecessary loss of design freedoms. INA has also been criticised for not being generally reliable in achieving the objectives [Cunningham & Pope], being overoptimistic about stability [Doyle^a], being suitable for only diagonal and "normal" systems [Doyle & Stein] with tight eigenvalue/singular value bounds, and for sometimes producing multivariable root-locus asymptotes not of minimal order [Kouvaritakis].

Another frequency-domain technique is the Characteristic Locus (CL) technique [MacFarlane^a, MacFarlane & Belletrutti]. This was developed as a direct extension of the Bode and Nyquist techniques to the multivariable problem. Initially the open-loop system response is analysed and shaped with a pre-compensator before the loop is closed using unitary feedback to make the closed-loop response easily predictable. The initial loop shaping involves phase compensation and decoupling at a high frequency before balancing the gains at a low frequency. This is followed by gain injection to improve the closed-loop performance. This technique, like INA, uses graphical information and is interactive with the designer. Even as the benefits are similar, many of the criticisms are too [e.g. Doyle &

Stein, Doyle^a, Cunningham & Pope]. Also the Computer-Aided Design (CAD) package [Edmunds], which implements the technique, whilst being comprehensive, requires extensive "hands-on" experience in order to design effective controllers. However, unlike INA, CL does minimise the order of the asymptotic root-locus structure [Kouvaritakis] and has been used in conjunction with the work of Kouvaritakis [MacFarlane & Kouvaritakis]. Finally, it must be said that neither INA nor CL have widespread use in the aerospace industry [Gangsaas et al].

The final frequency domain technique to be discussed is H^∞ [Postlethwaite et al^a for example]. This is a more recent technique based upon the H^∞ norm of a stable transfer function matrix, which is its maximum singular value over all frequencies (it may also be thought of as a measure of the maximum energy gain from input to output over all frequencies). Apparently many practical feedback control problems can be formulated as the minimisation of the H^∞ norm of a weighted closed-loop transfer function matrix. The weights are used by the designer to emphasise or de-emphasise maximum singular values of various transfer function matrices at various frequencies. This enables engineering objectives to be incorporated into the optimization procedure. Due to the complex mathematics involved a CAD package is needed and to the authors knowledge, only Stable-H is currently available [Postlethwaite et al^b]. Several design applications have been reported [Postlethwaite et al^a, Yue] which look promising but the following drawbacks should be noted. The controllers are often of very high order and need to be 'reduced', the CAD package needs considerable "hands on" experience similar to the CL CAD package, actuators can still cause design problems [Yue], the technique is a 'black box' technique giving limited insight to

the designer and finally it may prove difficult to implement the resulting controllers practically.

Linear optimal control is the first of the time domain techniques to be discussed. In fact it was the first of the modern techniques to be developed, and early contributions came from both the USSR [Pontryagin et al] and the USA [Bellman^{a,b}] founded on the state-space descriptions of dynamic systems. However, the first comprehensive design procedure for linear multivariable systems was developed by Kalman [Kalman^{a,b}] who introduced the quadratic performance criterion. This has subsequently given birth to a whole family of Linear Quadratic (LQ) techniques, of which the two main ones are listed below. An original and powerful member of the family is the LQ Regulator design (LQR), but the need for full state feedback with all LQ designs inspired the next derivative. Full state feedback could only be circumvented by the inclusion of an observer such as a Kalman filter. The complete system can then be optimised with respect to Gaussian white noise disturbances, resulting in 'LQG' designs.

The robustness of LQ SISO designs is well known and more recently singular value analysis of the return difference matrix has been incorporated with the LQ technique [Moomaw & Lowry, Lehtomaki et al, Safonov et al] to give truly multivariable stability margins. Furthermore, frequency domain trade-offs can now be incorporated with loop shaping techniques [Gansaa et al] and Loop Transfer Recovery (LQG/LTR) [Smith K L et al]. This illustrates the link now forged between time and frequency domain techniques which was mentioned earlier. Being a synthesis technique, LQ was often criticised for not being sufficiently iterative with the designer,

but even this has now been shown to be quite possible [Safonov et al, Lehtomaki et al]. To conclude the "good news", it is worth mentioning that several interesting aerospace paper studies have recently been produced using LQ techniques, and at least one application has gone beyond this to flight tests. For example: Ship-borne Vertical-Take Off and Landing (VTOL) aircraft [Bodson & Athans] and the QSRA [Blight & Gangsaas] as paper studies; the AFTI/F-16 (Advanced Fighter Technology Integration) [Anderson et al] being a relevant flying example.

Unfortunately though, the LQ technique is often criticised because full state feedback is generally required [Cunningham & Pope, MacFarlane^b, Sobel & Shapiro], which is often impractical, unless an observer is used adding complexity to the design and reducing the stability margins [Doyle^b]. It has also been said that there is no room for adding dynamic compensation and that the gain margin can be over specified [MacFarlane^b]. Moreover, it is difficult to relate performance criteria or handling qualities to the cost function due to their different modes of expression [Anderson et al, Sobel & Shapiro]. Finally it should be mentioned that LQ and classical root-locus techniques were both applied to the QSRA aircraft model [Blight & Gangsaas] for comparison. The optimal controller outperformed the simple proportional plus integral action controller until it was constrained to using only the airspeed error (like the classical controller) whereupon an observer had to be used. This resulted in a very similar performance from both the simple classical and the modern highly complex designs!

The next time domain technique to be discussed is Eigenstructure Assignment (EA) which is the assignment of closed-loop eigenvalues to the desired locations, and the shaping of eigenvectors, both by constant and dynamic gain feedback. At first it was only possible to move the poles and this was termed eigenvalue assignment, pole assignment or modal control. There is a vast literature on this subject but its origins can be traced back to remarks made by Rosenbrock [Rosenbrock^c] and may be summed up by "Modal Control Theory and Applications" by Porter and Crossley [Porter & Crossley]. The drawback of having to use full state feedback was addressed by using a subset of the full state and incorporating observers as necessary. This problem was also solved by using the outputs directly, with either constant or dynamic feedbacks. This work also generated a vast literature which is concisely reviewed by Patel [Patel & Munro]. The next improvement to the modal control technique was to use design freedoms to make it possible to shape the eigenvectors also [Moore], producing EA which is still under active development [Andry et al, Fletcher et al] (other workers are mentioned specifically below).

EA used to be criticised because whilst it was possible to assign poles and eigenvectors, it was not known where to assign them. Even when all the poles were assigned to a benign region in the complex plane, the system's transient response could still be poor and have little correlation to the pole positions [MacFarlane^b]. There were also numerical problems [Kautsky et al] associated with calculating the feedback matrix. Furthermore, the technique generally produces only PI Control and has been criticised for not giving any guidance for choosing dynamic compensation [MacFarlane^b]. However, EA is continuing to be developed and some of the most relevant advances are

described below:

- (i) A non-linear unstable canard aircraft model was linearised at several flight conditions and EA was used with singular value robustness analysis to achieve current handling qualities criteria [Cowling].
- (ii) Model following was coupled with EA to design a controller for the AFTI/F-16 for pitch pointing manoeuvres and to achieve current handling qualities criteria [Sobel & Shapiro].
- (iii) The above method was extended to improve robustness and was then applied to a vectored thrust aircraft model [Sobel & Lallman].
- (iv) The closeness of achievable eigenvectors to the desired eigenvectors can now be assessed graphically enabling trade-offs to be performed more easily [Smith P R]. Current handling qualities were also met in the fast-jet application used.
- (v) Finally, EA has been applied to an ASTOVL aircraft to design controllers for hover and transition flight cases, and for the achievement of satisfactory handling qualities [Lee et al].

Despite the above it is still not easy to use EA to design decoupling controllers which satisfy handling qualities criteria, whilst allowing sensible engineering trade-offs to be performed in both the

time and frequency domains. EA is highly mathematical and so needs a well designed computer analysis package to implement all the necessary features in a way that is useful to a designer. These and other criticisms have also been made in a paper which directly compares EA to the high-gain method using a V/STOL aircraft model as the basis of the comparison [Smith P R et al]. Furthermore, there are practicalities that need to be addressed concerning the structure of the resulting controller, and the ability to move from flight case to flight case. The last example mentioned illustrates this [Lee et al], whereby controllers are designed at the hover and at a transition case. The two controllers have a different structure and there is no indication of how the controller will progress from the hover to the higher speed case or vice versa.

The next technique to be reviewed is the multivariable root-locus technique [Kouvaritakis & Shaked, Kouvaritakis, Kouvaritakis & Edmunds, Owens^{a,b}]. This was developed as a MIMO generalisation of the SISO root-locus technique [Evans]. After the various types of multivariable zeros were characterised [Pugh, MacFarlane & Karcnias] it became possible to investigate multivariable root-loci. Rules that govern the structure of multivariable root-loci were derived and the rôle of the finite zeros and asymptotes was defined (asymptotes are also described as infinite zeros). It also became clear that for each input or output (square systems) there would be a Butterworth configuration for the asymptotes. The order of this configuration would depend on the rank of terms in the Markov Chain. These results were used to define feedback matrices which minimised the order of the Butterworth configurations and enabled their pivot points to be moved giving increased stability margins. This research [Kouvaritakis & Shaked, Owens^{a,b}, Kouvaritakis, Shaked] is

fundamental to the full understanding of multivariable systems, but it did not give rise to a comprehensive technique. It was only in conjunction with the CL method [Kouvaritakis et al, MacFarlane & Kouvaritakis] that the technique was used for design. However, the results from this research are used to describe the multivariable root-loci produced by application of the high-gain technique, and so are described in more detail in Chapter 3, Section 3.4.

Decoupling theory is the next technique discussed. Clearly, the simplest method of decoupling a system would appear to be placing a system inverse before the system. However, such a compensator is not always realisable and is usually unnecessarily complicated and difficult to implement. Consequently, decoupling by both constant gain and dynamic gain feedback has been developed. Decoupling theories have been developed using the geometric approach [Wonham & Morse] and the algebraic approach [Falb & Wolovich]. The algebraic approach is discussed here as it is closest to the technique which is used in this thesis. Indeed, there has been a study comparing the high-gain technique to the algebraic approach [Jackson]. The decoupling theory of Falb and Wolovich is very similar to the high-gain technique when the product of the output matrix (C) and the input matrix (B) is full rank. However, feedforward is used for steady state tracking rather than integral action, which is not robust with respect to plant changes. When CB is not full rank the Falb and Wolovich technique includes the plant matrix (A) in constructing the controller. This leads to better decoupling than the high-gain technique, but a reduction in robustness due to plant changes. In fact, the performance of the Falb and Wolovich technique is poor compared to the high-gain technique at the same off-design condition [Jackson]. Furthermore, the application for

which the two techniques were compared by Jackson was the AFTI/F-16 and it was noted that the Falb and Wolovich technique could not perform all the designs as the controller matrix was not invertible. Many of these problems have since been alleviated [Pautzke et al] but it is still not as robust as the high-gain technique and neither does it provide as much practical insight for the designer.

Linear system inverses are not generally used, as has been described. However, the digital computer has made it possible to develop non-linear system inverses which completely turn the dynamics of complex non-linear aircraft "inside-out". It is the exact opposite of self-adaptive or learning strategies whose central theme is to minimize the use of a priori information. The technique originally used dynamic trim maps which inverted the aircraft model and were used by interpolation over the whole flight envelope [Meyer & Cicolani, Smith & Meyer^{a,b}].

More recently the inversion has been achieved using a Newton-Raphson technique [Smith^{KL}/_h et al]. The model inversion in the forward path offers several benefits. Firstly, all the trim logic is taken care of so it is no longer the central issue, as it is in linear gain scheduled designs. Secondly, envelope limiting is relatively routine as the controller has access to detailed aircraft characteristics. Lastly, simple SISO design loops can be placed around the resulting system as the non-linearity and cross-coupling is dealt with. As external disturbances are expected, and perfect aircraft models do not exist, closed-loop feedback is used to correct the final response of the system.

Although the scheme has many obvious benefits, it would appear that the resulting controller is extremely complex and difficult to implement. However, the authors claim that the total control system complexity can be reduced by a factor of four compared to a conventionally designed system, when measuring the product of total memory used and execution time of the complete code! The method has been applied to simulation studies such as automatic aircraft carrier landing with an A-7E aircraft model [Smith & Meyer^a] and a Vertical Attitude Take-Off and Landing (VATOL) model aircraft [Smith & Meyer^b]; but more importantly it has been flight tested with a DHC-6 STOL aircraft (first flight test) [Smith & Meyer^a], the QSRA [Franklin & Hynes] and the Augmentor Wing Jet STOL research Aircraft [Meyer & Cicolani]. This is the most promising technique reviewed so far, especially if the comments about complexity are still valid when the technique is compared to an equivalent MIMO controller. However, the technique is most suitable for designing controllers for aircraft which already exist and have had accurate models developed. In contrast, the early stages of aircraft design have uncertain models which require feedback of design information from the control engineer before hardware is finalised. Consequently, a technique which gives insight into the system dynamics is preferable, so that trade-offs may be made knowledgeably.

It has already been stressed that the overriding design technique criteria are clarity, simplicity, high performance (and therefore high-bandwidth/high-gain) and practicality. Therefore, the following techniques have also been discounted : low gain theory [Porter^a], Quantitative Feedback Theory (QFT) [Horowitz], variable structure control [eg Hikita et al], model following and self-adaptive

techniques. Greater detail is not given here as these techniques are either too immature for serious consideration or on the fringe of those techniques which are suitable for this application.

2.4 The High-Gain Technique

The roots of the high-gain technique can be traced back to modal control, and later EA, which have been reviewed already. In parallel with this, the theory of singularly perturbed systems was also being investigated at Salford during the 1970's. There is an extensive literature produced during this period by Porter, Bradshaw and co-workers which shows in detail how research developed during this period. However, it will be more concise to set out the PhD theses produced in the period up to 1981 in date order with a precis of the contents, as shown in table (2.1) below:

TABLE 2.1

AUTHOR	SUPERVISOR	DATE	THEME
Shenton, A.T.	Porter, B.	1977	Modal control, singularly perturbed systems.
D'Azzo, J.J.	Porter, B.	1978	Eigenstructure assignment, sampled data systems.
Tsingus, A.	Porter, B.	1978	Singular perturbation methods, slow and fast modes.
Sangola, B.A.	Porter, B.	1980	Singular perturbation methods, eigenstructure assignment.
Hemani, A.	Bradshaw, A.	1980	High-gain controllers, singular perturbation methods.
Calderbank, J.A.	Bradshaw, A.	1981	Fast-sampling controllers, singular perturbation methods.
Garis, A.	Woodhead, M.A. (& Bradshaw, A. Porter, B.)	1981	Fast-sampling, flight control singular perturbation methods.

N.B. Full references for these theses appear among the other references.

From this table, it is clear that modal control developed into EA and that singular perturbation techniques were utilised with both of them. A major factor in the development of the high-gain technique at this time was the clarification of the rôle of zeros in multivariable systems [Pugh]. This, together with singular perturbation analysis which reveals the underlying dynamic structure [Porter & Bradshaw^a], gave the basis for the high-gain technique [Porter & Bradshaw^b]. This technique had to be extended though, to enable controllers to be designed even when output feedback resulted in a rank defective first Markov parameter [Porter & Bradshaw^c] (the significance of this is explained in Chapter 3).

It should be noted that throughout this development, sampled-data equivalents to the continuous-time techniques were being produced. This was in recognition of the powerful part that digital computers would play in the implementation of controllers. Whilst the essence of the high-gain theory is contained within Porter & Bradshaw^{b,c}, the essence of the sampled-data equivalent (fast-sampling theory) is contained within Bradshaw & Porter^{a,b}. From these papers it may be seen that although the analysis is different, the resulting continuous-time and discrete-time controller matrices are the same. This ability to switch from a high-gain design to the equivalent fast-sampling design without complex transformations is one of the strengths of this design technique.

Hence, by 1981 both the high-gain technique and the fast-sampling technique had been defined and both needed to be matured through practical application. From this time, the two techniques were used in final-year projects, MSc dissertations, MSc theses, PhD theses and

private contract work. The most relevant applications of the techniques, and extensions to them, are now described.

Fast-sampling controllers were designed for several linear YF-16 aircraft models at different flight cases [Garis], to enable pitch pointing and vertical translation manoeuvres to be performed. The aircraft was simulated using an analogue computer and the controller was implemented using a microprocessor which was connected to the aircraft model through Analogue to Digital (A-D) and Digital to Analogue (D-A) converters. Robustness to plant changes was demonstrated by simulating a controller designed at one flight condition with the aircraft model at a different flight condition. No actuator or sensor dynamics were included in the analysis or in the simulation; including these dynamics was suggested as an area of further research. The fast-sampling controller design technique used for this work was later extended to allow for computational time-delays of one or more sample periods [Bradshaw & Woodhead].

The fast-sampling controller design technique was also applied to linear models of a Handley Page VICTOR K Mk2 aircraft [Burge]. The objective was to design a MIMO controller which allowed relaxed static stability and yet gave improved pilot control, gust-load alleviation and manoeuvre load control. In addition to this, the influence of actuator and sensor dynamics was investigated. This showed that although the extra dynamics fundamentally alter the closed-loop root-locus structure, their presence does not affect the design procedure or performance provided "certain practically reasonable requirements are met" [Burge, Summary, Piii] (Unfortunately, these requirements are not met in the application described in this report as will be shown in subsection 3.2.2). The feasibility of implementing this controller was shown, once

again, by carrying out real-time microprocessor plus analogue computer simulations. The aircraft and representative actuator and sensor dynamics were simulated using the analogue computer, and the controller was implemented using a microprocessor via A-D and D-A converters. Several recommendations for further work appear, of which two are relevant to this discussion. Firstly, the actuators can become the limiting factor in any high performance design if the rate or deflection limits are too small. Research into these and other non-linear actuator effects is recommended. Secondly, it was noted that aircraft dynamics are also non-linear and that simulation of the linear controller with a non-linear aircraft model would be beneficial.

Following on directly from this research were two MSc dissertations [Fontane, Taylor]. A non-linear model of a VICTOR aircraft (similar to that used by Burge) was linearised at several flight cases and the state space matrices were obtained. Fast-sampling controllers were designed and simulated with the model at different flight conditions, thus robustness to plant changes was demonstrated. The effect of actuators and a delay of one sample period was also simulated, with appropriate changes to the controller. This is reported by Fontane. Taylor repeats some of this work but performs simulations using a linear controller and a non-linear large perturbation aircraft model (excluding actuator dynamics) at different flight conditions. One recommendation for further work is the investigation of gain scheduling as it is suggested that this would improve performance over a large flight envelope (in fact it is essential for V/STOL aircraft as the dynamic characteristics change considerably during the transition from jet-borne to fully wing-borne flight and vice versa).

Some other applications and developments of less relevance are described here briefly for completeness. The high-gain or fast-sampling technique has also been applied to Longitudinal vehicle dynamics (trains) [Calderbank], various F16, YF-16 and AFTI/F-16 linear models [Bradshaw ^a, Bradshaw et al, Bradshaw & Woodhead, Porter & Bradshaw ^c], helicopters [Bradshaw ^b, Porter ^b]. Missiles [Bradshaw & Counsell] and an early linear V/STOL model [Bradshaw & Davis]. Some developments to the technique include the incorporation of a certain class of non-linearity [Porter ^c] and self adaptive schemes [Porter & Bradshaw^d, Porter & Manganas^a].

The developments of interest here are summarised as follows:-

- (i) Practical implementation has been proved with digital-analogue simulations.
- (ii) Robustness to plant changes has been shown.
- (iii) The influence of actuator and sensor dynamics of a particular type has been investigated.
- (iv) Delays of one or more sample period can now be compensated for.
- (v) Controllers designed for a linearised flight case have been shown to operate satisfactorily with large perturbation non-linear models (no actuator dynamics).

The following is a summary of the most relevant areas of further research that were recommended:

- (i) The influence of non-linear actuators on the design problem.
- (ii) The influence of actuator dynamics which do not satisfy the requirements set down by Burge.
- (iii) The feasibility of implementing gain scheduling.
- (iv) The effect of implementing linear controllers in a representative large perturbation non-linear aircraft model, including actuator dynamics.

This concludes the historical evolution of the high-gain/fast sampling technique. It should be noted that the further developments needed that are listed above, have actually been accomplished and are described in this report.

CHAPTER 3

THE HIGH-GAIN CONTROLLER

DESIGN METHOD

THE HIGH-GAIN CONTROLLER DESIGN METHOD

3.1 Introduction

Despite the fact that the high-gain theory has been published many times in various forms, it is also presented here for completeness. The evolution of the high-gain technique has already been described in chapter 2, but in this chapter the actual characteristics of the technique are described. The next section (section 3.2) gives an overview of the high gain technique and highlights the main features. The new developments are then described in the same way. Finally the reasons for the new high-gain method being suitable are discussed referring to the requirements for a new controller design method which were given earlier.

Section 3.3 contains a mathematical description of the basic state-space system and the control theory. The closed-loop equations are defined and then the asymptotic analysis is performed. This exposes the underlying dynamic structure of the closed-loop system and shows how the controller matrices are defined.

Section 3.4 contains a description of the effects of adding actuators to the system and briefly reviews the theoretical work of Burge. Theoretical results for the exact calculation of the order and position of multivariable root-locus asymptotes (also called Butterworth patterns) are also given. A much simpler method, which closely approximates the same results, is then derived under certain realistic conditions. This allows the effects of relatively slow complex parasitic dynamics to be assessed and incorporated into the design. It is this new feature which transfers the high-gain

technique into the high-gain method which is suitable for this application.

There is, however, one strong condition concerning added actuator dynamics, each actuator should have unity steady state gain. In order to check this condition the SISO gain magnitude criteria is applied and this is described in section 3.5.

The breakdown of the multivariable problem into smaller classical SISO type problems enables simple tuning criteria to be applied. The definition of such criteria is contained in section 3.6. These tuning criteria enable the control law designer to undertake tuning of the system with a full understanding of the relationships and trade-offs involved

In the last section (section 3.7) all of this is brought together and the step-by-step method and how it is applied is described. Finally it should be noted that although in many cases the root-locus diagram is simplified (as will be shown) and the asymptotic structure is predictable, it is not suggested that hand sketching is a benefit of this design method. Rather, that these simplifications make it possible for the control engineer to obtain insight into the problem and hence to exercise judgment over the development of the design.

The method utilises root-locus diagrams, frequency-responses and time-responses. All of which can be generated by digital computers using suitable software which will allow the designer rapidly to see the effects of any design changes made. The design environment, and the software used in this thesis, are described in chapter 4, but a specific package is not needed to implement this method. Any software

which can generate the diagrams and responses mentioned above is sufficient for linear models. If a non-linear model is being used however, it becomes necessary to have software which can calculate time-responses of non-linear systems and also perform linearisation at spot points. Such a combination of non-linear design and analysis packages has been used for this project. Finally, it should be noted that the frequency responses are generated for the closed-loop system and that closed-loop equivalents to Bode's gain and phase margins are used throughout the rest of this thesis.

3.2 Overview of Design Method and Comparison to Requirements

3.2.1. Overview of the Basic High-Gain Technique

For simplicity here it is assumed that the plant has no parasitic dynamics (actuators, sensors etc) and that the system is square, functionally controllable [Rosenbrock^d], pointwise state (PS) controllable and observable [Rosenbrock^d, Patel], minimum phase and that it has a full rank first Markov parameter CB (where C is the output matrix and B is the input matrix of the state space system). Suitable controllers can be designed when some of these conditions are not met, as will be seen, but this is the very simplest case which enables a clear description of the main features of the technique to be made.

The high-gain technique produces error-actuated tracking controllers which feature multivariable Proportional plus Integral action (PI) utilising two square gain matrices (K_p and K_I respectively). Hence, each error and the integral of each error, has some effect on each actuator as defined by the controller matrices. This may be thought

of as m^2 SISO PI loops, where m is the number of inputs. Each controller matrix is multiplied by a scalar gain (g) which is made large during the singular perturbation analysis (also called asymptotic analysis). As has already been mentioned, doing this exposes the underlying dynamics of the closed-loop system and leads to the definition of the controller matrices. The controller matrices are simply defined in terms of the C and B matrices of the plant and two diagonal tuning matrices. The two diagonal tuning matrices do not have abstract properties (like those used in LQG for example) but correspond exactly to a multivariable equivalent of the two gains in a SISO PI controller.

During the asymptotic analysis, the plant-plus-controller dynamics split into "fast" and "slow" modes [Kokotović] associated with the infinite and finite zeros respectively. If the plant has n states and m inputs and outputs then the controller adds m integrators to the plant forming an $(n+m)$ th order closed-loop system. Consequently, there will be m first-order negative infinite zeros, $(n-m)$ finite transmission zeros associated with the plant only and m finite transmission zeros caused by the integrators. From a root-locus plot it is possible to see the coupled multivariable system decouple and assume the asymptotic form as g increases. If the open-loop system is unstable then it will be stabilised as g increases with $((n-m)+m)$ closed-loop poles approaching the negative finite zeros and m closed-loop poles approaching the negative first-order infinite zeros (or asymptotes). Similarly, using a frequency-response magnitude plot of the closed-loop transfer function matrix it is possible to see the diagonal dominance increase as g increases. The diagonal transfer function elements assume first-order dynamics which become increasingly fast (due to

the asymptotic poles) and the off diagonal transfer function elements become increasingly small as interaction between loops is reduced. Each diagonal transfer function element represents one decoupled loop of the closed-loop system, connecting the pilot input to the actual output (referred to throughout as control-modes).

The simplification of the root-locus and the decoupling of the transfer function is due to the choice of the gain matrices K_p and K_I , as a high-gain feedback alone will not achieve the simplification [Kouvaritakis]. The decoupling observed in the frequency domain, which asymptotically gives m non-interacting SISO loops, can also be observed using the root-locus. It exhibits the behaviour of m separate SISO root-locus diagrams overlaid as g increases. The m root-locus diagrams may be thought of as "layers" which are coupled to each other at low gain and which separate from each other as g increases. This is referred to again in subsection 3.2.2.

The basic design steps are as follows. Firstly, the root-locus diagram and the frequency-response may be used to tune g to give a suitable level of decoupling and approximately the desired bandwidth. Secondly, if different bandwidths are required for each decoupled loop then the diagonal proportional gain tuning matrix (Σ) may be used to fine tune the bandwidths. Finally, the closed-loop time-response may be examined and fine tuned using the diagonal integral gain tuning matrix (Ξ). The diagonal tuning matrices may be used in the same way that the P and I gains are used in a SISO PI controller.

The conditions which were defined at the start of this subsection are now discussed. If the first Markov parameter is not full rank and the

plant has no parasitic dynamics then extra measurements may be taken to augment the output matrix. This is also described as inner-loop compensation [Porter & Bradshaw^c, Bradshaw & Porter^b]. The need for extra measurement feedback most usually occurs when attempting tracking control of the lowest derivative in a second order dynamic equation (i.e. θ , the pitch attitude, where aircraft pitch dynamics are second order, including $\dot{\theta}$ and $\ddot{\theta}$ terms). It is interesting to note that the matrix algebra suggests augmenting the feedback variable with its rate of change (i.e. $\theta + \dot{\theta}$, or rather $\theta + q$ where q is the pitch rate) which is also the classical solution to an equivalent SISO problem. The rate feedback does not affect the steady-state tracking as it dies away to zero when the steady-state is approached, yet it improves the damping of the control-mode requiring this augmented feedback.

The condition of functional controllability is necessary for all servo/tracking systems and, as only square systems are considered in this thesis, the condition is satisfied if the determinant of the transfer function matrix is non-singular. This naturally leads on to discussions of square or non-square systems and the square system condition. Clearly there are two distinct cases of non-square systems $\ell > m$ or $\ell < m$, where for this discussion only, ℓ is the number of outputs and m the number of inputs. If $\ell > m$ then the system becomes functionally uncontrollable and it is impossible to track all of the outputs. Hence, the onus is upon the designer to choose only as many outputs for tracking control as there are inputs to the system. The alternative case is when $\ell < m$ for which the system is functionally controllable only if there exists at least one non-zero $\ell \times \ell$ minor of the closed-loop transfer function matrix. In practical terms this results in three possible courses of action. Firstly, more outputs

could be selected for control until the system is square. Secondly, "squaring down" by gearing actuators together could be used to form a square system (i.e. gearing canard and elevator as one pitch motivator, as in the EAP). This squaring down can also be performed by using the pseudo inverse of a non-square CB for the controller matrix. Thirdly, the designer can take advantage of $l < m$, which is termed redundancy, and use the extra motivators (inputs) to design reconfigurable controls for "fail-operate" flight controls. Reconfigurable control is a very wide area of current research and is not discussed here, but it is relevant to mention that the RAE are sponsoring research into reconfigurable control of ASTOVL aircraft (GVAM87) utilising the high-gain technique, as was mentioned in section 1.2. It can now be seen that the use of square systems only in this thesis is justified and does not restrict the applicability of the work.

There are two conditions which are interrelated and so are discussed together; these are controllability (PS) and observability. A system that is not completely controllable (PS) and/or observable will have input and/or output decoupling zeros respectively which correspond to certain open-loop poles. These poles and decoupling zeros cancel each other out when the transfer function matrix is formed. If the uncontrollable (PS) and/or unobservable modes are stable then the system is described as being stabilisable and/or detectable respectively. In past papers describing the high-gain technique [Porter & Bradshaw^{b,c}, Bradshaw & Porter^{a,b}] it has been required that the open-loop plant is controllable (PS) and observable, but it is now considered that this is too conservative. Indeed, the high-gain technique can be successfully applied to plants which are merely stabilisable and detectable, providing that the functional

controllability condition is not contravened. However, if the plant is completely controllable and observable then the only finite zeros which appear in the design are the transmission zeros, as was described for the simple case earlier in this section.

The final condition to be discussed is the minimum phase condition which refers to the system zeros [Patel] (which are finite). This condition is often quoted when the high-gain theory is being developed because the poles of the closed-loop system are driven towards the system zeros during singular perturbation analysis, which is used to derive the theoretical results. Clearly a non-minimum phase system (having system zeros in the right half plane) would become closed-loop unstable in the asymptotic case. However, practical gains are used in the final implementation of the controller and it may be possible to find a stable "gain-window" within which the closed-loop system performance is satisfactory. The gain-window would be defined by a minimum gain above which the closed-loop system is stable, and a maximum gain above which the closed-loop system is unstable. For square systems, the set of system zeros (SZ) is equal to the set of invariant zeros (IZ) which are given by

$$(SZ) = (IZ) \equiv (TZ) + (ODZ, IDZ) - (IODZ)$$

where TZ are the transmission zeros, ODZ are the output decoupling zeros, IDZ are the input decoupling zeros and IODZ are the input/output decoupling zeros. Consequently, as the set (ODZ, IDZ, IODZ) must be stable for the stabilisable and detectable conditions, only the set TZ can result in non-minimum phase systems for which it may still be possible to design a suitable controller using the

high-gain technique.

This concludes the overview of the basic high-gain technique and the discussion of the conditions which make the high-gain technique suitable.

3.2.2 Overview of the New Developments

When using the high-gain technique to design a controller the initial designs are performed with no parasitic dynamics. This enables the designer to produce a control scheme and to test the system's behaviour for the ideal case, where actuators and sensors have infinite bandwidth and are therefore infinitely fast. Having ascertained the functionality of the control scheme the parasitic dynamics must be included so that the realistic performance can be calculated. Work began on this aspect very soon after the high-gain technique was first published but initially only the effects of actuator dynamics were included. [Porter^d]. The actuators in this case were first-order and phase advance compensation was used to make the parasitic dynamics appear to be very fast. Indeed the phase compensation was unrealistically large so that the effective actuator dynamics and the plant dynamics were very well separated. The asymptotic analysis revealed second-order infinite zeros (or second-order asymptotes) for this case.

Subsequently, actuator and sensor dynamics were included and their effects on the resulting closed-loop dynamics were investigated [Burge]. In his work Burge stated that high-performance controllers require high-performance actuators and that the plant and parasitic dynamics should be well separated. Furthermore, the parasitic

dynamics studied were of simple dynamic structure (with poles but no zeros) and the expressions for asymptotes of order four or more become impractical to generate and use. These assumptions were practical and reasonable for the applications being considered by Burge and indeed for many other applications. However, these assumptions may not be practical for typical ASTOVL aircraft and are certainly not practical for this V/STOL application. It is characteristic of V/STOL aircraft that in the transition region they rely heavily on the engine to provide lift and control, consequently the engine and thrust vectoring actuation systems become primary actuators. An engine is invariably slow to respond to commands, compared with hydraulic jacks, due to the high inertias and the built in temperature and pressure limits which prevent surge and prolong engine life. Typical engine dynamics can also contain zeros which contravenes the assumption of simple dynamic structure made by Burge.

Usually, slow high-order actuators will possess dynamics which are not well separated from the plant dynamics and which interact strongly with them. Moreover, root-locus asymptotes of third or fourth order can be produced which are close to the origin and which result in unstable dynamics at relatively low gain. It has been suggested [Porter & Manganas] that these problems could be removed by placing phase advance compensation before the actuators, but the levels of phase advance compensation required are unrealistic for practical systems which possess actuator rate and position limits. Consequently, the problem of slow actuators remains to be dealt with and such actuators must become the critical part of any high performance design. The need to predict the asymptotic behaviour becomes important, therefore, but the lack of separation between the plant and actuator dynamics, the high-order and the appearance of

zeros in the actuator dynamics prohibits the use of Burge's results. It should be noted that only actuator parasitics are discussed with respect to these effects in the rest of this report because the actuator parasitics are those most likely to be relatively slow. Other parasitics such as sensors are usually relatively fast and so are well separated from the plant dynamics.

It was mentioned in subsection 3.2.1 that the high-gain technique results in a controller which greatly simplifies the root-locus structure. Indeed, at high gain the root-loci separate into m distinct SISO root-loci which appear to be overlaid (where m is the number of inputs/outputs). This phenomenon was also observed when typical slow high-order actuators were included in the analysis. These observations led to the derivation of very simple rules which predict the order and position of the multivariable root-locus asymptotes. These rules are presented in section 3.4 and are analogous to the rules used in classical control theory to predict the order and position of SISO root-locus asymptotes. These rules may be applied whatever the order of the actuator and whether its dynamics contain poles only or poles and zeros. The plant and actuator dynamics need not be well separated either. The only strong condition is that the actuator dynamics have a steady state gain of 1.0. This condition ensures that the controller matrices are still compatible with the system that includes actuator dynamics and it is explained in section 3.5.

These results have been corroborated by results produced for many variations of plant and actuator characteristics. Furthermore the same results apply when sensors or dynamic compensators are added making it a general theory for parasitic dynamics. The results have

also been checked against the original mathematically rigorous results of Owens and also Kouvaritakis (and co-workers). Their results are general but also very complex. However Owens' method for calculating the order and position of multivariable root-locus asymptotes has now been coded into Pro-Matlab, a linear algebra computer package. This makes the exact calculation of the root-locus asymptotes a trivial matter, but it is the insight given by the simpler technique which shows the designer the significance of this information and indicates the design options.

Studying the multivariable root-locus asymptotes has revealed another characteristic which is also of use to the designer. For V/STOL aircraft it is well known that the engine thrust controls the height in hover mode and that thrust vectoring controls the forward speed. These relationships reverse during the transition so that they are exactly the opposite in wing-borne flight. Hence it is found that the engine dynamics will dominate vertical control-modes at low speed and horizontal control-modes at higher speeds. By examining the effects of the individual diagonal Σ elements, $\text{diag} \{ \sigma_1, \sigma_2, \dots, \sigma_m \}$ on the root-locus asymptotes it is possible to discover which actuator is dominating a particular closed-loop control-mode. This aids the designer by correlating the critical actuator (with the slowest dynamics) to the control-mode which will be most compromised by the actuator's performance.

These new results enhance the high-gain technique and expand the range of problems which can be solved. The results were inspired by difficulties inherent in V/STOL aircraft but are equally applicable to other systems which have relatively slow high-order parasitic dynamics.

3.2.3. Reasons for Using the High-Gain Method

It is now possible to describe the reasons for the use of the high-gain method in this thesis. The properties that a suitable design method should have are listed below, summarising the points made in preceding chapters. The high-gain method which has been developed from the high-gain technique possesses each of these properties:

- (i) Interactive with the designer - not a "black-box" method.
- (ii) Capable of working backwards and therefore able to take part fully in an iterative CCV aircraft design project
- (iii) Gives the designer insight into the control problem.
- (iv) Capable of using design criteria or handling qualities criteria in several forms (time-domain and frequency-domain).
- (v) Makes real engineering trade-offs visible in the design .
- (vi) Uses graphical methods for the rapid communications of design information.
- (vii) Not tied to any particular CAD package and so it does not require extensive "hands-on" experience.

The previous chapters have defined the properties that a suitable controller should have. The controller which results from the application of the high-gain method, possesses each of these properties and they are listed below:

- (i) Obeys pilot commands non-interactively and tracks steady commands.
- (ii) Rejects unknown and unmeasured disturbances.
- (iii) Robust to plant parameter changes.
- (iv) Can easily be made into an equivalent digital controller with compensation for one or more sample periods delay (this has been proven with digital-analogue real-time simulations).
- (v) Results in a simple multivariable PI controller with a simple fixed structure (unlike a high-order filter).
- (vi) Only uses measurable outputs and does not require observers.
- (vii) The conditions which constrain the use of this method still allow a very wide class of practical problems to be solved.
- (viii) The tuning parameters have real physical meaning.
- (ix) The effects of relatively slow high-order actuators can be incorporated.

- (x) The linear controller works when implemented with a non-linear model (this has been proven by simulation).
- (xi) Task tailored control modes may be implemented and gain scheduling becomes possible due to the simple fixed structure.
- (xii) Other features may easily be built into or around the basic controller to produce a workable controller (i.e. protection from integrator wind-up due to actuator saturation, which is described in chapter 6).

Three disadvantages of using the high-gain method are described in this report but it is appropriate to list them here. The first is made apparent in chapter 5 and the second and third are given as recommendations for further work in chapter 9.

- (i) Although relatively slow high-order actuators can be incorporated into the design, they compromise the performance and limit the maximum practical feedback gain. In several cases this could result in some of the high-gain method's advantages disappearing. However, the actuators which compromise the high-gain design will also compromise other design techniques to a similar degree. Possible modification to the design may result in less cross-coupling, even at low gains, but it is possible that these modifications will also reduce the design's robustness to plant parameter changes.
- (ii) The high-gain method uses SISO gain and phase margins which are suitable for a diagonally dominant closed-loop system.

If the diagonal dominance is compromised (say by the situation described in (i) above) then the gain and phase margins may lose their validity. Truly multivariable stability margins are being developed using singular values of the return difference and inverse return difference matrices [e.g. Doyle^a, Safanov et al]. These results are currently immature and conservative, but they can easily be applied to a high-gain closed-loop system and could be used in the future.

- (iii) Although the tuning parameters have clear relationships with the tuning criteria, and some of the design may be performed loop-by-loop, there is a need for an optimisation routine. Initially, the designer should work through "by hand" and obtain insight into the problem and the design trade-offs. Then an optimisation routine could be employed to mechanise the tuning allowing the designer to find the "optimum" performance more quickly, whilst balancing several conflicting requirements [Fleming, Fleming & Pashkevich] [Grace & /]. A simple tuning algorithm has been implemented using Pro-Matlab, but it is very specific to this application and it sometimes gives results which are clearly ridiculous.

Weighing up the advantages and the criticisms, it is clear that the high-gain method is the most suitable for use with the V/STOL application which initiated this project and that it satisfies the criteria described at the beginning of this report. It should be remembered that all the other methods that have been reviewed failed to satisfy several of the criteria which were used to define the most suitable method.

3.3 Mathematical Definition of the Basic High-Gain Theory

3.3.1 General Definition of the Closed-loop System Incorporating Extra Measurement Feedback

It is assumed here that the designer has chosen particular outputs for control and thereby defined the output matrix. Furthermore, it is assumed that this choice of output matrix results in a rank defective first Markov parameter and so extra measurements will be required to augment the output feedback. For the purpose of developing the theory in the most concise way it is also assumed that the system is controllable (PS), observable, functionally controllable and minimum phase. Subsection 3.2.1 explains how and when these last conditions may be relaxed.

Figure (3.1) shows a block diagram of the plant and controller. The output, measurement, feedback, input, error and control signals are all shown and they are all vectors as it is a multivariable system.

The dynamic linear time-invariant system can be described by state, output and measurement equations of the respective forms

$$\begin{bmatrix} \dot{x}_1(t) \\ \dot{x}_2(t) \end{bmatrix} = \begin{bmatrix} A_{11} & A_{12} \\ A_{21} & A_{22} \end{bmatrix} \begin{bmatrix} x_1(t) \\ x_2(t) \end{bmatrix} + \begin{bmatrix} 0 \\ B_2 \end{bmatrix} u(t) \quad \dots \quad (3.1)$$

$$y(t) = [C_1 \ C_2] \begin{bmatrix} x_1(t) \\ x_2(t) \end{bmatrix} \quad \dots \quad (3.2)$$

and

$$w(t) = [F_1 \ F_2] \begin{bmatrix} x_1(t) \\ x_2(t) \end{bmatrix} \quad \dots \quad (3.3)$$

where $x_1(t) \in R^{n-m}$, $x_2(t) \in R^m$, $u(t) \in R^m$, $w(t) \in R^m$, $y(t) \in R^m$ and all the submatrices have conformable dimensions. It is assumed that

the input matrix is of full rank so that it is always possible to determine a set of state variables $\{x_1(t), x_2(t)\}$ such that the state equations can be expressed in the form (3.1) in which B_2 is a square invertible matrix. The input matrix rank condition is compatible with the conditions stated at the beginning of this section.

The high-gain error-actuated analogue controller is of the form

$$u(t) = g \{K_P e(t) + K_I z(t)\} \quad \dots \quad (3.4)$$

and is required to generate the control input vector $u(t)$ so as to cause the output vector $y(t)$ to track any constant command input vector $v(t)$ in the sense that

$$\lim_{t \rightarrow \infty} e(t) = \lim_{t \rightarrow \infty} \{v(t) - y(t)\} = 0 \quad \dots \quad (3.5)$$

as a consequence of the fact that the error vector

$$e(t) = v(t) - w(t) \quad \dots \quad (3.6)$$

assumes the steady state value

$$\lim_{t \rightarrow \infty} e(t) = \lim_{t \rightarrow \infty} \{v(t) - w(t)\} = 0 \quad \dots \quad (3.7)$$

for arbitrary initial conditions. In (3.4), (3.5) and (3.6),

$$e(t) \in R^m, v(t) \in R^m, g \in R^+, \text{rank } C_2 B_2 < m,$$

$$\text{rank } F_2 B_2 = m, K_P \in R^{m \times m}, K_I \in R^{m \times m} \text{ and}$$

$$z(t) = z(0) + \int_0^t e(\tau) d\tau \quad \dots \quad (3.8)$$

where $z(t) \in R^m$. Clearly then, the integral action introduces the extra state equation

$$\dot{z}(t) = e(t) \quad \dots \quad (3.9)$$

If the feedback matrices are defined as

$$[F_1 \ F_2] = [C_1 + MA_{11} \ C_2 + MA_{12}] \begin{bmatrix} x_1(t) \\ x_2(t) \end{bmatrix}, \quad \dots \quad (3.10)$$

where $M \in R^{m \times (n-m)}$, then it is evident from (3.2), (3.3) and (3.10) that the vector

$$w(t) - y(t) = [MA_{11} \quad MA_{12}] \begin{bmatrix} x_1(t) \\ x_2(t) \end{bmatrix} \quad \dots \quad (3.11)$$

of extra measurements is such that $v(t)$ and $y(t)$ satisfy the tracking condition (3.5) for any M if $e(t)$ satisfies the steady-state condition (3.7), since (3.1) implies that

$$\lim_{t \rightarrow \infty} [A_{11} \quad A_{12}] \begin{bmatrix} x_1(t) \\ x_2(t) \end{bmatrix} = 0 \quad \dots \quad (3.12)$$

in any steady-state. However, the condition that $\text{rank } F_2 B_2 = m$ requires that C_2 and A_{12} are such that M can be chosen so that

$$\text{rank } F_2 B_2 = \text{rank } (C_2 + MA_{12}) = m \quad \dots \quad (3.13)$$

Substituting (3.3) and (3.6) into (3.9) gives

$$\dot{z}(t) = v(t) - [F_1 \quad F_2] \begin{bmatrix} x_1(t) \\ x_2(t) \end{bmatrix} \quad \dots \quad (3.14)$$

and substituting (3.3) and (3.6) into (3.4) gives

$$u(t) = gK_p v(t) - g [K_p F_1 \quad K_p F_2] \begin{bmatrix} x_1(t) \\ x_2(t) \end{bmatrix} + gK_I z(t) \quad \dots \quad (3.15)$$

Finally, substituting (3.15) into (3.1) and including (3.14) the state vector yields closed-loop state and output equations of the respective forms

$$\begin{bmatrix} \dot{z}(t) \\ \dot{x}_1(t) \\ \dot{x}_2(t) \end{bmatrix} = \begin{bmatrix} 0 & -F_1 & -F_2 \\ 0 & A_{11} & A_{12} \\ gB_2 K_I & A_{21} - gB_2 K_p F_1 & A_{22} - gB_2 K_p F_2 \end{bmatrix} \begin{bmatrix} z(t) \\ x_1(t) \\ x_2(t) \end{bmatrix} + \begin{bmatrix} I_m \\ 0 \\ gB_2 K_p \end{bmatrix} v(t) \quad \dots \quad (3.16)$$

and

$$y(t) = [0 \quad C_1 \quad C_2] \begin{bmatrix} z(t) \\ x_1(t) \\ x_2(t) \end{bmatrix} \quad \dots \quad (3.17)$$

The transfer function matrix relating the system output vector to the command input vector for the system governed by (3.16) and (3.17) is given by

$$G(s) = [0 \ C_1 \ C_2] \begin{bmatrix} sI_m & F_1 & F_2 \\ 0 & sI_{n-m} - A_{11} & -A_{12} \\ -gB_2K_I & -A_{21} + gB_2K_P F_1 & sI_m - A_{22} + gB_2K_P F_2 \end{bmatrix}^{-1} \begin{bmatrix} I_m \\ 0 \\ gB_2K_P \end{bmatrix} \quad \dots \quad (3.18)$$

which is clearly not in a block diagonal form. However, the high-gain tracking characteristics of this system can be derived by applying block diagonalisation theory for a singularly perturbed system, as described in Appendix A. The results in Appendix A yield the asymptotic form of $G(s)$ as the gain parameter $g \rightarrow \infty$. It will be shown that this not only makes the determination of the matrices K_P , K_I and M clear, but that it also exposes the underlying dynamic structure of the closed-loop system.

3.3.2 Definition of the Closed-Loop Asymptotic Structure

The results of Appendix A indicate that as $g \rightarrow \infty$ the transfer function matrix $G(s)$ assumes the asymptotic form (A21) with "slow" and "fast" parts given by

$$G(s) = G_S(s) + G_f(s) \quad \dots \quad (3.19)$$

where the "slow" transfer function matrix is

$$G_S(s) = [C_2 F_2^{-1} K_p^{-1} K_I \quad C_1 - C_2 F_2^{-1} F_1]$$

$$\begin{bmatrix} sI_m - K_p^{-1} K_I & 0 \\ -A_{12} F_2^{-1} K_p^{-1} K_I & sI_{n-m} - A_{11} + A_{12} F_2^{-1} F_1 \end{bmatrix}^{-1} \begin{bmatrix} 0 \\ A_{12} F_2^{-1} \end{bmatrix} \dots (3.20)$$

and the "fast" transfer function matrix is

$$G_f(s) = [C_2] [sI_m + gB_2 K_p F_2]^{-1} [gB_2 K_p] \dots (3.21)$$

(from (A22), (A23), (A41), (A42), (A43), (A44), (A45) and (A46).

Furthermore, it is clear that the set of "slow" modes Z_S of the tracking system correspond as $g \rightarrow \infty$ to the poles $Z_1 U Z_2$ of $G_S(s)$ where

$$Z_1 = \{s \in C: |sI_m + K_p^{-1} K_I| = 0\} \dots (3.22)$$

and

$$Z_2 = \{s \in C: |sI_{n-m} - A_{11} + A_{12} F_2^{-1} F_1| = 0\} \dots (3.23)$$

and that the set of "fast" modes Z_f of the tracking system correspond as $g \rightarrow \infty$ to the poles Z_3 of $G_f(s)$ where

$$Z_3 = \{s \in C: |sI_m + gF_2 B_2 K_p| = 0\} \dots (3.24)$$

It may be seen that the asymptotic structure of (3.20) is such that

$$G_S(s) = (C_1 - C_2 F_2^{-1} F_1) (sI_{n-m} - A_{11} + A_{12} F_2^{-1} F_1)^{-1} A_{12} F_2^{-1} \dots (3.25)$$

and that rearranging (3.21) and bringing F_2 outside the expression gives

$$G_f(s) = C_2 F_2^{-1} (sI_m + gF_2 B_2 K_p)^{-1} gF_2 B_2 K_p \dots (3.26)$$

Consequently by substituting (3.25) and (3.26) into (3.19) the asymptotic transfer function matrix $G(s)$ becomes

$$G(s) = (C_1 - C_2 F_2^{-1} F_1)(sI_{n-m} - A_{11} + A_{12} F_2^{-1} F_1)^{-1} A_{12} F_2^{-1} + C_2 F_2^{-1} (sI_m + g F_2 B_2 K_p)^{-1} g F_2 B_2 K_p \quad \dots \quad (3.27)$$

due to the fact that both the "slow" modes corresponding to the poles Z_2 and the "fast" modes corresponding to the poles Z_3 possibly remain both controllable and observable as $g \rightarrow \infty$. However, the "slow" transfer function matrix $G_s(s)$ reduces to the form (3.25) because the "slow" modes corresponding to the poles Z_1 become asymptotically uncontrollable as $g \rightarrow \infty$ in view of the block structure of the matrices given by (3.20).

3.3.3 Definition of the Controller Matrices

It is evident that the use of integral action only requires the condition of asymptotic stability before steady-state tracking is achieved in the sense of (3.5) because of (3.9). This is guaranteed if

$$Z_s \cup Z_f \in C^- , \quad \dots \quad (3.28)$$

where C^- is the open left half-plane. In view of (3.22), (3.23) and (3.24), the "slow" and "fast" modes will satisfy the tracking requirements (3.2.8) for sufficiently large gains if the controller and extra measurements matrices K_p , K_I and M are chosen such that $Z_1 \in C^-$, $Z_2 \in C^-$, $Z_3 \in C^-$ and (3.13) is satisfied.

Furthermore, if K_p is chosen such that

$$F_2 B_2 K_p = \text{diag} \{ \sigma_1, \sigma_2, \dots, \sigma_m \} = \Sigma \quad , \quad \dots \quad (3.29)$$

where $\sigma_j \in \mathbb{R}^+$ ($j = 1, 2, \dots, m$), then $G_f(s)$ becomes increasingly fast and diagonally dominant as $g \rightarrow \infty$. This results in fast non-interactive behaviour associated with $G_f(s)$.

$G_s(s)$ may also, in many cases, be diagonalised by choosing

$$K_p^{-1} K_I = \text{diag} \{ \rho_1, \rho_2, \dots, \rho_m \} = \Xi \quad , \quad \dots \quad (3.30)$$

where $\rho_j \in \mathbb{R}^+$ ($j = 1, 2, \dots, m$). Then substituting (3.29) into (3.24) and (3.30) into (3.22) gives

$$Z_3 = \{ -\sigma_1 g, -\sigma_2 g, \dots, -\sigma_m g \} \quad \dots \quad (3.31)$$

and

$$Z_1 = \{ -\rho_1, -\rho_2, \dots, -\rho_m \} \quad \dots \quad (3.32)$$

respectively.

It is also usually possible to exploit freedoms in choosing M in order to make the resulting transfer function $G(s)$ as near diagonal as possible. This will be shown in the case study, chapter 6. Indeed, if the steady-state conditions expressed by (3.12) correspond to kinematic relationships which hold between the state variables (i.e. $\dot{\theta} = q$ for the pitch dynamics of an aircraft) then correct choice of M results in the definition of the basic plant transmission zeros as

well as producing a diagonal transfer function matrix $G(s)$.

3.3.4 Definition of the Resultant Zeros and Asymptotic Closed-Loop Transfer Function

It is appropriate to point out now that as $g \rightarrow \infty$ the poles of the closed-loop transfer function matrix approach the zeros of the system. Consequently the sets of poles Z_1 , Z_2 and Z_3 of the asymptotic transfer function matrix are also the sets of zeros of the open-loop plant. The sets Z_1 and Z_2 are the finite transmission zeros where Z_1 contains the transmission zeros caused by the integrators and Z_2 contains the transmission zeros of the basic plant. The set of transmission zeros Z_1 are easily assigned by the diagonal integral action tuning matrix Ξ , whereas the set of transmission zeros Z_2 may usually be assigned by a suitable choice of M , as described above. The set Z_3 contains the infinite zeros defined by (3.31) and clearly they are first-order infinite zeros making first-order asymptotes aligned along the negative real-axis. They may be assigned by a suitable choice of Σ the proportional action diagonal tuning matrix.

The asymptotic closed-loop transfer function matrix $G(s)$ is given by (3.27) and it is simplified here as follows. The expression (3.29) is substituted into the "fast" part of $G(s)$ and it is assumed that the "slow" part of $G(s)$ is made diagonal by a suitable choice of M . For the case where (3.12) represents a kinematic relationship $G(s)$ may be written in the form

$$G(s) = (I_m - C_2 F_2^{-1}) \begin{bmatrix} \frac{1/m_1}{s+1/m_1} & 0 & 0 \\ 0 & \frac{1/m_2}{s+1/m_2} & 0 \\ 0 & 0 & \frac{1/m_m}{s+1/m_m} \end{bmatrix} + C_2 F_2^{-1} \begin{bmatrix} \frac{g\sigma_1}{s+g\sigma_1} & 0 & 0 \\ 0 & \frac{g\sigma_2}{s+g\sigma_2} & 0 \\ 0 & 0 & \frac{g\sigma_m}{s+g\sigma_m} \end{bmatrix} \quad \dots (3.33)$$

where m_j (for $i = 1, 2, \dots, m$) are finite and $g \rightarrow \infty$.

This clearly illustrates the effects of extra measurements upon the closed-loop transfer function $G(s)$. Each of the elements $((1/m_j)/(s+1/m_j))$ (for $j = 1, 2, \dots, m$) only exists where extra measurement augmentation is used on output channel $y_j(t)$ (for $j = 1, 2 \dots, m$) where

$$y(t) = [y_1, y_2, \dots, y_m]^T \quad \dots \quad (3.34)$$

Furthermore, any element $((1/m_j)/(s+1/m_j))$ that does exist will be in $G(s)$ in place of an element $(g\sigma_j/s+g\sigma_j)$ which shows how extra measurement feedback introduces "slow" modes in place of the "fast" modes. Finally it should be said that the simpler case, for which the first Markov parameter is full rank, results in very similar expressions for the equations given in this section, but the asymptotic transfer function matrix has no "slow" modes, only "fast" modes.

3.4 Mathematical Description of the "New Developments" and their Roots

3.4.1 Review of the Effects of Relatively Fast Parasitic Dynamics on Systems with High-Gain Controllers

This subsection briefly reviews some of the theoretical work of Burge which investigated the effects of explicit actuator and sensor dynamics on systems incorporating high-gain (and fast-sampling) controllers. The type of parasitic dynamics that were considered can be expressed by state and output equations of the form

$$\dot{x}_a(t) = A_a x_a(t) + B_a u(t) \quad \dots \quad (3.35)$$

and

$$y_a(t) = C_a x_a(t) \quad \dots \quad (3.36)$$

for

$$x_a(t) = [x_{a_1}(t), x_{a_2}(t), \dots, x_{a_m}(t)] \quad , \quad \dots \quad (3.37)$$

$$A_a = \text{block diag } [A_{a_i}] \quad , \quad \dots \quad (3.38)$$

$$B_a = \text{block diag } [B_{a_i}] \quad \dots \quad (3.39)$$

and

$$C_a = \text{block diag } [C_{a_i}] \quad , \quad \dots \quad (3.40)$$

where $x_a(t) \in \mathbb{R}^a$, $x_{a_i}(t) \in \mathbb{R}^{a_i}$, $A_a \in \mathbb{R}^{a \times a}$, $A_{a_i} \in \mathbb{R}^{a_i \times a_i}$, $B_a \in \mathbb{R}^{a \times m}$, $B_{a_i} \in \mathbb{R}^{a_i \times 1}$, $C_a \in \mathbb{R}^{m \times a}$, $C_{a_i} \in \mathbb{R}^{1 \times a_i}$, ($i = 1, 2, \dots, m$) and m is the number of inputs/outputs.

It is assumed that

$$\text{rank } C_{a_i} A_{a_i}^{(a_i-1)} B_{a_i} = 1 \quad (i = 1, 2, \dots, m) \quad , \quad \dots \quad (3.41)$$

$$\text{rank } C_{a_i} A_{a_i}^i B_{a_i} = 0 \quad (i = 1, 2, \dots, < a_i-1) \quad \dots \quad (3.42)$$

and

$$C_{a_i} (-A_{a_i})^{-1} B_{a_i} = 1 \quad (i = 1, 2, \dots, m) \quad . \quad \dots \quad (3.43)$$

The conditions (3.41), (3.42) and (3.43) merely imply that each actuator block is of simple dynamic structure with poles only, and that the input-output relationship in the steady state is one-to-one. Parasitics such as this are incorporated with the basic plant and block diagonalisation of the singularly perturbed closed-loop system yields the asymptotic terms. This is then used to derive expressions for first-order or second-order actuators, first-order or second-order sensors and later first-order actuators and second-order sensors together.

The simplified expressions, rely in part, on the parasitics being "high-performance" and therefore relatively fast, with eigenvalues well separated from the plant. Two important points are summarised from the simplified expressions below:-

- 1) First-order parasitics produce second-order asymptotes; second order parasitics produce third-order asymptotes and so on.
- 2) The pivot-points for second-and third-order asymptotes, corresponding to first and second-order actuators, are given as follows:

Second order:- Pivot-point = $(\alpha_i + \rho_i + \gamma_i)/2$... (3.44)

where $(-\alpha_i)$ is the parasitic pole $(-\rho_i)$ is the integrator zero and $(-\gamma_i)$ is the transmission zero associated with extra measurement feedback for the i th control-mode

Third-order:- Pivot-point - $(2.\zeta_i\omega_i+\rho_i+\gamma_i)/3$... (3.45)

where ζ_i is the damping ratio and ω_i is the natural frequency of the second-order parasitic dynamics, ρ_i and γ_i are as before, for the i th control-mode.

Results for stability were also given which were based upon the asymptotes crossing the imaginary axis. Furthermore, it was stated that results for asymptotes of order four or more could be derived, but that the resultant expressions and stability conditions would become unweildy.

These results were fundamental in the understanding of the effects of parasitic dynamics on the closed-loop asymptotic root-locus structure. The results are still valid for a wide range of aircraft control problems where actuator and/or sensor dynamics need to be included. However subsection 3.2.2 discussed the fact that typical V/STOL aircraft do not come within the range of validity for this work.

3.4.2. Review of Relevant Results from Multivariable Root-Locus Theory

The fundamental work in this field was performed by Owens and Kouvaritakis (and co-workers) as reported in section 2.3. The reasons behind the development of multivariable root-locus theory and the use it was put to are described in that section, whereas the relevant mathematical results are defined here. Many papers were produced

covering many aspects of multivariable root-locus theory and most of them were of a very general nature. This resulted in expressions to calculate the various properties of multivariable root-loci which were extremely complicated. The references [Owens^{a,b,c,d}, Kouvaritakis & Shaked, Kouvaritakis & Edmunds, Kouvaritakis, Kouvaritakis et al] may be consulted for full details, but the references [Owens^a, Kouvaritakis & Shaked] contain the main results. Consequently, the results from this work have been simplified and are presented here for systems which are strictly proper with no direct pass operator (i.e. $y(t) = Cx(t)$ and not $y(t) = Cx(t) + D u(t)$, as $D = 0$).

The early work by Kouvaritakis (and co-workers) and Owens did not consider any specific controller as part of the closed-loop system because the main aim was to discover the properties of multivariable root-loci. Consequently, their feedback systems may be depicted as shown by Figure (3.2a), where the controller is simply kI , as shown by block A where I is the identity matrix. The scalar gain k is varied to generate the root-locus, and the dynamics of block B are analysed to determine what the root-locus structure will be like. The high-gain feedback system is shown in Figure (3.2b) and clearly block C is quite different from block A. Consequently analysing block D in the same way that block B can be analysed WILL NOT give the correct root-locus structure for the entire closed-loop high-gain system.

However it is obvious that the controller (block C) can be split as shown in Figure (3.2c) such that (block E * block F) is exactly the same as block C. Furthermore, block E is exactly the same as block A and so (block F * block G) is equivalent to block B. This shows that analysis of the dynamics of (block F * block G) WILL give the correct

root-locus structure for the entire closed-loop high-gain system. The last comparison to be made is that block F is exactly the same as block C in the case where $g = 1$.

These results are used so that calculation of the root-locus structure for high-gain systems becomes amenable to the application of Kouvaritakis' (and co-workers) and Owens' results. If the scalar gain (g) is set to one ($g = 1$) and the resultant high-gain controller (block C, for $g = 1$) is connected in series with the open-loop dynamics represented by block D (or equivalent block G), then the open-loop dynamics of the resultant high-gain system may be derived and used subsequently to calculate the root-locus structure of the closed-loop high gain system as will be shown.

The first results to be presented are those concerning the calculation of the order and angles of multivariable root-locus asymptotes. The Markov parameters are fundamental in calculating the properties of multivariable root-loci and are defined as

$$M_j = C A^{j-1} B, \quad j = 1, 2, \dots, n, \quad \dots \quad (3.46)$$

where n is the number of states, so that $M_1 = CB$, $M_2 = CAB$ etc. In (3.46) the Markov parameters were generated up to M_n . In general though fewer than n parameters need to be generated to perform the calculations. It is necessary to define a parameter d_j which denotes the rank defect of M_j (these start at $j = 1$ as M_1 is the lowest Markov parameter, but d_0 is defined as $d_0 = m$ for systems with no direct pass operator, where m is the number of inputs/outputs. A parameter ν is also defined such that ν is the smallest integer for which M_j is full rank and $1 \leq \nu \leq n$. Now several results may be

defined.

There will be n_{FZ} finite zeros where

$$n_{FZ} = n - \sum_{j=0}^{\nu-1} d_j \quad \dots \quad (3.47)$$

and n_{IZ} infinite zeros where

$$n_{IZ} = \sum_{j=0}^{\nu-1} d_j \quad \dots \quad (3.48)$$

Of the infinite zeros, $(d_0 - d_1)$ will be first-order, $2*(d_1 - d_2)$ will be second-order and generally $j*(d_{j-1} - d_j)$ will be j th order, for all $j = 1, 2, \dots, \nu$.

The angles that the asymptotes (or infinite zeros) make with the positive real axis are given by

$$\alpha_{i,t}(j) = \frac{1}{j} [\angle(-\lambda_i(j)) + 2t\pi], \quad \begin{matrix} j = 1, 2, \dots, \nu, \\ i = 1, 2, \dots, (d_{j-1} - d_j) \\ t = 0, 1, \dots, j-1 \end{matrix} \quad \dots \quad (3.49)$$

where all the terms are defined as follows:

j - j counts through the Markov chain up to the first full rank Markov parameter, M_ν .

i - i counts through the number of asymptote sets, of order j , at each step through the Markov chain. The maximum i is given by $(d_{j-1} - d_j)$, so clearly if $d_{j-1} = d_j$ then no calculations need be performed for this j as there are no asymptote sets of order j .

t - t counts through each asymptote of order j in the i th asymptote set when $d_{j-1} \neq d_j$ and t generates multiples of 2π

radians so that the exact angle of each asymptote of the i th set of j th order asymptotes may be calculated.

$\lambda_i(j)$ - $\lambda_i(j)$ denotes the i th non-zero eigenvalue of the j th Markov parameter. It determines the direction of the asymptotes. For example, using first-order asymptotes, if $\lambda_i(j)$ is positive then the asymptote will be along the negative real axis as $\angle(-\lambda_i(j)) = \pi$ rads, for $\lambda_i(j) > 0$.

$\alpha_{i,t}(j)$ - $\alpha_{i,t}(j)$ denotes the angle of the t th asymptote of the i th asymptote set of order j .

To illustrate these points, an example is given.

Example 3.1

A system with 8 states ($n=8$) and 2 inputs/outputs ($m=2$) has the first four Markov parameters M_1, M_2, M_3 and M_4 such that

$$\begin{aligned} \text{rank } M_1 &= 0 \therefore d_1 = 2 \\ \text{rank } M_2 &= 1 \therefore d_2 = 1 \\ \text{rank } M_3 &= 1 \therefore d_3 = 1 \\ \text{and rank } M_4 &= 2 \therefore d_4 = 0 \end{aligned}$$

hence $d_0 = m = 2$, and $v = 4$. From (3.47) it is clear that

$$n_{FZ} = n - (d_0 + d_1 + d_2 + d_3) = 8 - (2+2+1+1) = 2$$

and from (3.48) it is clear that

$$n_{IZ} = (d_0 + d_1 + d_2 + d_3) = (2+2+1+1) = 6$$

hence, there are 6 infinite zeros and 2 finite zeros.

There will be: $1(d_0-d_1)$ first-order infinite zeros, $(2-2) = 0$
 $2(d_1-d_2)$ second-order infinite zeros, $2(2-1) = 2$
 $3(d_2-d_3)$ third-order infinite zeros, $3(1-1) = 0$
 and $4(d_3-d_4)$ fourth-order infinite zeros, $4(1-0) = 4$

Given that the first non-zero eigenvalue of M_2 is greater than zero and that the second non zero eigenvalue of M_4 is less than zero. Then by application of (3.49)

For $j = 1$, $(d_0 - d_1) = 0$, therefore no asymptotes

For $j = 2$, $(d_1 - d_2) = 1$, therefore one second-order asymptote set

Hence, for $j = 2$.

$$\alpha_{1,0}^{(2)} = 1/2 [\pi + 2(0)\pi] = \pi/2$$

and

$$\alpha_{1,1}^{(2)} = 1/2 [\pi + 2(1)\pi] = 3\pi/2$$

For $j = 3$, $(d_2 - d_3) = 0$, therefore no asymptotes

For $j = 4$, $(d_4 - d_3) = 1$, therefore one fourth-order asymptote set

Hence, for $j=4$,

$$\alpha_{1,0}^{(4)} = 1/4 [0 + 2(0)\pi] = 0$$

$$\alpha_{1,1}^{(4)} = 1/4 [0 + 2(1)\pi] = \pi/2$$

$$\alpha_{1,2}^{(4)} = 1/4 [0 + 2(2)\pi] = \pi$$

and

$$\alpha_{1,3}^{(4)} = 1/4 [0 + 2(3)\pi] = 3\pi/2$$

This is illustrated in Figure (3.3). The two asymptote sets are shown separately, and the positions of the pivot-points (where the asymptotes cut the real axis) are not given precisely as they have not been calculated (End of Example 3.1).

It can be shown that it is not necessary to calculate the asymptote angles for each asymptote individually, and for each case, as there is a general pattern. In fact there are two distinct patterns; pattern A for $\lambda_i(j) > 0$ and pattern B for $\lambda_i(j) < 0$. These patterns are shown on Figures (3.4) and (3.5) respectively. It is significant

that correct application of the high-gain method always results in asymptotes which correspond to pattern A. Asymptotes conforming to pattern A never have an asymptote along the positive real axis and consequently they result in a more "stabilizing" asymptote set than those conforming to pattern B which always have an asymptote along the positive real axis.

The last aspect of multivariable root-locus asymptote theory to be reviewed is the pivot-point calculation. The simplest form is that presented by Owens [Owens^a] as one part of a systematic technique to calculate the asymptotic pivot-points and directions of square invertible systems (which is the case for systems resulting from the correct application of the high-gain method). A complete description of Owens' systematic technique is not included here as it is easily obtained from the reference. However, a description of how the technique is implemented as a Pro-Matlab function (see section 4.5 for a description of this matrix calculator package) is described below in a form suitable for systems which result from the application of the high-gain method.

Step 1 A matrix $M^{(1)}$ is formed such that

$$M^{(1)} = [M_{\mu}, M_{\mu+1}, \dots, M_{\nu+1}] \quad \dots \quad (3.50)$$

where M_j ($j = \mu, \mu+1, \dots, \nu+1$) are Markov parameters as defined previously, M_{μ} is the first Markov parameter for which $\text{rank } M_{\mu} = r_{\mu} \neq 0$ and M_{ν} is the first Markov parameter which is full rank (note r_j ($j = \mu, \mu+1, \dots, \nu+1$) is the rank of each Markov parameter in $M^{(1)}$).

Step 2 The non-singular eigenvector matrix T_μ of M_μ is calculated and a unimodular transformation is performed on $M^{(1)}$ to form $\bar{M}^{(1)}$ such that

$$\bar{M}^{(1)} = [T_\mu^{-1} M_\mu T_\mu, T_\mu^{-1} M_{\mu+1} T_\mu, \dots, T_\mu^{-1} M_{\nu+1} T_\mu] = [\bar{M}_\mu, \bar{M}_{\mu+1}, \dots, \bar{M}_{\nu+1}] \quad \dots \quad (3.51)$$

and

$$\bar{M}_\mu = \begin{bmatrix} \Lambda_\mu & 0 \\ 0 & 0 \end{bmatrix} \quad \dots \quad (3.52)$$

where Λ_μ is a diagonal matrix of size $(r_\mu \times r_\mu)$ which contains the r_μ non-zero eigen values of M_μ .

Step 3: The \bar{M}_k ($k = \mu+1, \mu+2, \dots, \nu+1$) are reduced to the form

$$\tilde{M} = \begin{bmatrix} R_k & 0 \\ 0 & S_k \end{bmatrix} \quad (k=\mu+1, \mu+2, \dots, \nu+1) \quad \dots \quad (3.53)$$

where R_k is a diagonal matrix of size $(r_\mu \times r_\mu)$, and S_k is a matrix of size $(d_\mu \times d_\mu)$, by using elementary row and column operations using the rows and columns of \bar{M}_μ , taking care that the diagonal elements of R_k remain unchanged during the operations.

Step 4 The i th pivot-point of the μ th order asymptote set may be calculated from

$$P_i^{(m)} = \frac{(\Lambda_\mu(i, i) / R_{\mu+1}(i, i))}{\mu} \quad (i = 1, 2, \dots, r_\mu) \quad \dots \quad (3.54)$$

Here, there are r_μ sets of μ th order asymptotes and hence r_μ pivot-points to be calculated.

Step 5 If $d_\mu \neq 0$ then create a new matrix $M^{(2)}$ similar to the matrix $M^{(1)}$ in step 1, but using again the matrices S_k ($k = \mu+1, \mu+2, \dots, \nu+1$), again omitting any S_k where $\text{rank } S_k = 0$ until $\text{rank } S_k \neq 0$ such that

$$M^{(2)} = [S_\phi, S_{\phi+1}, \dots, S_{\nu+1}] \quad \dots \quad (3.55)$$

where $\text{rank } S_\phi \neq 0$ and $\text{rank } S_\nu = (m-r_\mu) = d_\mu$.

Having created this matrix $M^{(2)}$ (similar to $M^{(1)}$ in step 1) the steps 2 to 5 may be repeated, and so on until all asymptote pivots are found.

The above steps have been implemented in software using the package Pro-Matlab and so the multivariable asymptote pivot-points can easily be found. However, it should be noted that the unimodular transformation of step 2 does not always result in the block diagonal form \bar{M}_μ shown in equation (3.52). Indeed, the diagonal elements of Λ_μ may appear anywhere along the diagonal of \bar{M}_μ in practice. This does not affect the validity of the method which performs row and column operations on \bar{M}_k ($k = \mu+1, \mu+2, \dots, \nu+1$) to produce \tilde{M}_k ($k = \mu+1, \mu+2, \dots, \nu+1$) with the block diagonal form of \bar{M}_μ (as given by (3.53)). It simply means that the same type of row and column operations are performed, but that the resulting block structure of the matrices \bar{M}_μ and \tilde{M}_k ($k = \mu+1, \mu+2, \dots, \nu+1$) is more complicated. The pivot-point calculation and a more complex block structure for \bar{M}_μ and \tilde{M}_k ($k = \mu-1, \mu+2, \dots, \nu+1$) is demonstrated in the following example.

Example 3.2

In this example a high-gain controller is coupled with a linear V/STOL aircraft model (which includes actuator parasitic dynamics) and the multivariable root-locus asymptotes are investigated for the resulting system. The derivation of the controller is not described because a full worked example appears in chapter 5. Neither is the aircraft model described as it is merely used to provide a basis for the example. Full details of the calculations appear in Appendix B, and consequently only the main points are described here. The system is depicted by Figure (3.6).

A basic plant with four states ($n=4$) and three inputs/outputs ($m=3$) is used for this example and is described by equations (B1) and (B2). The basic plant has actuator parasitic dynamics added where actuator 1 is assumed to have negligible dynamics, actuator 2 is represented by a first-order lag and actuator 3 is represented by third-order dynamics and has a zero in addition to the three poles, two of which are a complex conjugate pair. The poles and zeros for these actuators are given in Appendix B and the equivalent state and output equations are given by (B3), (B4), (B5), (B6), (B7) and (B8). The actuators are connected in series with the basic plant such that input 1 is fed through actuator 1, and so on for the other two inputs, resulting in the composite system given by (B9), (B10) and B(11). A high-gain controller was added to this (as described earlier and by Figure (3.2)) which resulted in the composite open-loop system described by (B12), (B13) and (B14). The Markov parameters of the high-gain open-loop system are given in Table (B1), along with the rank and rank defect of each parameter. The 5 finite and 6 infinite zeros are:

3 finite zero due to integrators

1 finite zero due to the third-order actuator

1 finite zero due to the transmission zero of the basic plant

1 first-order infinite-zero

2 second-order infinite zeros

and 3 third-order infinite zeros.

As was described earlier, the asymptotic patterns produced by correct application of the high-gain method always result in asymptotes of pattern A, given by Figure (3.4). Consequently the first-order, second-order and third-order asymptotes produced by this example correspond to those given in Figure (3.4).

The pivot-point calculation begins at step 1 in Appendix B and follows the 5 steps which were described previously. It is clear from (B17) and (B18) that the block structure of (3.52) is not produced by the unimodular transformation, but it is also apparent how the calculation proceeds whilst keeping the block structure of (B17). The correct form of $M1bar$ (equivalent \bar{M}_1) is given by (B24), and (B26) shows how $M2$ (equivalent M_2) may be extracted from $M1bar$ after the first pivot-point is found. The steps are followed until each of the three pivot-points are found and the results are given in Table (B2).

To perform a check on this calculation, the closed-loop system representing the example was derived and its root-locus was generated. The asymptotes are shown by Figure (3.7a) and the fine detail of the root-locus near to the origin is shown by Figure (3.7b). It is possible to calculate the pivot points using Figure (3.7a) or by calculating the roots for a very high gain (so that the roots are very close to the asymptotes and then exploiting the simple geometry of the asymptotes given by Figure (3.4). In this way the

asymptote pivot-points were calculated using the closed-loop system and are given in Table 3.2 (below) for comparison with the results given in Table B2.

Table 3.2

Asymptote Order	Pivot-point (from closed-loop root-locus)	Pivot-point (from Appendix B)
1st	-	0.085557
2nd	-2.038	-2.0380
3rd	-5.507	-5.5072

It should be noted that using the closed-loop system it is not possible to calculate the pivot-point for the first-order asymptote due to the amount of "activity " at low gain on the real-axis. However, knowledge of the first-order pivot-point is of no real use or interest to the designer when the first-order asymptotes follow pattern A (of Figure (3.4)) which is always the case when the high-gain method is correctly applied.

This example has shown how multivariable root-locus asymptotes may be calculated using a step-by-step method which has been given in subsection 3.4.2. Furthermore, the results have been shown to be correct by comparing them with the pivot-points of the root-locus diagram (Figure (3.7)) of the closed-loop system.

(End of example 3.2).

This subsection has reviewed the relevant results from multivariable root-locus theory and has illustrated them with two worked examples. Appropriate software is used to simplify the calculation of the

asymptote characteristics. However, these methods do not give as much insight into the dynamics of the control problem as the simple SISO rules which calculate asymptote characteristics. A multivariable equivalent to the simple SISO rules is presented in the next subsection.

3.4.3 Description of the "New Developments"

Before describing these "new developments" it is relevant to review briefly the results of classical SISO root locus theory. Given an open-loop transfer function $F(s)$ such that

$$F(s) = K \frac{(s+z_1)(s+z_2)\dots(s+z_{nz})}{(s+p_1)(s+p_2)\dots(s+p_{np})}, \quad \dots \quad (3.56)$$

where nz is the number of zeros and np is the number of poles, then the closed-loop transfer function is given by $H(s)$ where

$$H(s) = \frac{F(s)}{1+F(s)} \quad \dots \quad (3.57)$$

and the characteristic equation is $1+F(s)$. For $K \geq 0$, SISO root-locus theory defines the asymptote angles (with respect to the real-axis) as

$$\phi_a = \left(\frac{2i+1}{np-nz} \right) \pi, \quad (i = 0, 1, \dots, (np-nz-1)) \quad \dots \quad (3.58)$$

and the asymptote pivot-point as

$$P_a = \frac{\sum_{j=1}^{np} P_j - \sum_{k=1}^{nz} Z_k}{(np-nz)}, \quad \dots \quad (3.59)$$

where P_j ($j = 1, 2, \dots, np$) and Z_k ($k = 1, 2, \dots, nz$) are given by (3.56). The order of the asymptotes is clearly $(np-nz)$. A full discussion of SISO root-locus theory may be found in any good control

engineering undergraduate text book such as Richards [Richards,]. These results are simple to use and they clearly show the designer the effects of increasing the number of poles or zeros in the system and also the effects of moving poles or zeros to the left or to the right. It is also clear that adding phase advance compensation moves the asymptote pivot-point P_a to the left so that the asymptotes are "deeper" in the stable region, increasing the stability margin. The results described in the previous subsection do not give this insight.

It was mentioned in subsection 3.2.2. (and in 3.2.1 briefly) that the multivariable system decomposes into m SISO decoupled systems as the gain increases (where m is the number of inputs/outputs). This is true whether there are no parasitic dynamics or high-order parasitic dynamics. However the issue is clouded in the frequency and time responses when the parasitics are of order two or more, because the asymptotes will become unstable at high gain, possibly before the multivariable system is fully decomposed into the m SISO systems. Despite this fact, it is still possible to view this decomposition using the root-locus diagram which displays m asymptote sets and resembles m SISO root-loci overlaid to form a composite diagram. This simplification is caused by the selection of the controller matrix defined by the high-gain method.

If the parasitic dynamics are removed, then many multivariable plants (including aircraft) may be described by coupled first-order and second-order dynamic equations. Correct application of the high-gain method will decouple this basic system and will asymptotically result in m SISO root-locus diagrams formed from the following poles and zeros:

(i) first-order: One plant pole, one integrator pole (at 0.0 in the open-loop) and one of the integrator zeros at $-\rho_i$ ($i = 1, 2, \dots, m$) (where ρ_i ($i=1, 2, \dots, m$) is given by equation (3.30)).

(ii) second-order: Two plant poles, one plant transmission zero (assigned by the use of extra measurement feedback), one integrator pole and one integrator zero as described in (i) above.

N.B. It should be noted that the addition of integrators effectively increases the order of each set of dynamics by 1. They are still referred to as first-order and second-order for simplicity.

Clearly, for the first-order case (i), $n_p = 2$, $n_z = 1$ and the asymptote is first-order (order = $2-1$). Similarly, for the second-order case (ii), $n_p = 3$, $n_z = 2$ and the asymptote is again first-order (order= $3-2$). Each first-order asymptote is aligned with the negative real-axis and so increasingly fast dynamics are exhibited (as shown previously by equation (3.33)). Furthermore, each SISO root-locus "layer" represents a control-mode such as pitch attitude control (a pitch control-mode) or forward velocity control (a horizontal control-mode). Consequently, adding parasitic dynamics simply adds poles and/or zeros to the original poles and zeros, representing each control-mode, given by either (i) or (ii) above. The parasitic dynamics most closely related to a particular control-mode combine with the dynamics of that control-mode. This implies that the engine parasitic dynamics would most likely

influence the vertical control-mode for a V/STOL aircraft in the hover, which is the case in practice. However, the association of parasitic dynamics with a particular control-mode depends upon the following:

(i) The values of the proportional action tuning parameters

$$\sigma_i \quad (i = 1, 2, \dots, m) \quad (\text{see equation 3.29}).$$

(ii) The pole and zero positions of the parasitic dynamics.

(iii) The flight conditions (i.e. changing the thrust vector from vertical to horizontal swaps the engine dynamic effects from the vertical control-mode to the horizontal control-mode for V/STOL aircraft).

This complex association means that the designer can alter the natural associations between parasitic dynamics and control-modes. This is achieved by tuning (see (i) above) or altering the parasitic dynamics (see (ii) above) (the associations automatically change as the flight case changes). Once the association of particular parasitic dynamics to a particular control-mode is established, then the following simplification may be made. The asymptote angles (with respect to the real-axis) are given by

$$\phi_{j_i} = \frac{(2j+1)\pi}{(np_i - nz_i)} \quad \begin{array}{l} (i = 1, 2, \dots, m) \\ (j = 0, 1, \dots, (np_i - nz_i - 1)) \end{array} \quad \dots (3.60)$$

the asymptote pivot-point is given by

$$PP_i = \frac{\sum_{k=1}^{np_i} P_{i_k} - \sum_{\ell=1}^{nz_i} z_{i_\ell}}{(np_i - nz_i)} \quad (i = 1, 2, \dots, m) \quad \dots (3.61)$$

and the asymptote order is given by

$$\text{Asymptote order} = (np_i - nz_i) \quad (i = 1, 2, \dots, m) \quad \dots \quad (3.62)$$

where the terms are as follows:

ϕ_{j_i} is the angle of the j th asymptote of the i th asymptote set

np_i is the number of poles associated with the i th control-mode

nz_i is the number of zeros associated with the i th control-mode

PP_i is the i th pivot-point

P_{i_k} is the k th pole of the i th control-mode

z_{i_l} is the l th zero of the i th control-mode

i denotes the control modes ($i = 1, 2, \dots, m$)

j denotes each asymptote of the i th asymptote set
($j = 0, 1, \dots, (np_i - nz_i - 1)$)

In practice (3.60) is not required because once the asymptote order is found from (3.62) then the angles correspond to asymptotes of pattern A in Figure (3.4).

The pivot point equation (3.61) may be separated into two parts representing the contributions of the parasitic dynamics and the basic system dynamics respectively, given by

$$PP_i = \frac{\overbrace{\sum_{k=1}^{(np_i - npp_i)} Pa_{i_k} - \sum_{l=1}^{(nz_i - nzp_i)} Za_{i_l}}^{\text{parasitic dynamics}} + \overbrace{(Pb_{i_1} + Pb_{i_2} + Pb_{i_3}) - (Zb_{i_1} + Zb_{i_2})}^{\text{basic system dynamics}}}{(np - nz)}$$

for ($i = 1, 2, \dots, m$) ... (3.63)

- PP_i , np_i & nz_i - are as before (3.61).
- Pa_{i_k} is the k th parasitic pole of the i th control mode
- Za_{i_k} - is the k th parasitic zero of the i th control mode
- Pb_{i_1} , Pb_{i_2} - represent the effects of the poles from first order or second order plant dynamics associated with the i th control-mode. If this control-mode is associated with first-order plant dynamics than Pb_{i_2} does not exist and $npp_i=2$
- Zb_{i_1} - is a transmission zero from second-order plant dynamics associated with the i th control-mode. If this i th control mode is associated with first order plant dynamics then Zb_{i_1} , does not exist and $nzp_i = 1$
- Pb_{i_3} - is the pole caused by the integrator which is associated with the i th control-mode ($Pb_{i_3} = 0.0$ in all cases and may be dropped from (3.63).
- Zb_{i_2} - is the transmission zero caused by the integrator associated with the i th control-mode ($Zb_i = -\rho_q$, where ρ_q is the integral action tuning parameter (see equation (3.30)) which affects the i th control-mode).
- npp_i - is the number of poles that are associated with the i th control-mode, excluding the parasitic poles. Hence, $npp_i = 3$ unless Pb_{i_2} does not exist, in which case $npp_i = 2$.
- nzp_i - is the number of zeros that are associated with the i th control-mode, excluding the parasitic zeros. Hence, $nzp_i = 2$ unless zb_i does not exist in which case $nzp_i=1$.

The expression (3.63) may be simplified further when the plant pole effects represented by Pb_{i1} and Pb_{i2} are negligible and so do not significantly change the result of (3.63) to give

$$\overline{PP}_i = \frac{(\sum_{k=1}^{np_i-npp_i} Pa_{ik} - \sum_{\ell=1}^{nz_i-nzp_i} Za_{i\ell}) - (Zb_{i1} + Zb_{i2})}{(np_i - nz_i)}, \quad (i = 1, 2, \dots, m)$$

... (3.64)

where \overline{PP}_i is an estimate of PP_i and the other terms have already been defined. This expression is very similar to (3.59) for SISO theory, with the slight complication that it has to be used m times for each i (where $i = 1, 2, \dots, m$) to calculate the m pivots of the m asymptote sets for the multivariable case.

Clearly, (3.60) and (3.61) are very similar to (3.58) and (3.59) respectively. Also, the expanded and simplified version of (3.61) (i.e. (3.64)) is very similar to (3.59). This similarity means that the insight gained by using SISO root-locus rules for SISO systems may now also be gained by using (3.64) for multivariable high-gain systems. Furthermore, the equation (3.64) is the same as the equations derived by Burge for second-order and third-order root-locus asymptotes as given by (3.44) and (3.45). The following table (Table (3.3)) compares like terms from each of the equations (3.64), (3.44) and (3.45).

Table 3.3

Table of Equivalent Terms	
Equation (3.44) (first order parasitic)	Equations (3.64)
α_i	1 $\sum_{k=1} Pa_{i_k}$
ρ_i	$-Zb_{i_2}$
γ_i	$-Zb_{i_1}$
2	$(np_i - nz_i)$
Equation (3.45)	Equation (3.64)
(second-order parasitic)	
$-2c_i\omega_i$ *	2 $\sum_{k=1} Pa_{i_k}$
ρ_i	$-zb_{i_2}$
γ_i	$-zb_{i_1}$
3	$(np_i - nz_i)$

* NB a second-order equation with poles P_1 and P_2 has the form $(s-P_1)(s-P_2) \equiv s^2 - (P_1+P_2)S + P_1P_2$. Alternatively, it may be written as $(s^2+2c\omega s+\omega^2)$ which shows that $-2c\omega \equiv (P_1+P_2)$.

The terms for (3.44) and (3.45) are defined where the equations appear. Furthermore, in each of the above cases there are no parasitic zeros and so

$$(nz_i - nzp_i) \sum_{l=1}^{\ell} za_{i_l} = 0, \quad (i = 1, 2, \dots, m).$$

Expression (3.64) is derived from (3.63) under the condition that the plant pole effects represented by Pb_{i_1} and Pb_{i_2} do not significantly affect the value of PP_i . This condition is not as strict as Burge's condition of modal separation between plant and parasitic dynamics as will be shown.

The contribution of the plant poles to the expression for PP_i (3.63) is not straight forward due to the multivariable nature of the plant. However, the contribution of the plant poles represented by Pb_{i_1} and Pb_{i_2} may be written as $\bar{P}b_i$. This makes it possible to write the percentage error that results from using the estimate (3.64), rather than the full expression (3.63), as follows

$$e_i = \left[\frac{\bar{P}b_i}{PP_i (np_i - nz_i)} \right] * 100\% \quad (i = 1, 2, \dots, m), \quad \dots (3.65)$$

where e_i is the percentage error associated with the i th control mode. Clearly the error will be small whenever $(\bar{P}b_i \ll \bar{P}P_i * (np_i - nz_i))$ which occurs when there is good modal separation between plant dynamics and parasitic dynamics as defined by Burge. Furthermore, the error will also be small whenever the nett effect of the parasitic dynamics (given by (3.63)) is larger than the plant dynamic effects. This can occur for relatively slow high order actuators that are not well separated from the plant, as is the case for this V/STOL example.

In order to define the "new developments" precisely, the notation is somewhat complex, but the following worked example demonstrates the simplicity of the new results.

Example 3.3

In this example the results of subsection 3.4.3 are used in conjunction with the system described and used in example 3.2. The basic 4th-order plant has extra measurement augmentation on output y_3 which results in control-mode 3 being second-order and control-modes 1 and 2 being first-order until the actuator parasitic dynamics are added. In this example actuator 1 is associated with control-mode 2, actuator 2 is associated with control-mode 1 and actuator 3 is associated with control-mode 3 (this may be found by analysing the root-locus diagram). Each control-mode, and hence each asymptote set, is analysed in turn below.

Control-mode 1

For this control mode $i = 1$, $n_{pp1} = 2$, $n_{zp1} = 1$, $n_{p1} = 3$, $n_{z1}=1, Z_{b1}_1$

does not exist, $Z_{b1}_2 = -1$, $\sum_{k=1}^1 P a_{1k} = -5$ and $\sum_{l=1}^0 z a_{1l} = 0$

Hence, from (3.62)

$$\text{Asymptote order} = (3-1) = 2$$

and from (3.64)

$$PP_1 = \frac{(-5) - (0) - (-1)}{2} = -2$$

Table 3.2 gives the exact answer as -2.038 and so the percentage error in this case is 1.9%.

Control-mode 2

For this control-mode $i=2$, $npp_2=2$, $nzp_2 = 1$, $np_2 = 2$, $nz_2 = 1$. zb_{1_1} does not exist,

$$zb_{1_2} = -1, \sum_{k=1}^0 pa_{2_k} = 0 \text{ and } \sum_{l=1}^0 za_{2_l} = 0.$$

Hence, from (3.62)

$$\text{Asymptote order} = (2-1) = 1$$

and from (3.64)

$$pp_2 = \frac{(0) - (0) - (-1)}{1} = 1$$

Table 3.2 gives the exact answer as 0.086, which is clearly quite different, but this error is because for first-order asymptotes, when there are no parasitic dynamics involved, Pb_{i_1} and Pb_{i_2} are not negligible. Consequently (3.64) should not be used in such a case. This is not a hindrance as first-order asymptote pivot points are of no use to the designer when using the high-gain method.

Control-mode 3:

For this control-mode $i=3$, $npp_3=3$, $nzp_3=2$, $np_3=6$, $nz_3=3$,

$$zb_{3_1} = -1, zb_{3_2} = -1,$$

$$\sum_{k=1}^2 Pa_{3_k} = -22, \text{ and } \sum_{l=1}^2 Za_{3_l} = -4.$$

Hence, from (3.62)

$$\text{Asymptote order} = (6-3) = 3$$

and from (3.64)

$$PP_3 = \frac{-(-22) - (-4) - (-1-1)}{3} = -5.33$$

Table 3.2 gives the exact answer as -5.5072 and so the percentage error is 3.2%.

The asymptote order and pivot-point has been closely estimated for each asymptote set with the exception of the non critical first order pivot point. The calculation was made much simpler than that presented in the previous subsection (and Appendix B), by using (3.64). The root-locus asymptote patterns may be found using the asymptote order calculated from (3.62) and Figure (3.4).

(End of example 3.3).

In this subsection simple expressions that determine the characteristics of multivariable root-locus asymptotes have been derived. Furthermore, equations (3.62) and (3.64) give the designer the same insight into the closed loop system dynamics that SISO root locus rules give (i.e.(3.59). It has also been shown that these simple expressions not only agree with the precise (yet complex) calculation methods of Kouvaritakis (and co workers) and Owens, but that they also agree with the algebraic results derived by Burge.

These new developments enhance the high-gain technique and result in a control law design method which satisfies the criteria described at the beginning of this thesis.

3.5 Assessing Actuator Compatibility

The new developments allow the effects of relatively slow high-order actuators, with or without zeros, to be assessed and incorporated into the design. The only strict condition is that the actuator has a steady state gain of 1.0. It is this condition which defines actuator compatibility.

The controller matrices are defined using the basic system with no actuator dynamics and the same matrices are used when actuators are added though retuning may be necessary. The controller on the basic system issues simultaneous commands to each actuator which drive the system to perform a given manoeuvre with the minimum of cross coupling. The introduction of actuator dynamics will disrupt the "simultaneous" nature of the controller commands by making them out of phase with each other and this will promote cross coupling. The situation is made even worse if there is any gain loss in an actuator as this reduces its effect, increasing cross coupling and reducing system performance still further. Consequently, there is a strict condition that all actuators have a steady state gain of 1.0.

This condition is trivial for most cases as this will be true automatically. The difficulty arises when an actuator model is being used for which there is incomplete information. This situation arises in this project due to the nature of the GVAM87 and the way the engine dynamics are modelled. Fortunately though, the poles and zeros for the engine dynamics are known exactly and this information can be used. The difficulty is explained fully in section 5.3 and it is resolved using these results in subsection 5.5.1.

The need in this case is for a simple test that confirms actuator compatibility when other methods of calculating the steady state gain cannot be used. The basis for the actuator compatibility test here relies upon the simplification of the MIMO system and the SISO root locus gain magnitude criterion.

The simplification of the MIMO system is brought about by the choice of controller matrices as described previously. It allows the control-modes to be analysed individually as evidenced by the new developments described in the previous subsection. Consequently, the SISO gain magnitude condition can be applied to each control-mode in turn to calculate its gain magnitude. The SISO gain magnitude condition is defined below but can also be obtained from any good basic control engineering text book [Van De Vegte, Franklin et al].

A general transfer function may be defined as

$$G(s) = K \frac{(s+z_1)(s+z_2) \dots (s+z_{nz})}{(s+p_1)(s+p_2) \dots (s+p_{np})} \quad \dots (3.66)$$

and a point on the root-locus of this transfer function is S_0 . If lines are drawn from each open-loop pole to the point S_0 on the root locus, then the vector magnitude from the pole at $-P_i$ to the point S_0 may be given by p_{m_i} ($i = 1, 2, \dots, np$). Likewise, the vector magnitude from the zero at $-z_j$ to the point S_0 may be given by z_{m_j} ($j = 1, 2, \dots, nz$). Hence the gain magnitude condition may be defined as

$$K = \frac{p_{m_1} * p_{m_2} * \dots * p_{m_{np}}}{z_{m_1} * z_{m_2} * \dots * z_{m_{nz}}} \quad \dots (3.67)$$

In order to apply this condition to the control-modes that occur in a system incorporating a high gain controller, a point (or several) on the appropriate root locus asymptote can be selected and pm_i ($i = 1, 2, \dots, np$) and zm_j ($j = 1, 2, \dots, nz$) can be calculated for every pole and zero associated with the control mode. In the same way that only certain poles and zeros are used to calculate asymptote pivot points using (3.64), only the poles and zeros of the associated actuator dynamics should be used, plus any basic plant open-loop poles and transmission zeros that are associated with the control mode. The basic plant open loop poles that are also associated with the control mode can be approximated as poles at the origin with negligible errors, especially when S_0 is chosen to be far away from these poles.

The fact that makes the test complete is that the i th control-mode has a gain magnitude (GM_i) that is given by

$$GM_i = g\sigma_i K_i \quad \dots (3.68)$$

where g is the controller's scalar gain, σ_i is the controller's tuning parameter which is associated with the i th control-mode and K_i is the actuator gain. In this instant GM_i is equivalent to K of equation (3.67) and so GM_i may be calculated for any point on the root-locus (S_0). For each Point S_0 , the corresponding values of g and σ_i are known enabling K_i to be calculated. The value of K_i is the "apparent" actuator gain and it may be compared with the actuator gain value that satisfies the unity steady state gain condition.

The relationship between the actuator gain (K_{ai}) and the steady state gain (G_{SS}) may be shown for the general actuator model given by

$$G_{ai}(s) = K_{ai} \frac{(s+z_1)(s+z_2) \dots (s+z_{nz})}{(s+p_1)(s+p_2) \dots (s+p_{np})} \quad \dots (3.69)$$

to be

$$G_{ss} = K_{ai} \frac{z_1 * z_2 * \dots * z_{nz}}{p_1 * p_2 * \dots * p_{np}} \quad \dots (3.70)$$

for $s \rightarrow 0$. Consequently, for the unity steady state gain condition $G_{ss} = 1.0$ and so

$$K_{ai} = \frac{p_1 * p_2 * \dots * p_{np}}{z_1 * z_2 * \dots * z_{nz}} \quad \dots (3.71)$$

Therefore, when the actuator poles and zeros are known exactly the actuator gain (K_{ai}) that satisfies the unity steady state gain condition can be found. This value may be checked against the apparent actuator gain (K_i), which is calculated using (3.67) and (3.68), to verify the actuator compatibility.

If K_i does not equal K_{ai} then the actuator signal must be multiplied by K_i/K_{ai} in order to restore actuator compatibility. This gain correction factor may be introduced in several different ways and Section 5.3 illustrates one simple way that is derived naturally from the problem. Section 5.5.1 uses the results defined in this subsection to assess the compatibility of the engine dynamics and it may be referred to as a worked example.

The main calculation to be performed in this actuator compatibility check is that represented by (3.67). A Pro-Matlab function called GMAG has been written which accepts three vector arguments and returns a vector answer. The first two vectors should contain the

poles and zeros that are associated with the control-mode that is being assessed. The third vector should contain a series of points (or a single point) taken from the root locus at particular gain settings. The vector answer contains the gain magnitudes that correspond to each point in the third input vector. A useful method is to feed in several points from a root locus asymptote at several different gain settings such as $g = 10, 10^2, 10^3, 10^4, 10^5$ etc. The user can then observe the answer converging onto the correct solution as the gain increases. This is due to the approximation errors being reduced as the test points move away from the basic plant open-loop poles.

3.6 Tuning Criteria for the High-Gain Method

Tuning criteria for systems with no actuator dynamics will not be discussed here as that situation is both trivial and unrealistic. Indeed, it is the addition of realistic actuators which made the original high-gain technique unsuitable and for which the high-gain method has been developed. The new developments of the high-gain method make simple SISO tuning criteria applicable to the high-order control-modes which result from adding realistic actuator dynamics. The first step is to define the relationship between the control mode's performance and its dominant roots.

It is well known that the performance of many systems is dominated by a complex conjugate pole pair. The exception to this is when there is a single pole on the real axis that is much closer to the imaginary axis than the pole pair. In this situation the single pole will dominate the performance and this occurrence will be discussed at the end of this section. Assuming that there are no dominant poles on the

real axis it is easy to see that the high-gain method will result in control-modes with a dominant complex conjugate pole pair (control modes associated with first order asymptotes excepted). This is because the correct application of the high-gain method always results in asymptotes conforming to pattern A (Figure (5.4)) and each control-mode will be associated with an asymptote set.

The second step is to link performance measures to a complex conjugate pole pair. It is appropriate to consider the frequency response of a lightly damped second order system as given by

$$G(s) = \frac{\omega_n^2}{s^2 + 2\zeta\omega_n s + \omega_n^2} \quad \dots (3.72)$$

where ω_n is the natural frequency and ζ is the damping ratio. A typical frequency response of such a system is shown as Figure (3.8) where the peak magnitude (M_p) the peak frequency (ω_p) and the bandwidth (ω_b) are shown.

N.B. The bandwidth here is defined as the frequency at which the magnitude falls below 0.707 or -3dB.

It may be shown that the three main performance measures (ω_b, ω_p, M_p) are all functions of natural frequency and damping (ω_n, ζ). The relationships are given here as

$$\frac{\omega_p}{\omega_n} = (1 - 2\zeta^2)^{1/2}, \quad (\zeta \leq 0.707) \quad \dots (3.73)$$

$$M_p = (2\zeta(1 - \zeta^2)^{1/2})^{-1}, \quad (\zeta \leq 0.707) \quad \dots (3.74)$$

and

$$\frac{\omega_b}{\omega_n} = [1 - 2\zeta^2 + (2 - 4\zeta^2(1 - \zeta^2))^{1/2}]^{1/2} \quad \dots (3.75)$$

These relationships have been plotted to aid visualisation. Figure (3.9) shows the three performance parameters as functions of the damping ratio, diagram (1) for M_p , diagram (2) for ω_p and diagram (3) for ω_D .

The main tuning criterion that will be applied is a minimum damping level because the three performance measures mentioned above all depend upon the damping ratio. Such a criterion is easy to apply using the high-gain method as the tuning parameter Σ can be used to push each control-mode to its minimum damping limit. Figure (3.10) shows the root locus of a theoretical system with three control-modes of different orders where each has been pushed to the minimum damping line by setting the diagonal elements of Σ . In this figure each control-mode has been tuned to the same minimum damping level but this could of course be varied to suit each control-mode if necessary.

Once a value for the damping ratio of a control-mode has been set, the peak magnitude is defined completely and the bandwidth and peak frequency will be defined by the resulting natural frequency. In this way the designer will be able to see a clear trade-off between good performance (measured in terms of bandwidth) and poor performance (measured in terms of resonance and oscillatory behaviour).

The final link between the root-locus and performance is the relationship between the gain and the root's position on the root-locus. This relationship has already been defined to a certain extent in section 3.5 where the gain magnitude criterion was discussed. Explicit relationships for asymptote sets of every order

will not be derived here but the general relationship is as follows

$$\Delta R \propto (\Delta g)^{1/n} \quad \dots (3.76)$$

where ΔR is the root's displacement along its asymptote, Δg is the feedback gain and n is the excess of poles over zeros for that control mode. For example, this states that, for a control-mode with second-order root locus asymptotes, the two complex conjugate poles' imaginary parts will grow in proportion to \sqrt{g} . This relationship enables the designer to visualise the effects of increasing the feedback gain upon the two dominant asymptotic poles of a control-mode. The position of the dominant pole pair in the complex plane defines the natural frequency and damping and therefore the performance of the control-mode. Thus knowledge of the asymptotic structure of the system enables simple SISO tuning rules to be applied to each control mode.

The condition where there is a complex conjugate pole pair and a single dominant pole on the real axis is now discussed. Such a pole will drastically alter the performance of the control-mode and it will limit the bandwidth too. One beneficial factor is that it will also suppress any resonant effects of the complex conjugate pole pair. The effect that the tuning parameters have on this control-mode should be found as it should be possible to speed up the control-mode using one of the diagonal Σ tuning parameters. This will also make the complex conjugate pole pair more lightly damped but as the complex conjugate pole pair are not dominant in the control-mode it will be possible for the designer to find a satisfactory trade-off. One other possibility is that neither the complex conjugate pole pair nor the single pole on the real axis is dominant. This will produce a mixed response.

Whether or not there is a single dominant pole on the real axis, applying the above criteria will help the designer to set g and Σ . The tuning parameters associated with the extra measurement feedback gains can be set in a similar way to Σ and this is illustrated in chapter 5. The final tuning parameter is Ξ which defines the transmission zeros caused by the integrators and sets the integral action levels. Very little tuning needs to be performed using Ξ and setting each element to be between 0.2 and 0.4 is usually satisfactory. The step response of the closed-loop transfer function matrix should be generated and Ξ should be reduced if the diagonal elements exhibit undesirable overshoot. Conversely, Ξ should be increased if steady state tracking is poor. Typically a value of 0.2 will be chosen using the linear model, but if cross coupling is found to be more severe in the non linear model a higher value may be required.

3.7 The High-Gain Method A. Step-By-Step Procedure

The high gain technique plus the new developments forms the high-gain method. This method may be applied most easily using a step-by-step procedure which allows the designer to increase his knowledge of the control problem as the system becomes increasingly complex. The initial design is performed using the basic plant, stripped of all parasitic dynamics. These parasitic dynamics may be added and their effect on the closed-loop system may be ascertained. Finally, if the system cannot be tuned to give satisfactory performance in the presence of parasitic dynamics then dynamic compensation may be introduced and it is treated by the method in the same way that parasitic dynamics are treated.

Another aspect of the step-by-step method is that although used upon multivariable systems, the resulting closed-loop system may be analysed loop-by-loop. In this way weak parts of the design and problem areas may be isolated more easily. A designer who is aware of the limitations of a design is able to perform the necessary engineering trade-offs effectively.

The step-by-step procedure is described below:

1. Determine the mathematical model for the plant and its systems
(these include the actuator and sensor dynamics).
2. Derive a linearised model from the above (1) at the design point.
3. Extract the basic plant dynamics leaving off parasitic dynamics.

4. Express these dynamics in the form of (3.1).
5. Determine the control objectives and hence generate the appropriate output equation (3.2).
6. Select extra measurements, where appropriate, according to (3.3) and (3.10).
7. Calculate the system zeros and check that the system is stabilizable and detectable. (Note that this condition is not absolute, see 3.2.1).
8. Determine the controller matrices K_p and K_I using (3.29) and (3.30) respectively.
9. Use root loci diagrams, frequency-responses and time-responses as necessary, to find a suitable value for g with $\Sigma = \Xi = I_m$.
10. Repeat 9 altering Σ and Ξ to gauge their effect and to tune them, as described in section 3.6. Perform the same tests with the extra measurement gains.
11. Include the parasitic dynamics in easy stages and use (3.62) in conjunction with Figure (3.4) to predict the asymptotic structure. Use results from section 3.5 to assess the actuator compatibility. Use root loci to determine the association of parasitic dynamics to control-modes and then check the pivot points using (3.64). Once these relationships are discovered the insight given by (3.62) and (3.64) becomes relevant and so does the tuning criteria of section 3.6. Steps

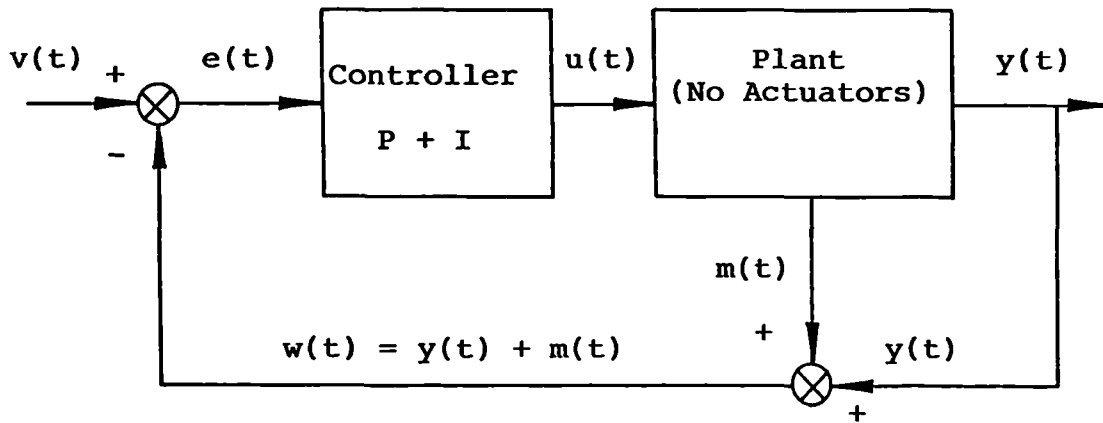
(9) and (10) should be repeated at each stage and g , Σ , Ξ and the extra measurement gains retuned as necessary.

12. If closed-loop performance is not satisfactory after retuning, then dynamic compensation may be included. This is designed in a loop by-loop fashion and is analysed in the same way that the effects of parasitic dynamics are analysed. Indeed, (3.62) and (3.64) give insight into the use of dynamic compensation. (9) and (10) should be repeated in conjunction with tuning the dynamic compensation.

13. Simulate with the full mathematical model and retune if necessary. Special attention should be paid to the effect of non-linearities such as rate limits and absolute limits on actuator dynamics. At this stage extra features may be needed to enable the linear controller to function in a non-linear environment. This could include command-rate limiting, integrator wind-up protection, weight-on-wheels conditions and similar features.

This step by step procedure is used to design a set point controller for each flight case and for each control strategy. Hence, a task tailored controller for a wide flight-envelope can involve considerable effort. This may be alleviated using optimisation techniques once the designer understands the control problem. However, it should be realised that no manual or automatically tuned designs may be produced unless suitable design aims are first defined in terms that are compatible with the design method. This is described in chapter 6 where a design brief is defined.

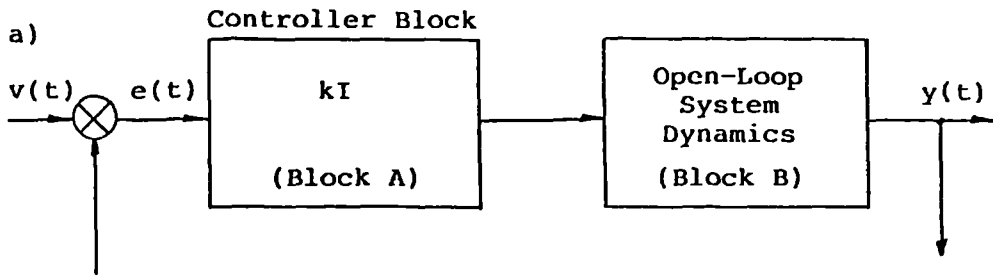
Subsequently, these set point controllers are combined into a gain scheduling controller which operates over a wide flight envelope, including the transition region. Before this though, it is appropriate to describe the V/STOL aircraft model which is the basis for this design study.



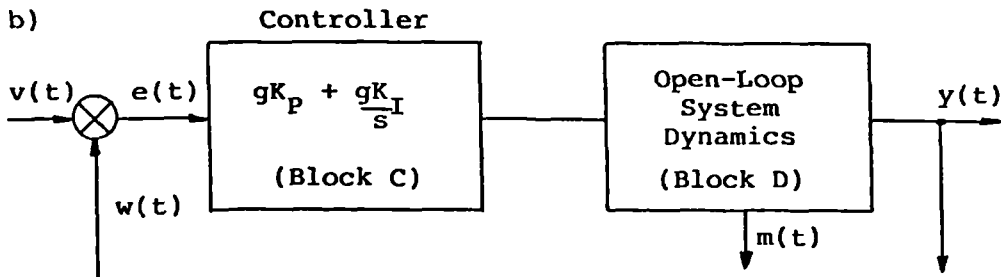
Key:

- $v(t)$ - Command input vector
- $e(t)$ - Error vector
- $u(t)$ - Control signal vector
- $y(t)$ - Output vector
- $m(t)$ - Extra measurement vector
- $w(t)$ - Feedback vector

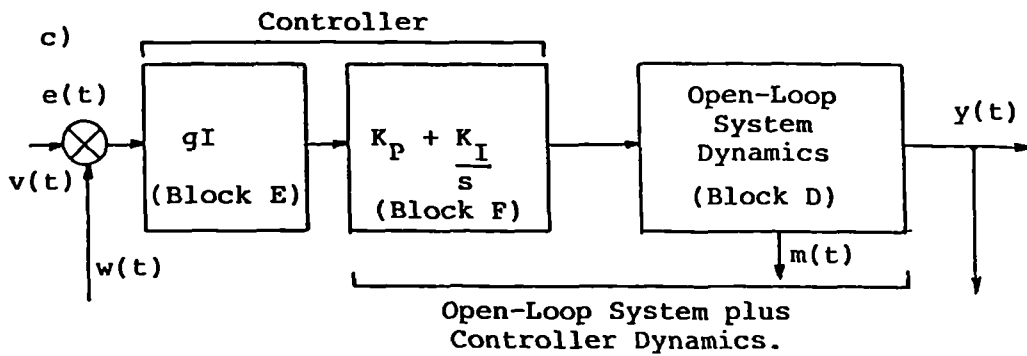
Figure (3.1) Block Diagram of Controller Plus Plant



Block Diagram of the Feedback System
for Original Root-Locus Studies.



Block Diagram of the Feedback System for the
High-Gain Method Root-Locus Studies.



Block Diagram of the Equivalent Feedback System for
High-Gain Method Root-Locus Studies.

Key:

- $v(t)$ - Command input vector
- $y(t)$ - Output vector
- $m(t)$ - Extra measurement vector
- $w(t)$ - Feedback vector
- $e(t)$ - Error vector
- I - Identity matrix
- k - Scalar gain
- g - Scalar gain
- K_p - Proportional gain matrix
- K_I - Integral gain matrix
- s - Laplace operator

Figure (3.2)

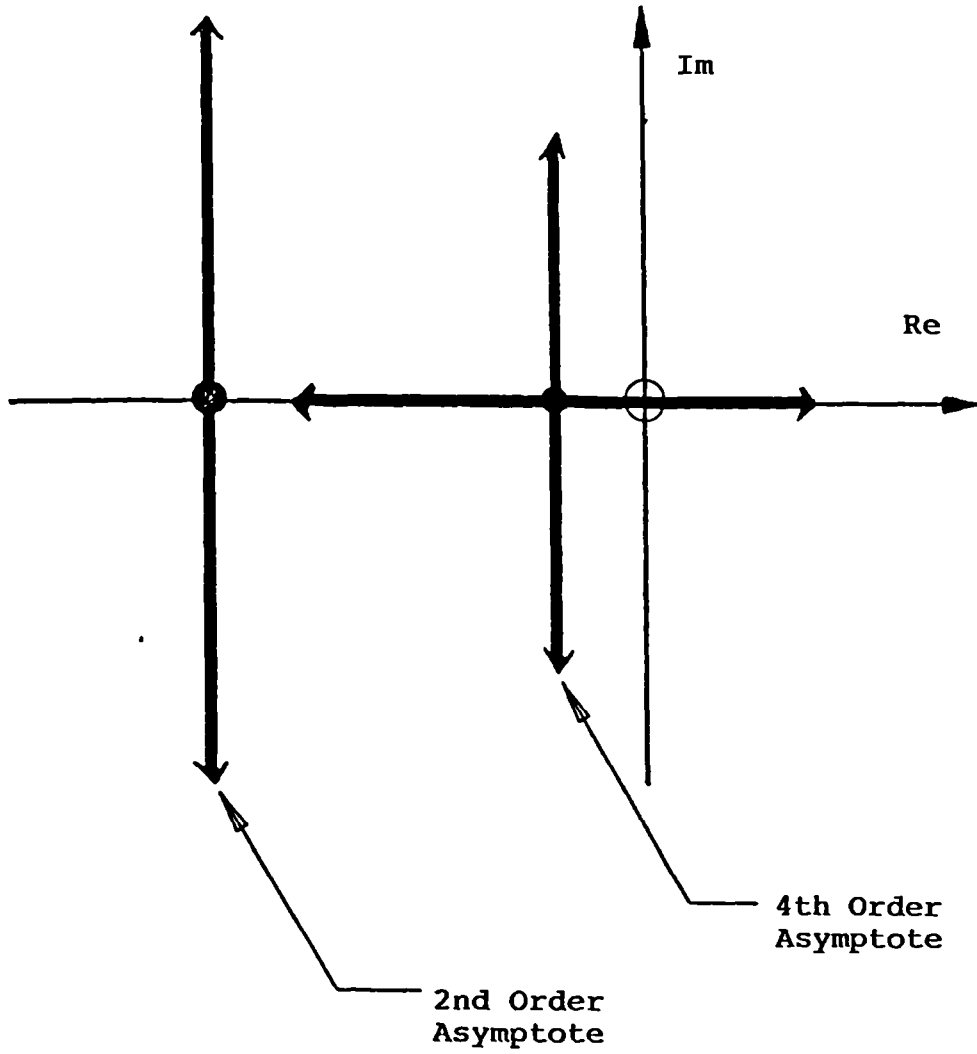
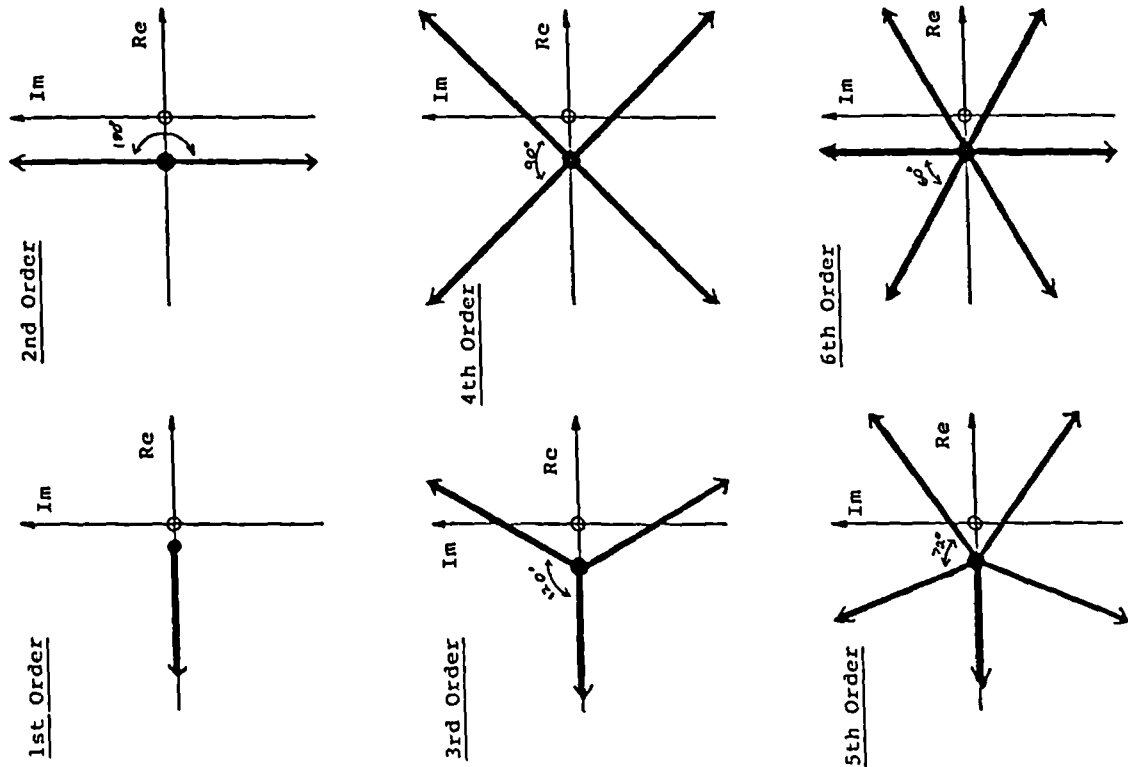


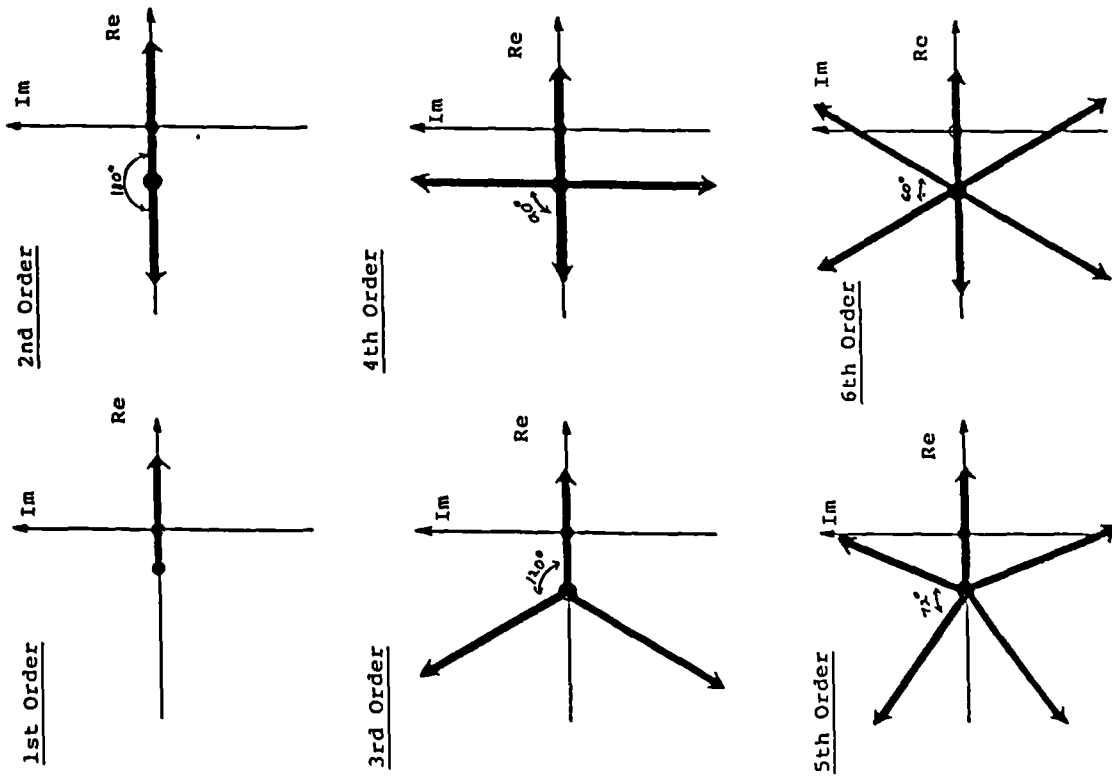
Figure (3.3) Asymptotic Structure for Example (3.1)

Figure (3.4) Pattern A Asymptotes for Root-Loci



1st order	2nd order
$\alpha_{1,0}^{(1)} = \pi$	$\alpha_{1,0}^{(2)} = \pi/2$; $\alpha_{1,1}^{(2)} = 3\pi/2$
3rd order	
$\alpha_{1,0}^{(3)} = \pi/3$; $\alpha_{1,1}^{(3)} = \pi$; $\alpha_{1,2}^{(3)} = 5\pi/3$	
4th order	
$\alpha_{1,0}^{(4)} = \pi/4$; $\alpha_{1,1}^{(4)} = 3\pi/4$; $\alpha_{1,2}^{(4)} = 5\pi/4$	
$\alpha_{1,3}^{(4)} = 7\pi/4$	
5th order	
$\alpha_{1,0}^{(5)} = \pi/5$; $\alpha_{1,1}^{(5)} = 3\pi/5$; $\alpha_{1,2}^{(5)} = \pi$	
$\alpha_{1,3}^{(5)} = 7\pi/5$; $\alpha_{1,4}^{(5)} = 9\pi/5$	
6th order	
$\alpha_{1,0}^{(6)} = \pi/6$; $\alpha_{1,1}^{(6)} = \pi/2$; $\alpha_{1,2}^{(6)} = 5\pi/6$	
$\alpha_{1,3}^{(6)} = 7\pi/2$; $\alpha_{1,4}^{(6)} = 3\pi/2$; $\alpha_{1,5}^{(6)} = 11\pi/6$	

Figure (3.5) Pattern B Asymptotes for Root-Loci



1st order	2nd order
$\alpha_{1,0}^{(1)} = 0$	$\alpha_{1,0}^{(2)} = 0$, $\alpha_{1,1}^{(2)} = \pi$
3rd order	
$\alpha_{1,0}^{(3)} = 0$, $\alpha_{1,1}^{(3)} = 2\pi/3$, $\alpha_{1,2}^{(3)} = 4\pi/3$	
4th order	
$\alpha_{1,0}^{(4)} = 0$, $\alpha_{1,1}^{(4)} = \pi/2$, $\alpha_{1,2}^{(4)} = \pi$	
$\alpha_{1,3}^{(4)} = 3\pi/2$	
5th order	
$\alpha_{1,0}^{(5)} = 0$, $\alpha_{1,1}^{(5)} = 2\pi/5$, $\alpha_{1,2}^{(5)} = 4\pi/5$	
$\alpha_{1,3}^{(5)} = 6\pi/5$, $\alpha_{1,4}^{(5)} = 8\pi/5$	
6th order	
$\alpha_{1,0}^{(6)} = 0$, $\alpha_{1,1}^{(6)} = \pi/3$, $\alpha_{1,2}^{(6)} = 2\pi/3$	
$\alpha_{1,3}^{(6)} = \pi$, $\alpha_{1,4}^{(6)} = 4\pi/3$, $\alpha_{1,5}^{(6)} = 5\pi/3$	

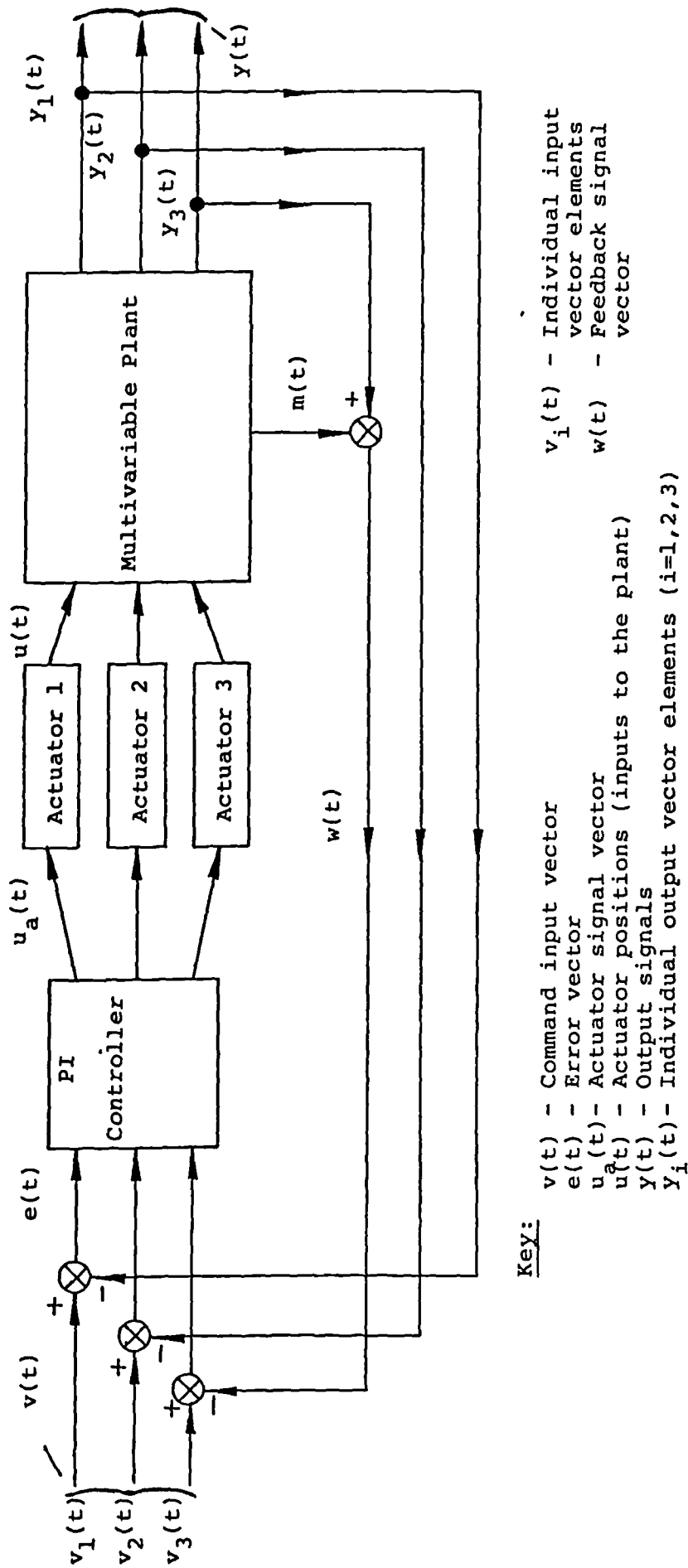


Figure (3.6) Block Diagram of the Control System for Example 3.2

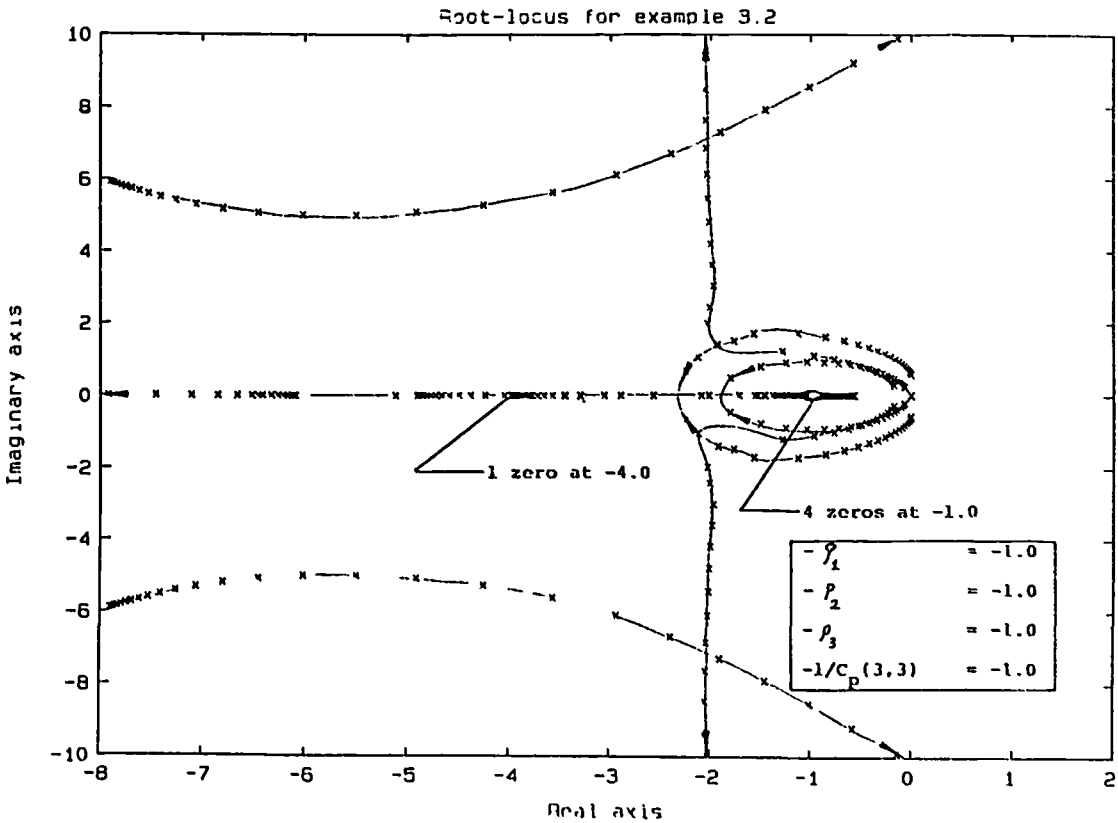
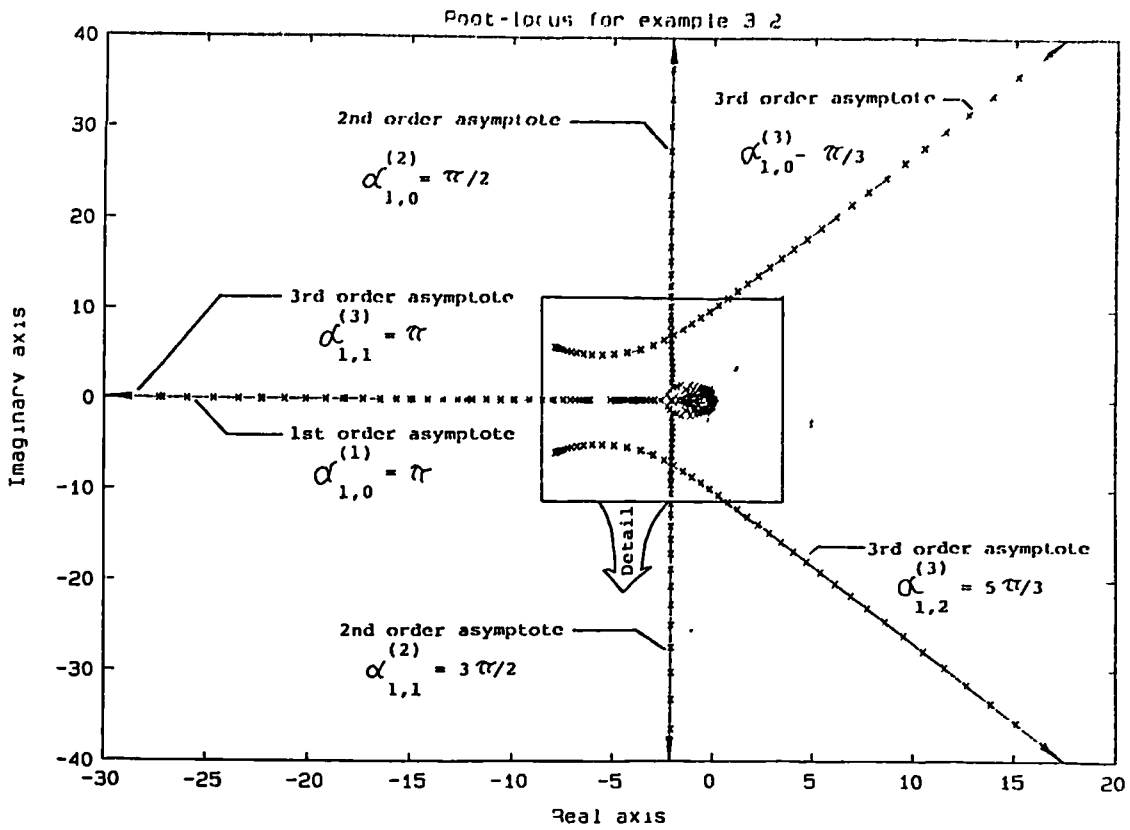


Figure (3.7) Asymptotic Structure for Example 3.2

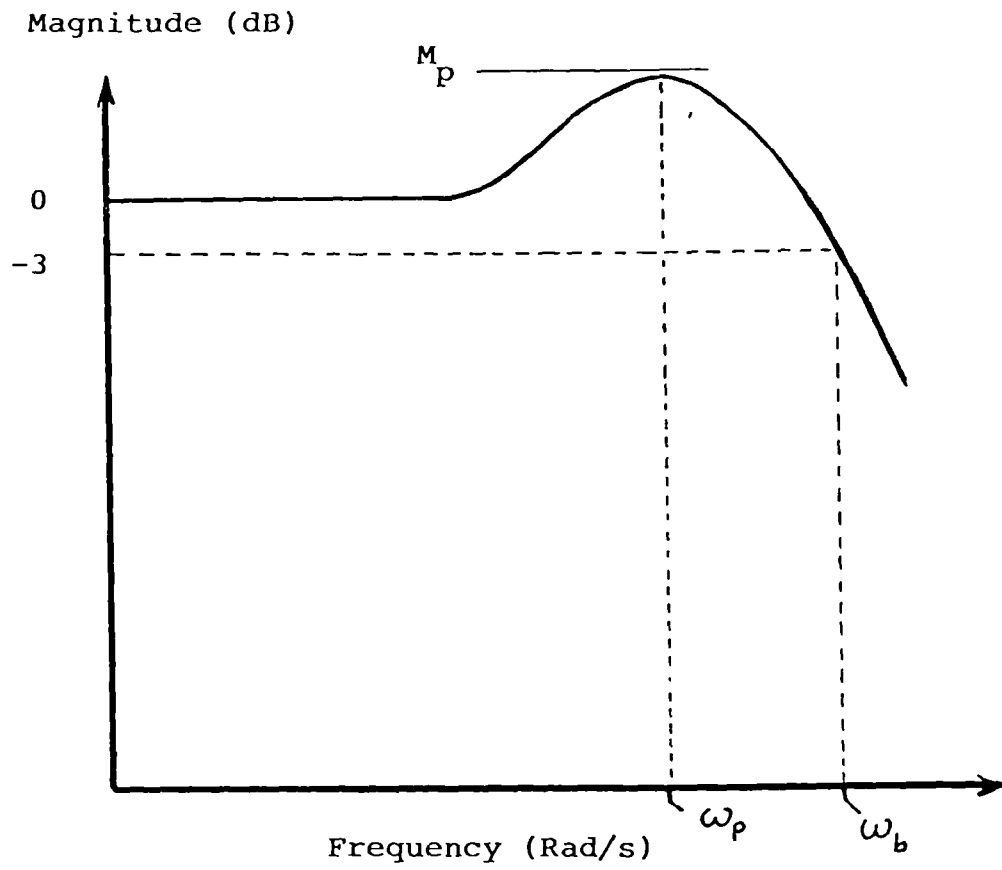
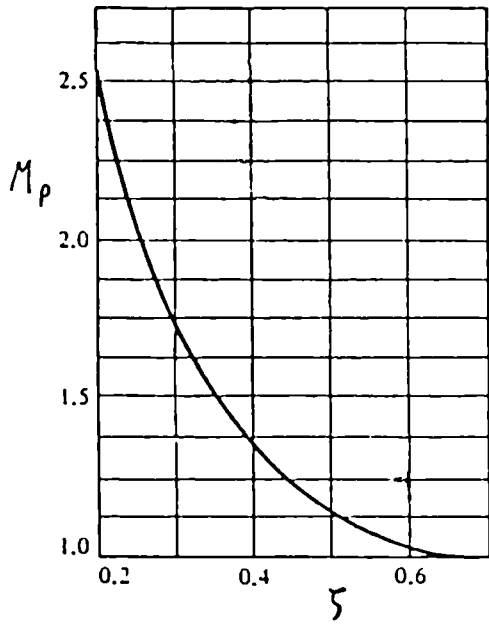


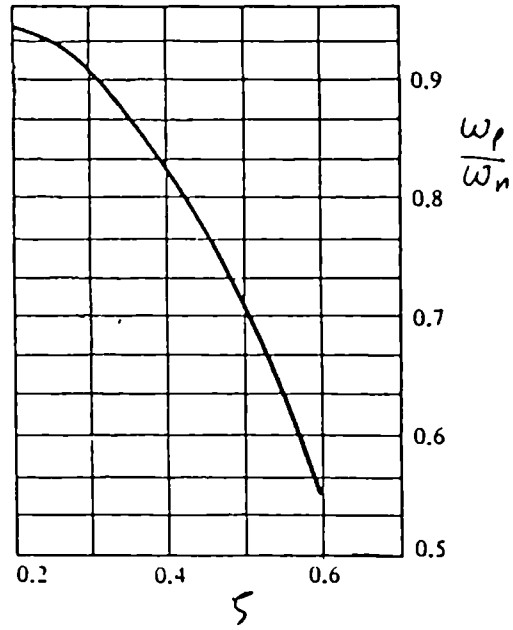
Figure (3.8) Frequency Response of a Second-Order Dominant Mode

(1)



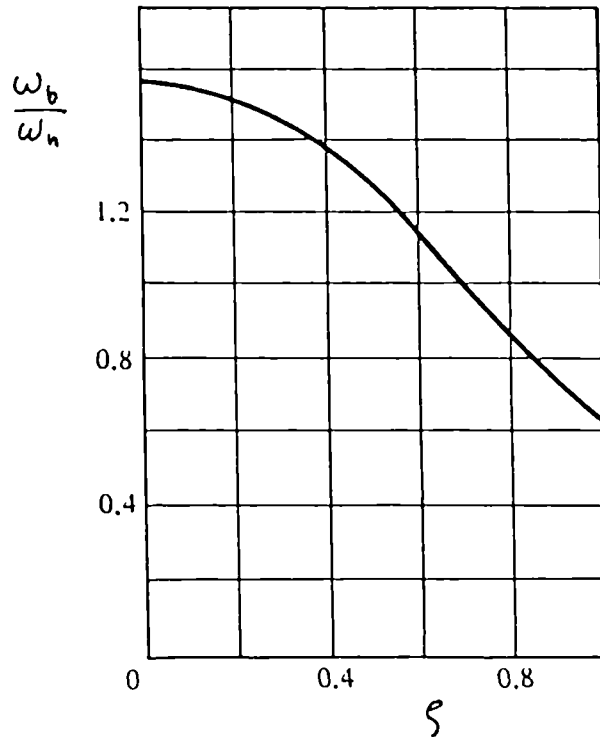
M_p vs ζ

(2)



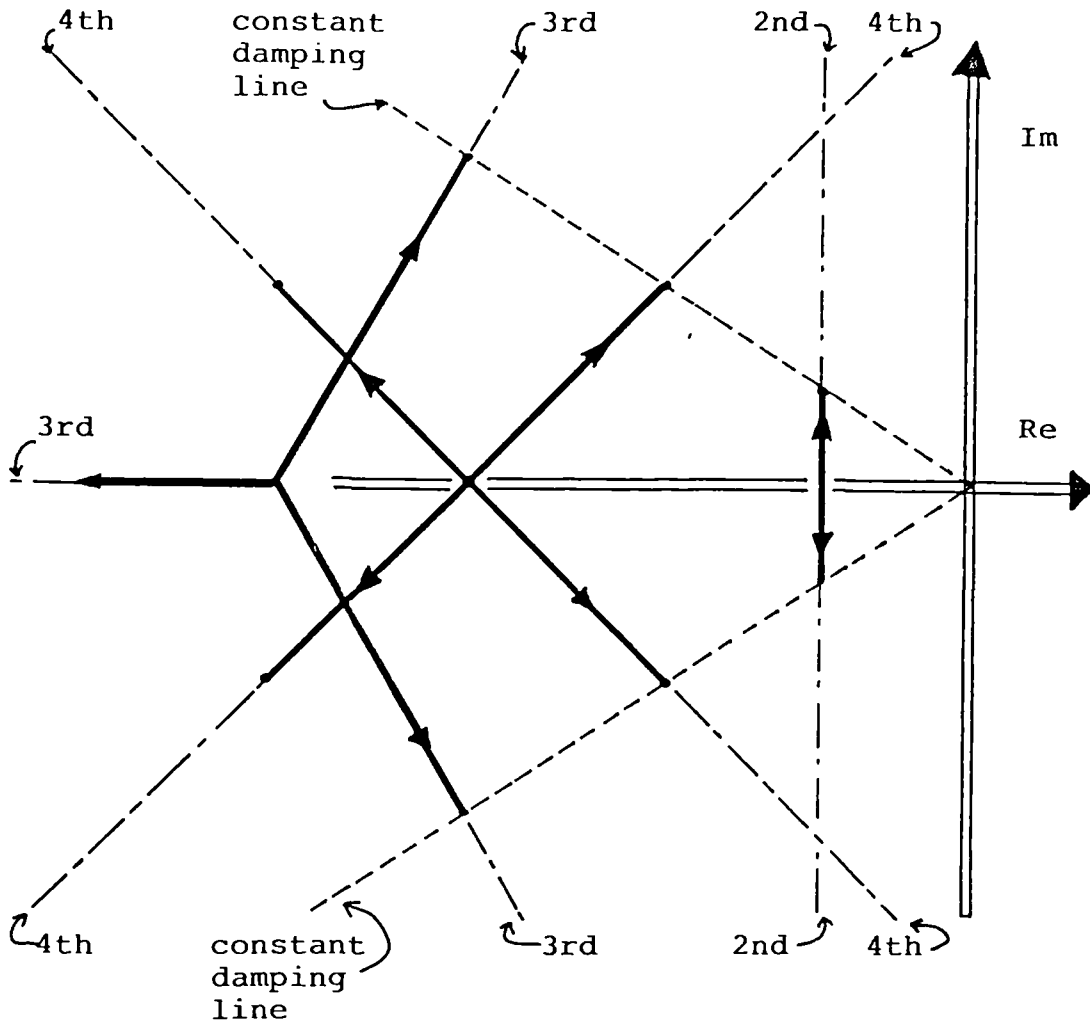
$\frac{\omega_p}{\omega_n}$ vs ζ

(3)



$\frac{\omega_b}{\omega_n}$ vs ζ

Figure (3.9) Relationships Between Key Performance Parameters and the Damping



This shows a system with second, third and fourth order asymptotes. Each has been tuned to a constant damping line. This would be achieved using the diagonal tuning elements of .

Figure (3.10) Example of Tuning to a

Constant Damping Line

CHAPTER 4

THE GVAM87 AND THE

DESIGN/ANALYSIS/SIMULATION ENVIRONMENT

THE GVAM87 AND THE DESIGN/ANALYSIS/SIMULATION ENVIRONMENT

4.1 Introduction

This chapter describes the Generic V/STOL Aircraft Model (GVAM87) [Muir & Kellett] and the Design/Analysis/Simulation (DAS) environment which has been used for this project. The GVAM87 has been developed by the RAE to provide a comprehensive, non-linear, vectored thrust aircraft model for use in Advanced Short Take-Off and Vertical Landing (ASTOVL) control law design studies and real-time piloted simulation. The model has evolved from an earlier model which was configured for open-loop pilot control. This has resulted in the GVAM87 possessing some dynamic features which actually complicate the closed-loop control problem. These features will be pointed out in this chapter and referred to in future chapters. Section 1.2 gives further background information on the model and its use within the VAAC programme.

The GVAM87 incorporates many dynamic effects which are characteristic of V/STOL aircraft and it possesses realistic engineering constraints which impose limits on the closed-loop performance. The aircraft model is able to "fly" within an extensive and representative flight envelope and is able to perform large perturbation manoeuvres. Furthermore, this takes place within a flight environment which can include turbulent and steady wind effects. Because of this complexity the description of the aircraft model is divided into

eight sections as follows: the aircraft model configuration (Section 4.2), the rigid body dynamics and SESAME* (Section 4.3), the model structure (Section 4.4), the aircraft aerodynamic modelling (Section 4.5), the actuator (or parasitic dynamics) modelling (Section 4.6), the engineering constraints and non-linearities (Section 4.7) and the "flight" environment (Section 4.8). The last section (4.9) describes the DAS environment and the relationship between GVAM87, TSIM** and Pro-Matlab*** (these two packages are briefly described individually also).

Finally, it should be noted that throughout the rest of this report the model and its features are often referred to as if they represent real hardware, so that explanations do not become cumbersome.

* SESAME - a System of Equations for the Simulation of Aircraft in a Modular Environment [Tomlinson]. This software package performs the standard aircraft dynamics calculations and axis transformations.

** TSIM (Time SIMulation) is a DAS package that handles general non-linear dynamic equations
[Winter et al, Cambridge Control Ltd.a.b.]

*** Pro-Matlab - is an interactive MATrix LABoratory package
[Mathworks].

4.2 The Aircraft Configuration

The GVAM87 may be configured in several different ways, but only the default configuration was used throughout this project. The default configuration is shown by Figure (4.1) and the primary and secondary control inputs (which define the configuration) are now described.

4.2.1 Primary Control Inputs

(i) Thrust

The thrust is a primary control input on V/STOL aircraft and the engine model is described fully in subsection 4.6.6. In the default configuration, the thrust varies from minimum to maximum (0.26 - 1.0) only, (i.e. no thrust augmentation from plenum chamber combustion is modelled) and it is divided almost equally between all four nozzles. The engine is shown by Figure (4.2).

(ii) Thrust Vectoring

The thrust may be vectored by rotating the nozzles, as shown in Figure (4.2), between the limits of nozzles aft (0°) and nozzles forwards ($98\frac{1}{2}^\circ$). The splay angles are fixed at 5° - front pair and 10° - rear pair. The nozzle system is described fully in subsection 4.6.5.

(iii) Reaction Control System

The reaction control system consists of high-pressure hot air "puffer jets" operated by valves situated at:

the nose and tail to provide pitching moments, the upper and lower wing-tips to provide rolling moments and the port and starboard side of the tail for yawing moments. To roll to port the upper port and lower starboard wing-tip valves are opened, whilst to roll to starboard this operation is reversed. However, the pitching control valves both point down so that lift is not reduced by pitching. Consequently, the front and rear valves never operate together. The yaw control valve is integral with the tail pitch control valve and the yaw valve can only select port or starboard. The required hot high-pressure air is bled from the high pressure stage of the engine (see section 4.6.1 and Figure (4.2)) and is switched on gradually as the nozzles move down from 4° to 34°.

(iv) Pitch Control

Pitch moments are produced by an all moving tailplane in normal fully wing-borne flight. At low speeds, where the aerodynamic effects are not sufficient, the reaction control system augments the aerodynamic pitch moment as described above (iii). Generally, the nozzles will be selected forwards of 34° during a decelerating manoeuvre which ensures the reaction control bleed air is fully on before the aerodynamic control effects are lost. The pitch reaction control valves are linked to the tailplane actuation system so that normal commands to the tailplane also produce reaction control forces at low speed. This ensures that only pitch commands need to be given whatever the flight case, and not separate tailplane and reaction control commands. The tailplane is constrained between - 10.25° to + 11.25° which is 1.5° less than the default maximum limits. These limits were chosen to be conservative for development purposes which are beyond the scope of this report. The tailplane actuation system is described in subsection 4.6.1.

(v) Roll Control

Rolling moments are produced by conventional ailerons which are linked to the reaction control system in a similar way to the pitch controls (Range $\pm 14^\circ$). The actuation is described in subsection 4.6.1.

(vi) Yaw Control

Yawing moments are produced by a conventional rudder which is also linked to the reaction control system in a similar way to the pitch and roll controls. (Range $\pm 15^\circ$). The actuation is described in subsection 4.6.1.

4.2.2 Secondary Control Inputs

(i) Flaps

The flaps are used for increasing the lift for take-off landing and any other relatively low speed flight phases. The flaps are selected by the pilot (or they can be scheduled with speed by the controller). They are not fast acting and are not used directly for control of the aircraft. (Range 0° to 50° , the rate limit is 10° per second.) The actuation is described in subsection 4.6.2.

(ii) Air Brake

The air brake is used to increase drag for decelerating manoeuvres and for added stability when the undercarriage is down. Hence the air brake has three positions : in (0), out (1) and a mid

position (0.4) which corresponds to the "undercarriage out" configuration. The mid position is part of the default configuration and it improves open-loop piloting control. The actuation is described in subsection 4.6.2.

The other possible control variables, which are not part of the default configuration, are as follows : Common mode aileron, differential flap, chin fin, fast acting flaps and air brake, extended nozzle range (-20° to 180°), independent nozzle actuation (or paired common modes), variable splay angle, thrust modulation port-to-starboard, thrust augmentation for front nozzles and the independent use of the reaction control system. This independent use of the reaction control system allows the following two modes of operation : switching on the reaction control bleed air independent of the nozzle position, operating the reaction control valves independent of the aerodynamic surface positions.

Other degrees of freedom within the GVAM87 concern the geometry, weight, inertias, engine power and the relative positions and magnitudes of the control forces and moments. These degrees of freedom cannot be used for active control purposes, but may be used to push the GVAM87 into the mould of a particular ASTOVL configuration. However, the GVAM87 was used in the default configuration throughout this project, as described previously, and

the other degrees of freedom mentioned above took their default values. The limits mentioned previously are summarised below in Table (4.1).

TABLE 4.1

MOTIVATOR LIMITS

<u>MOTIVATOR</u>	<u>RANGE</u>	<u>MEANING</u>
Tail plane	-10.25° to +11.25°	Tail plane down to up
Aileron	± 14°	Aileron down to up
Rudder	± 15°	Rudder port to starboard
Nozzles	0° to 98½°	Nozzles aft to forwards
Engine	0.26 to 1.0	Idle speed to maximum speed
Flap	0 to 50°	Flaps in to flaps down
Air brake	0 to 1	Air brake in to out

4.3 The Rigid Body Aircraft Dynamics and SESAME

Aircraft have six degrees of freedom and each degree of freedom has a position, a rate of change and an acceleration associated with it. These eighteen variables may be expressed by six second-order equations which may be equated with the three forces and three moments which are acting upon the aircraft. The six second order equations may be expressed by twelve first-order equations in state-space form. However, before describing the twelve states that describe the rigid body dynamics, it is first necessary to describe the four axis systems which are used : earth axes, body axes, wind axes and flight path axes (each axis system is a right-hand orthogonal triad).

(i) Earth Axes

The earth axes are defined as an inertial frame which assume a flat, non-rotating earth. The x_e axis points northward, the y_e axis points eastward and the z_e axis points down normal to the surface of the earth. The xy plane is parallel to the surface of the earth and the origin of the axes is at some datum, such as the runway threshold.

(ii) Body Axes

The body axes used in the GVAM87 are geometric body axes which have their origin at the centre of gravity of the aircraft and are aligned with the aircraft longitudinal fuselage datum line. The x_b axis points forwards (through the nose), the y_b axis points to starboard and the z_b axis points down (through the floor of the aircraft).

(iii) Wind Axes - Flight Path Axes

The wind axes have their origin at the centre of gravity and are aligned with the aircraft velocity vector, relative to the wind or airflow. Hence, the x_w axis points along this velocity vector, the z_w axis lies in the aircraft plane of symmetry and the y_w axis is defined by the x_w axis and the z_w axis. In cases where the atmosphere is at rest, then the x_w axis represents the instantaneous flight path of the aircraft (the tangent to the flight trajectory at any instant) and the wind axes may then be termed the "flight path" axes. Conditions where the wind is not at rest are only used for disturbance rejection tests in this report; these conditions are made clear when they occur and the calculations are handled by SESAME as can be seen on Figures (4.3) and (4.4). Consequently, flight path axes and not wind axes are used mainly in this report and are denoted x_{fp} , y_{fp} , and z_{fp} .

The relationships between these axes are given by Figures (4.5) and (4.6). The relationship between the body and earth axes is given by the Euler angles ϕ , θ and ψ . The roll angle ϕ (or bank angle) is measured from the horizontal plane and lies in the range -180° to $+180^\circ$. The pitch angle θ is measured from the horizontal and lies

in the range -90° to $+90^\circ$. The heading angle ψ is measured from North and lies in the range 0° to 360° .

The relationship between the body and flight path axes is given by the angles α and β . The angle α represents the angle of attack and the angle β represents the side slip angle. The angle of attack and the side slip angle are important parameters used for calculating aerodynamic forces, as they represent angles between the aircraft body reference axis and the airflow. Often, the incidence (or angle of attack) of the wing is slightly higher than the incidence of the body axes as the wing is inclined up (longitudinally), relative to the body axes.

The relationship between the earth and flight path axes is the flight path angle γ which is measured without reference to the heading. It is used as a measure of the glide slope, or climb rate along which the aircraft is travelling, relative to the earth. It is an important parameter for pilot control, especially during landing.

The need for different axis systems may be illustrated by the following account. It is usual to calculate the effect of the airflow on the aircraft in body axes as the position and attitude of all surfaces is known relative to the centre of gravity making force and moment calculations easier. However, the "relative wind" or airflow direction must be known which is defined by α and β , which implies flight path axes. For flight simulation, some representation of the real world is needed and it may include a steady, gusting or a turbulent wind. This last situation is usually represented in earth axes.

The way in which these axis transformations and other calculations are handled is shown by Figures (4.3) and (4.4) which are taken from the SESAME report [Tomlinson]. These two figures essentially describe the necessary calculations that derive all the important flight variables from just the three forces and three moments which act upon the aircraft, along with the various other constants (e.g. mass, inertias, geometry and atmospheric conditions). The names in each box represent the names of the SESAME routines which perform the calculations depicted in that box. The force and moment data from the model is used each frame time by SESAME to calculate flight data; this flight data is in turn used by the model to calculate the forces and moments. Hence, the GVAM87 and SESAME are interlinked and interdependent. It is together that they make it possible for the rigid body aircraft dynamics to be calculated for the model. These rigid body dynamics may be expressed by twelve state variables as shown in Table (4.2) below.

TABLE 4.2

<u>State</u>	<u>Definition</u>
X	Horizontal displacement North ($\dot{X} = VKN$)
Y	Horizontal displacement East ($\dot{Y} = VKE$)
H	Vertical displacement Up ($\dot{H} = -VKD$)
VKN	Velocity in knotts North (Horizontal, along x_e axis)
VKE	Velocity in knotts East (Horizontal, along y_e axis)
VKD	Velocity in knotts Down (Vertical, along z_e axis)
ϕ	Roll angle, about the x_b - axis
θ	Pitch angle, about the y_b - axis
ψ	Heading or Yaw angle, about the z_b - axis
	The Euler } angles
P	Roll rate ($\dot{\phi} = P$)
Q	Pitch rate ($\dot{\theta} = Q$)
R	Yaw rate ($\dot{\psi} = R$)

Note:

The velocities VKN, VKE and VKD in earth axes may be replaced by UB, VB and WB respectively in body axes for a body axis representation of the model (In that case generally $\dot{X} \neq UB$, $\dot{Y} \neq VB$ and $\dot{H} \neq WB$).

These twelve states are not the only twelve states that can be used to express the rigid body dynamics of an aircraft but they are the twelve states used in this thesis. The earth axis velocities are used in preference to the body axis velocities for disturbance rejection tests as the body axis velocities are wind relative (as shown in Figure (4.5)) making them quite unsuitable for gust rejection control. However, in still air simulations both earth and body axis velocities may be used, depending on which seems most suitable at the time. This is expanded upon in Chapter 6 which also discusses the variables which are most likely to be available for measurement (or which could be reconstructed) in reality.

For more detailed information on the operation of SESAME the references should be consulted. Likewise, if more detailed information concerning flight dynamics is required a good reference book such as

"Automatic Control of Aircraft and Missiles", [Blakelock]

or

"Dynamics of Atmospheric Flight", [Etkin]

should be consulted.

4.4 The Structure of the GVAM87

The main structure of the GVAM87 is shown in block form by the schematic in Figure (4.7). Each subroutine shown is called in turn from top to bottom and from left to right by branches (i.e. CONTROLS and all of its subroutines). The following briefly describes each module.

USRSIM

This is a TSIM module (see section 4.10) which handles the communication between TSIM and SESAME. It is the top level model routine.

USERCMI

This is also a TSIM module and it is used to introduce interactive or calculated inputs from the user via TSIM.

SESAME

The SESAME package has already been briefly described. It receives its initial data from USRSIM and whilst performing its calculations and transformations it calls many subroutines. The most significant to this discussion are CONTROLS and TOTM.

CONTROLS

This contains the calling sequence for the control inputs which include the actuator and servo dynamics and most importantly, the engine dynamics. It calls DEMAND, SJACT and ENGINE.

DEMAND

This places bounds upon the actuator demands so that the limits are enforced. It also calls CLMAST.

CLMAST

This is the master routine for the control laws and it interfaces the model and the controller. This module and its calls are discussed in Chapter 7.

SJACT

This contains the continuous-time actuator's dynamic models which correspond to the first-order and second-order actuators and servos. It does not include the main engine dynamics which are called next.

ENGINE

This calls the engine modules in sequence for initialising and for simulation. The engine is a large part of the model reflecting the fact that in V/STOL aircraft, the engine dominates the dynamic response. The engine model calculates a solution for each time step as the balance between spool speeds, air mass flow, and fuel flow. It calls INTAKE, ENGDYN, ENGOUT, FLOCON and ADDEFF.

INTAKE

This calculates the airmass flow and the intake efficiency.

ENGDYN

This estimates the fan and compressor acceleration rates and the spool speeds.

ENGOUT

This calculates the gross thrust produced by the engine and it calls REACT.

REACT

This calculates all the pressures and flows in the reaction control system caused by the control inputs. The actual forces and moments are calculated also.

FLOCON

This calculates the fuel flow to the engine and simulates the fuel control system.

ADDEFF

This literally ADDs the EFFects and produces the resultant engine forces and moments in body axes.

TOTM

This calls the modules which calculates the rigid body aerodynamics and it sums the various force and moment components. It calls AERSUB, INTFR and AERODY.

AERSUB

This simply calculates some of the variables and aerodynamic coefficients needed by INTFR.

INTFR

This calculates the interference forces and moments occurring in the longitudinal plane. These are caused by the jet exhaust impinging upon the flaps and the tailplane. It calls XSICAL and CMICAL.

XSICAL

This calculates the longitudinal interference force coefficients.

CMICAL

This calculates the interference pitching moment coefficients.

AERODY

This calculates the aerodynamic force and moment coefficients for the wing and the primary and secondary control surfaces.

USERCMO

This is used so that variables calculated within the aircraft model can be "fed back" to the user and examined within TSIM.

Once again, the references should be consulted if further information is required [Muir & Kellett]. However, this section shows something of the scope and complexity of the aircraft model and shows the structure of the modules which generate the various dynamics effects. These dynamic effects are described in the following sections.

4.5 The Aircraft Aerodynamics

The rigid body aerodynamics are modelled to a first-order approximation and may be split into three distinct areas: normal aerodynamic effects, interference effects and effects that are V/STOL specific. Firstly, the normal aerodynamics are based upon calculations involving aerodynamic derivatives. However, the aerodynamic derivatives change with Mach number, and also with incidence in some cases, so that the equations are representative over the full flight envelope. The force and moment contributions of the intake, the wing, the tail, each control surface and each secondary control surface are calculated from these equations.

Non-linearity is introduced in these calculations because some aerodynamic coefficients are bounded between their maximum and minimum limits. Furthermore, the wing drag and lift is bounded by an incidence limit which represents the stalled case. Other non-linearities are introduced by the use of conditional statements which select the most appropriate equation for the conditions, such as supercritical or subcritical drag conditions.

Secondly, the aircraft configuration shown by Figure (4.1) is prone to interference effects caused by the engine jet exhaust from the nozzles impinging upon the tailplane and the flap, and also interference effects caused by the flap and nozzle deflections. These effects are modelled and they vary with nozzle angle, thrust, flap angle, Mach number and incidence.

Thirdly, two characteristic V/STOL effects are included, namely Hot Gas Reingestion (HGR) and suck down. The first effect (HGR) is caused by hot gases from the nozzles circulating and being reingested by the engine through the intake. This causes an inlet temperature rise which leads to a loss in thrust. HGR is at its maximum in the hover case and reduces as speed increases. The second effect, suck down is caused by the engine gases hitting the floor and radiating out like a fountain. The engine gases entrain ambient air which is replaced by a downdraft which in turn causes a down force on the wing. Suck down for this "four-poster" jet configuration is found to reduce as height increases, indeed the effect is zero above 58.5 ft in the GVAM87.

This variety of aerodynamic effects increases the complexity of the

model but it also increases its realism. This is emphasised by the fact that all of the aerodynamic derivatives in the look-up tables are derived from representative wind tunnel data. Hence, this section has shown that despite the simplistic first-order representation of some aerodynamic effects, the resulting overall aerodynamics are both complex and realistic (due in part to the non-linearity which has been modelled.)

4.6 The Actuator Modelling

The actuators provide the control inputs for the GVAM87. They were briefly discussed in section 4.2 so that the configuration of the GVAM87 could be defined. The dynamic models which describe the actuators are based upon hardware assumptions which reflect the characteristics that could be expected of real actuators. Therefore, the theoretical hardware is described for each actuator so that the dynamic models of the actuators may be understood more clearly. The tailplane aileron and rudder actuation systems are essentially the same, as are each of the associated reaction control valves, so these are described together in subsection 4.6.1. The flap undercarriage and airbrake actuation systems are described in subsections 4.6.2, 4.6.3 and 4.6.4 respectively whilst the nozzle actuation system is described in subsection 4.6.5. Finally, subsection 4.6.6 describes the engine which is a significant part of the GVAM87, indeed, the engine dynamics dominate the control problem as will be seen.

4.6.1 Aerodynamic Surfaces and Reaction controls

It is assumed that each actuator is powered by a hydraulic servo system which obeys commands given in the form of a desired position. The aerodynamic surfaces of tailplane, aileron and rudder are each modelled as having first-order actuators of this form with time constants of 0.025s (i.e. poles at -40).

The roll reaction control valves are directly linked to the ailerons and the rear pitch reaction control valve is directly linked to the tailplane. Consequently, the valve action is assumed to be simultaneous with the aerodynamic surface movement. However, in the GVAM87 the front pitch reaction control valve and the rear yaw reaction control valve are driven by actuators represented as first-order lags with time constants of 0.02s (i.e. poles at -50). Despite this difference in actuator dynamics the front pitch and rear yaw reaction control valves are still configured to operate in harmony with the aerodynamic surfaces.

4.6.2 Flaps

The port and starboard flaps move in parallel and are not used as primary flight control motivators. Consequently, the actuation system is represented by a slow screw jack actuator which is rate limited to 10° per second. Therefore, as the full range of deflection is 0° to 50° the flaps take 5 seconds to cross the full range in or out.

4.6.3 Undercarriage

Although the undercarriage is neither a primary nor a secondary control input it is described in this motivator section as its operation is governed by an actuation system. The actuator is assumed to be hydraulic and it is slow acting. The result is a rate limited system which can extend the undercarriage (for landing) in 10 seconds and can raise it (after take-off) in 7 seconds. The undercarriage has no drag forces modelled and so it only effects the aircraft because of the airbrake (see below, subsection 4.6.4) or when the "wheels touch the floor". This phenomenon is discussed in section 4.8, as it is part of the flight environment.

4.6.4 Air Brake

The airbrake is not a primary flight control input consequently its actuation systems is modelled as a slow acting hydraulic system. This system extends the airbrake in 2 seconds and retracts it in 1 second. It was mentioned earlier (section 4.2) that the airbrake will move to a mid-position of 0.4 when the undercarriage is selected down (the mid-position is part of the GVAM87 default configuration and is used for added stability). The airbrake will move in or out to achieve the mid-position depending on the previous setting and it will take 0.6 or 0.8 seconds respectively.

4.6.5 Nozzles

All four nozzles move together and in the GVAM87 they are powered by an air motor which runs on high pressure air that is bled from the engine. The air motor is represented as a first-order lag with a time constant of 0.2s (i.e. a pole at -5). The nozzles are operated close-loop and there is a servo control which ensures that the desired nozzle angle is achieved. This servo control could be mechanical, hydraulic, electrical or a hybrid, but in the GVAM87 it is represented simply as a second-order dynamic equation with a natural frequency of 10 rads/sec and a damping of 0.575. This second order servo is in series with the air motor lag such that the resulting nozzle actuation system dynamics are third-order. Finally, it should be remembered that the reaction control bleed air master valve is opened by the nozzles moving from 4° to 34° , but that there is no additional actuation dynamics modelled for this.

4.6.6 Engine

The engine is modelled as an axial flow, twin spool, turbofan jet propulsion engine, see Figure (4.2). The two spools are assumed to be contra-rotating so that the gyroscopic effects are minimised and can be assumed to be negligible. Air from the low pressure compressor is split and some is exhausted through the front nozzles as relatively cool low pressure air whilst the rest passes through to the high pressure compressor. Some high-pressure air is bled off to power the nozzle actuation system (a negligible amount which is not modelled) and some to the reaction control system (which is modelled). After the high pressure compressor stage comes the

combustion chamber followed by high pressure and low pressure turbine stages. These turbine stages are on the same shafts as the respective compressor stages and so supply the power for the compression cycle. The hot gases are then exhausted through the rear nozzles. The engine is assumed to produce thrust which is divided almost equally between the front and rear nozzles such that the thrust vector passes very close to the centre of gravity of the engine and the aircraft for all nozzle angles.

The control input to the engine is via a second-order servo which changes the fuel flow to the engine. This second-order servo has the same dynamics as the second-order servo in the nozzle actuation system (i.e. a natural frequency of 10 rads/sec and a damping of 0.575). The change in desired fuel flow is the input to a complex and comprehensive engine model which is basically third-order. Two states represent the two spool speeds and one state represents the fuel control system which is part of the engine controller. There are several other internal states which simply represent internal filters (lag and lead/lag) which do not affect the closed-loop control and vice versa.

The mathematical modelling of the engine is complex as it dynamically models the processes which occur in an engine of this type. Furthermore, many of the parameters used are taken from look-up tables and they can vary with Mach number, air mass flow, fuel flow, spool speeds and other factors. Various temperature limits are built into the engine as practical constraints and the fuel control system which is modelled adds its own constraints.

The fuel control system has to balance the demand with the various

practical limits which are set to increase engine life, to keep within fuel pump capacity and to remove the risk of surge (where the engine blades stall due to temperature and pressure differentials being exceeded). In addition to this, the fuel control system modifies the engine response to make the throttle-to-thrust relationship suitable for open-loop piloted control. In low speed flight the thrust controls the aircraft height above the ground and so the pilot needs a reasonably linear throttle-to-thrust relationship which gives a rapid response. However, in normal flight this rapid almost linear response is unnecessary. Consequently, the engine is governed to give a throttle-to-thrust response as shown by Figure (4.8). The difference in engine response is considerable either side of Point 'A' in Figure (4.8) and it leads to control problems. This is described in more detail in the next chapter, but an illustration of the change in engine dynamics is given here also.

The engine model, along with the aircraft rigid body dynamics, may be linearised at spot points. The eigenvalues of the engine change with speed and altitude for a given throttle setting but not significantly. However, the change in eigenvalues given by a throttle change which passes through the 60% throttle position is given by Figure (4.9). Areas A, B and C show the regions where the three open-loop engine eigenvalues are for throttle settings greater than 60%, whereas areas D, E and F show the regions where the three open-loop engine eigenvalues are for throttle settings less than 60%. Clearly, the onset of the engine governor causes a gross non-linearity in the engine response and a step change in dynamics. However, the linearisation process is such that a root-locus can be produced for the engine eigenvalue changes versus throttle setting, see Figure (4.9).

One more complication characterises the engine dynamics demand and that is the engine thrust loss due to bleed air. As the bleed air is high pressure air, considerable work must have been performed on it by the two compressor stages. If this air does not pass through the combustion and turbine stages then it provides no useful energy in return (unless it exits from the nose or tail pitch reaction control valves, which makes the loss slightly less). This effect is modelled and so reaction control demands for bleed air result in a thrust loss, which is magnified, pound for pound, because the bleed air is not burnt.

The actuation systems described in subsections 4.6.1 to 4.6.5 are summarised in the table below, Table (4.3). The main engine dynamics do not appear as they vary considerably with flight condition and demand, however Figures (4.8) and (4.9) give a good indication of the dynamic behaviour of the third-order system. The second-order engine servo is included in Table (4.3),

Table 4.3

Motivator or actuator	dynamic order	Poles	Characteristic equations
Tail plane } Aileron } Rudder }	1st	-40	$s + 40 = 0$
Aileron RCV } Rear Pitch } RVC }	1st	geared to surfaces above	
Front Pitch } RCV } Rear Yaw RCV }	1st	-50	$s + 50 = 0$
Nozzle air motor	1st	-5	$s + 5 = 0$
Nozzle servo	2nd	$-5.75 \pm 8.18j$	$s^2 + 11.50s + 100 = 0$
Engine servo	2nd	$-5.75 \pm 8.18j$	$s^2 + 11.50s + 100 = 0$

Key: RCV is Reaction Control Valve, decimals are to 2 significant figures.

4.7 Engineering Constraints and Non-Linearities

The GVAM87 modelling includes many engineering constraints and non-linearities. Some of which have been described in previous sections. These and others yet to be described, are set out in this section for easy reference.

Each engineering constraint can introduce non-linearity into the model and each non-linearity is usually the result of some engineering constraint. However, the more obvious engineering constraints are described first here, and the remaining non-linearities are described afterwards.

There are many engineering constraints included in the GVAM87 which make the simulation model more realistic. The aerodynamic stalling effects for instance require that controller designs should incorporate incidence limiting to prevent stall. This contributes to carefree handling characteristics which are desirable for CCV's. The need to prevent surge and to prolong engine life has resulted in acceleration limits (implemented by fuel flow control) and temperature limits which vary depending upon flight condition. These effects seriously compromise the controller if they reduce the motivator bandwidth such that it is not much greater than the desired closed-loop control bandwidth. The final engineering constraint discussed here (that was mentioned in previous sections) is the engine governor which gives specific throttle-to-thrust characteristics for open-loop piloted control of the GVAM87. This additional engine controller could not be by-passed for this study

and its significant effects influence the controller design considerably. It is hoped that a CCV aircraft could be designed from the start with actuators that possess characteristics that are more compatible with active control technology!

Engineering constraints that were not mentioned previously are now discussed. Engine life depends upon several factors but cycling the engine is definitely a factor that reduces engine life. Consequently, control strategies which cycle the engine should be avoided or kept to a minimum. This is particularly difficult in low speed transition as the engine is then a primary actuator controlling height.

Moreover, the engine acceleration and deceleration rates are different and the engine is slow to accelerate from low revs into the faster dynamic region at high revs. This requires the constraint that engine control inputs should not put the engine revs too low when failure to accelerate fast enough could be catastrophic.

Another constraint requires that the reaction controls are not used for long periods of time as the hot high pressure air needs to be ducted through the airframe. Consequently, a time limit of 5 minutes is imposed upon use of the reaction controls. This is made easier by the fact that the GVAM87 is seldom required to loiter at low speed and the transition is usually completed in much less than 5 minutes. It should be remembered that the reaction control air is off at the end of a transition because the nozzles are then aft.

A further constraint concerns landing speeds which should be kept within a descent rate of 12 feet per second due to realistic

undercarriage compression limits. These are not modelled by the undercarriage routine but it is good practice to observe such a limit. The last constraint concerns high speed or wing-born aerodynamic effects upon the flap and undercarriage. In practice there are maximum speeds above which it is unsafe to have either of these two services extended. The following speed limits were chosen for each:

flaps	30° only below 525 kts
	50° only below 300 kts
undercarriage	out only below 250 kts

As each of these are secondary controls they are normally left for the pilot to select, although they can easily be scheduled with speed. Many of the other non-linearities are caused simply because the GVAM87 is a large perturbation model and so trigonometric terms such as SIN, COS and TAN are not eliminated. Furthermore, accelerations are caused by the aircraft kinematics because the cross products of velocity vectors and angular rate vectors are no longer negligible. In addition to this it is not trivial to state that gravity only acts downwards and so all manoeuvres affected by gravitational pull are going to be dependent on aircraft orientation with respect to the earth.

Other non-linearities are caused by physical limits such as actuator position limits, rate limits and acceleration limits (see Table (4.1), earlier in this chapter and subsection 4.6.6.). There are also bounds put upon some aerodynamic coefficients such as the coefficient of lift (incidence limits). Temperature limits, time

limits and speed limits have already been mentioned in the previous section. Another significant non-linearity is the wide-spread use of look-up tables for empirical data which is used in the aerodynamic and engine modelling; it makes the GVAM87 a time-varying model. Two other effects that cause non-linearity were described in section 4.2, namely HGR and suck-down.

The last area of non-linearity to be discussed is that of cross-coupling caused by the actuators. The demand for bleed air results in thrust losses which can be significant. This results in cross-coupling between pitch (or roll or yaw) and vertical or horizontal translation. In addition to this there are interference effects caused by interaction between the flaps, the nozzles and the tailplane. This results in cross-coupling between vertical or horizontal translations and pitching moments. The secondary motivators also produce cross-coupling as the drag and pitch moment changes when the airbrake is used and lift, drag and pitch moment are all affected by flap setting. Finally, it should be noted that the centre of gravity, the centre of lift and the thrust centre are not completely coincident. Consequently, lift, nozzle angle or thrust changes all cross-couple into the pitch moment and cause pitch oscillations if not compensated for.

The reasons for mentioning each engineering constraint and each non-linearity is because each should be taken into account when designing a controller. The way in which the engineering constraints are incorporated is explained where the constraints are mentioned in future sections. Of the other non-linearities, some may be accounted for by special conditions within the controller and others simply by ensuring that they do not produce limit-cycles. A typical example of

a special condition is freezing the integrators to prevent integrator wind-up during actuator saturation. For limit cycle tests, unfortunately, the only method currently available for MIMO systems is time simulation. However, the nature of the high-gain theory is such that multivariable describing function developments should be possible. This concludes the discussion of the engineering constraints and non-linearities.

4.8 The "Flight" Environment

The "flight" environment is provided by the undercarriage routine, SESAME and some code added by the author. The result is an environment that allows landings, take-offs and a wide variety of atmospheric effects. The undercarriage could be considered as part of the aircraft dynamics but it is not essential to this study and is only used to aid the realistic assessment of the controller.

Furthermore, the undercarriage model is only a simple mass/damper system which calculates forces and moments that are combined with all the other forces and moments in TOTM. Hence the undercarriage model is not suitable for ground handling tests but is quite adequate for this study.

Within SESAME the atmospheric conditions are based upon the ICAO International Standard Atmosphere [Tomlinson] at sea level and the atmospheric properties are calculated as a function of height. In this study these effects are negligible as the flight conditions are around the transition region and so high speed high altitude conditions are not achieved. However, SESAME also allows wind velocities to be fed in (relative to the earth axes) and it generates the body axis velocities (relative to the wind) which allow the effect of relative wind on the aircraft to be calculated.

The wind is specified by a vertical component (VWDLO) a horizontal wind speed (VWKTO) and a heading angle (PSIWD) which orients the wind with respect to the earth axes (PSIWD = 0, horizontal wind is from the north). From these three parameters wind in all three earth axis

directions is calculated. An addition to this by the author has been to provide a gust model (such as 1-COSINE ramps or 1-COSINE gusts) which shapes VWDLO or VWKTO so that gust response tests may be performed with the controller. No suitable data could be found for low altitude gusts and so a gust that is similar in magnitude to the British Civil Airworthiness standard "once in a lifetime" gust, has been used. Thus a gust of 60 ft/s with a width of 4 seconds is used for both vertical and horizontal gusts. This test may be overly pessimistic but it does provide a thorough test for the controller.

The RAE also provided a random amplitude random frequency turbulence generation routine which models atmospheric turbulence based on statistical discrete gust theory [Tomlinson]. The turbulence is weighted by parameters which define the RMS intensities in each of the three earth axis directions. These turbulence components are superimposed onto any steady wind there might be and the resultant is used to calculate the wind relative body axis velocities as before.

The turbulence and the shaped wind functions allow the disturbance rejection properties of the controller to be assessed, as will be seen in Chapter 8. These wind functions, together with the atmospheric conditions and the undercarriage model constitute the "flight" environment.

4.9 The Design/Analysis/Simulation Environment

The DAS environment used for this study is a computer environment which makes the control engineer's task of DAS much simpler. It is implemented on a VAX 750 mini-computer and it comprises the software packages TSIM [Winter et al, Cambridge Control^{a,b}] and Pro-Matlab [The Mathworks]. Some changes of the model software and some menu-based routines have been added by the author to provide a simple method of re-configuring and re-building the complex model within this environment.

The GVAM87 is written in Fortran 77 and it consists of several subroutines which are called from within SESAME. SESAME handles the usual aircraft calculations and transformations and was described in sections 4.3 and 4.4, SESAME is in turn interfaced to TSIM via the routines USERCMI, USERCMO and SESSIM (see section 4.4). An interface also exists between TSIM and Pro-Matlab which is used for exchanging data concerning linearised models. However, before describing this DAS environment in detail (subsection 4.9.3) it is appropriate to describe TSIM and Pro-Matlab and this is performed in subsections 4.9.1 and 4.9.2 respectively.

4.9.1 Description of the Package TSIM

TSIM [Winter et al, Cambridge Control^{a,b}] is a general DAS package that can handle both linear and non-linear dynamic equations. The simulation is written in a superset of Fortran 77 that is translated into standard Fortran 77. This can then be compiled and linked to

the TSIM package which is held as a shareable image. The result is an executable programme which appears to the user as a command driven package. The package has many different DAS features and those used in this study are listed below:-

- i) Trimming non-linear systems to an equilibrium condition
- ii) Linearising non-linear systems
- iii) Time responses of non-linear systems
- iv) Frequency responses of linearised systems
- v) Root-loci of linearised systems
- vi) Linear system data output to Pro-Matlab.

The GVAM87 has already been described and its relationship to SESAME has been described also. The routine called SESSIM simply equates various Fortran model variables into equivalent TSIM variables so that all the dynamics of the GVAM87 are accessible to TSIM. This makes it possible for the user to analyse and simulate the GVAM87 during each design stage. Many design changes can be made on-line through TSIM, but some, mainly those requiring code changes, have to be implemented in the original controller or model software. This then requires that some or all of the model and controller routines are re-compiled and that the executable programme is re-built.

The user can define trimming inputs (such as throttle, nozzle and tailplane and trimming outputs (such as forward, vertical and pitch acceleration) and then set TSIM to find the trimming inputs which minimise the trimming outputs (DAS feature i). In this way a trimmed flight condition can be found such that the aircraft is in equilibrium. These steady flight equilibrium points are used as baseline design points throughout this study, but linear models at non-equilibrium conditions have also been used.

Whether or not the aircraft is in equilibrium, the user can linearise the aircraft at its current flight condition (DAS feature ii). To do this each TSIM variable must be given a perturbation parameter which is typically 0.01, but which should be approximately 1% of the variables range. Each variable is then perturbed by $\pm 1\%$ (approx.) and the partial derivatives relating this variable to every other is found by the slope of each result. In this way a matrix of partial derivatives is built up and the linearised state-space matrices may be found. These linearised state-space matrices may then be used for any linear DAS work that is required. However, it should be noted that discontinuities need to be "hidden" from TSIM during linearisation and care should be taken near discontinuities as linearised results can be misleading in such circumstances.

The time response of the non-linear system may easily be generated using TSIM (DAS feature iii). A variety of different command inputs may be generated by the user so that various system responses may be examined. Typical inputs include steps, lagged steps, ramps, cubic ramps and 1-cosine ramps. These inputs are basically crude open-loop pilot models and are not part of TSIM.

Frequency responses between a particular input and output pair, or between the input vector and the output vector, may be generated (DAS feature (iv)) once the linearised model is obtained. This may be generated in several forms, but the Bode diagram has been used most extensively to check results obtained using Pro-Matlab.

Root-loci are generated for changing gain or for changing tuning parameters (DAS feature v). In all cases, the non-linear closed-loop system is generated at each step and then it is

linearised so that the closed-loop A-matrix eigenvalues can be found. The routine is found to be reliable but large eigenvalue changes can occur occasionally when passing near or through a discontinuity. This though is a function of the linearisation and is not a problem if monitored by the user (for example, see Figure (4.8) and subsection 4.6.6).

Finally, the linearised state space matrices may be put into a file suitable for Pro-Matlab to read (DAS feature vi) which makes many powerful linear algebra methods available (see next subsection). Much of the early design and early analysis can be performed using Pro-Matlab and the linearised model. If further information is required concerning TSIM, the references should be consulted.

4.9.2 Description of the Package Pro-Matlab.

Pro-Matlab [The Mathworks] is a MATrix LABoratory package which is interactive with the user. It provides easy access to matrix software developed by the LINPACK and EISPACK projects which represent the state of the art in software for matrix computation. The package is written in the computing language C and it provides the user with a high level language that looks very much like normal mathematical notation. The basic data element is a matrix which does not require dimensioning.

The package has a set of fundamental core functions which provide elementary matrix operations and other functions to help the user such as : plotting capability, programming capability (via conditional statements and counting loops) and various input and

output facilities. These core functions are used to build up still higher level functions which are also part of the package. Indeed, several higher level functions have been derived especially to help with control engineering, systems identification and signal processing. These specialised functions are contained in various "tool-boxes" which can be used or extended as required. Furthermore, the user can define his own tool-box of higher level functions specific to his work.

This has been done by the author and several functions now exist which help the designer to generate the controller and perform the initial analysis tests. The more important of these functions are listed by name in Appendix C and a brief description of each appears there. It is intended to produce a Pro-Matlab tool-box in the future which allows a designer to use the high-gain method and which provides all the necessary design and analysis tools. This is discussed further in Chapter 9.

The functions that have been developed already, include: control law generator, closed-loop system builder, root-locus generator, frequency response generator, time-response generator and multivariable root-locus asymptote analysis. The root-locus generator can provide a standard root-locus for a fixed gain step or alternatively a root-locus with a self adaptive gainstep. The self adaptive gain step algorithm allows each branch of the root-locus to be traced separately. Each function has been of use at various stages of the design and the worked examples illustrate this. Once the controller has been generated and analysed within Pro-Matlab it may be transferred to TSIM for further analysis. The operations between the model and the two packages TSIM and Pro-Matlab are part

of the DAS environment, which is described in the next subsection.

4.9.3 Description of the DAS Environment.

The purpose of the DAS environment is to make the control system designer's task easier. This is mainly achieved by the use of the software packages TSIM and Pro-Matlab which have already been described. In addition to these packages there is a menu based programme written by the author which allows the user to select different model configurations. This programme also handles the translation, re-compilation and building of complex models which requires that all the correct subroutines and data files are put together for any particular model configuration. The rest of this subsection describes how the whole DAS environment functions.

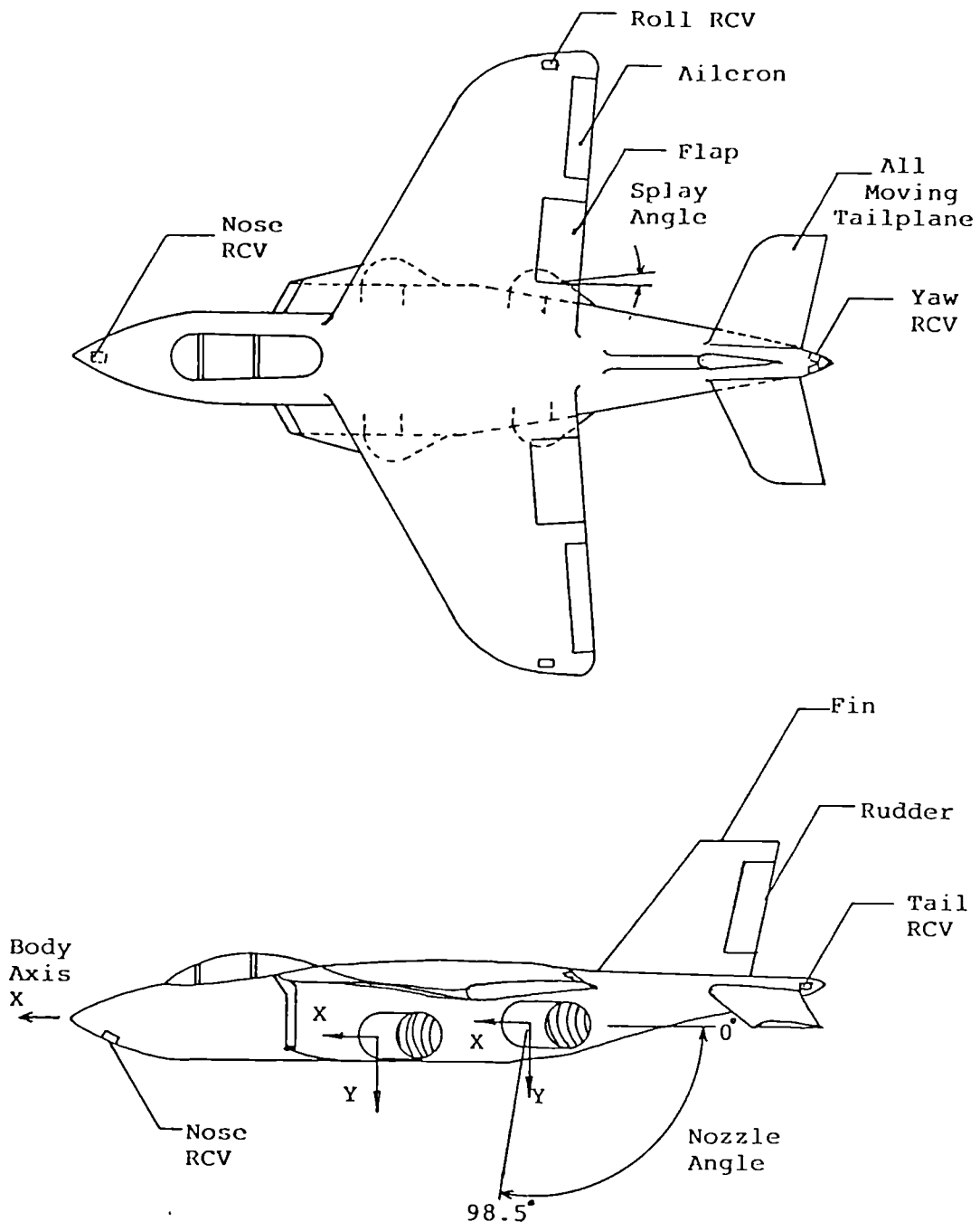
When starting an interactive DAS session the default model configuration is automatically selected so that the user has access to the model configuration utilised most. Alternatively, the user may select options from a menu to define the desired model configuration. This then assigns "logical names" and "symbols" which may be thought of as variables which can contain programme names, directory names, data file names and object library names. These variables are then used to define the model configuration and their use relieves the user of ensuring that all the right components of the model are correctly compiled and brought together. In this way the correct model can easily be built and connected to TSIM as described in section 4.4 and subsection 4.9.1.

With the correct model configuration functioning with the TSIM

package the user can select the design flight condition, trim the aircraft (if necessary), linearise the aircraft and then pass the data to Pro-Matlab. The data passing stage may be checked by comparing the open-loop eigenvalues calculated by Pro-Matlab with those calculated by TSIM. Within Pro-Matlab the linear design may be performed and the linear system may be investigated as described in subsection 4.9.2 and Chapter 3.

The resulting controller may then be passed back from Pro-Matlab to TSIM for further analysis using the non-linear model. At the design flight condition the root-locus and frequency-response of the linearised system may be examined in TSIM and compared to the results generated by Pro-Matlab to ensure that the controller was transferred correctly. Then time-responses may be used to check the effects of non-linearity and to assess the closed-loop system response to various pilot commands or external disturbances. Results and data generated during this process can be stored and the files are then named using an appropriate naming convention. This could be improved upon with a data-base to manage the DAS environment which should be object orientated. However, such innovations are being pursued elsewhere and ECSTASY is one example [Munro].

This concludes the description of the GVAM87 and the DAS environment which have been used throughout this report. The theory described in Chapter 3 may now be applied to this model; this application is described in the next Chapter.



Key

- RCV - Reaction Control Valve
- X - x-axis force
- Y - y-axis force

Figure (4.1) The Default Configuration for GVAM87

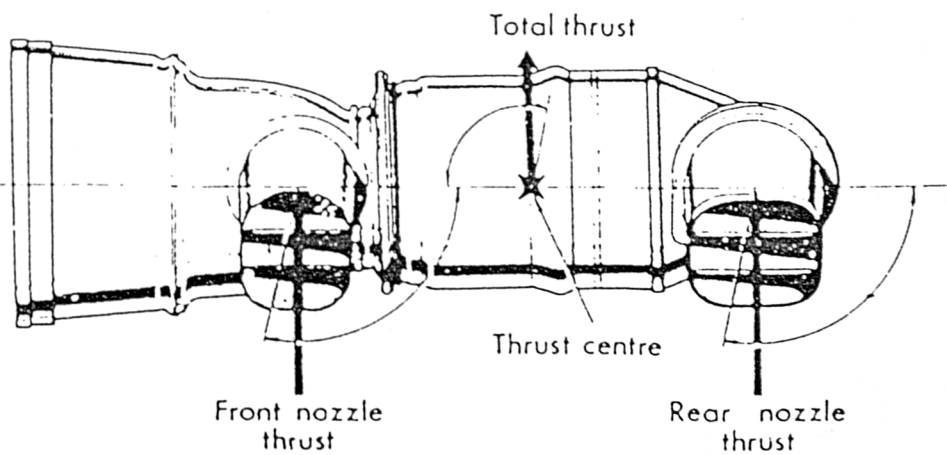
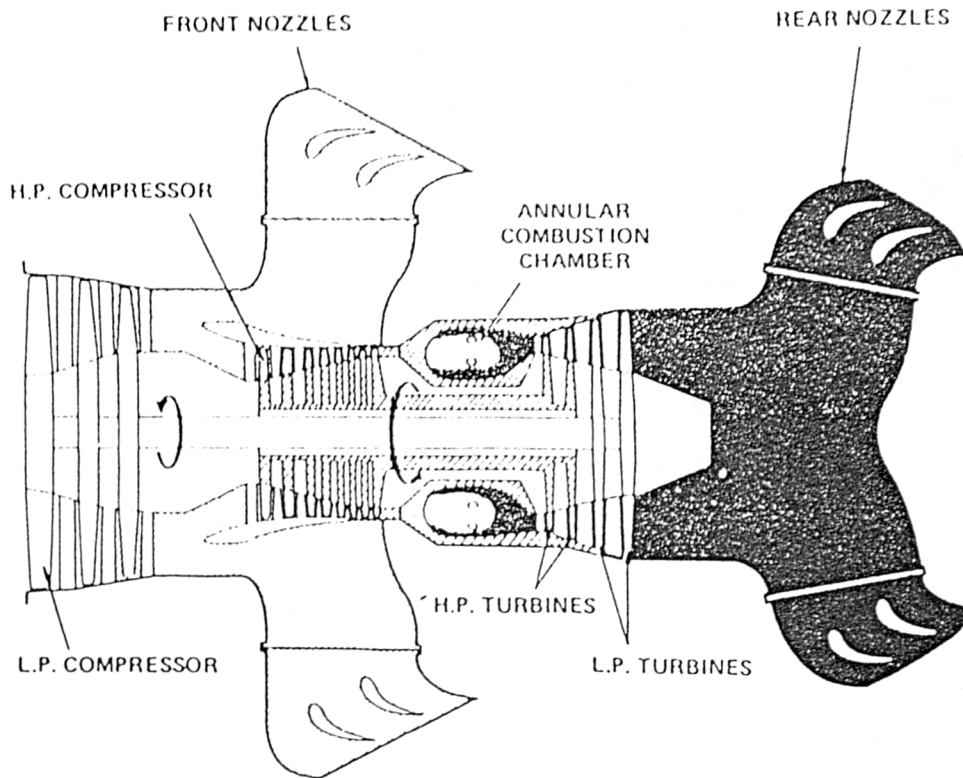


Figure (4.2) Typical Layout for GVAM87-Type Engine

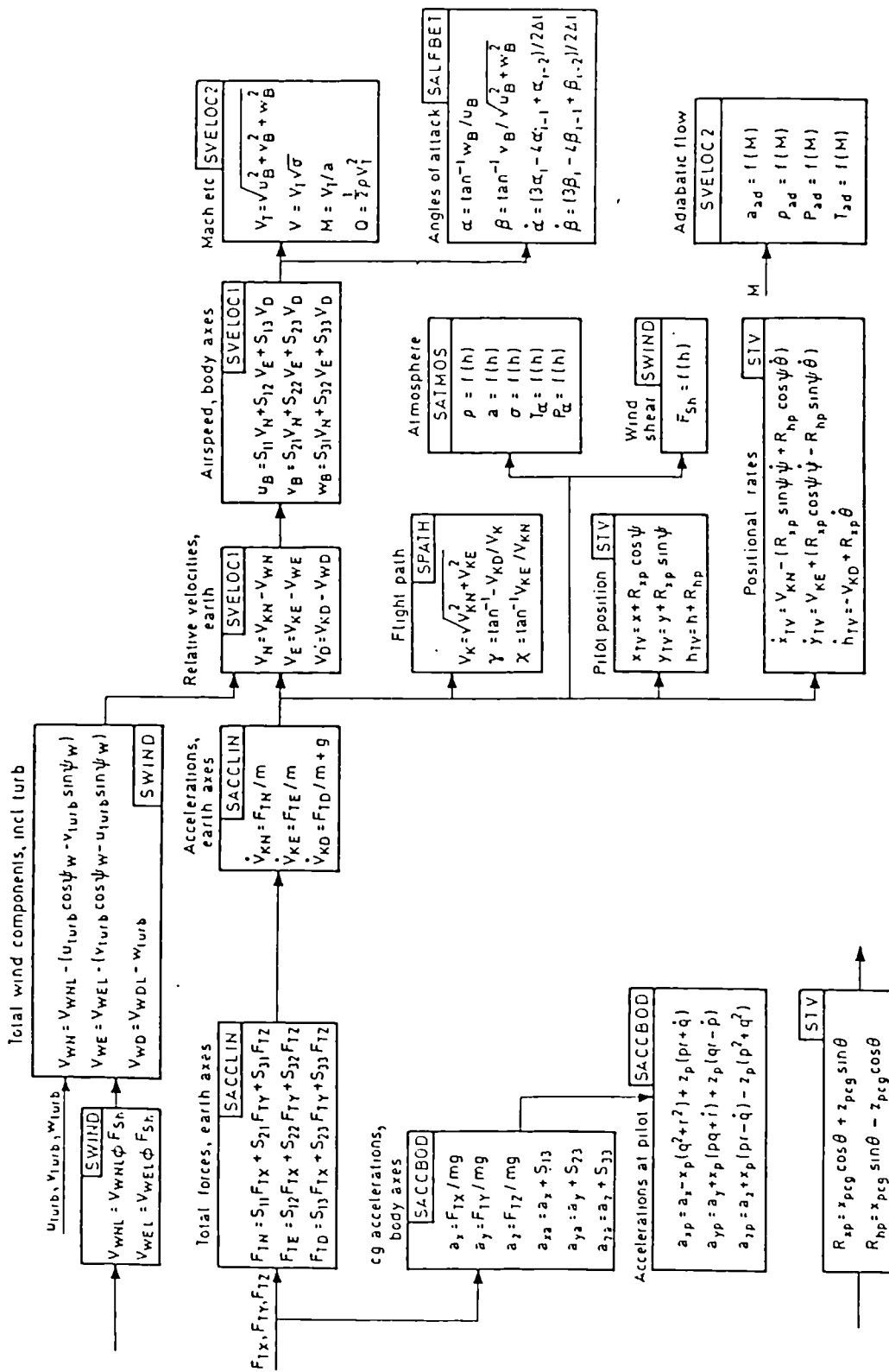


Figure (4.3) Block Diagram of Translational Equations from SESAME Report

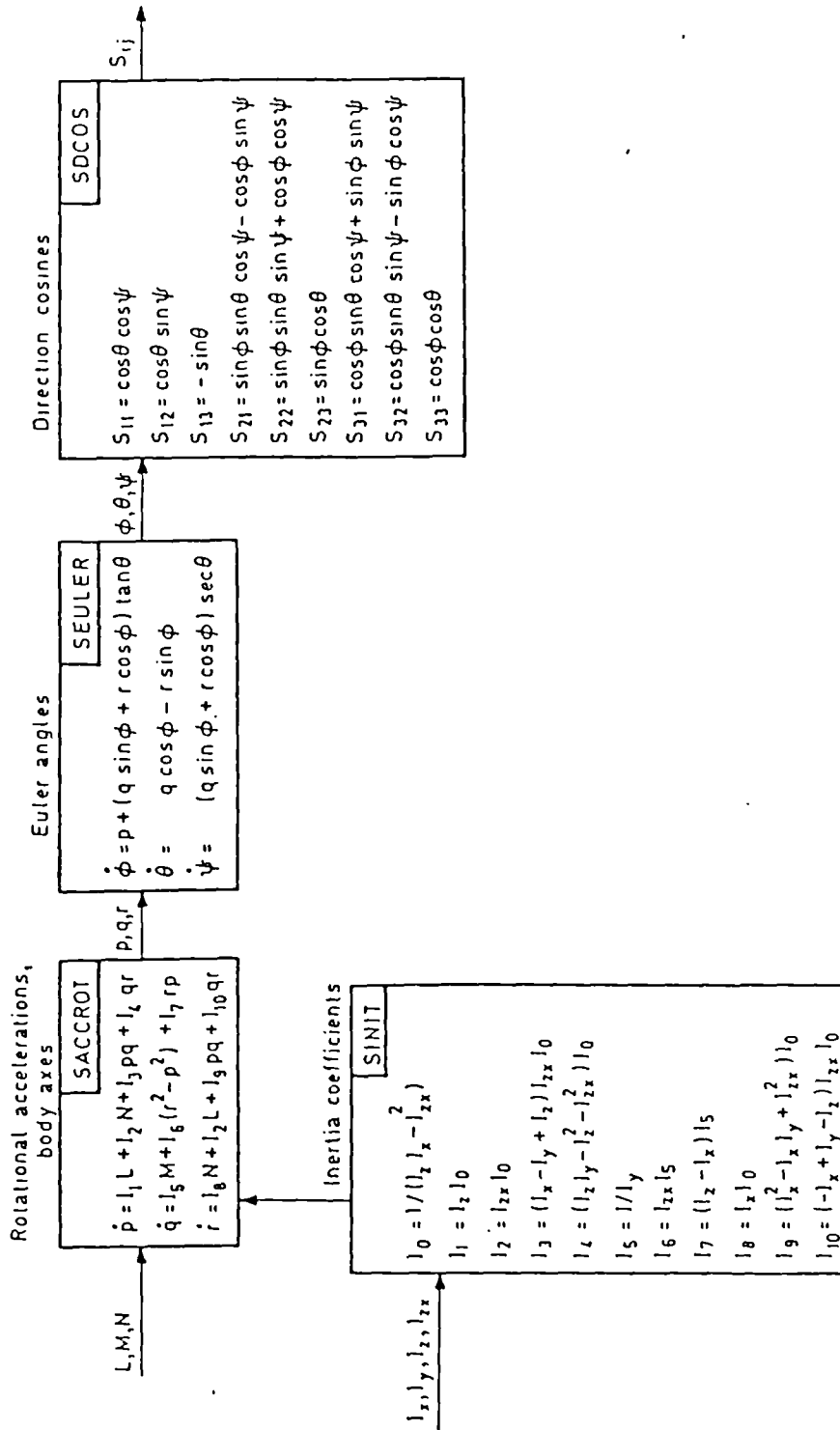
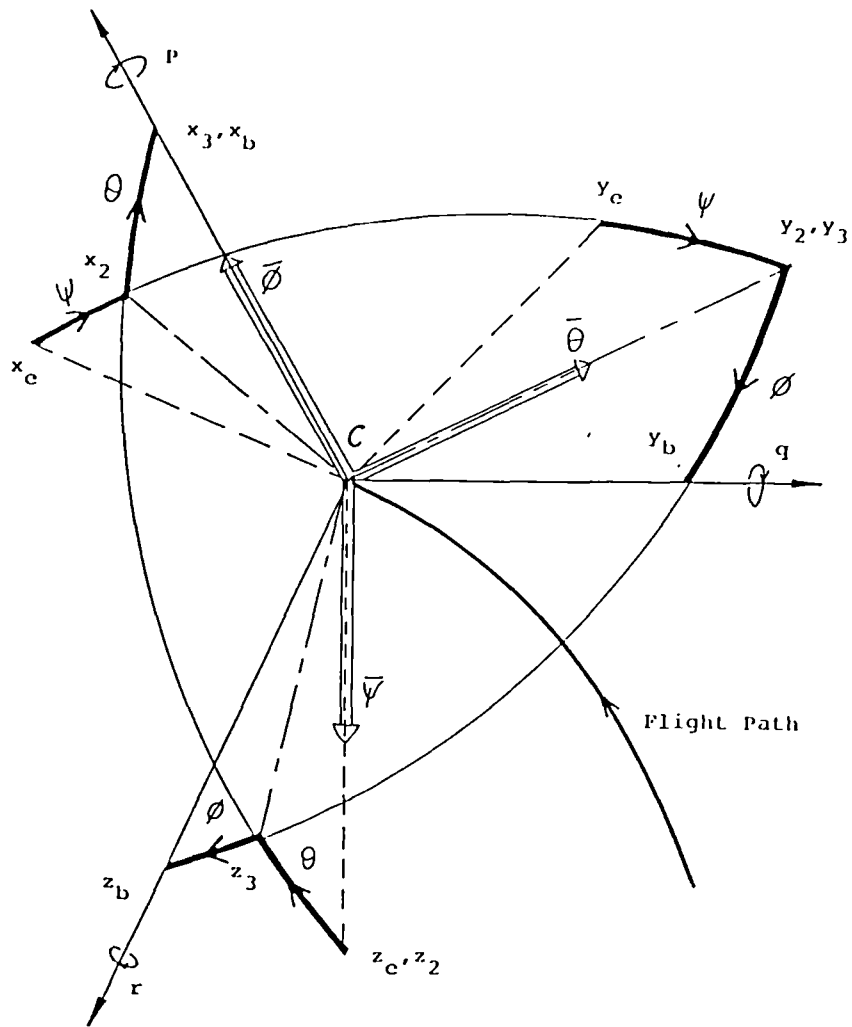


Figure (4.4) Block Diagram of Rotational Equations from SESAME Report



Key:

x_e, y_e, z_e - Earth axes

x_b, y_b, z_b - Body axes

p, q, r - Roll, pitch and yaw rates

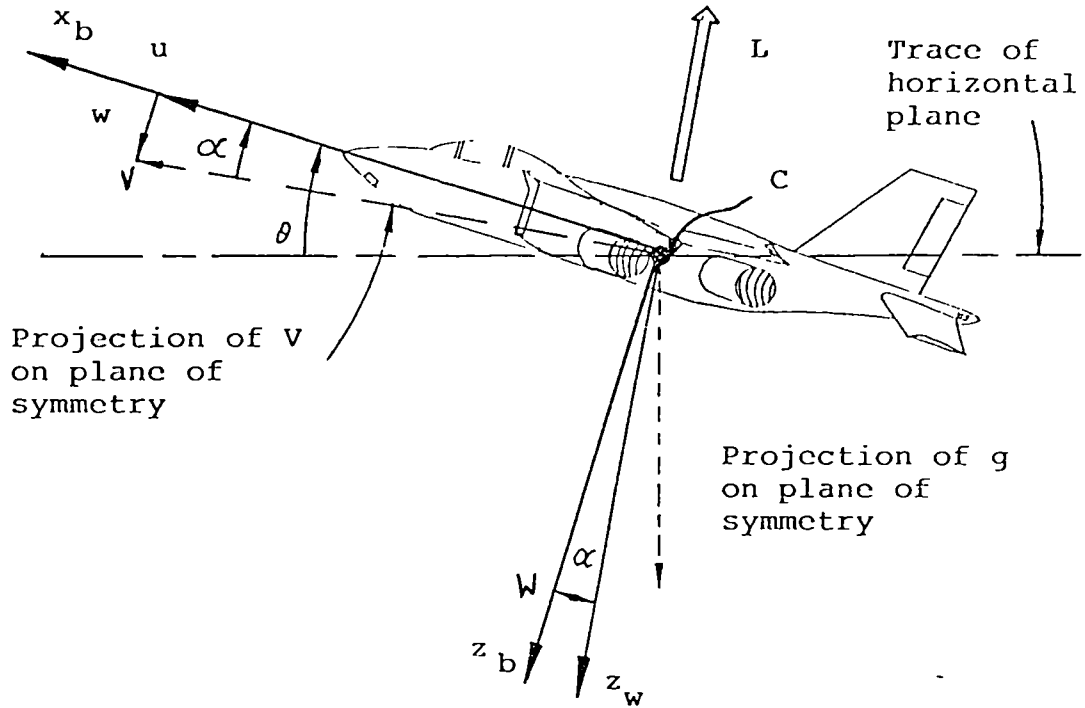
ψ, θ, ϕ - Euler angles (yaw, pitch, roll)

$\vec{\psi}, \vec{\theta}, \vec{\phi}$ - Euler angle vectors

Axis Transformation Process

- 1) A rotation ψ about $O_e z_e$ carrying the axes to $O_e x_2 y_2 z_2$
- 2) A rotation θ about $O_e y_2$ carrying the axes to $O_e x_3 y_3 z_3$
- 3) A rotation ϕ about $O_e x_3$ carrying the axes to $O_e x_b y_b z_b$

Figure (4.5) Illustration of the Euler Angles

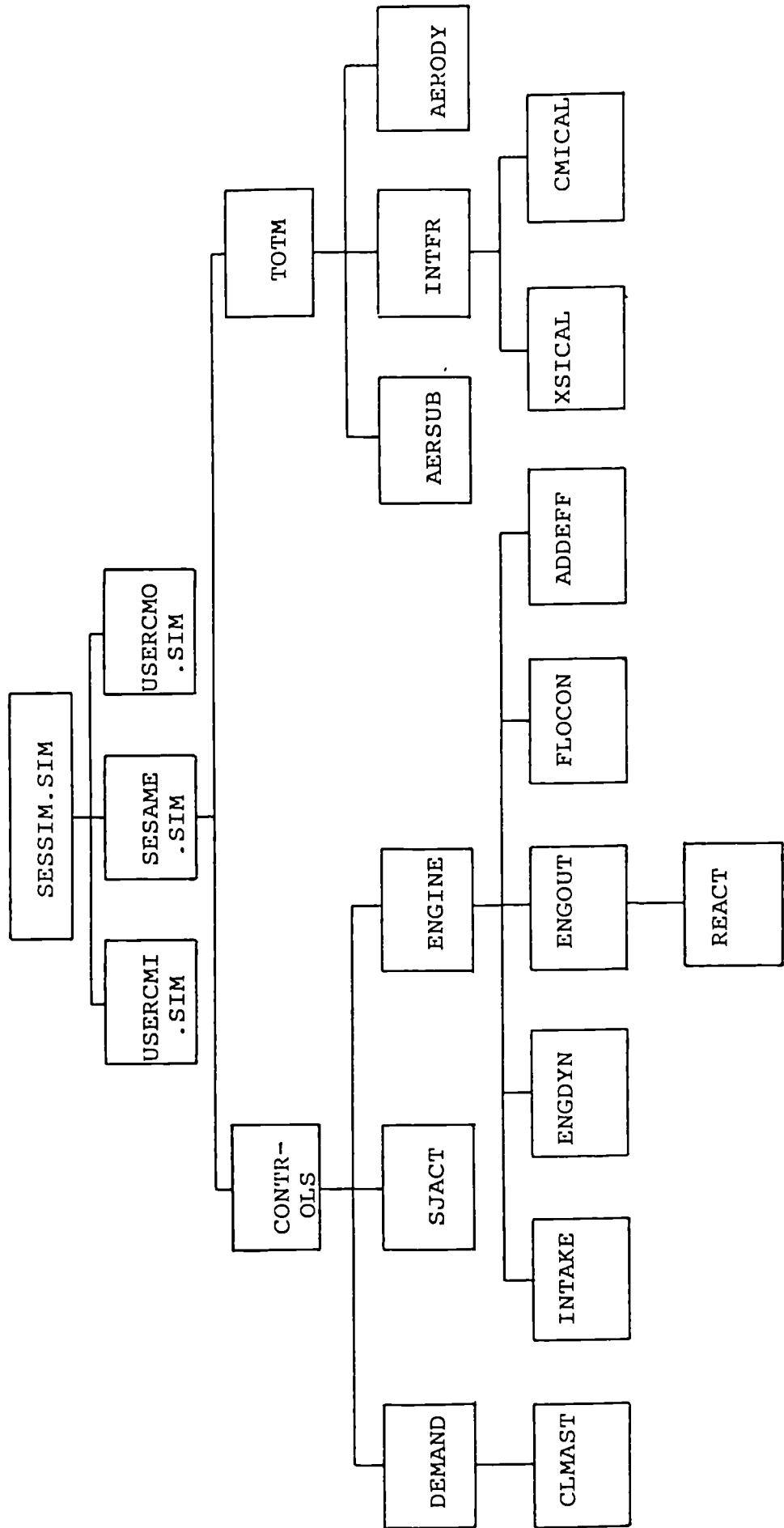


Key:

- x_b - body axis (forwards .)
- u - forward speed in body axes
- w - vertical speed in body axes
- z_b - body axis (normal -)
- L - lift vector
- V - velocity vector
- C - centre of gravity
- α - angle of incidence
- θ - pitch attitude
- g - gravitational constant

Figure (4.6) Illustration of the Relative Wind Angle

Figure (4.7) Subroutine Calling Structure for the GVAM87



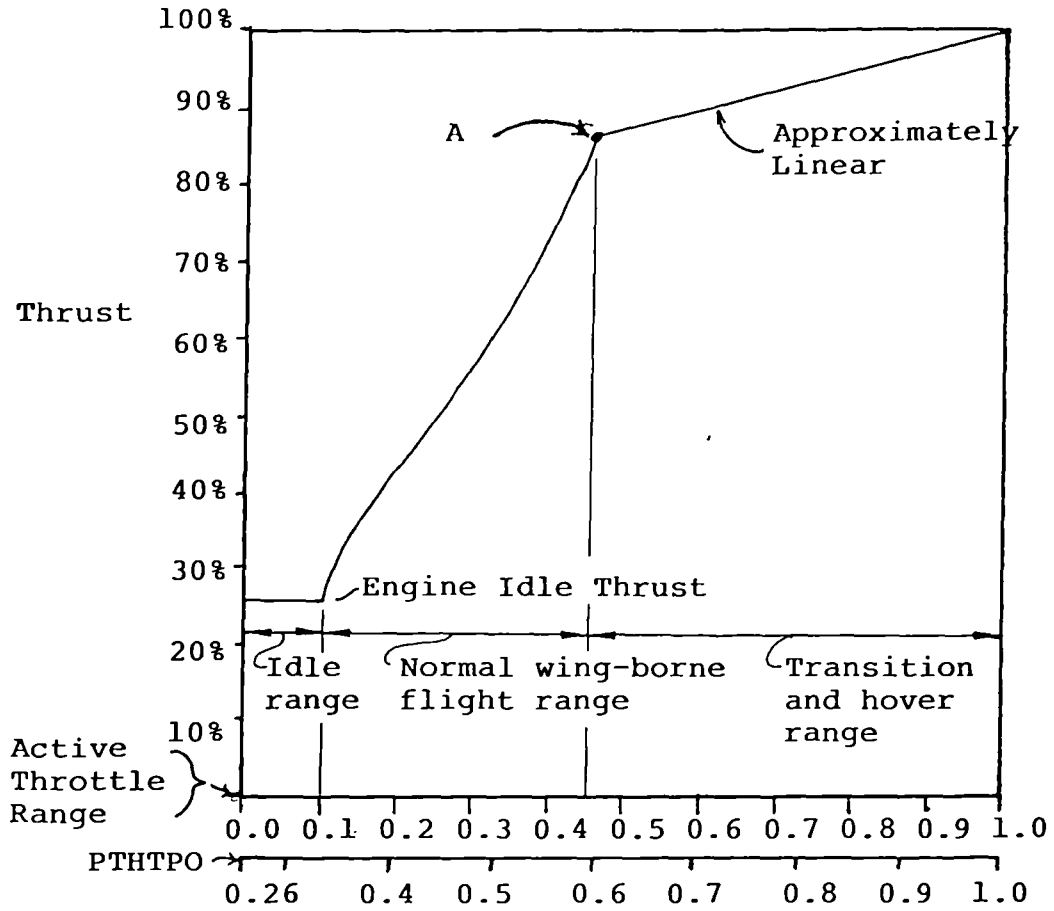


Figure (4.8) Throttle to Thrust Relationship

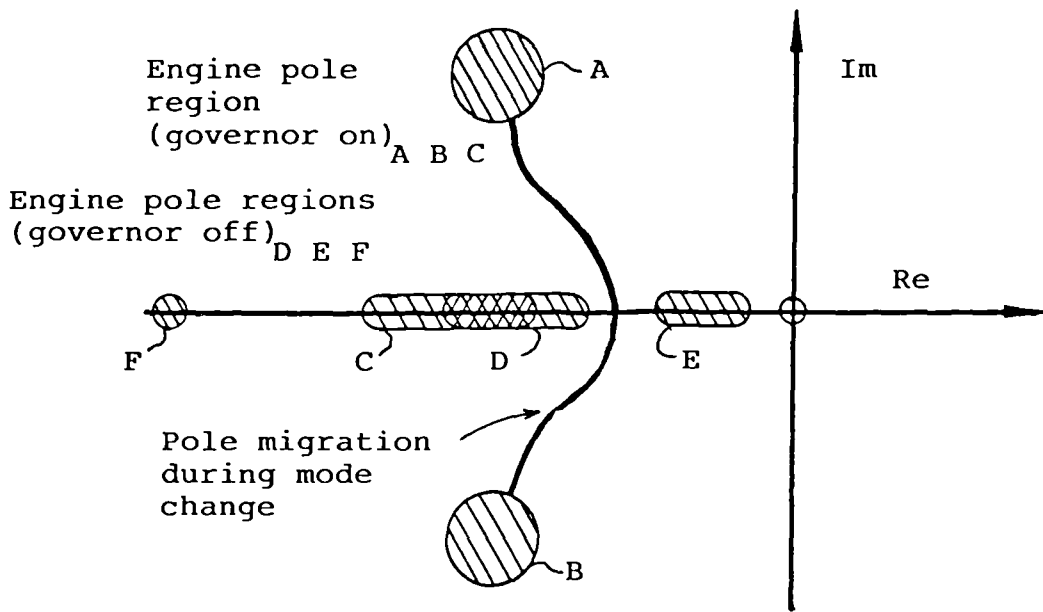


Figure (4.9) Engine Dynamic Changes Caused By the Engine Governor System

CHAPTER 5

APPLICATION OF THE HIGH-GAIN METHOD

TO V/STOL AIRCRAFT - CASE STUDIES

APPLICATION OF THE HIGH-GAIN METHOD TO

V/STOL AIRCRAFT - CASE STUDIES

5.1 Introduction

The purpose of this chapter is to bring together the high-gain method and the V/STOL aircraft GVAM87, which have been described in chapter 3 and chapter 4 respectively. The case studies will illustrate features of the high-gain method by example and will show how the new developments can be used. The calculation of results from the new developments are not shown as this was explained in chapter 3 with the aid of three worked examples (section 3.4). The case studies will also illustrate certain features of the aircraft model, but more importantly they will show what affect these features have on the controller design.

This chapter is divided into eight sections. Section 5.2 contains a definition of the flight case which is mainly used throughout this chapter and the reasons for this choice are explained. Section 5.3 contains a description of the way in which the basic plant (with no actuator dynamics) can be extracted from the full linearised model. The basic plant is then used for the first stage of the design which is described in section 5.4. In this section the main features of the basic high-gain method are illustrated.

In section 5.5 the engine dynamics are added and their effects upon the design are described. The other parasitic dynamics are then added and this is described in section 5.6. In both sections 5.5 and 5.6 the new developments are used to analyse the effects of adding the extra dynamics and to tune the resulting system. Section 5.7 contains a brief analysis of the controller's robustness by applying the

controller of section 5.6 to a different flight case.

A simple SISO technique for designing dynamic compensation for MIMO systems is described in section 5.8 illustrating a further aspect of the new developments. The last section (section 5.9) contains a demonstration of an important feature of the high-gain method which was defined at the start in section 1.1; the ability to work two ways. This refers to the concept of "working backwards" and defining the necessary hardware (actuator performance) from a desired system performance. The more usual method of "working forwards" from a design specification including the hardware description is important, but the ability also to "work backwards" means the design method is particularly suited to the early "paper" design stages for the fully integrated design of aircraft. This feature allows the control system designer to interact with a multi-disciplinary design team and to feed-back useful design information. It is the advent of CCV's that makes this especially important as the control laws are no longer an afterthought and the actuators together with the control laws define the aircraft handling qualities and performance.

Throughout this chapter, the designs are performed using a linear model and all results are derived using linear models also. Results using a non-linear model are described in chapter 8 where particular non-linear features are also demonstrated. In this chapter the design follows the steps given in section 3.7 and wherever steps are mentioned it refers to those given in section 3.7.

5.2 Flight Case Definition

In order to show the increased complexity that is inherent in V/STOL

aircraft, a transition flight case has been selected. Only the aircraft longitudinal dynamics are considered here and so all manoeuvres occur in the pitch plane. The longitudinal states and other variables which are used to describe the aircraft are given in table (5.1) below.

Table 5.1

Variable	Description
VKN	- Forward velocity (North) in earth axes (Ft/s)
VKD	- Vertical Velocity (down) in earth axes (Ft/s)
UB	- Forward velocity in body axes (Ft/s)
WB	- Vertical velocity in body axes (Ft/s)
THETR/THETD	- Pitch attitude (Rads)/(Deg)
Q/QD	- Pitch rate (Rads/s)/(Deg/s)
ALFAR/ALFAD	- Angle of attack or incidence (Rads)/(Deg)
GAMMAR/GAMMAD	- Flight path angle (Rads)/(Deg)
X	- Forward displacement (North) (Ft)
H	- Vertical displacement or height (Ft)
PTHPTO	- Throttle setting (%/100)
THDFPO	- Nozzle setting (Deg)
ETADO	- Tailplane setting (Deg)
FNP	- Low pressure fanspeed (%/100)
HNP	- High pressure fan speed (%/100)
QEF	- Fuel flow rate (Gal/hour)
AIRBRO	- Airbrake setting (%/100)
FLAPDO	- Flap angle (Deg)
AXCGF	- Horizontal acceleration of C.G. (g)
AZCGF	- Vertical acceleration of C.G. (g)
VT	- Total airspeed (Ft/s)
VTKT	- Total airspeed (Kts)

The flight condition chosen is for straight and level trimmed 1g flight at 120 Kts, at a height of 100 ft. The aircraft is pitched up at 8° relative to the earth which makes the angle of attack 8° also, as the flight path angle is zero. Full details of the flight case are given below in table (5.2).

TABLE 5.2

Variable	Value
VKN	202.5 Ft/s
VKD	0.0 Ft/s
THETR/THETD	0.1396 Rads/ 8° (Deg)
Q/QD	0.0 Rads/s / 0.0 Deg/s
ALFAR/ALFAD	0.1396 Rads/ 8.0° (Deg)
GAMMAR/GAMMAD	0.0 Rads/ 0.0 (Deg)
X	0.0 Ft
H	100.0 Ft
PTHTPO	0.6036 %/100
THDFPO	57.21° (Deg)
ETADO	4.141° (Deg)
FNP	0.8725 %/100
HNP	0.9233 %/100
QEF	984.8 Gall/Hr
AIRBRO	0.4 %/100
FLAPDO	50.0° (Deg)
AXCGF	0.0 g
AZCGF	0.0 g
VT	202.5 Ft/s
VTKT	120 Kts

At 8° angle of attack, in the default configuration, the aircraft will attain "wing-borne flight" at 167 Kts. In fact this is really the nozzles aft condition and not truly the fully wing-borne condition as the angle of attack implies that 14% of available thrust is still supporting the aircraft (i.e. Thrust & SIN (8°)). The wing and flaps generate aerodynamic lift as speed increases and at 120 Kts, the design case, the aerodynamic lift and the jet lift are nearly equal. The condition of exact equality between aerodynamic lift and jet lift was not sought, as there are additional reasons for choosing 120 Kts which are given below.

For the design flight condition the trimmed throttle setting places the engine dynamics at the end of the "governor on" linear throttle-to-thrust curve (close to point 'A' on Figure (4.8)). This enables the effects of gross engine non-linearities to be shown for a slightly "off-design" condition and a possible solution to the problem is then demonstrated using dynamic compensation (section 5.7). Furthermore the aircraft speed at this flight condition is sufficient for useful aerodynamic forces to be generated and the reaction controls are also operative (the nozzles are below 34° and the engine is at 60%, so the reaction controls are fully on and effective). The final point to note is that the nozzles are at 57° which, allowing for offsets, places the thrust vector at approximately 65° to the earth. Consequently, thrust changes will dominate the vertical motion and nozzle changes will dominate the horizontal motion. All of these factors combine to make this flight condition one of the most varied and interesting to study.

5.3 Derivation of the Basic Plant Dynamics

The step-by-step method begins with the derivation of a mathematical model of the plant and its systems. This step has already been achieved and is represented by the GVAM87. The second step of the method is the derivation of a linearised model from the full mathematical model and this is achieved through the use of the package TSIM. The third step of the method is the removal of the parasitic dynamics to leave just the basic system dynamics. This step is not straight forward in this case due to the structure of the GVAM87 and it is described here.

The GVAM87 has been developed, from the outset, as a representative V/STOL aircraft model. This means that the engine is a significant and integral part of the model and consequently it is not easy to separate the engine dynamics from the rigid body aircraft dynamics as required by step 3 of the method. In particular, it is not obvious what the direct effects of thrust changes are on the rigid body dynamics, whereas the direct force and moment effects of the nozzle and elevator are known. This difficulty is caused by the engine state space representation which does not contain a state representing thrust. Instead, the three main engine states are the low pressure fan spool speed FNP (normalised and non-dimensional), the high pressure fan spool speed HNP (normalised and non-dimensional) and the fuel flow rate QEF (gallons per hour (200-1300)). The relationship between these three states and the thrust is not available and so the direct thrust effects cannot be found from the composite state space system which includes the actuator dynamics (the composite state space system is given overleaf in Table (5.3) and was obtained directly from the non-linear model using the package TSIM). This is

Table (5.3).

The Open-Loop State Space Equations Representing Plant-2.

$$\begin{bmatrix} \text{THETR} \\ Q \\ \text{VKN} \\ \text{VKD} \\ \text{FNP} \\ \text{HNP} \\ \text{QEF} \end{bmatrix} = \begin{bmatrix} 0.0 & 1.0 & 0.0 & 0.0 & 0.0 & 0.0 & 0.0 & 0.0 & 0.0 & 0.0 & 0.0 & 0.0 & 0.0 \\ -2.3280e-1 & -3.9647e-1 & 2.9458e-3 & -1.1173e-3 & 1.0673e+0 & -1.1771e+0 & -1.3725e-4 & 0.0 & 0.0 & 0.0 & 0.0 & 0.0 & 0.0 \\ -5.5743e+1 & 2.4128e-2 & -5.4596e-2 & -1.1640e-1 & 1.0711e+1 & 4.8101e+0 & 1.5214e-3 & 0.0 & 0.0 & 0.0 & 0.0 & 0.0 & 0.0 \\ -5.6823e+1 & -1.8454e+0 & -1.6279e-2 & -2.8060e-1 & -3.0437e+1 & -8.3488e+0 & -2.7403e-3 & 0.0 & 0.0 & 0.0 & 0.0 & 0.0 & 0.0 \\ 0.0 & 0.0 & -1.9448e-5 & 0.0 & -3.7749e+0 & 2.5557e+0 & 7.1782e-4 & 0.0 & 0.0 & 0.0 & 0.0 & 0.0 & 0.0 \\ 0.0 & 0.0 & -6.1894e-5 & 0.0 & -5.8899e-3 & -2.7347e+0 & 5.2474e-4 & 0.0 & 0.0 & 0.0 & 0.0 & 0.0 & 0.0 \\ 0.0 & 0.0 & 2.6245e+0 & 0.0 & -8.6208e+4 & 1.3835e+2 & -1.3333e+1 & 0.0 & 0.0 & 0.0 & 0.0 & 0.0 & 0.0 \end{bmatrix} \begin{bmatrix} \text{PHTPA} \\ \text{THDFPA} \\ \text{ETADA} \end{bmatrix} + \begin{bmatrix} 0.0 & 0.0 & 0.0 & 0.0 & 0.0 & 0.0 & 0.0 & 0.0 & 0.0 & 0.0 & 0.0 & 0.0 & 0.0 \\ 0.0 & 0.0 & 2.6129e-3 & -1.2823e-1 & 0.0 & 0.0 & 0.0 & 0.0 & 0.0 & 0.0 & 0.0 & 0.0 & 0.0 \\ 0.0 & 0.0 & -3.9209e-1 & -9.8574e-2 & 0.0 & 0.0 & 0.0 & 0.0 & 0.0 & 0.0 & 0.0 & 0.0 & 0.0 \\ 0.0 & 0.0 & -6.7902e-2 & -3.9692e-1 & 0.0 & 0.0 & 0.0 & 0.0 & 0.0 & 0.0 & 0.0 & 0.0 & 0.0 \\ 0.0 & 0.0 & 0.0 & 0.0 & 0.0 & 0.0 & 0.0 & 0.0 & 0.0 & 0.0 & 0.0 & 0.0 & 0.0 \\ 0.0 & 0.0 & 0.0 & 0.0 & 0.0 & 0.0 & 0.0 & 0.0 & 0.0 & 0.0 & 0.0 & 0.0 & 0.0 \\ 2.4399e+4 & 0.0 & 0.0 & 0.0 & 0.0 & 0.0 & 0.0 & 0.0 & 0.0 & 0.0 & 0.0 & 0.0 & 0.0 \end{bmatrix} \begin{bmatrix} \text{THEID} \\ \text{VTKT} \\ \text{GAMMAD} \end{bmatrix} = \begin{bmatrix} 5.7296e+1 & 0.0 & 0.0 & 0.0 & 0.0 & 0.0 & 0.0 & 0.0 & 0.0 & 0.0 & 0.0 & 0.0 & 0.0 \\ 0.0 & 0.0 & 5.9248e-1 & 0.0 & 0.0 & 0.0 & 0.0 & 0.0 & 0.0 & 0.0 & 0.0 & 0.0 & 0.0 \\ 0.0 & 0.0 & 0.0 & -2.8294e-1 & 0.0 & 0.0 & 0.0 & 0.0 & 0.0 & 0.0 & 0.0 & 0.0 & 0.0 \end{bmatrix} \begin{bmatrix} \text{THETR} \\ Q \\ \text{VKN} \\ \text{VKD} \\ \text{FNP} \\ \text{HNP} \\ \text{QEF} \end{bmatrix}$$

now described in more detail.

The basic system dynamics may be represented by state and output equations of the form

$$\dot{x}_{bs} = A_{bs} x_{bs} + B_{bs} u_{bs} \quad \dots (5.1)$$

and

$$y_{bs} = C_{bs} x_{bs} \quad \dots (5.2)$$

where the basic system state vector is x_{bs} , the basic system input vector is u_{bs} , the basic system output vector is y_{bs} and the state space triple (A_{bs}, B_{bs}, C_{bs}) are of conformable dimensions. Similarly, the dynamics of the actuators may be represented by state and output equations of the form

$$\dot{x}_a = A_a x_a + B_a u_a \quad \dots (5.3)$$

and

$$y_a = C_a x_a \quad \dots (5.4)$$

where the actuator state vector is x_a , the actuator input vector is u_a , the actuator output vector is y_a and the state space triple (A_a, B_a, C_a) are also of conformable dimensions. If the actuators are put in series with the basic system, such that the actuator output vector becomes the basic system input vector, then a composite system is formed. This composite system has u_a as its input vector, y_{bs} as its output vector and the relationship.

$$u_{bs} = y_a \quad \dots (5.5)$$

connecting the two components of the composite system. Substituting (5.5) and (5.4) into (5.1) and rewriting the equations of the composite system yields

$$\dot{x}_{CS} = A_{CS} x_{CS} + B_{CS} u_{CS} \quad \dots (5.6)$$

and

$$y_{CS} = C_{CS} x_{CS} \quad \dots (5.7)$$

where

$$x_{CS} = \begin{bmatrix} x_a \\ x_{bs} \end{bmatrix} ; \quad \dots (5.8)$$

$$u_{CS} = u_a ; \quad \dots (5.9)$$

$$y_{CS} = y_{bs} . \quad \dots (5.10)$$

$$A_{CS} = \begin{bmatrix} A_{bs} & B_{bs}C_a \\ 0 & A_a \end{bmatrix} ; \quad \dots (5.11)$$

$$B_{CS} = [0] \quad \dots (5.12)$$

and

$$C_{CS} = [C_{bs} \ 0] . \quad \dots (5.13)$$

The composite linear system ((5.6)to(5.13)) is very similar to the composite linear system which is derived from the GVAM87 using TSIM. Indeed the GVAM87 composite linear system may be partitioned so that it corresponds to the system given by (5.6)to(5.13) except that the block A_{CS} (2,1) given by (5.11), may not be null for the GVAM87 derived model. This is caused by the linearisation algorithm of TSIM which senses the effect of forward speed on the engine dynamics (changes in forward speed will affect the air inlet conditions and hence the engine dynamics) and causes the block A_{CS} (2,1) to be

non-zero, though negligible.

It is now possible to define the problem exactly. The design method requires the information contained within the matrix B_{bs} but the

designer in this case only has access to the GVAM87 derived composite linear system and hence the matrix $(B_{bs}C_a)$. Clearly then, B_{bs} is only known if C_a is exactly known. Taking this one actuator at a time, C_a is exactly known for the nozzle and the elevator but C_a is not known for the engine because the relationship between FNP, HNP, QEF and the thrust is not known. This problem may be solved by the assumption that the thrust effects of the engine are proportional to the low pressure fan speed effects (FNP). This fan speed has been normalised by the normal-running maximum fan speed (the engine can be overdriven) and so its range is from a minimum value (engine idle speed) to approximately 1.0.

Consequently C_a may take the form

$$C_a = [K_e \ 0 \ 0] \quad \dots \quad (5.14)$$

where

$$x_a = \begin{bmatrix} \text{FNP} \\ \text{HNP} \\ \text{QEF} \end{bmatrix} \quad \dots \quad (5.15)$$

and K_e is a scalar constant

This in turn defines $B_{bs}K_e$, for the engine thrust effects only, as the first four elements of column 5 of the A matrix given by Table (5.3). Therefore B_{bs} , for the engine thrust effects only, may be written as

$$B_{bs} = \begin{bmatrix} 0 \\ (1.0673e+0)/K_e \\ (1.0711e+1)/K_e \\ (-3.0437e+1)/K_e \end{bmatrix} \quad \dots \quad (5.16)$$

The value of K_e is not known exactly at this stage and it cannot be calculated from the data that is already available due to the structure of the model. However, it may easily be found by applying the, "gain magnitude" results described in section 3.5, as will be shown in subsection 5.5.1. The objective is that K_e is set to a value that gives a steady state engine gain of 1.0, which is equivalent to the condition

$$C_a (-A_a)^{-1} B_a = 1 \quad \dots (5.17)$$

that applies to all actuators added to the basic system when using the high gain method (in (5.17) A_a , B_a and C_a represent the plant, input and output matrices, respectively, for an actuator). This means that although the thrust effects may be considered to be proportional to the FNP effects, they are unlikely to be identical. Calculating K_e , as described above, will remove any discrepancies caused by this assumption and will ensure that the engine dynamics satisfy the unity steady state gain conditions.

As explained above, a value for K_e will be calculated in subsection 5.5.1,, and it is only important at that stage. For the purpose of the initial examples in section 5.4, $K_e = 1.0$ will be used. This enables the basic plant dynamics to be derived as given by (5.1) where x_{bs} , u_{bs} , A_{bs} and B_{bs} are given by

$$x_{bs} = \begin{bmatrix} \text{THETR} \\ Q \\ \text{VKN} \\ \text{VKD} \end{bmatrix} \quad \dots (5.18)$$

$$u_{bs} = \begin{bmatrix} \text{PTHTPO} \\ \text{THDFPO} \\ \text{ETADO} \end{bmatrix} \quad \dots (5.19)$$

$$A_{bs} = \begin{bmatrix} 0 & 1.0000 & 0 & 0 \\ -2.3280e-1 & -3.9647e-1 & 2.9458e-3 & -1.1173e-3 \\ -5.5743e+1 & 2.4128e-2 & -5.4596e-2 & -1.1640e-1 \\ -5.6823e+1 & -1.8454e+0 & -1.6279e-2 & -2.8060e-1 \end{bmatrix} \dots (5.20)$$

and

$$B_{bs} = \begin{bmatrix} 0 & 0 & 0 \\ 1.0673e+0 & 2.6129e-3 & -1.2823e-1 \\ 1.0711e+1 & -3.9209e-1 & -9.8574e-2 \\ -3.0437e+1 & -6.7902e-2 & -3.9692e-1 \end{bmatrix} \dots (5.21)$$

NB B_{bs} here represents the input matrix for all three inputs and not just the engine thrust effects.

In order to distinguish the basic plant dynamics from other plants used later, the basic plant will be referred to as Plant-1.

Results obtained using the above assumption have been very good, but the results could possibly be improved if the correct relationship between FNP, HNP, QEF and thrust could be found. It is important to note, however, that the manipulations described in this section are only necessary when the force and moment effects of the actuators cannot be obtained directly from the model.

5.4 Application of the Design Method to the Basic Plant Dynamics

(Plant 1)

5.4.1 Case 1

The plant-1 dynamics are given by equations (5.18), (5.19), (5.20) and (5.21) and it is clear that the basic system is already in the form of equation (3.1) if

$$x_1 = [\text{THETR}] \quad \dots (5.22)$$

and

$$x_2 = \begin{bmatrix} Q \\ \text{VKN} \\ \text{VKD} \end{bmatrix} \quad \dots (5.23)$$

Using the same notation as section 3.3 it is clear that the number of states (n) is 4, therefore n=4. Furthermore from equation (5.19) it is clear that the number of inputs (m) is 3, therefore m=3.

Step 5

The objective has been given as control of QD, VKN and VKD. However, QD (the pitch rate in degrees per second) is not a state variable whilst Q (the pitch rate in radians per second) is a state variable. Fortunately, a simple conversion may be used whereby QD = 57.296*Q as 57.296 is the conversion factor from radians to degrees. The output matrix can now be defined as

$$C = \begin{bmatrix} 0 & 57.296 & 0 & 0 \\ 0 & 0 & 1 & 0 \\ 0 & 0 & 0 & 1 \end{bmatrix} \quad \dots (5.24)$$

Step 6

The matrix $C_2B_2 \in \mathbb{R}^{3 \times 3}$ can easily be calculated from (5.24) and (5.21) and the rank of C_2B_2 in this case is 3. As C_2B_2 is therefore full rank, there is no need for any extra measurements. This being so, it is clear that $F_2 = C_2$ and $F_1 = C_1$ and so from (3.33), for $m = 3$, the asymptotic transfer function may be written as

$$G(s) = \begin{bmatrix} \frac{g\sigma_1}{s+g\sigma_1} & , & 0 & , & 0 \\ 0 & , & \frac{g\sigma_2}{s+g\sigma_2} & , & 0 \\ 0 & , & 0 & , & \frac{g\sigma_3}{s+g\sigma_3} \end{bmatrix} \dots (5.25)$$

which indicates three fast modes (pitch rate, forward speed and vertical speed).

Step 7

The transmission zeros are then calculated giving one at the origin. This would normally indicate a marginally stable system which is undesirable, but in this case it is merely a consequence of the kinematic relationship between pitch attitude and pitch rate and it causes no problem. The basic system is also controllable and observable and so there are no decoupling zeros. Hence, the set of system zeros is {0} which is the set of transmission zeros, as described at the end of subsection 3.2.1. Consequently, the system zeros present no hinderance to the design.

Step 8

From (3.29) and (3.30) it is possible to calculate the two controller matrices. It is clear that with no extra measurements $F_2 = C_2$ and so

$$K_p = (C_2 B_2)^{-1} \Sigma \dots (5.26)$$

giving

$$K_p = \begin{bmatrix} 1.4429e-3, & 5.4089e-3, & -2.8052e-2 \\ 7.0254e-2, & -2.4017, & -7.0398e-1 \\ -1.2267e-1, & -3.9186e-3, & -2.4783e-1 \end{bmatrix}$$

$$* \begin{bmatrix} \sigma_1 & 0 & 0 \\ 0 & \sigma_2 & 0 \\ 0 & 0 & \sigma_3 \end{bmatrix} \quad \dots (5.27)$$

and also that

$$K_I = (C_2 B_2)^{-1} \Sigma \Xi \quad \dots (5.28)$$

$$K_I = \begin{bmatrix} 1.4429e-3, & 5.4089e-3, & -2.8052e-2 \\ 7.0254e-2, & -2.4017, & -7.0398e-1 \\ -1.2267e-1, & -3.9186e-3, & -2.4783e-1 \end{bmatrix}$$

$$* \begin{bmatrix} \sigma_1 & 0 & 0 \\ 0 & \sigma_2 & 0 \\ 0 & 0 & \sigma_3 \end{bmatrix} * \begin{bmatrix} \rho_1 & 0 & 0 \\ 0 & \rho_2 & 0 \\ 0 & 0 & \rho_3 \end{bmatrix} \quad \dots (5.29)$$

These matrices together with values for Σ , Ξ and g will completely define the controller as given by (3.4). Furthermore, the controller in series with the plant-1 system will add three transmission zeros as defined by (3.32) and they will be at $-\rho_1$, $-\rho_2$ and $-\rho_3$.

Steps 9 and 10

For this simple illustrative example the parameters Σ , Ξ and g will not be tuned to achieve any specific criteria. Instead, each parameter will be varied to show what effect it has on the closed-loop system.

Effects of g

The simplest way of examining the effects of the feedback gain g on the closed-loop system is to plot the eigenvalues of the closed-loop

system as this parameter increases, while $\Sigma = \Xi = I_3$. Figure (5.1) shows this root-locus for the plant-1 as g varies from 0.0 to 7.0 in steps of 0.1. The open-loop poles ($g = 0$) and a set of closed-loop poles ($g = 7$) are given below in table (5.4).

Table 5.4

open loop ($g = 0$)	closed-loop $g = 7.0$
$-1.0663e-2 + 5.0472e-1j$	-6.3117) Asymptotic "fast"
$-1.0663e-2 - 5.0472e-1j$	-6.1295) poles tending
-0.49357	-5.7896) to $-g$ (-7.0)
-0.21676	0.0
0.0)	-1.2517) 'Slow' poles
0.0) due to the	-1.1498) heading for
0.0) integrators	-1.0995) zeros at -1.0

The open-loop poles are marked on Figure (5.1) and from there it is possible to see that the two lightly damped poles form pole pair a, the pole at -0.21676 joins one of the poles at the origin and forms pole pair b and that the pole at -0.49357 joins another of the poles at the origin to form pole pair c. Each of the pole pairs a, b and c rejoin the real axis beyond the transmission zeros at -1.0 and each pole pair splits, one heading towards the transmission zeros and the other forming one of the three first-order asymptotes. Clearly, the dynamic modes represented by the "fast" poles (or asymptotes) become increasingly stable as $g \rightarrow \infty$. The third open-loop pole at the origin does not move and is cancelled by the transmission zero at the origin.

This simple root-locus structure was predicted by the high-gain technique theory and is a consequence of the choice of gain matrices. Furthermore, the diagram is representative of three SISO second-order root-loci overlaid on one diagram. It is also obvious from Figure (5.1) that the closed-loop dynamics have split into "fast" and "slow" modes with only moderate feedback gains (each pole pair has rejoined the real axis and began to separate into "fast" and "slow" modes for $g > 4.2$).

Other effects of increasing the feedback gain may be confirmed by examining the frequency response of the closed-loop transfer function matrix. This frequency response has been generated for $\Sigma = \Xi = I_3$ and for $g = 2.5, 5.0$ and 10.0 as shown in Figure (5.2). Diagram (1) of Figure (5.2) shows the response, to a pitch rate demand, of each of the three outputs. The forward speed and vertical speed outputs are almost identical and are consequently overlaid. This diagram corresponds to the first column of the transfer function matrix and columns 2 and 3 correspond to diagrams (2) and (3) respectively. A key is given on Figure (5.2) identifying each curve.

Before examining the figure it is necessary to define the term "bandwidth". The bandwidth of a response is defined here as the frequency at which the response drops below -3dB , having been above -3dB at all lower frequencies. It is a measure of speed-of-response. Table (5.5) below lists the bandwidths of each response shown in Figure (5.2).

Table 5.5

Response	Bandwidths		
	$g = 2.5$	$g = 5.0$	$g = 10.0$
Pitch rate (Deg/s)	3.18	5.65	10.62
Forward speed (Ft/s)	3.40	5.92	10.93
Vertical speed (Ft/s)	3.21	5.72	10.71

Table (5.5) shows that the bandwidth of each diagonal transfer function element increases as the feedback gain increases, and also that the bandwidth is proportional to the feedback gain. This feature illustrates exactly (5.25) which gives the asymptotic transfer function matrix. It is also clear that the correlation between feedback gain and bandwidth improves as the feedback gain increases; this is due to the closed-loop system becoming more like the asymptotic system as $g \rightarrow \infty$.

The figure also shows that the cross coupling reduces as the feedback gain increases, as evidenced by the curves representing off-diagonal transfer function elements. The forward and vertical speed demands both produce negligible cross coupling where the cross coupling is still below -20dB even at the peak (-20 dB represents 10%, but as the system is not non-dimensional it represents 1/10th of a degree per second or 1/10th of a foot per second). However, the pitch rate demand exhibits relatively high cross coupling at low frequencies which falls below -20dB for feedback gains greater than 10.0. This strong cross coupling between pitch rate and speed at low frequencies is natural in aircraft dynamics, especially where these speeds are

represented in earth axes. Despite this it is interesting to note that for $g = 2.5$ the cross coupling at low frequency is -9dB which corresponds to 0.35 ft/s change in speed in response to 1.0 deg/s of pitch rate and a 0.35 ft/s perturbation is negligible at 202.5 ft/s (less than 0.2%).

The main effects of increasing the feedback gain may also be observed by examining the time response of the closed-loop system. Although step inputs are neither practical nor realistic in real systems, they are used here with linear models as they give an idea of the maximum speed of response and also because a step response excites all frequencies. The step response of the transfer function matrix is shown as Figure (5.3) and it shows how the speed of response of the system becomes faster as the feedback gain increases. The cross coupling due to speed demands is negligible as shown by diagram (2) and (3), but the cross coupling due to a pitch rate demand is more evident (diagram (1)). However, it should be remembered that this represents 0.35 ft/s speed perturbation for each 1.0 deg/s of pitch rate. The forward and vertical speed cross coupling is identical in diagram (1) and the two curves are overlaid, both nearing zero as the feedback gain increases.

Effects of Σ

The effects of Σ are identical to the effects of g , but the effects are manifest on each control-mode individually as each individual diagonal element of Σ is changed. This may be illustrated by a frequency response in which the feedback gain is 2.5 , $\Xi = I_3$ and σ_2 is varied as 1.0 , 2.0 and 4.0 as shown by Figure (5.4). This figure shows that the bandwidth of the middle diagonal transfer function

element has increased in the same way that it did when the feedback gain was varied in Figure (5.2). The bandwidth for $\sigma_2 = 1.0, 2.0$ and 4.0 for $g = 2.5$ corresponds exactly to the bandwidth for $g = 2.5, 5.0$ and 10.0 respectively, the values being identical to those given in table (5.5). This confirms the validity of the asymptotic transfer function matrix of (5.25) which gives the forward speed diagonal transfer function element as

$$G_{22}(s) = \frac{g\sigma_2}{s+g\sigma_2} \quad \dots (5.30)$$

This figure also shows that the cross coupling of pitch rate into forward speed (diagram (1)) and of vertical speed into forward speed (diagram (3)) has been reduced as σ_2 increases. Furthermore, other cross coupling terms in these two diagrams have remained unchanged showing that σ_2 only affects the forward speed mode, and cross coupling into it.

Finally, this figure shows that the cross coupling from forward speed to pitch rate and vertical speed (diagram (2)) has increased, as σ_2 has increased, at high frequencies ($\omega > 3$ rads/s). This is due to the increase in forward speed bandwidth at these frequencies for $\sigma_2 = 2.0$ and 4.0 . The increase in bandwidth places greater demands upon the whole system and produces an increase in cross coupling at these frequencies.

Effects of Ξ

The effects of increasing individual Ξ elements is to increase the amount of integral action present on that control channel. These effects are most easily illustrated using a step response and this is

shown as Figure (5.5) for $\Sigma = I_3$, $g = 2.5$ and for $\rho_1 = \rho_2 = 0.2, 1.0$ and 5.0 and $\rho_3 = 1.0$ throughout. The middle condition where $\rho_1 = \rho_2 = \rho_3 = 1.0$ and $g = 2.5$ is identical to the $g = 2.5$ condition in Figure (5.3). This figure shows that the diagonal transfer function element of vertical speed (diagram (3)) does not change whilst the other two diagonal transfer function elements (diagram (1) and (2)) have altered.

This figure also shows that for $\rho_2 = 0.2$ the forward speed step response has less overshoot than for $\rho_2 = 1.0$ or $\rho_2 = 5.0$. The pitch rate step response shows similar characteristics but it also shows a reduction in steady state tracking for $\rho_1 = 0.2$. To the other extreme, $\rho_1 = 5.0$ gives very good steady state tracking and also gives a lightly damped oscillatory response. An oscillatory response is also produced by $\rho_2 = 5.0$.

This figure illustrates another feature which is clear from diagram (1), but not diagrams (2) and (3), as diagram (1) shows greater levels of cross coupling. The cross coupling from pitch rate to vertical speed remains unchanged throughout but the cross coupling from pitch rate to forward speed reduces as ρ_2 increases.

The reason for the oscillatory response when $\rho_1 = \rho_2 = 5.0$ may be illustrated with the aid of a root-locus as shown by Figure (5.6) for $\Sigma = \Xi = I_3$ and for g varying from 0.0 to 0.7 in steps of 0.1 . It should be remembered that this particular condition will produce two transmission zeros at -5.0 as defined by (3.32). Accordingly, two of the pole pairs, a and c , do not move towards the real axis like before (Figure (5.1)), but are "pushed out" by the presence of the two zeros at -5.0 . The dashed lines indicate the previous root-locus

from Figure (5.1), and Figure (5.6) is produced for the same range of feedback gains. The two pole pairs a and c clearly form lightly damped oscillatory modes for a large range of gains and the actual position for $g = 2.5$ is marked on Figure (5.6). The natural frequency and damping of each mode is respectively 3.5925 Rads/s and 0.35386 for the pitch rate mode and 3.5109 rads/s and 0.41492 for the forward speed mode which is confirmed by the step responses of Figure (5.5). This figure also shows how the high-gain controller splits the root-locus into several SISO layers. Although pole pair b have formed a slightly different pattern to that displayed in Figure (5.1), they clearly show the same behaviour that they displayed in Figure (5.1). It is as if the two "layers" containing pole pairs a and c have been "peeled back" to reveal pole pair b. The coupling between "layers" at low gain is evidenced by the change in the locus shape for pole pair b. It is caused by the change in position of the pole pair c which previously interacted with the pole pair b, forcing them further from the zeros at -1.0.

This case study has illustrated the effects of g , Σ and Ξ and also shown the validity of certain theoretical results from Chapter 3. Furthermore, the decomposition of the closed-loop system has been shown to occur for quite moderate gains, despite using the "high-gain" theory! The next case study illustrates the conditions where extra measurements are required.

5.4.2. Case 2

The objective here is to give the pilot direct non-interacting control of the pitch attitude (THETA), the forward speed (VTKT) and the flight path angle (GAMMA).

Step 4

The plant-1 system dynamics are given by equations (5.18), (5.19), (5.20) and (5.21) and it is clear that the plant-1 system is already in the form of (3.2) if once again,

$$x_1 = [\text{THETR}] \quad \dots (5.31)$$

and

$$x_2 = \begin{bmatrix} Q \\ VKN \\ VKD \end{bmatrix} \quad \dots (5.32)$$

Using the same notations section 3.3 it is clear that as before $n = 4$ and $m = 3$.

Step 5

The objective has been given as control of THETD, VTKT and GAMMAD, none of which are state variables. This does not present any problems providing that the desired output variable can be expressed as a linear combination of the state variables. The relationship between THETD and THETR is the radians to degrees conversion constant and the relationship between VTKT and VKN is the ft/s to knots conversion constant, providing that the aircraft is in straight and level flight. The conversion for GAMMAD is not so straight forward as the conversion factor will be speed dependant even in straight and level flight. Furthermore, VTKT and GAMMAD both become functions of VKN and VKD when the flight path is no longer straight and level. This would result in a C matrix as follows

$$C = \begin{bmatrix} C_{11} & 0 & 0 & 0 \\ 0 & 0 & C_{23} & C_{24} \\ 0 & 0 & C_{33} & C_{34} \end{bmatrix} \quad \dots (5.33)$$

where c_{23} , c_{24} , c_{33} and c_{34} could vary with flight condition. This variation in the C matrix would be paralleled by variations in the B matrix and both can be handled by gain scheduling, as will be described in Chapter 7.

The package TSIM produces a linear model from the full non-linear model utilising small perturbation theory and consequently it is possible to obtain C matrices for any flight condition where the desired output variables are calculated in the model. From TSIM the C matrix for this flight condition was given as

$$C = \begin{bmatrix} 57.296 & 0 & 0 & 0 \\ 0 & 0 & 0.59248 & 0 \\ 0 & 0 & 0 & -0.28294 \end{bmatrix} \quad \dots (5.34)$$

which can be verified as follows. The conversion factor from radians to degrees is 57.296 and the conversion factor from ft/s to knots is 0.59248, both to five significant figures. The conversion from VKD to GAMMAD (K_{con}) is

$$K_{con} = -ARCTAN \left(\frac{1}{202.5} \right) \text{ Deg}/(\text{Ft/s}) \quad \dots (5.35)$$

where 202.5 is the forward speed in feet per second and the ARCTAN is in degrees. This gives $-0.28294 \text{ Deg}/(\text{Ft/s})$ and the negative sign is to maintain conventions; VKD is positive down whereas GAMMAD is positive up.

Step 6

The matrix $C_2 B_2 \in R^{3 \times 3}$ is calculated from equations (5.21) and

(5.34). The rank of C_2B_2 is found to be 2 which demonstrates that C_2B_2 is not full rank (a rank defect of 1) and so extra measurements are needed. It is obvious why C_2B_2 has a rank defect of one when C_2 and B_2 are examined and they are written symbolically below for this purpose:

$$C_2 B_2 = \begin{bmatrix} 0 & 0 & 0 \\ 0 & c_{23} & 0 \\ 0 & 0 & c_{34} \end{bmatrix} \times \begin{bmatrix} b_{21} & b_{22} & b_{23} \\ b_{31} & b_{32} & b_{33} \\ b_{41} & b_{42} & b_{43} \end{bmatrix} \dots (5.36)$$

Clearly, $C_2 B_2$ is rank defective due to c_{12} being zero.

Equation (3.10) gives the formula for F where in this case M is a real 3×1 matrix written as

$$M = \begin{bmatrix} M_1 \\ M_2 \\ M_3 \end{bmatrix} \dots (5.37)$$

and the matrices A_{11} and A_{12} are found from (5.20) to be

$$A_{11} = [0] \dots (5.38)$$

and

$$A_{12} = [1 \ 0 \ 0], \dots (5.39)$$

such that

$$[F_1, F_2] = \left[\begin{bmatrix} c_{11} \\ 0 \\ 0 \end{bmatrix} + \begin{bmatrix} m_1 \\ m_2 \\ m_3 \end{bmatrix} [0], \begin{bmatrix} 0 & 0 & 0 \\ 0 & c_{23} & 0 \\ 0 & 0 & c_{34} \end{bmatrix} + \begin{bmatrix} m_1 \\ m_2 \\ m_3 \end{bmatrix} [1 \ 0 \ 0] \right] \dots (5.40)$$

or rather

$$[F_1, F_2] = \left[\begin{bmatrix} c_{11} \\ 0 \\ 0 \end{bmatrix} \quad \begin{bmatrix} m_1 & 0 & 0 \\ m_2 & c_{23} & 0 \\ m_3 & 0 & c_{34} \end{bmatrix} \right] \dots (5.41)$$

The requirement from (3.13) is that $F_2 B_2$ be full rank which will be so if $m_1 \neq 0$, by comparison with (5.36). To simplify the result, only m_1 will be non-zero here and $m_2 = m_3 = 0$ will be used as there is no need to introduce extra measurements onto the speed and flight path feedback signals. Only the pitch attitude output requires extra measurement compensation in this case.

With extra measurements being used, the feedback equation is taken from (3.3) as

$$w(t) = F x(t) \quad \dots (5.42)$$

which may be represented as

$$w(t) = \begin{bmatrix} 57.296 & m_1 & 0 & 0 \\ 0 & 0 & 0.59248 & 0 \\ 0 & 0 & 0 & -0.28294 \end{bmatrix} \begin{bmatrix} \text{THETR} \\ Q \\ \text{VKN} \\ \text{VKD} \end{bmatrix} \quad \dots (5.43)$$

and rewritten as

$$w(t) = \begin{bmatrix} \text{THETD} + m_1 x Q \\ \text{VTKT} \\ \text{GAMMAD} \end{bmatrix} \quad \dots (5.44)$$

Equation (5.43) clearly shows the presence of extra measurements on the pitch attitude channel only, and that the extra measurement is pitch rate. This shows that whilst extra measurement are based upon matrix algebra, the final result is analogous to a classical SISO solution to a similar problem, as described in Chapter 3.

Next, in order to make the units of (5.44) consistent, QD will be fed back instead of Q and so F_2 becomes

$$F_2 = \begin{bmatrix} m_1 * 57.296 & 0 & 0 \\ 0 & 0.59248 & 0 \\ 0 & 0 & -0.28294 \end{bmatrix} \dots (5.45)$$

Finally, substituting F_1 , F_2 , C_1 and C_2 into (3.33) the resulting asymptotic transfer function matrix may be written as

$$G(s) = \begin{bmatrix} \frac{1/m_1}{s+1/m_1} & 0 & 0 \\ 0 & \frac{g\sigma_2}{s+g\sigma_2} & 0 \\ 0 & 0 & \frac{g\sigma_3}{s+g\sigma_3} \end{bmatrix} \dots (5.46)$$

which clearly indicates that there will be two "fast" modes (forward speed and flight path angle) and one "slow" mode (pitch attitude).

Step 7

The transmission zeros can be calculated algebraically for this case study and it may be shown that there is one transmission zero for the plant-1 system in this case, with extra measurement feedback of pitch rate on the pitch attitude channel. This basic system is also controllable and observable and so there are no decoupling zeros. Hence the set of system zeros is equal to the set of transmission zeros which is $\{-1/m_1\}$. Furthermore, the fact that choosing M also influences the transmission zeros was mentioned at the very end of subsection 3.3.3 and this feature has now been demonstrated. The system zeros present no hindrance to the design if $m_1 \in \mathbb{R}^+$.

Step 8

From (3.29) and (3.30) the two controller matrices can be calculated for $m_1 = 1.0$ as follows:

$$K_p = (F_2 B_2)^{-1} \Sigma \quad \dots (5.47)$$

giving

$$K_p = \begin{bmatrix} 1.4429e-3 & 9.1293e-3 & 9.9145e-2 \\ 7.0254e-2 & -4.0336 & 2.4881 \\ -1.2267e-1 & -6.6139e-3 & 8.7590e-1 \end{bmatrix}$$

$$* \begin{bmatrix} \sigma_1 & 0 & 0 \\ 0 & \sigma_2 & 0 \\ 0 & 0 & \sigma_3 \end{bmatrix} \quad \dots (5.48)$$

and

$$K_I = (F_2 B_2)^{-1} \Sigma \Xi \quad \dots (5.49)$$

giving

$$K_I = \begin{bmatrix} 1.4429e-3 & 9.1293e-3 & 9.9145e-2 \\ 7.0254e-2 & -4.0336 & 2.4881 \\ -1.2267e-1 & -6.6139e-3 & 8.7590e-1 \end{bmatrix}$$

$$* \begin{bmatrix} \sigma_1 & 0 & 0 \\ 0 & \sigma_2 & 0 \\ 0 & 0 & \sigma_3 \end{bmatrix} \quad * \begin{bmatrix} \rho_1 & 0 & 0 \\ 0 & \rho_2 & 0 \\ 0 & 0 & \rho_3 \end{bmatrix} \quad \dots (5.50)$$

Once again, these two matrices, together with values for Σ , Ξ , g and m_1 will completely define the controller as given by (3.4). Furthermore, the controller in series with the plant-1 system will add three transmission zeros as defined by (3.32) and they will be at $-\rho_1$, $-\rho_2$, and $-\rho_3$. Finally, the implication of the above equation is that K_p and K_I have to be recalculated for every new value of m_1 .

This could become tedious when tuning the controller. However, for many cases F_2 may be rewritten due to the diagonal nature of MA_{12} (which very often occurs) and the fact that F_2 and B_2 are often individually invertible. For example, $(F_2 B_2)^{-1} \Sigma$ may be rewritten as $(B_2^{-1} F_2^{-1}) \Sigma$ when both F_2 and B_2 are invertible. Next, F_2^{-1} may be rewritten as

$$F_2^{-1} = \begin{bmatrix} 1 & 0 & 0 \\ 0 & 0.59248 & 0 \\ 0 & 0 & -0.28294 \end{bmatrix}^{-1} * \begin{bmatrix} 1/m_1 & 0 & 0 \\ 0 & 1 & 0 \\ 0 & 0 & 1 \end{bmatrix} \dots (5.51)$$

taking F_2 from (5.43). This enables a general K_p to be defined for m_1 such that

$$K_p = \begin{bmatrix} 1.4429e-3 & 9.1293e-3 & 9.9145e-2 \\ 7.0254e-2 & -4.0336 & 2.4881 \\ -1.2267e-1 & -6.6139e-3 & 8.7590e-1 \end{bmatrix} * \begin{bmatrix} \sigma_1/m_1 & 0 & 0 \\ 0 & \sigma_2 & 0 \\ 0 & 0 & \sigma_3 \end{bmatrix} \dots (5.52)$$

and a similar equation may be derived for K_I . This is more general than the expression given by (5.48) and similar expressions to (5.52) can be derived in most cases. This makes programming of the controller easier, especially when gain scheduling m_1 , and avoids that on-line matrix inversion and all hazards that brings to flight safe software.

Steps 9 and 10

As for case 1, the parameters Σ , Ξ , g and m_1 will not be tuned to achieve any specific criteria but g and m_1 will be varied to

illustrate the effects that extra measurements have on the closed-loop system system.

Effects of g :

Figure (5.7) shows the root-locus for this closed-loop system for g varying from 0.0 to 7.0 in steps of 0.1 while $\Sigma = \Xi = I_3$ and $m_1 = 1.0$. This system has a different root-locus structure than that of case 1 due to the movement of the transmission zero from 0.0 to $-1/m_1$ (or -1.0 in this instance). This change gives the following root-locus structure. Pole pair a is formed from the two periodic lightly damped open-loop poles, pole pair b is formed from two of the integrator poles at the origin and pole pair c is formed from the open-loop pole at -0.21676 and the third integrator pole at the origin. Each pole pair moves beyond the four transmission zeros at -1.0 before rejoining the real axis where each pole pair splits up; one going to the zeros at -1.0 and one forming a first-order asymptote. The fourth open-loop rigid body aircraft pole is at -9.49357 and it moves towards the zeros at -1.0 completing the pattern. Clearly, the closed-loop system has again split into "fast" and "slow" subsystems for only moderate feedback gains. It is also possible to see the "layered" SISO effect as described previously.

Other effects of increasing the feedback gain may be confirmed by examining the frequency response of the closed-loop transfer function matrix. The frequency response has been generated for $\Sigma = \Xi = I_3$, $m_1 = 1$ and $g = 2.5, 5.0$ and 10.0 as shown in Figure (5.8). The forward speed and flight path angle diagrams ((2) and (3) respectively) compare almost exactly with their counterparts in Figure (5.2) and require no further explanation. Any small

differences are due to the fact that different quantities are involved and different units. The different units also account for the different levels of cross coupling from pitch attitude into forward speed and flight path angle, shown in diagram (1), which was identical to that shown in Figure (5.2).

The main feature of Figure (5.8) is that the bandwidth of the pitch attitude response is almost invariant under increasing feedback gain. Table (5.6) below shows the bandwidth of each response for each gain, similar to Table (5.5). Indeed the results for forward speed and flight path angle are identical to the forward and vertical speed responses respectively, showing the bandwidth characteristics to be independent of the units chosen for output variables.

Table (5.6)

Response	Bandwidth (Rad/s)		
	$g = 2.5$	$g = 5.0$	$g = 10.0$
Pitch Attitude (Deg)	1.64	1.23	1.09
Forward speed (Kts)	3.40	5.93	10.93
Flight Path Angle (Deg)	3.21	5.72	10.71

Clearly, although the forward speed and flight path angle responses behave as expected, the pitch attitude response is independent of gain and converges asymptotically to a bandwidth at 1.0 as $g \rightarrow \infty$. This obviously agrees with (5.44) exactly for $m_1 = 1.0$.

This may be illustrated further with the step response of the closed loop transfer function matrix shown by Figure (5.9) for $\Sigma = \Xi = I_3$,

$m_1 = 1$ and $g = 2.5, 5.0$ and 10.0 . Diagrams (2) and (3) show no change from their counterparts in Figure (5.3) with the speed of response increasing as the feedback gain increases. However, the pitch attitude response (Diagram (1)) shows little change due to feedback gain increases.

Another feature to be noted is that the shape of the forward speed and flight path angle step responses are first-order dominant, initially, with some "second-order-like" overshoot due to the integral action. Whereas the pitch attitude step response is second-order dominant from the start. This is confirmed by the fact that in Figure (5.8), both the forward speed and flight path angle responses drop off at -20 dB per decade after the bandwidth frequency, whereas the pitch attitude response drops off at -40 dB per decade.

Effects of m_1

The effects of m_1 are illustrated here with a frequency response of the closed-loop transfer function matrix for $\Sigma = \Xi = I_3$, $g = 2.5$ and $m_1 = 2.0, 1.0$ and 0.2 in Figure (5.10). This figure shows that the forward speed and flight path angle diagonal transfer function elements are not affected by m_1 changes (diagrams (2) and (3)). The off diagonal term representing flight path angle cross coupling into forward speed (diagram (3)), shows no change as m_1 decreases, but the cross coupling of forward speed into flight path angle (diagram (2)) shows a slight improvement at low frequencies due to m_1 decreases. This last feature is to be expected because pitch attitude and flight path angle are closely coupled and it is caused by the improved pitch attitude control as m_1 decreases.

This figure also shows (diagram (1)) that the pitch attitude response's bandwidth increases as m_1 decreases. The bandwidths of each response are given below in Table (5.7) for different values of m_1 .

Table (5.7)

Response	Bandwidth (Rad/s)		
	$m_1 = 2.0$	$m_1 = 1.0$	$m_1 = 0.2$
Pitch Attitude (Deg)	0.521	1.64	5.28
Forward Speed (Kts)	3.40	3.40	3.39
Flight Path Angle (Deg)	3.21	3.21	3.21

Clearly, the pitch attitude bandwidth is proportional to $1/m_1$ and this is found to become more exact, asymptotically, as $g \rightarrow \infty$. This confirms the validity of the asymptotic transfer function matrix given by (5.46) which gives the pitch attitude diagonal transfer function element as

$$G_{11}(s) = \frac{1/m_1}{s+1/m_1} \quad \dots (5.53)$$

The effect of insufficient gain (g) is shown by the $m_1 = 0.2$ case which is shown in diagram (1) to have a small resonant peak, typically a second-order feature. This has occurred because for $m_1 = 0.2$ the pitch control-mode needs a high gain in order to assume the asymptotic form of (5.53). This is discussed further when the root-locus for this case is shown.

Another feature to note is that the forward speed and flight path bandwidths are the same as those given in Case 1, Table (5.5), and the same relationships also apply (i.e. the relationship defined by (5.30)).

Finally, this figure shows that the cross coupling from pitch attitude into forward speed and flight path angle increases as m_1 decreases in diagram (1). This is because the increase in performance of the pitch attitude control at higher frequencies puts greater demands upon the whole system and it results in an increase in cross coupling.

These features are also illustrated using a step response of the transfer function matrix for $\Sigma = \Xi = I_3$, $g = 2.5$ and $m_1 = 2.0, 1.0$ and 0.2 in Figure (5.1). The forward speed and flight path angle responses (diagrams (2) and (3)) are unaffected by m_1 changes, whereas the pitch attitude response becomes faster as m_1 decreases. Indeed, for $m_1 = 0.2$ the pitch response is lightly damped and oscillatory, as shown previously by the resonant peak in the corresponding frequency response.

In order to show the reason for this lightly damped oscillatory mode, the root-locus for the system is given as Figure (5.12) for $\Sigma = \Xi = I_3$, $m_1 = 0.2$ and g varies from 0.0 to 7.0 in steps of 0.1 . The point which corresponds to $g = 2.5$ is marked and here the pitch attitude control-mode has a natural frequency of 3.66 (Rads/s) and a damping of 0.267 . This corresponds exactly to the time response given by Diagram (1) of Figure (5.11). Figure (5.12) shows how setting $m_1 = 0.2$ places a transmission zero at $(-1/0.2)$, or -5.0 , and it is this which causes pole pair a to move out around that zero and so

give a lightly damped control mode for $g = 2.5$. A higher gain would move this pole pair further along the root-locus until eventually the asymptotic form of (5.53), would be reached. This figure also illustrates the "layered" nature of the root-locus , the pitch attitude layer being "peeled back" to reveal the other two control-modes beneath. The slight change in the shape of the loci of pole pairs b and c, compared to their loci in Figure (5.7), is due to the interaction which occurs between control-modes (and "layers") at low feedback gain.

The case study has illustrated the effects of g and m_1 , the extra measurement gain, and shown the validity of further theoretical results from chapter 3. This completes the case studies that use the basic system dynamics only and which illustrate the fundamentals of the high-gain method. The next case studies illustrate the high-gain method as it relates to more realistic systems.

5.5 Controller Design with Engine Dynamics Included - Case 3

The objective here is the same as that for case 2, section 5.4.2. It is required that the pilot has direct control of the pitch attitude (THETAD), the forward speed (VTKT) and the flight path angle (GAMMAD). This case study covers step 11 of the method only, but it uses results from the previous worked example, steps 4 to 10, and so it is a continuation of that work. The analysis of the system and its subsequent tuning are described in subsections 5.5.1 and 5.5.2 respectively.

5.5.1 Analysis of the Asymptotic Root-Locus Structure for the Plant-2 System

The linear aircraft equations, including the engine parasitic dynamics, are given by Table (5.3). To distinguish this plant from the plant used in the previous two case studies it will be referred to a Plant-2. The output matrix used for this case study is the same as that used for case study 2 and is given by (5.34). Furthermore, the same extra measurements are taken and so the feedback matrix is given by (5.43) or (5.45). This in turn yields the same controller matrices as given by (5.48) and (5.50). For this case study the number of plant-2 states is 7 ($n=7$) and the number of inputs is 3 ($m=3$). The open-loop eigenvalues for the Plant-2 system in series with the controller are given below in Table (5.8) (note that adding the controller introduces three more states, three more poles and also three more transmission zeros, all due to the integrators).

Table (5.8)

Eigenvalues	Mode type
-1.0223e-2 +5.0457e-1 j -1.0223e-2 -5.0457e-1 j -4.9380e-1 -2.1716e-1	Aircraft rigid body modes
-7.4388 +5.4527 j -7.4388 -5.4527 j -4.9636	Engine modes
0 0 0	Integrator poles

Similarly, the transmission zeros of plant-2 are given below in Table (5.9)

Table (5.9)

Transmission Zeros	Source of the zeros
1.0	From the integrators, algebraically they are equal to $-\rho_1$, $-\rho_2$ and $-\rho_3$.
1.0	
-1.0	From the basic plant-1 dynamics, algebraically it is equal to $-1/m_1$.
-1.0	
-4.6760	From the engine dynamics
12.725	

The Markov parameters for this may easily be calculated according to (3.46) and it may be shown that the first Markov parameter has a rank defect of 1 ($d_1 = 1$) and that the following are of full rank ($d_2 = 0$ and therefore $v=2$). Equations (3.47) and (3.48) may then be used indicating that there are 6 finite zeros and 4 infinite zeros forming the closed-loop asymptotic structure. Further calculations shows that two of the infinite zeros are first-order ($d_0-d_1=2$) and two are second order $2(d_1-d_2)=2$. All of the infinite zeros, or asymptotes, conform to pattern A, shown in Figure (3.4).

The second-order pivot point may be approximated using (3.64) where

$$\overline{PP}_1 = ((-7.4388+5.4527j \ -7.4388-5.4527j \ -4.9656) - (-12.725 \ -4.6760 \ -1.0))/2 = -0.7211 \quad \dots (5.51)$$

The Pro Matlab function may also be used to calculate the asymptote characteristics and these are given below in Table (5.10).

Table (5.10)

Pro-Matlab		Equation (5.51)
Pivot Points	Asymptote order	Pivot Point Approximation
+0.4435	1	-
-0.070568	1	-
-0.9442	2	-0.7211

To confirm this asymptotic structure the root-locus of the system has been plotted and is shown as Figure (5.13) for g varying from 0.1 to 100.0 logarithmically while $\Sigma = \Xi = I_3$ and $m_1 = 1.0$. This figure also displays constant damping lines for damping ratios from 0.0 to 0.9 in steps of 0.1, where the imaginary axis corresponds to a damping ratio of 0.0 and the real axis corresponds to a damping ratio of 1.0 or more. From this figure it is possible to verify that the second-order asymptote and pivot point have been calculated correctly and that increasing the gain results in a system containing one lightly damped second-order control-mode. The other two control-modes are associated with the first-order asymptotes.

Now that the closed-loop system has been formed, it is necessary to check the engine dynamics to assess this actuator for compatibility with the design method (i.e. whether its steady state gain is 1.0). The correct actuator gain may be calculated using (3.71) from subsection 3.4.4. In this instance $n_p = 3$ and $n_z = 2$. The actual values for p_1, p_2, p_3, z_1 and z_2 may be taken from Table (5.9) to give

$$K_{ai} = \frac{[(7.4388)^2 + (5.4527)^2] \cdot (4.9636)}{(4.6760) \cdot (12.725)} = 7.0963 \quad \dots (5.54)$$

Next, the apparent actuator gain should be calculated from the root-locus (Figure (5.13)) using the Pro-Matlab function GMAG which is described in section 3.5. The poles and zeros used to represent the control mode are given below in Table (5.11) as are the results for 5 different gains ($g = 10, 10^2, 10^3, 10^4$ and 10^5).

Table (5.11)

Control mode open-loop poles:		$-7.4388 \pm 5.4527j$	
		$-4.9636, 0, 0$	
Control-mode zeros:		$-12.725, -4.6760, -1.0$	
Feedback Gain (g)	Pole on the second order asymptote	Gain Magnitude (GMAG)	Apparent Engine Gain - K (GMAG/g)
10	$-5.7784 \pm 5.5377j$	18.0574	1.8057
10^2	$1.9601 \pm 14.473j$	178.478	1.7848
10^3	$-0.96612 \pm 42.991j$	1797.74	1.7977
10^4	$-0.79418 \pm 134.34j$	17992.9	1.7993
10^5	$-0.7525 \pm 424.27j$	17994.5	1.7995

Clearly, the engine does not exhibit a steady state gain of 1.0 as the apparent engine gain (1.7995) is less than the correct value (7.0963) by a factor of 3.94458. The discrepancy could be resolved by multiplying all inputs to the engine by 3.94458 or by setting K_p of

equation (5.14) to be 3.94458. This second option will be used here and it results in B_{bs} , for the engine effects only, being given by

$$B_{bs} = \begin{bmatrix} 0 \\ (1.0673e+0)/3.94458 \\ (1.0711e+1)/3.94458 \\ (-3.0437e+1)/3.94458 \end{bmatrix} \quad \dots (5.55)$$

and then \dot{B}_{bs} , for all three inputs, can be written as

$$\dot{B}_{bs} = \begin{bmatrix} 0 & 0 & 0 \\ 2.7057e-1 & 2.6129e-3 & -1.2823e-1 \\ 2.7150e+0 & -3.9209e-1 & -9.8574e-2 \\ -7.7162e+0 & -6.7902e-2 & -3.9692e-1 \end{bmatrix} \quad \dots (5.56)$$

Clearly \dot{B}_{bs} is in the required form of (3.1) already and as F_2 was defined by (5.45), then for $m_1 = 1$ the controller matrices K_p and K_I are given by

$$K_p = \begin{bmatrix} 5.6917e-3 & 3.6012e-2 & 2.9109e-1 \\ 7.0254e-2 & -4.0536e+0 & 2.4881e+0 \\ -1.2267e-1 & -6.6139e-3 & 8.7590e-1 \end{bmatrix} \\ * \begin{bmatrix} \sigma_1 & 0 & 0 \\ 0 & \sigma_2 & 0 \\ 0 & 0 & \sigma_3 \end{bmatrix} \quad \dots (5.57)$$

and

$$K_I = \begin{bmatrix} 5.6917e-3 & 3.6012e-2 & 2.9109e-1 \\ 7.0254e-2 & -4.0536e+0 & 2.4881e+0 \\ -1.2267e-1 & -6.6139e-3 & 8.7590e-1 \end{bmatrix} \\ * \begin{bmatrix} \sigma_1 & 0 & 0 \\ 0 & \sigma_2 & 0 \\ 0 & 0 & \sigma_3 \end{bmatrix} * \begin{bmatrix} \rho_1 & 0 & 0 \\ 0 & \rho_2 & 0 \\ 0 & 0 & \rho_3 \end{bmatrix} \quad \dots (5.58)$$

These "new" gain matrices do not alter the root-locus structure as they simply increase the gains that effect the engine by 3.94458. This can be verified by comparing (5.57) and (5.58) with (5.48) and (5.49) which shows the top row of each "new" controller matrix to be larger by 3.94458. Figure (5.14) shows the root-locus for this system which has the same structure as the previous root-locus (Figure (5.13)); both figures being generated for the same range of gains and with $\Sigma = \Xi = I_3$ and $m_1 = 1.0$. The main difference is that the poles representing the second order control-mode have progressed further

along their asymptotes as they are affected by the increased engine gain.

The gain magnitude of the engine may be calculated once again and the results are tabulated below in Table (5.12)

Table (5.12)

Feedback gain (g)	Pole on the second-order asymptote	Gain Magnitude (GMAG)	Apparent Engine gain - K (GMAG/g)
10	-2.9942 ± 9.4176	69.6476	6.9647
10 ²	-1.2198 ± 27.418	706.550	7.0655
10 ³	-0.8265 ± 84.551	7095.18	7.0952
10 ⁴	-0.77863 ± 266.53	70983.9	7.0984
10 ⁵	-0.77367 ± 842.57	70987.2	7.0987

Clearly, the apparent engine gain is now correct as it compares almost exactly with k_{ai} given by (5.54).

Figure 5.15 shows the same root-locus in more detail for g varying from 0.0 to 14.0 in steps of 0.1 while $\Sigma = \Xi = I_3$ and $m_1 = 1.0$. Pole pairs b and c behave very similarly to their equivalents in Figure (5.7), but both poles of pair a are heading towards the transmission zeros at -1.0. In addition to this there are various pole-to-pole and pole-to-zero interactions occurring on the real axis which are not described in detail here. It is clear that even this relatively simple root-locus has some complex features at low gain which can be

investigated using root-loci with fine gain steps. However, whilst this phenomena can be of general interest, they do not yield any additional insight to the control system designer at this stage. Consequently, detailed analyses of the various interactions which occur in root-loci will not be given for every root-locus diagram hereafter.

5.5.2 Investigation of the Closed-Loop Performance and Tuning

Setting the parameter K_e to give a steady state engine gain of 1.0 also defines the core of the controller matrices. The design can now proceed with selection of the tuning parameter, but first certain relationships must be established. These are the relationships between control-mode performance, asymptote sets and tuning parameters.

The relationships between tuning parameters and the two control-modes associated with the two first-order asymptotes has already been described in section 5.4. These relationships still hold for this case study. Consequently the emphasis here will be upon the effects of the engine dynamics and the second-order asymptotes.

Effects of g

Figure (5.16) shows the frequency response of the closed-loop transfer function matrix for gains of 2.5, 5.0 and 10.0 where $\Sigma = \Xi = I_3$ and $m_1 = 1.0$. To prevent crowding the individual sub-diagrams, only cross-coupling for the gain = 5.0 case is shown. From this figure it is possible to match the flight path angle control-mode with the second-order asymptotic pole pair caused by

the engine dynamics. This is sensible as the vertical motion is still dominated by the thrust effects at this flight condition. The second-order asymptotic pole pair are the dominant complex conjugate pole pair within this control-mode. The characteristics of this control-mode are taken from the frequency response and tabulated below (Table 5.13) alongside the equivalent results derived from equations (3.73), (3.74) and (3.75).

Table (5.13)

Analysis of the second-order control-mode for gain = 10.0		
Closed loop pole:	-2.9942 ± 9.4176j	
Natural frequency (ω_n):	9.8821 rads/s	
Damping ratio (ζ):	0.30299	
Characteristic	Graphical	Theoretical
Bandwidth (rad/s) [ω_b]	13.12	14.345
Peak frequency (rad/s) [ω_p]	8.70	8.9289
Peak magnitude ratio [M_p]	3.75	5.2318

NB:

Discrepancies between the two sets of results are to be expected as the control-mode may not be totally dominated by the complex conjugate pole pair, as described in the section 3.6.

The cross coupling in diagram (3) does not reduce at all frequencies as the gain increases, unlike the cross coupling in diagrams (1) and (2). High gains cause resonance* as the flight path angle control-mode becomes lightly damped. This resonance causes high cross

coupling levels at the resonant frequency (ω_p), even though cross coupling is reduced at other frequencies. The cross coupling from flight path angle into pitch attitude is high for the $g = 5.0$ case reaching 5.7 dB (a magnitude ratio of 1.93). This untuned design is clearly unacceptable due to cross coupling levels.

The effect of increasing the gain is also illustrated in Figure (5.17) which shows the step response matrix of the transfer function for gains of 2.5, 5.0 and 10.0 (once again $\Sigma = \Xi = I_3$ and $m_1 = 1.0$). This shows the speed of response increasing with gain in diagrams (2) and (3) but no speed of response change in diagram (1), as expected. Clearly, cross coupling levels are reducing as the gain increases, but the flight path angle control-mode also becomes oscillatory.

Effects of Σ

Plotting the frequency response of the closed-loop transfer function matrix whilst varying the diagonal elements of Σ establishes the association between tuning parameters and asymptote sets. The results are summarised in Table (5.14) below

* Resonance - this refers to peaks in the magnitude of any response due to lightly damped poles, both on-diagonal and off-diagonal transfer-function elements.

Table 5.14

Control-mode	Tuning parameter	Actuator/asymptote set
Pitch attitude	σ_1	Tailplane/first-order
Forward Speed	σ_2	Nozzle angle/first-order
Flight Path Angle	σ_3	Engine (thrust)/second-order

Effects of m_1

Figure (5.18) shows the frequency response of the closed-loop transfer function matrix for a gain of 5.0, with $\Sigma = \Xi = I_3$ and m_1 varying ($m_1 = 2.0, 1.0$ and 0.2). Features illustrated by diagrams (1) and (2) are the same as their equivalents in Figure (5.10); the accompanying explanation is also the same. The main feature to note in diagram (3) is that cross coupling into pitch angle from flight path angle is reduced at low frequencies, but remains high at approximately 5 rads/s due to the resonance present in the pitch angle control-mode.

Figure (5.19) shows the step response of exactly the same system (for the same tuning parameter values). It illustrates the increase in speed of response of the pitch angle control-mode and the accompanying decrease in damping (diagram (1)) as well as a decrease in cross coupling (diagram (3)) which is also accompanied by a decrease in damping.

Figure (5.20) shows the root-locus for the plant-2 system with g varying from 0.1 to 100.0 logarithmically, $m_1 = 0.2$ and $\Sigma = \Xi = I_3$. Clearly, the pitch angle control-mode is dominated by pole pair a which give a lightly damped response for $g = 5$ as marked on the figure. However, it also becomes apparent that increasing σ_1 (which is associated with the pitch angle control-mode) will move pole pair a to the left giving a less oscillatory response,

Tuning the Closed-loop system

Having analysed the various affects of the tuning parameters it is now possible to tune the closed-loop system with a full understanding of the approach. The method described in section 3.6 is to choose a minimum damping level to tune to and the level chosen here is $\zeta \approx 0.6$ (this allows a fast speed of response without the draw back of a large overshoot and a long settling time). The two control-modes associated with the first-order asymptotes could theoretically be tuned to give very high bandwidths but a bandwidth of 5 rad/s is sufficient for this example.

The forward speed control-mode has an asymptotic transfer function identical to (5.30) and so here σ_2 is set to be 1.0 and g is set to be 5.0. The pitch angle control-mode has an asymptotic transfer function identical to (5.53) and so m_1 is set to be 0.2. In order to prevent the pitch angle control-mode from being lightly damped σ_1 will be set to 5.0. The last tuning parameter to be set here is σ_3 which was varied until the complex conjugate pole pair associated with the second-order asymptote (and the flight path angle control-mode) had a damping ratio of 0.6. The setting to give this is $\sigma_3 = 0.3222$ (The parameter $\Xi = I_3$ as before).

Figure (5.21) shows the root-locus for this tuned system with g varying from 0.1 to 100.0 logarithmically. The asymptotic structure is identical to that of the untuned system but clearly the root-locus is of a quite different shape. The open-loop engine poles no longer form the second-order asymptote and it is formed by two different poles (pole pair a of Figure (5.20)). However this "shape change" does not affect the relationships defined in Table (5.14).

Figure (5.22) shows the root-locus for this tuned system and it is clear that the cross coupling is now down to an acceptable level. The bandwidths of the pitch angle and forward speed responses are 6.6985 and 6.2905 respectively as expected and the bandwidth of the flight path angle control mode is 2.8683.

The complex conjugate pole associated with this control-mode is $-4.9288 \pm 6.5717j$ which has a natural frequency of 8.2147 rads/s and a damping ratio of exactly 0.6. Applying (3.75) gives the theoretical bandwidths of 9.4325 which is clearly very different from the actual value. The conclusion is that the complex conjugate pole pair are not the dominant poles of this control-mode.

Figure (5.23) shows the frequency response of the closed-loop transfer function matrix with the same tuning parameter settings as those used for Figure (3.22), but σ_3 is varied from its original setting of 0.3222 to 0.7 and 1.1. Clearly, the bandwidth increases as σ_3 increases but unfortunately the cross coupling into forward speed and pitch angle also increases. Setting $\sigma_3 = 0.7$ gives adequate improvement in bandwidth for the flight path angle response, and yet maintains cross couplings below -10 dB (30%) at the resonant

frequency. This is a clear example of a performance versus cross coupling trade-off where the designer would exercise judgement.

Figure (5.24) shows the step response for this design which is acceptable except for the slight overshoot apparent in the forward speed and the flight path angle responses. This may be reduced by setting $\rho_2 = 0.2$ and $\rho_3 = 0.2$. As the pitch angle response is acceptable ρ_1 will not be altered. Figure (5.25) shows the step response for this final design with the previous step response ($\Xi = I_3$) overlaid for comparison. The root-locus for the final design has the same general shape and characteristics as the root-locus shown by Figure (5.21) and so it is not shown here. The frequency response of the closed-loop transfer function for the final design is very similar to the response for $\sigma_3 = 0.7$ shown in Figure (5.23) and so it is also not shown here. Table (5.15) below gives various performance parameters for the final closed-loop system.

* The phase margin here is calculated at the bandwidth frequency as not every magnitude curve passes through 0dB. This is a more severe criterion.

(Note for Table (5.15), see overleaf)

Table (5.15)

Performance parameter	Pitch attitude control-mode	Forward speed control-mode	Flight path angle control-mode
Bandwidth (rad/s)	6.8686	5.5506	6.3453
Gain Margin (dB)	∞	∞	∞
Phase margin * (deg)	111.8 ⁰	131.0 ⁰	91.6 ⁰
Maximum cross coupling to:			
Pitch Attitude (dB)	-	-28.23	-9.996
Forward speed (dB)	-18.57	-	-9.826
Flight path angle (dB)	-20.06	-25.84	-

It is clear from Table (5.15) that the closed-loop system performance is good, (this is confirmed by the design objectives in Chapter 6) the bandwidths are adequate, the gain and phase margins are high and cross coupling levels are low. The closed-loop transfer function matrix is diagonally dominant and exhibits good tracking control up to 5-6 rad/s followed by a smooth roll off.

This case study has illustrated the effects of adding the engine dynamics and how the method copes with the related problems. Recovery of the steady state engine gain was demonstrated early on using results from section 3.5. The controller was then tuned using tuning criteria from section 3.6 and the effects of a non-complex dominant mode were shown. The final result was simple to achieve and at each stage the designer was aware of the effects that his decisions would have on the system performance. Furthermore, an engineering trade-off became apparent during the design which was clear to the designer, leaving him in control of the final design.

5.6 Controller Design with the Full Actuation System

Included - Case 4

The objective here is the same as that for case 2, section 5.4.2. It is required that the pilot has direct control of the pitch attitude (THETAD), the forward speed (VTKT) and the flight path angle (GAMMAD). This case study, like case 3, covers step 11 of the method only. It not only draws upon results from the case 2 worked example (steps 4 to 10) but it also draws upon results from the case 3 worked example. This is a continuation of the work presented as case 3 and case 4 and may be considered as the culmination of the work as all the actuator dynamics are included. The analysis of the system and its subsequent tuning are described in subsections 5.6.1 and 5.6.2 respectively.

5.6.1 Analysis of the Asymptotic Root-locus Structure for the plant-3 system

The linear aircraft equations, including the engine parasitic dynamics, are given by Table (5.3). However, this does not include the dynamics which represent the tailplane actuation system (see subsection 4.6.1), the nozzle actuation system (see subsection 4.6.5) and the engine servo system (see subsection 4.6.6). The actuator dynamics are summarised in Table (4.3) and it is these dynamics which are added to the plant-2 system, given in Table (5.4). This new composite system will be referred to as plant-3.

It should be mentioned here that the GVAM87 splits the front and rear reaction control signals and puts them through simple first order lag actuation models with different time constants (0.025 and 0.02 respectively). This is neither convenient nor necessary here as the pitch actuators are very fast and very well separated from the open-loop aircraft rigid body dynamics. Consequently, to simplify the implementation in Pro-Matlab the entire "pitch-motivator" signal will be passed through a first order lag with a time constant of (0.025). The time constant of 0.025 was chosen as a worst case. Table (5.16) below contains the A and B matrices of the actuators which were added to plant-2 to form plant-3.

The output matrix used for this case study is the same as that used for case study 2 and it is given by (5.34). The same extra measurements are taken and so the feedback matrix is given by (5.43) and (5.45). This in turn yields the same controller matrices as given by (5.48) and (5.50). For this case study the number of plant-3

states is 13 ($n=13$) and the number of inputs is 3 ($m=3$). The open-loop eigenvalues for the plant 3 systems in series with the controller are given below in Table (5.17).

Table (5.16)

<u>A Matrix:</u>					
-11.5	-100.0	0.0	0.0	0.0	0.0
1.0	0.0	0.0	0.0	0.0	0.0
0.0	0.0	-16.5	-157.51	-500.0	0.0
0.0	0.0	1.0	0.0	0.0	0.0
0.0	0.0	0.0	1.0	0.0	0.0
0.0	0.0	0.0	0.0	0.0	-40.0
<u>B Matrix:</u>					
1.0	0.0	0.0			
0.0	0.0	0.0			
0.0	1.0	0.0			
0.0	0.0	0.0			
0.0	0.0	0.0			
0.0	0.0	1.0			
<u>C Matrix:</u>					
0.0	100.0	0.0	0.0	0.0	0.0
0.0	0.0	0.0	0.0	500.0	0.0
0.0	0.0	0.0	0.0	0.0	40.0

Table (5.17)

Eigenvalues	mode type	
$1.0223e-2 + 5.0457e-1j$ $-1.0223e-2 - 5.0457e-1j$ $-4.9380e-1$ $-2.1716e-1$	Aircraft rigid body modes	
$7.4388 + 5.4527j$ $7.43888 - 5.4527j$ -4.9656	Engine modes	Engine Actuation System
$-5.75 + 8.182j$ $-5.75 - 8.182j$	Engine servo	
$-5.75 + 8.182j$ $-5.75 - 8.182j$	Nozzle servo	Nozzle Actuation System
-5.0	Airmotor lag	
-40.0	Pitch motivator lag (tailplane and reaction controls)	
0 0 0	Integrator poles	

Similarly, the transmission zeros of Plant-2 are given below in Table (5.18).

Table (5.18)

Transmission zeros	Source of the zeros
$\left. \begin{array}{l} -1.0 \\ -1.0 \\ -1.0 \end{array} \right\}$	From the integrators, algebraically they are equal to $-\rho_1, -\rho_2, -\rho_3$
-1.0	From the basic plant dynamics, This is caused by extra measurement feedback. Algebraically it is equal to $-1/m_1$.
$\left. \begin{array}{l} -4.6760 \\ -12.725 \end{array} \right\}$	From the engine dynamics

The Markov parameters for this system may easily be calculated according to (3.45) and it may be shown that the first Markov parameter has a rank defect of three ($d_1 = 3$) and the next two Markov parameters have rank defects of 2 each ($d_2 = d_3 = 2$) whilst the fourth Markov parameter is full rank ($d_4 = 0$ and therefore $\nu = 4$). Equation (3.47) and (3.48) may then be used indicating that there are 6 finite zeros and 10 infinite zeros forming the closed-loop asymptotic structure. Further calculation shows that there are two second-order infinite zeros ($2(d_1-d_2)=2$) and eight fourth-order infinite zeros ($4(d_3-d_4) = 8$).

Each set of infinite zeros, or each asymptote set, conforms to pattern A, shown in Figure (3.4).

The pivot points may be approximated using (3.64) as follows

$$\bar{pp}_1 = ((-40.0) - (1.0 - 1.0))/2 = -19.0 \quad \dots (5.59)$$

$$\begin{aligned} \bar{pp}_2 &= ((-5.75+8.182j-5.75-8.182j-5.75-8.182j-5.0)-(-1.0))/4 \\ &= -3.875 \\ &\dots (5.60) \end{aligned}$$

$$\begin{aligned} \bar{pp}_3 &= \\ &((-7.4388+5.4527j-7.4388-5.4527j-4.9656-5.75+8.182j-5.75-8.182j) \\ &\quad (-12.725-4.676-1.0))/4 = -3.2355 \\ &\dots (5.61) \end{aligned}$$

The Pro-Matlab function ASYMPTOTES may also be used to calculate the asymptote characteristics and these are given below in Table (5.19).

Table (5.19)

Pro-Matlab pivot points	Asymptote order	Actuator	Equation (3.64) pivot-point approximation
-19.21	2	Tailplane	-19.0
-3.952	4	Nozzle	-3.875
-3.293	4	Engine	-3.2355

There is obviously good correlation between the Pro-Matlab results and the approximation. To confirm this asymptotic structure the root locus of the system has been plotted as Figure (5.26) for g varying from 0.1 to 100.0 logarithmically and for $\Sigma = \Xi = 1_3$, $m_1 = 1.0$. From this figure it is possible to verify that the asymptote order and pivot points have been calculated correctly (setting a very high gain, so that the root-loci draw near to the asymptotes, enables the pivot points to be checked by utilising the simple geometry of the asymptote sets). Clearly, the closed-loop system becomes unstable at high gain due to the two fourth-order asymptotes which cross the imaginary axis.

It is possible to find the gain at which stability is lost using the root-locus and small gain steps.

Pole pair a become unstable for $g > 24.16$ and pole pair b become unstable for $g > 6.118$. Pole pairs c and d are the second order servo poles and they complete the other two branches of the two fourth order asymptote sets. Pole C is the pitch motivation pole, pole pair a are the engine poles, and pole pair f are the second order asymptotic poles. The root-locus has been replotted using a different set of axes to show the fourth order asymptotes in more detail (Figure (5.27)).

Now that the closed-loop system has been formed, it is possible to check each asymptote set to verify that the associated actuators are compatible with the high-gain method. All the actuators that have been added, excluding the engine, have been given a steady state gain of 1.0. This means that no checks actually need to be performed as

the engine has already been assessed in subsection 5.5.1 and the results of that subsection may be applied here directly. Figure (5.28) shows the root-locus of the system using the correct steady state engine gain (all the other parameters are the same as for Figure (5.26)).

It is possible to find the gain at which stability is lost as described before (subsection 5.5.1). Pole pair a become unstable for $g > 6.3898$ and pole pair b become unstable for $g > 6.2892$. Slight differences in the root-locus shape can be seen when comparing Figures (5.26) and (5.28), but the most significant difference is that pole pair a and pole pair c now move considerably further due to the engine gain being increased. Pole pair g have also been labelled on this figure as they represent the pitch attitude mode and they are referred to later.

This particular change shows that pole pair a and pole pair c are part of the same asymptote set and they form the fourth-order asymptotes that have a pivot point at -3.293 . Likewise, pole pairs b and d form the fourth order asymptote set that has a pivot-point at -3.952 and finally pole pair f form the second order asymptote set that has a pivot-point at 19.21 .

5.6.2 Investigation of the Closed-Loop Performance and Tuning

The first step is to establish the relationships between the tuning parameters, the control-modes and the asymptote sets.

Gain Effects

Figures (5.29a) and (5.29b) show the frequency response of the closed-loop transfer-function matrix for gains of 2.5 and 5.0 respectively, where $\Sigma = \Xi = I_3$ and $m_1 = 1.0$. The two figures are not overlaid this time as the resulting figure would be confusing. The figures show that for $g = 2.5$ the pitch attitude is second-order dominant and lightly damped, whereas for $g = 5.0$ the pitch attitude response nears its asymptotic form and becomes heavily damped, approximating a first-order response. The figures also show that both the forward speed and the flight path angle responses are second-order dominant and lightly damped.

Another feature to note is that cross coupling is high between every input and output, especially cross coupling into flight path angle. Furthermore, increasing the gain reduces the cross coupling at low frequencies but actually increases it where there is resonance (and at frequencies higher than the resonant frequency). There are also "troughs" of anti-resonance caused by interactions between the poles and the zeros.

The most important information to come from the figure is the connection between asymptote sets and control-modes. This connection is easily found by examining the bandwidth (ω_B), peak frequency (ω_p) and peak magnitude (M_p) of each response and comparing them to results derived from equations (3.73), (3.74) and (3.75) using the dominant poles. The dominant complex conjugate pole pairs are shown below in Table (5.20) for the two different gains.

Table (5.20)

Pole pair/actuator	g = 2.5	g = 5.0
a/Engine	-2.5625 ± 4.7939j	-0.63461 ± 5.7668j
b/Nozzle	-1.0347 ± 2.5646j	-0.35163 ± 4.2894j
g/-*	-0.48406 ± 1.2675j	[Dominant mode is not complex]

* This pole pair (g) is not actually directly associated with an actuator pole pair.

The corresponding theoretical values of ω_b , ω_p and M_p are given below in Table (5.21) for the two different gains.

Table (5.21)

Pole pair/actuator	gain	ω_b (Rad/s)	ω_p (Rad/s)	M_p (Rad/s)
a/Engine	2.5	7.0864	4.0515	3.0642
b/nozzle	2.5	3.8641	2.3467	3.9451
g -	2.5	1.9153	1.1714	4.2075
a/engine	5.0	8.9380	5.7318	13.305
b/nozzle	5.0	6.6556	4.2750	15.793
g/-	5.0	-	-	-

The graphical values of ω_b , ω_p and M_p from Figure (5.29a) and (5.29b) are now given, for each control-mode and each of the two gains, in Table (5.22) below.

Table (5.22)

Control-mode	gain	ω_b (Rad/s)	ω_p (Rad/s)	M_p (Rad/s)
Flight path angle	2.5	5.80	3.39*	-0.285*
Forward speed	2.5	4.88	2.56	7.22
Pitch attitude	2.5	1.99	1.26	3.72
Flight path angle	5.0	8.14	4.50	10.69
Forward speed	5.0	7.32	4.50	15.29
Pitch attitude	5.0	-	-	-

* ω_p and M_p for $g = 2.5$ (flight path angle control-mode) are taken from the second peak on diagram (3), Figure (5.29a).

Allowing for the crude frequency step used for the frequency response, and the fact that each pole pair may not be completely dominant in each control mode, there is a clear correlation between control-modes and pole pairs. This links each control-mode to its dominant poles and hence in two cases to its dominant actuator (the tailplane dynamics only dominate if higher gains are achieved). The two tables (5.21) and (5.22) have been ordered such that the link is between corresponding rows (i.e. Flight path angle control-mode and pole pair a, forward speed control-mode and pole pair b, pitch attitude control-mode and pole pair g).

Effects of Σ

Plotting the frequency response of the closed-loop transfer function matrix whilst varying the diagonal elements of Σ establishes the association between the tuning parameters and the control-modes. A similar procedure using the root-locus diagram establishes the association between tuning parameters and asymptote sets. These results are summarised below in Table (5.23).

Table (5.23)

Control-mode Pole-Pairs	Tuning Parameter	Actuator	Asymptote Pivot-point	Asymptote	
				Order	Set
Pitch attitude	σ_1	Tailplane	-19.21	2nd	i
Forward speed	σ_2	Nozzle	-3.952	4th	b & d
Flight path angle	σ_3	Engine	-3.213	4th	a & c

Clearly, this defines the link between control-modes, asymptote sets and tuning parameters.

The previous case study also assessed the effects on the closed-loop system of changing the extra measurement feedback gain m_1 . This is not necessary here as the effects on this closed-loop system will be basically the same. Consequently, tuning of the closed-loop system can now proceed.

Tuning the Closed loop System

Having analysed the various effects of the tuning parameters it is now possible to tune the closed-loop system with a full understanding of the approach. The method described in section 3.6 is to select a minimum damping level. In this case there are three lightly damped pole pairs which can be tuned to a minimum damping criteria. Once again, the desired minimum damping level is 0.6 ($\zeta \geq 0.6$). The desired bandwidth chosen here is 5 rad/s for each control-mode.

The pitch rate control-mode has an asymptotic transfer function given approximately by (5.30) and so here m_1 is set to be 0.2 to achieve a bandwidth of 5.0 rad/s. However, it has already been seen that setting m_1 alone can give oscillatory results (subsections 5.4.2 and 5.5.2) and so here σ_1 is increased to 5.0. This ensures that the pole pair which are dominant in the pitch attitude control-mode are not lightly damped. These two changes will alter the shape of the root-locus and so σ_2 and σ_3 are not changed at this stage, however it is appropriate to decrease the level of integral action as before, giving $\rho_1 = \rho_2 = \rho_3 = 0.2$.

The root-locus for this closed-loop system is shown as Figure (5.30) for g varying from 0.1 to 100.0 logarithmically. The asymptotic root-locus structure has changed due to the movement of the four transmission zeros at $-1/m_1$, $-\rho_1$, $-\rho_2$ and $-\rho_3$. The new asymptote pivot-points are only slightly different and they are given below in Table (5.24) for comparison with those given in Table (5.19).

Table_(5.24)

Pro-Matlab Pivot-points	Asymptote order	Actuator	Equation (3.64) Pivot-point approximation
-17.64	2	Tailplane	17.0
-3.892	4	Nozzle	4.075
3.89	4	Engine	3.4356

Although the asymptotic structure has changed little, the root-locus shape is quite different now to that shown by Figure (5.2.8). The main feature to note here is that pole pair a reach a maximum damping of only 0.51 which is less than the desired maximum damping level. This asymptote set is dominated by the engine dynamics and so it is clear here that the engine dynamics are limiting the performance of the closed loop system by producing lightly damped modes. This insight comes from using the high-gain method and would probably not be given using other methods.

The initial design point now is to achieve damping of 0.5 for pole pair a and damping of 0.6 for pole pair b as shown on Figure (5.30). This was performed by setting $g = 2.5$, $\sigma_2 = 0.8$ and $\sigma_3 = 0.1$, with other parameters remaining unchanged. The frequency response of the resulting closed-loop transfer function matrix is shown as Figure (5.31). Clearly, the pitch attitude control-mode gives a fast tracking response but also high cross coupling into the other two outputs. Indeed, the bandwidth of 7.57 rad/s is really too high. The forward speed control-mode exhibits good performance, low cross

coupling into the other two outputs and a bandwidth of 3.90 rad/s. The flight path angle control-mode exhibits low cross coupling into the other two outputs but also a very low bandwidth (1.94 rad/s). The two pole pairs a and b are given below in Table (5.2.5) along with the performance characteristics that would normally be associated with them as dominant modes (this is calculated using equations (3.73), (3.74) and (3.75).

Table (5.25)

Characteristics	Pole pair a	Pole pair b
Actual value	$-3.3694 \pm 5.8266j$	$-1.9087 \pm 2.5091j$
Natural frequency (ω_n)	6.7307 rad/s	3.1526 rad/s
Damping	0.5	0.6
Theoretical bandwidth (ω_b)	8.561 rad/s	3.620 rad/s
Theoretical peak frequency (ω_p)	4.759 rad/s	1.668 rad/s
Theoretical peak magnitude (M_p)	1.155	1.042

The flight path angle control-mode was previously dominated by pole pair a but Table (5.25) shows that this is no longer the case. This control-mode must therefore be dominated by a pole on the real axis which allows the associated tuning parameter gain to be increased. Consequently σ_3 should be increased to achieve a bandwidth 5.0 rad/s for this control-mode. The forward speed control-mode has a bandwidth of 3.90 rad/s, a peak magnitude of 1.04 and a peak frequency of 1.68 rad/s which shows excellent correlation with the equivalent theoretical results for pole pair b given in Table (5.25). This

indicates that pole pair b are the dominant poles of the forward speed control-mode. The system should now be tuned by decreasing $1/m_1$ and σ_1 to achieve a bandwidth of 5.0 rad/s for the pitch attitude control-mode, increasing σ_2 to achieve bandwidth of 5.0 rad/s for the forward speed control-mode and by increasing σ_3 to achieve a bandwidth of 5.0 rad/s for the flight path angle control-mode.

The frequency response of the new tuned system is given as Figure (5.32) and it shows a good response generally with seemingly high cross coupling from pitch attitude demands into forward speed and especially flight path angle demands into the other two outputs. The bandwidths were not tuned to be exactly 5.0 rad/s but they are all close to this value as can be seen from Table (5.26) below.

Table (5.26)

Control-mode	bandwidth (rad/s)
Pitch attitude	5.6614
Forward speed	5.0171
Flight path angle	5.2424

The parameters that give this response are $g = 2.5$, $m_1 = 0.25$, $\Sigma = \text{diag} (4.0, 1.05, 0.85)$ and $\Xi = \text{diag} (0.2, 0.2, 0.2)$. Figure (5.33) shows the step response of this system which exhibits quite lightly damped behaviour in diagram (1) and diagram (2) where the two most lightly damped modes are beginning to increase in dominance as the gain is increased. The solution to this is to reduce σ_2 and σ_3

slightly to obtain a satisfactory step response, but this also reduces the bandwidth of the forward speed mode. The final setting is $\Sigma = \text{diag} (4.0, 0.7, 0.75)$ and all the other parameters are as given above.

Figure (5.34) shows the frequency response for this system and Figure (5.35) shows its step response. Table (5.27) below gives various performance parameters for the final design. It should be noted that the gain and phase margins are all better than 6dB and 45° respectively, This satisfies part of the design requirements as will be described later in Chapter 6.

Table (5.27)

Performance parameter	pitch attitude control-mode	forward speed control mode	Flight path angle control-mode
Bandwidth (rad/s)	5.70	3.34	4.45
Gain margin (dB)	19.59	10.11	7.23
Phase margin (deg)	86.60°	55.61°	50.48°
Maximum cross coupling to:			
Pitch attitude (dB)	-	-28.5	-2.06
Forward speed (dB)	-7.84	-	-2.62
Flight path angle (dB)	-15.7	-32.0	-

From the step response (Figure (5.35)) it is evident that the cross coupling levels (diagrams (1) and (3)) are not as severe as those shown by the frequency response (Figure (5.34), diagrams (1) and (3)). This is because the high cross coupling levels indicated in the

frequency response figure are at high frequencies (approx 5 rad/s) and a step input is not a sustained high frequency input. Furthermore, cross coupling into forward speed is negligible when the actual units are considered as described previously in subsection 5.4.1. Conversely though, cross coupling from forward speed into the other two outputs will be higher, in real terms, when the actual units are considered.

The final design indicates that high frequency flight path tracking tasks will result in relatively high levels of cross coupling. However it should be noted that at this flight condition it is not necessary to be able to track a flight path command at 0.71 Hz (4.45 rad/s). Furthermore, the main actuators used for flight path and speed changes are the nozzle and engine which are relatively slow to respond as they were not originally designed to operate at such high frequencies. This indicates that there is a trade-off here between speed of response (in terms of bandwidth) and quality of response (in terms of cross coupling levels). Indeed, by detuning this system to a lower bandwidth cross coupling levels can be reduced slightly.

Unfortunately, though, the reduction in cross coupling is not as great as the reduction in performance and this can lead to poor handling qualities. This fact was demonstrated in the AFTI/F-16 programme [Anderson et al], where it was stated that "... decoupled purity was not as important as adequate control bandwidth in producing a useful control capability for many tasks", (see also subsection 6.2.1 (d)). Consequently, the final word on the trade-off rests with the handling qualities test pilot, but, the control law designer has full engineering insight into the trade-off when using the high-gain method.

This case study has illustrated the effects of adding complex actuator dynamics to the basic system and has shown how the high-gain method deals with the added complexity. After the asymptotic structure was analysed various tuning parameter effects were investigated. This revealed the associations between tuning parameters, asymptote sets, actuators and control-modes. Knowledge of these associations enabled the complex system to be tuned to achieve a satisfactory performance and also exposed a fundamental engineering trade-off. Throughout the design the designer was aware of various trade-offs and consequently was able to retain control over the final solution.

5.7 Analysis of Controller Robustness to Plant Changes - case 5

This section contains a simple analysis of controller robustness to plant dynamic changes. A linear model was derived from GVAM87 at 100 Kts flying straight and level at 8° angle of incidence. Thus, the 100 Kts flight condition only differed from the 120 Kts flight condition due to speed and actuator settings. A linear model was derived, and its plant and input matrices are given overleaf in Table (5.28). The

Table (5.28).

The Open-Loop State Space Equations Representing Plant-4.

$$\begin{bmatrix} \text{THETR} \\ \text{Q} \\ \text{VKN} \\ \text{VKD} \\ \text{FNP} \\ \text{HNP} \\ \text{QEF} \end{bmatrix} = \begin{bmatrix} 0.0 & 1.0 & 0.0 & 0.0 & 0.0 & 0.0 & 0.0 & 0.0 & 0.0 & 0.0 \\ -2.1573e-1 & -3.3562e-1 & 2.3862e-3 & -1.2389e-3 & 1.0152e+0 & -1.3386e+0 & -1.5266e-4 & 0.0 & 0.0 & 0.0 \\ -4.6213e+1 & 2.4526e-2 & -5.7514e-2 & -8.3325e-2 & 7.3837e+0 & 3.2513e+0 & 1.1477e-3 & 0.0 & 0.0 & 0.0 \\ -4.1429e+1 & -1.4952e+0 & -4.4346e-2 & -2.4558e-1 & -3.9761e+1 & -1.0067e+1 & -3.6074e-3 & 0.0 & 0.0 & 0.0 \\ 0.0 & 0.0 & -2.2587e-5 & 0.0 & -3.6694e+0 & 2.5091e+0 & 6.9846e-4 & 0.0 & 0.0 & 0.0 \\ 0.0 & 0.0 & -5.7784e-5 & 0.0 & -6.0990e-3 & -2.6898e+0 & 5.2018e-4 & 0.0 & 0.0 & 0.0 \\ 0.0 & 0.0 & 2.2420e+0 & 0.0 & -9.0976e+4 & 1.4632e+2 & -1.3333e+1 & 0.0 & 0.0 & 0.0 \end{bmatrix} \begin{bmatrix} \text{PHTPA} \\ \text{THDFPA} \\ \text{ETADA} \end{bmatrix} + \begin{bmatrix} 0.0 & 0.0 & 0.0 & 0.0 & 0.0 & 0.0 & 0.0 & 0.0 & 0.0 \\ 0.0 & 1.4738e-3 & -1.1952e-1 & 0.0 & 0.0 & 0.0 & 0.0 & 0.0 & 0.0 \\ 0.0 & -4.2731e-1 & -9.0789e-2 & 0.0 & 0.0 & 0.0 & 0.0 & 0.0 & 0.0 \\ 0.0 & -8.9264e-2 & -2.9736e-1 & 0.0 & 0.0 & 0.0 & 0.0 & 0.0 & 0.0 \\ 0.0 & 0.0 & 0.0 & 0.0 & 0.0 & 0.0 & 0.0 & 0.0 & 0.0 \\ 0.0 & 0.0 & 0.0 & 0.0 & 0.0 & 0.0 & 0.0 & 0.0 & 0.0 \\ 3.9467e+4 & 0.0 & 0.0 & 0.0 & 0.0 & 0.0 & 0.0 & 0.0 & 0.0 \end{bmatrix} \begin{bmatrix} \text{THETD} \\ \text{VTKT} \\ \text{GAMMAD} \end{bmatrix} = \begin{bmatrix} 5.7296e+1 & 0.0 & 0.0 & 0.0 & 0.0 & 0.0 & 0.0 & 0.0 & 0.0 \\ 0.0 & 0.0 & 5.9249e-1 & 0.0 & 0.0 & 0.0 & 0.0 & 0.0 & 0.0 \\ 0.0 & 0.0 & 0.0 & -3.3947e-1 & 0.0 & 0.0 & 0.0 & 0.0 & 0.0 \end{bmatrix} \begin{bmatrix} \text{THETR} \\ \text{Q} \\ \text{VKN} \\ \text{VKD} \\ \text{FNP} \\ \text{HNP} \\ \text{QEF} \end{bmatrix}$$

standard elevator, nozzle servo and engine servo actuators were added and this plant will be referred to as plant-4. The controller which has been designed for the 120 Kts flight case with full actuators is used in conjunction with this plant at a different flight condition (i.e. at an "off-design" flight condition). The parameter settings are identical to those used for the final design and so the results may be compared to those achieved in the final design.

The frequency response of the transfer function matrix is shown as Figure (5.36) and the step response is shown as Figure (5.37). These two figures may be compared directly to Figures (5.34) and (5.35) respectively. The frequency responses are of the same basic shape though the off-design case is clearly more lightly damped, it exhibits more cross coupling generally and the bandwidths are also slightly different. The step responses show this decrease in damping and increase in cross coupling also.

The speed of response of the off-design case is acceptable but the stability, in terms of damping, is not acceptable. The deterioration in performance progresses as the off-design flight case moves further from the on-design condition, as expected. However, the deterioration is more severe when the on-design controller is highly tuned, as in this case. This clearly indicates a trade-off between performance (in terms of highly tuned controllers for maximum speed of response) versus robustness (in terms of stability at off-design flight conditions). This is particularly important here as the final controller will be gain scheduling between on-design spot point controllers as the airspeed changes (airspeed changes coincide with flight condition changes under certain circumstances which are explained in chapter 7).

The gain scheduling controller will vary the gains from one on-design flight condition to another smoothly using linear interpolation. Consequently, there will be less of a disparity between the controller and the flight condition at off-design points when gain scheduling is used than in this example where the controller gains were not altered at all. Consequently, using less highly tuned controllers with on-design spot points 40 Kts apart should give satisfactory performance when scheduling with air speed. The 40 Kts gap between on-design flight conditions is based on the fact that a 20 Kts gap (as used in this example) will give satisfactory performance if the controller is less highly tuned. Therefore 40 Kts gaps will ensure that the controller is never further than 20 Kts from an on-design condition.

The last feature to note concerning robustness, as defined here, is that it alters with flight condition. The early part of the flight envelope 0 - 80 Kts shows as much dynamic change as the next 40 Kts (80-120 Kts) and the dynamics change completely in the next 20 Kts (120-140 Kts). This indicates that there is an optimum step length for gain scheduling which varies depending upon two factors. The first is the amount of significant changes in dynamics that occur as the scheduling variable changes; a type of sensitivity function. The second factor is in the hands of the designer as it concerns the off-design performance of the controller. A finite number of on-design spot point controllers implies that the controller is usually working in off-design conditions. Hence the "performance versus robustness" trade-off translates into a "performance versus number of design points" trade-off. The conclusion here is that high performance highly tuned controllers will require many design points which is not possible in this study. Therefore moderately tuned controllers will be used throughout this study.

Clearly, the high-gain method can produce robust controllers which function satisfactorily at off-design flight conditions. Furthermore, the high-gain method enables important robustness trade-offs to be viewed and exploited by the designer.

5.8 Design of Dynamic Compensators for High-Gain MIMO Systems - Case 6

In this section a slightly different design case is used to illustrate the way in which dynamic compensation can be designed for

MIMO systems using simple SISO techniques. The flight case used is for straight and level flight at 8° angle of incidence as before, but at 136 Kts; 16 Kts faster than the flight condition defined at the start of this chapter. This faster flight condition generates greater wing lift and so the supportive thrust requirement is reduced. This requires a lower throttle setting which places the engine dynamics in the "governor off" section of the throttle-to-thrust curve (close to point 'A' on Figure (4.8)). This small change in flight condition causes a gross change in engine dynamics which makes the control problem even more difficult. A dynamic compensator is designed here to show how such difficulties may be overcome.

The plant and input matrices are given below in Table (5.29) for this new design case. The plant will be referred to as plant-6. The open-loop eigenvalues for this plant are given below in Table (5.30)

Table (5.29).

The Open-Loop State Space Equation Representing Plant-5.

$$\begin{bmatrix} \text{THETR} \\ \text{Q} \\ \text{VKN} \\ \text{VKD} \\ \text{FNP} \\ \text{HNP} \\ \text{QEF} \end{bmatrix} = \begin{bmatrix} 0.0 & 1.0 & 0.0 & 0.0 & 0.0 & 0.0 & 0.0 & 0.0 & 0.0 & 0.0 & 0.0 & 0.0 & 0.0 \\ -3.3506e-1 & -4.4217e-1 & -1.8031e-3 & -1.4315e-3 & 1.6180e+0 & -1.0621e+0 & -1.1304e-4 \\ -6.3915e+1 & 2.3166e-2 & -7.2727e-2 & -1.3856e-1 & 2.2277e+1 & 5.5723e+0 & 1.9085e-3 \\ -7.4830e+1 & -2.1336e+0 & -1.9930e-1 & -3.2650e-1 & -2.9543e+1 & -5.4615e+0 & -1.9810e-3 \\ 0.0 & 0.0 & 2.4935e-5 & 0.0 & -4.0809e+0 & 2.6282e+0 & 7.5931e-4 \\ 0.0 & 0.0 & -4.0864e-5 & 0.0 & -5.5284e-3 & -3.0475e+0 & 5.3453e-4 \\ 0.0 & 0.0 & 0.0 & 0.0 & 0.0 & 0.0 & -1.3333e+1 \end{bmatrix} \begin{bmatrix} \text{THETR} \\ \text{Q} \\ \text{VKN} \\ \text{VKD} \\ \text{FNP} \\ \text{HNP} \\ \text{QEF} \end{bmatrix}$$

$$+ \begin{bmatrix} 0.0 & 0.0 & 0.0 & 0.0 & 0.0 & 0.0 & 0.0 & 0.0 & 0.0 & 0.0 & 0.0 & 0.0 \\ 0.0 & 0.0 & 3.6989e-3 & -1.3573e-1 & 0.0 & 0.0 & 0.0 & 0.0 & 0.0 & 0.0 & 0.0 & 0.0 \\ 0.0 & 0.0 & -3.3310e-1 & -1.0380e-1 & 0.0 & 0.0 & 0.0 & 0.0 & 0.0 & 0.0 & 0.0 & 0.0 \\ 0.0 & 0.0 & -4.5013e-2 & -4.8065e-1 & 0.0 & 0.0 & 0.0 & 0.0 & 0.0 & 0.0 & 0.0 & 0.0 \\ 0.0 & 0.0 & 0.0 & 0.0 & 0.0 & 0.0 & 0.0 & 0.0 & 0.0 & 0.0 & 0.0 & 0.0 \\ 0.0 & 0.0 & 0.0 & 0.0 & 0.0 & 0.0 & 0.0 & 0.0 & 0.0 & 0.0 & 0.0 & 0.0 \\ 6.4348e+4 & 0.0 & 0.0 & 0.0 & 0.0 & 0.0 & 0.0 & 0.0 & 0.0 & 0.0 & 0.0 & 0.0 \end{bmatrix} \begin{bmatrix} \text{PHTPA} \\ \text{THDFPA} \\ \text{ETADA} \end{bmatrix}$$

$$\begin{bmatrix} \text{THETD} \\ \text{VTKT} \\ \text{GAMMAD} \end{bmatrix} = \begin{bmatrix} 5.7296e+1 & 0.0 & 0.0 & 0.0 & 0.0 & 0.0 & 0.0 & 0.0 & 0.0 & 0.0 & 0.0 & 0.0 \\ 0.0 & 0.0 & 5.9246e-1 & 0.0 & 0.0 & 0.0 & 0.0 & 0.0 & 0.0 & 0.0 & 0.0 & 0.0 \\ 0.0 & 0.0 & 0.0 & -2.4961e-1 & 0.0 & 0.0 & 0.0 & 0.0 & 0.0 & 0.0 & 0.0 & 0.0 \end{bmatrix} \begin{bmatrix} \text{THETR} \\ \text{Q} \\ \text{VKN} \\ \text{VKD} \\ \text{FNP} \\ \text{HNP} \\ \text{QEF} \end{bmatrix}$$

Table (5.30))

Eigenvalues	mode type	
-4.7961e-1 ± 6.3491e-1j -7.8088e-2 1.9590e-1	Aircraft rigid body modes	
-4.0671 -3.0613 -13.333	Engine modes	Engine Actuation System
-5.75 ± 8.182j	Engine Servo	
-5.75 ± 8.182j	Nozzle servo	Nozzle Actuation System
-5.0	Air motor lag	System
-40.0	Pitch motivator lag (tailplane and reaction controls)	
0 0 0	Integrator poles	

The open-loop poles can be compared to those given for the 120 Kts flight case in Table (5.17). This reveals that the aircraft rigid body modes have altered slightly and that the aircraft is open-loop unstable. However the most significant difference is that the engine

mode no longer contains a complex conjugate pole pair as the two poles have migrated onto the real-axis, as shown previously in Figure (4.9). The transmission zeros are essentially identical to those derived in case study 4, but those associated with the engine dynamics change with flight condition and have altered slightly. The transmission zeros are given below in Table (5.31) which may be compared with Table (5.18).

Table (5.31)

Transmission zeros	source of the zeros
<p>-1.0 -1.0 -1.0</p>	<p>From the integrators, algebraically they are equal to $-\rho_1, -\rho_2, -\rho_3$.</p>
<p>-1.0</p>	<p>From the basic plant dynamics, caused by extra measurement feedback. Algebraically it is equal to $-1/m_1$</p>
<p>-18.286 -4.9637</p>	<p>From the engine dynamics</p>

A controller was derived for the flight case but no working is shown as the method was identical to that used for the previous case studies. The resulting asymptotic structure is essentially identical to that which was derived for case study 4 for $\Xi = \text{diag}(1,1,1)$ and $m_1 = 1$. The asymptote pivot-points are slightly affected by the flight condition change but the most significant change is the pivot-point which is dependent upon the engine dynamics. The

asymptotic structure is given below in Table (5.32) with pivot-points calculated using both Pro-Matlab and equation (3.64). The results may be compared to those given by Table (5.19) for

Table (5.32)

Pro-Matlab Pivot-Points	Asymptote order	Actuator	Equation (3.64) Pivot-Point Approximation
-19.354	2	Tailplane	-19
-3.8819	4	Nozzle	-3.625
-2.0787	4	Engine	-1.928

The main difference is that the asymptote set dependent upon the engine dynamics is now nearer to the imaginary axis and closer to instability. The effect that this has upon the root-locus is shown by Figure (5.38) which is plotted for g varying from 0.1 to 100.0 logarithmically and for $m_1 = 1.0$ and $\Sigma = \Xi = I_3$. Pole pair a are associated with the engine dynamics and they become unstable for $g > 3.5$ which is quite low. Pole pair b are associated with the nozzle dynamics and they become unstable for $g > 6.5$ but they only become stable for $g > 2.8$ which gives a very small stability window for $3.5 < g < 2.8$. In addition to these stability problems pole pair a reach a maximum damping of 0.33 and pole pair b reach a maximum damping of 0.22, which is very low in each case.

For this case study, the effects of tuning the controller will not be examined but dynamic compensation will be used to improve the system. The dynamic compensation used will be phase advance compensation.

It is clear that the engine dynamics are quite slow and that they produce an asymptote very close to the imaginary axis. Consequently, it is the engine dynamics which are the limiting factor in this design and so moving this critical asymptote set to the left will improve the system. In order to move this asymptote set to the left phase advance compensation should be placed in series with the engine dynamics. The amount of phase advance compensation required generally depends the severity of the problem and the practicality of using phase advance compensation. Very strong phase advance compensation can be impractical due to actuator rate and position limits. Considering this, it was decided to relocate the engine asymptote set close to -5.0.

The new developments make this design very simple as equation (3.64) can be used directly. The asymptote set is required to move to the left by approximately -3.0 (from -2.07 to -5.0). The original (uncompensated) pivot-point equation for this asymptote set is given below

$$\bar{pp}_3 = \frac{((-4.0671-3.0613-5.75+8.182j)-5.75-8.182j)-(-18.286-4.9637-1.0-1.0)}{4} = -1.928 \quad \dots (5.62)$$

Adding dynamics in series with the engine dynamics merely adds poles and zeros to expression (5.62) above. Consequently, to move the pivot-point by -3.0 means that the nett sum of the poles minus the zeros is decreased by (-3.0)x4 or -12.0. Conventionally, SISO dynamic compensation is performed by stable pole zero cancellations and the high-gain method makes this possible for MIMO systems also. The dynamic compensation element (C(s)) to be used is given below by (5.63)

$$C(s) = K_c \frac{(s+z_{1c})(s+z_{2c})}{(s+p_{1c})(s+p_{2c})} \quad \dots (5.63)$$

where $(z_{1c} * z_{2c}) < (p_{1c} * p_{2c})$ for phase advance compensation, and

$$K_c = \frac{(p_{1c} * p_{2c})}{(z_{1c} * z_{2c})} \quad \dots (5.64)$$

for the unity steady state gain condition.

The two zeros at z_{1c} and z_{2c} can be used to cancel the two slow engine poles at -4.0671 and -3.0613 and the two poles at p_{1c} and p_{2c} should be placed further to the left. Indeed as the sum of the poles minus the sum of the zeros must be increased by -12.0 then clearly

$$(p_{1c} + p_{2c}) = (z_{1c} + z_{2c}) - 12 =$$

$$(-4.0671 - 3.0613 - 12) = -19.1284 \quad \dots (5.65)$$

The dynamic compensation design does not need to be absolutely precise and so setting $(p_{1c} + p_{2c}) = -19.0$ and letting $p_{1c} = p_{2c}$ gives $p_{1c} = p_{2c} = -9.5$. Different values of p_{1c} and p_{2c} could be used providing that (5.65) is still true. K_c can now be defined using (5.64) giving

$$K_c = \frac{(-9.5 * 9.5)}{(-4.0671) * (-3.0613)} = 7.2486 \quad \dots (5.66)$$

Thus the phase compensator design is given by

$$7.2486 * \frac{(s-9.5)(s-9.5)}{(s-4.0671)(s-3.0613)} \quad \dots (5.67)$$

The dynamic compensator is placed in series with the engine dynamics and the asymptote pivot-point that was at -2.0787 moves to -4.9811 , close to -5.0 as desired (this was calculated using the Pro-Matlab

function). The actual root-locus for this system is shown as Figure (5.39) for g varying from 0.1 to 100.0 logarithmically and for $m_1 = 1.0$ and $\Sigma = \Xi = I_3$. Clearly, the asymptotes associated with the engine have moved to the left as desired and pole pair a are now the other side of pole pair b. The stability and maximum damping of the two pole pairs (a and b) has been improved and the stability window has been widened. The results are given below in Table (5.33) with the previous uncompensated results alongside.

Table (5.33)

Characteristic	uncompensated system	compensated system
pole pair a -stability	$g < 3.5$	$g < 3.9$
pole pair b -stability	$2.8 < g < 6.5$	$g < 6.8$
pole pair c -stability*	-	$1.0 < g$
stable gain window	$2.8 < g < 3.5$	$1.0 < g < 3.9$
pole pair a - maximum damping	0.33	0.63
pole pair b - maximum damping	0.22	0.62

* pole pair c only exist on Figure (5.40) where pole pair b are not initially unstable

This shows that the overall system can be improved with phase compensation which is designed using SISO techniques. Despite the MIMO nature of the problem, each asymptote set (and therefore each control-mode) can be analysed and phase compensated individually using the high-gain method and the new developments. The only caution added here is that phase advance compensation reduces robustness, adds complexity, increases the order of the system and promotes

actuator rate and position saturation. Consequently it is recommended that phase advance compensation is only used when a satisfactory result cannot be obtained by tuning the controller. This is especially true when a gain scheduling controller is being designed. Furthermore, if phase advance compensation is used it should be kept to the lowest level possible and the linear model results should be checked with a non-linear simulation that incorporates actuator rate and position limits.

The final point to be made here concerns the engine non-linearity. The engine governor forces the engine into two distinctly different dynamic modes and it allows the engine to change from one mode to the other quite quickly. This causes a robustness problem which becomes critical when gain scheduling is used.

The 120 Kts on-design controller was quite robust in that it gave reasonable results when linked to a plant representing a 100 Kts flight case. However, the 120 Kts on-design controller drives the 136 Kts flight condition even more unstable. Clearly, non-linearity can cause serious control problems in gain scheduling controllers which cannot easily be alleviated. One solution to this problem is described in chapter 7.

5.9 Working Backwards

This section demonstrates the concept of "working backwards" which is an important feature of the high-gain method. "Working backwards" involves specifying the required actuator dynamics from a given

system performance specification. This feature enables the control engineer to interact with the other aircraft design disciplines in the early stages of the design of a CCV.

It has already been shown that relatively slow high-order actuator dynamics can seriously affect and compromise the overall system performance. Consequently, if the desired system performance is known then the minimum actuator speed of response can be calculated such that the actuators do not compromise the overall system to a lower performance level. However, there are invariably several actuators of different speeds which affect the overall system performance in different ways and it is usual that the slowest actuator compromises the whole system. The reason for this is that decoupling controllers drive coupled MIMO plants through all actuators simultaneously to achieve the decoupled response.

The flight case used in section 5.8 (case study 6) demonstrates a situation where one particularly slow actuator comprises the overall system performance. One strength of the high-gain method is that it enables the designer to discover this "weak link" in the whole design and to take appropriate action. In case study 6 the weak link was the engine dynamics (see (Figure (4.8))) and dynamic compensation was used to improve the actuator's phase characteristics. Had this been a preliminary design for a new aircraft, the control law designer could have discussed the problem with the engine design team, pressed for an increase in the engine bandwidth and settled upon a compromise solution.

In this study it is not possible to alter the engine dynamics of the GVAM87 as they are too complex, even in the linear model. Therefore an example is constructed here in which the nozzle dynamics are the slowest of the actuators and are changeable. The basic plant plus engine dynamics are used at the 120 Kts flight condition, as defined at the start of this chapter, and the plant and input matrices are given by Table (5.3). The tailplane dynamics are represented by a simple lag with a pole at -25.0 and the nozzle dynamics are represented by two simple lags in series with poles at -6.0 and -4.0. These extra actuator dynamics were added to the plant-3 system of Table (5.3) to form Plant-6. The open-loop eigenvalues for this system are given by Table (5.8) plus the three poles given above. Transmission zeros are given by Table (5.9) with one exception. For this example the desired bandwidth of each control-mode is 10 rad/s and based on previous results the following tuning parameters are set: $m_1 = 0.1$, $\sigma_1=10.0$, $\sigma_2=1.0$, $\sigma_3=1.0$ and $\Xi = I_3$. Hence, the exception is that one transmission zero is now at -10.0. The asymptotic structure of this system is given below in Table (5.34).

Table 5.34

Pro-Matlab		Equation 5.51
Pivot-Points	Asymptote Order	Pivot-Points (approximation)
-0.55292	2	-0.7211
-7.452	2	-7.5
-3.009	3	-3

This asymptotic structure is confirmed by the root-locus shown in Figure (5.40) for g varying from 0.1 to 100.0 logarithmically while the other tuning parameters are set to the values given previously. Pole pair c form the complex conjugate poles of the third-order asymptote set and they are obviously the most limiting factor of the whole design, becoming unstable for $g > 6.85$. The third-order asymptote are caused by the nozzle dynamics and so the nozzles are the "weak link" in this design. To see how this affects the overall system performance the frequency response of the closed-loop transfer function matrix is given as Figure (5.41) for $g = 6.0$, all other tuning parameters being unaltered.

From Figure (5.41) it is clear that the nozzle dynamics produce a lightly damped mode which dominates the overall system performance by giving high resonant peaks. The forward speed control-mode is dominated in this way as it is most closely associated with the nozzles at this flight case whereas the other two control-modes have high resonant peaks in their off-diagonal cross coupling transfer-function elements. It is apparant that the desired performance of 10 rad/s bandwidth cannot be reached due to the limitations of the slow nozzle dynamics.

Treating this case study as the early stage of a theoretical design, it is possible to move the nozzle actuator poles to the left making the nozzle dynamics faster until the desired system performance becomes possible. As an example here, the actuator speed is doubled by moving the pole at -6.0 to -12.0 and moving the pole at -4.0 to -8.0 forming Plant-7. This in turn moves the third-order asymptote pivot-point from -3.009 to -6.342 (calculated using the Pro-Matlab

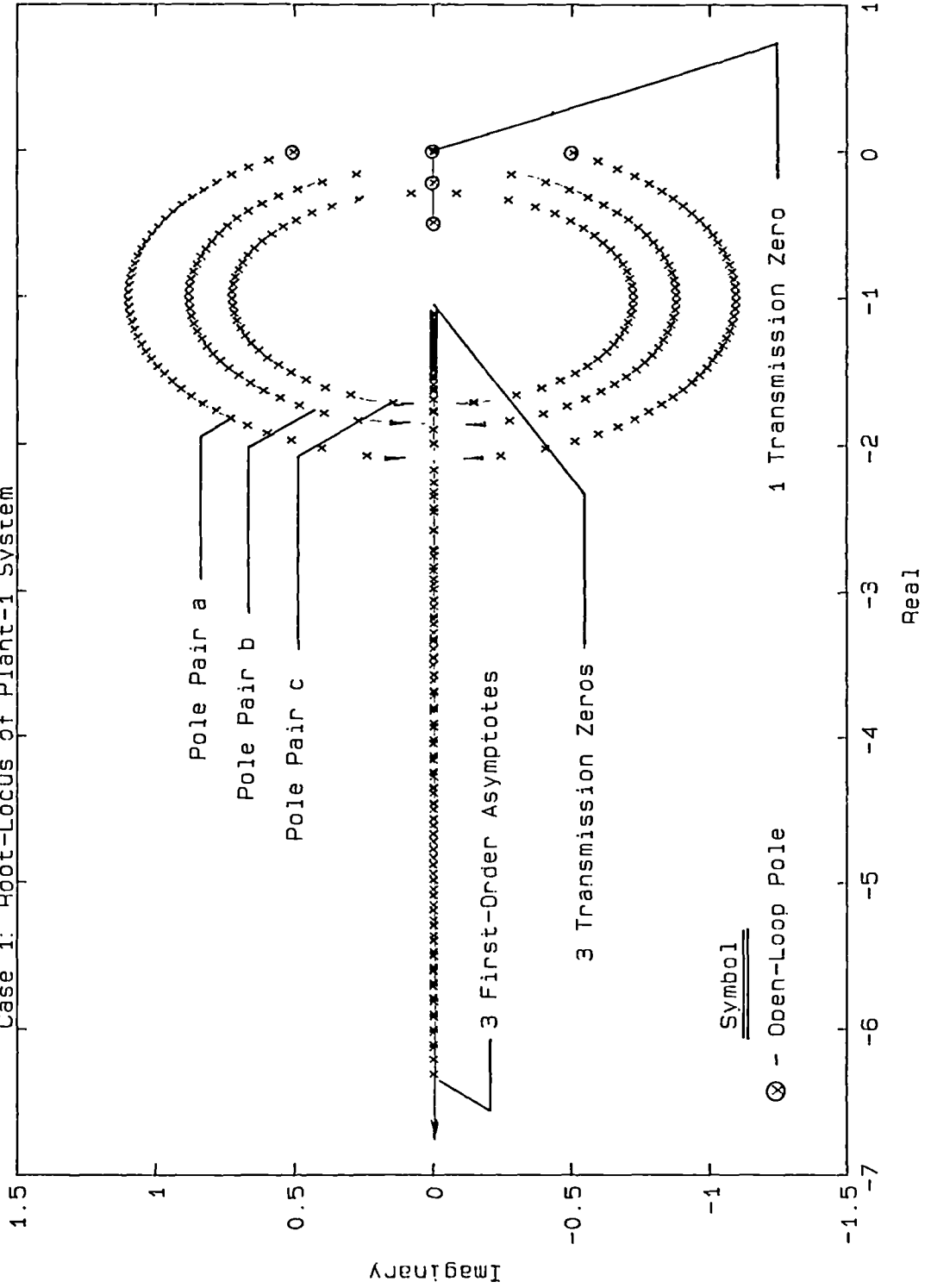
function). This new root-locus structure is confirmed by Figure (5.42) which is plotted for the same parameter settings as Figure (5.40).

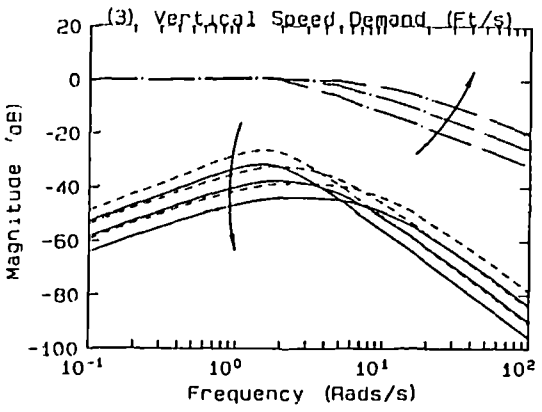
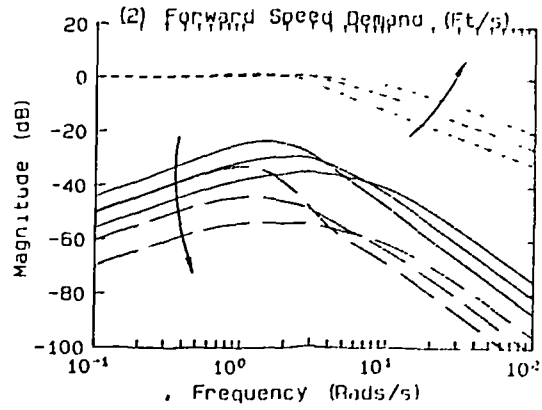
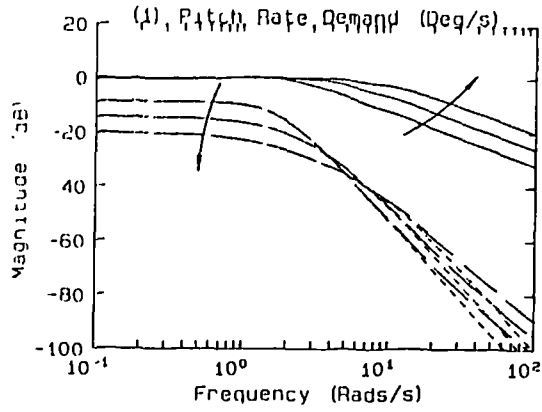
Pole pair C are now stable for $g > 15.5$, a large improvement over the previous condition ($g > 6.85$). This is further confirmed by the frequency response of the closed-loop transfer function matrix (Figure (5.43)) plotted once again for $g = 6.0$ so that direct comparisons can be made between Figure (5.43) and Figure (5.42). Comparing the two frequency responses shows that the resonant peaks have now been greatly reduced. Although the response is still not ideal, the bandwidths are close to 10 rad/s and tuning will improve the overall response. In this way the designer can tune the actuators to meet a specific system performance specification. Thus the high-gain method provides the means for "working backwards" an essential feature for any control law design method that is used for CCV's.

The high-gain method has now been applied to a typical V/STOL aircraft model at a representative transition flight condition with full actuator dynamics included. Various features of the high-gain method have now been illustrated including the effect of the engine non-linearity. A full discussion of this and other non-linear effects that influence the controller design are discussed in Chapter 7. But first the overall design brief for the full gain scheduling controller is presented in the next chapter (chapter 6).

Figure 5.1

Case 1: Root-Locus of Plant-1 System

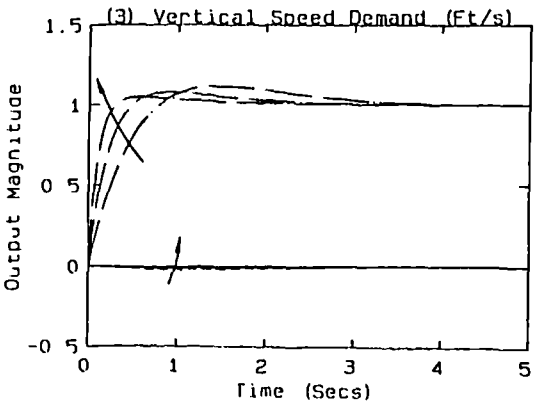
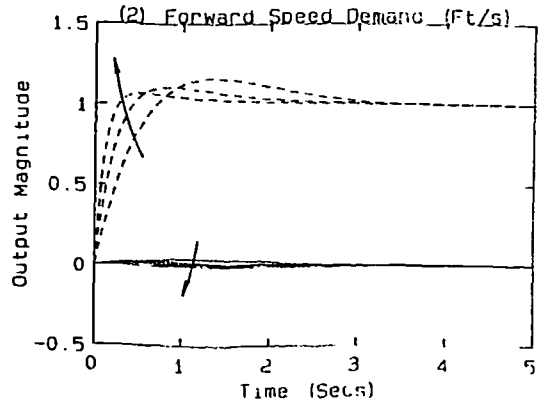
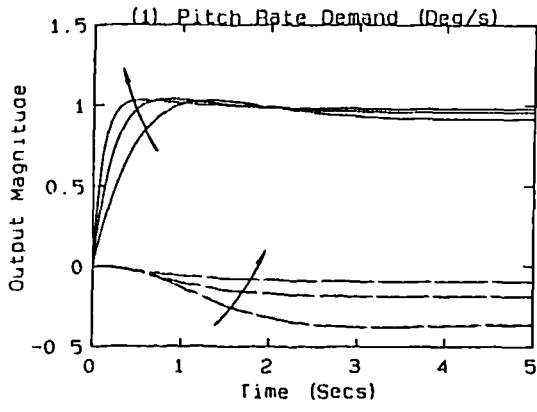




Key
 ——— Pitch Rate (Deg/s)
 - - - Forward Speed (Ft/s)
 - · - Vertical Speed (Ft/s)

Arrows represent increasing gain for gain = 2.5, 5.0, 10.0

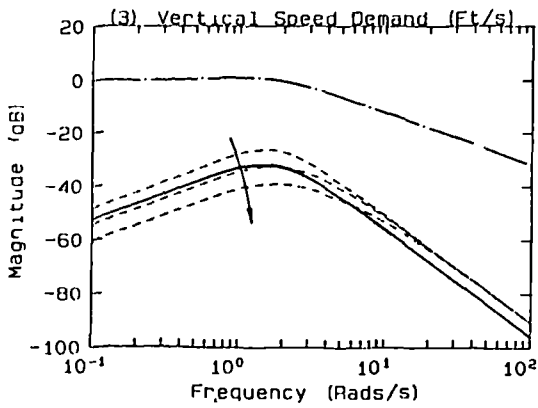
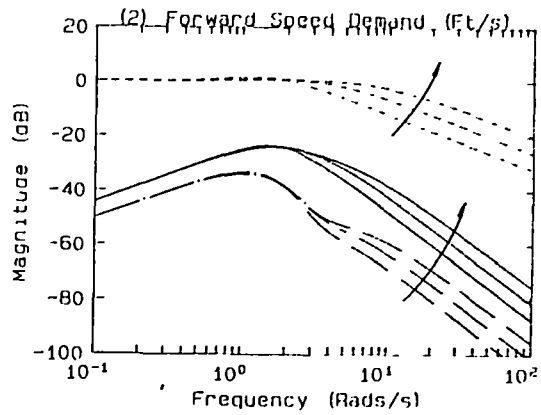
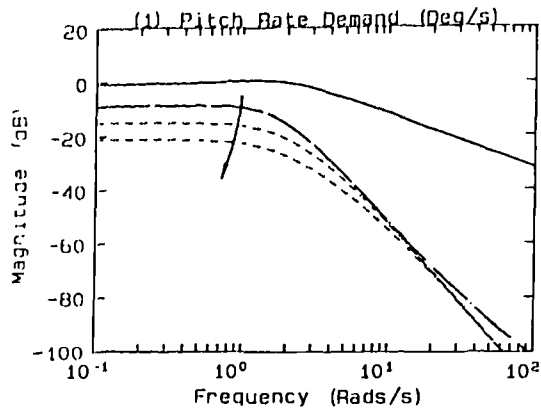
Figure 5.2
 Case 1:
 Frequency Response for Plant-1 System



key
 ——— Pitch Rate (Deg/s)
 - - - Forward Speed (Ft/s)
 - · - Vertical Speed (Ft/s)

Arrows represent increasing gain for gain = 2.5, 5.0, 10.0

Figure 5.3
 Case 1:
 Step Response for Plant-1 System



Key

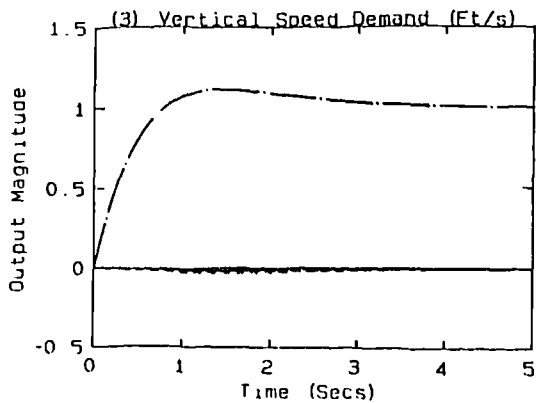
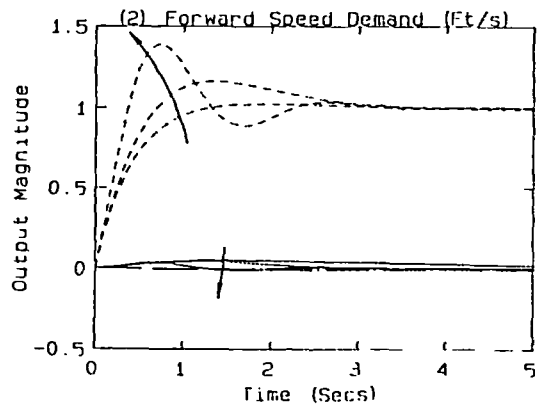
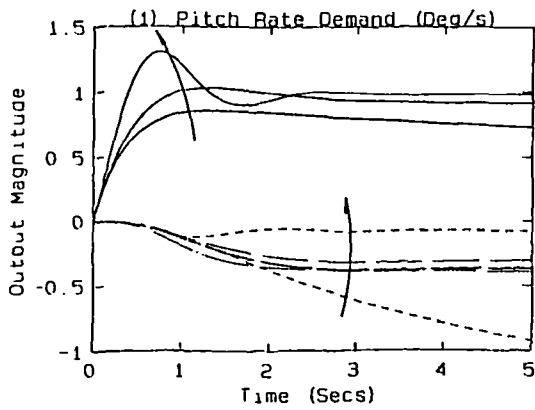
- - Pitch Rate (Deg/s)
- - - - Forward Speed (Ft/s)
- · - Vertical Speed (Ft/s)

Arrows represent increasing σ_2 for $\sigma_2 = 1.0, 2.0, 4.0$ and for a gain of 2.5

Figure 5.4

Case 1.

Frequency Response for Plant-1 System



Key

- - Pitch Rate (Deg/s)
- - - - Forward Speed (Ft/s)
- · - Vertical Speed (Ft/s)

Arrows represent increasing ρ_1 or ρ_2 taking the values 0.2, 1.0, 5.0 and for a gain of 2.5

Figure 5.5

Case 1.

Step Response for Plant 1 System

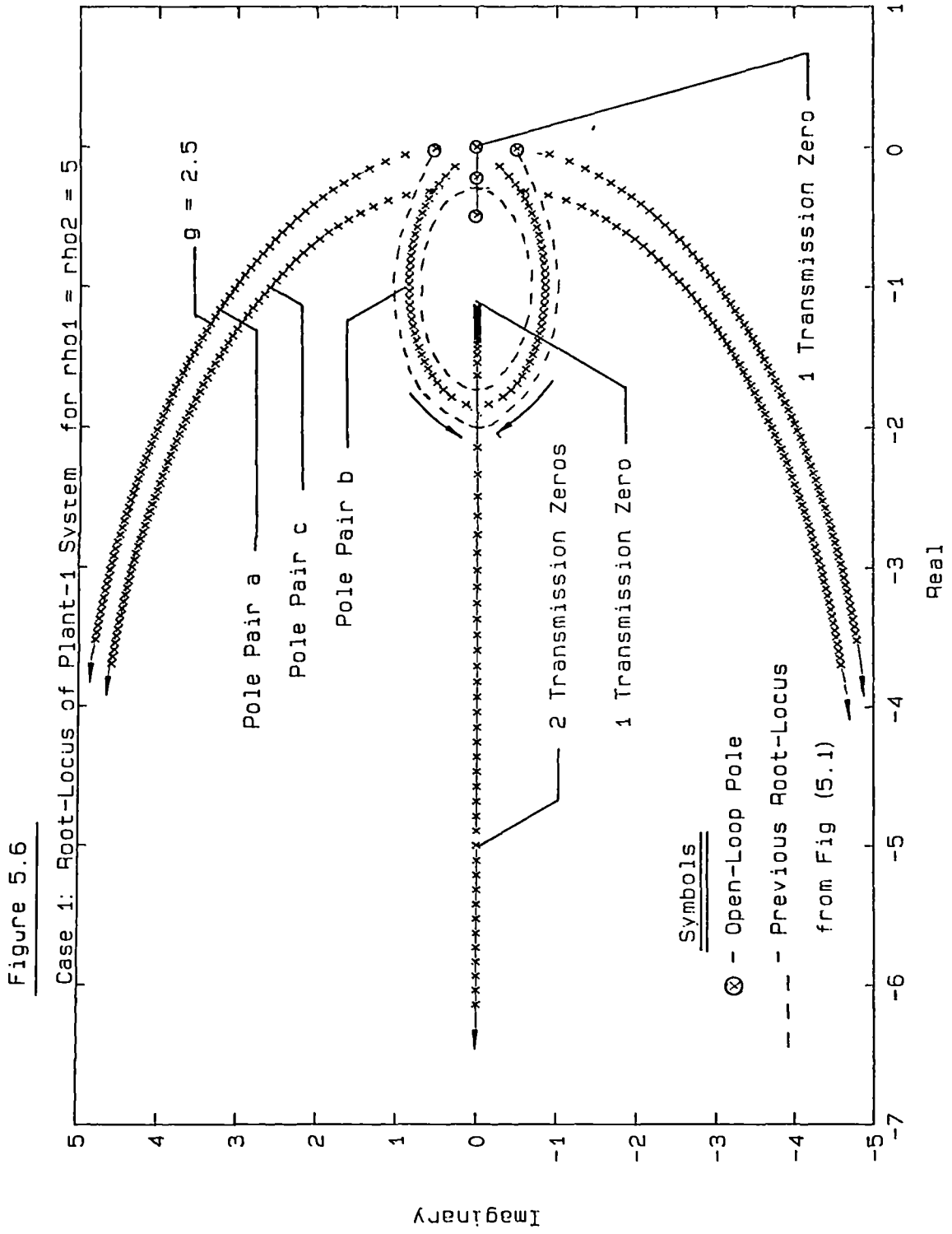
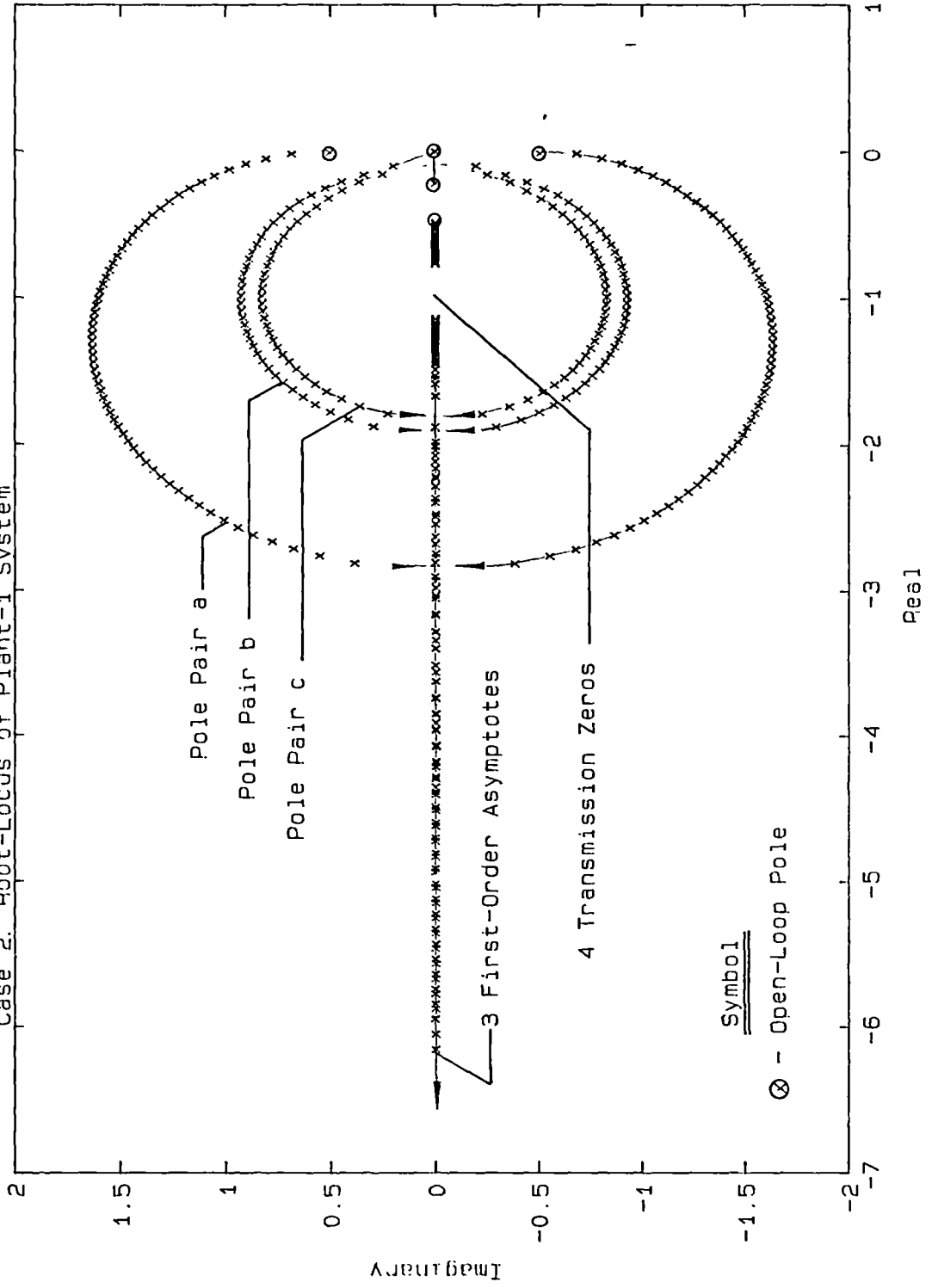
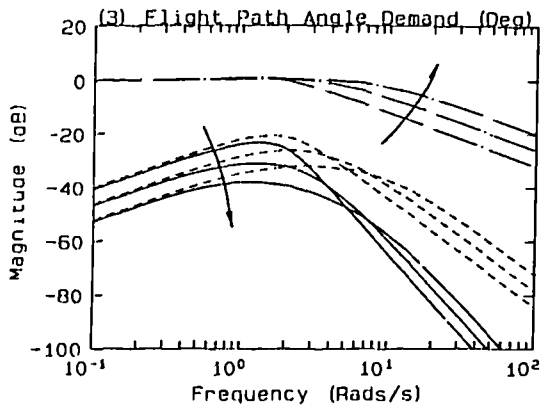
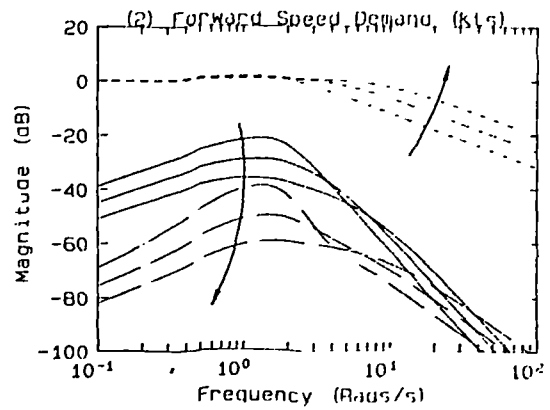
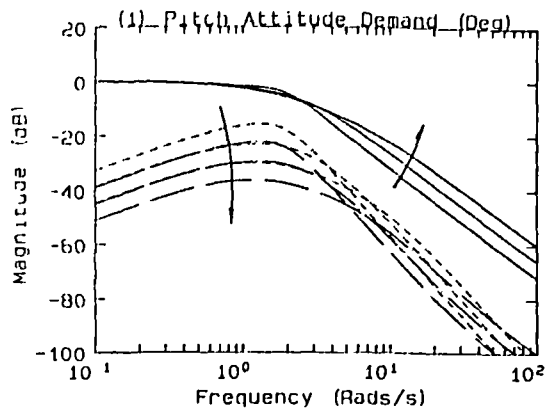


Figure 5.7
Case 2. Root-Locus of Plant-1 System



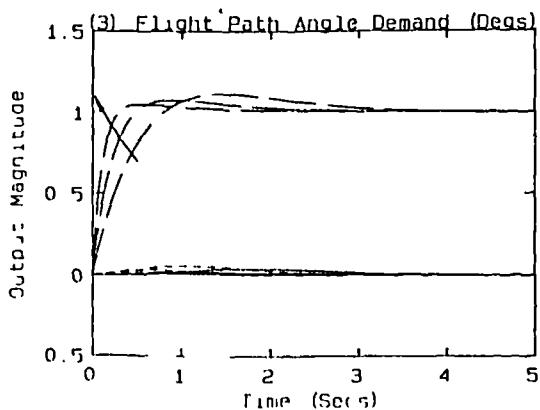
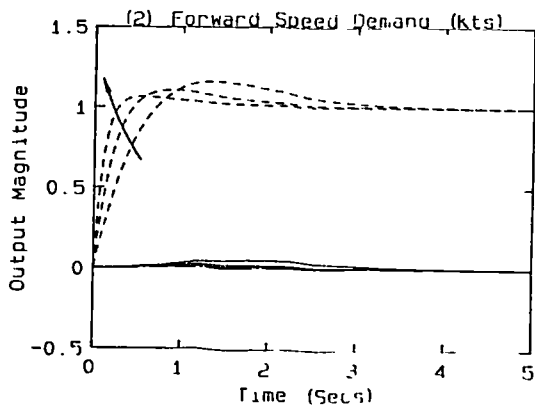
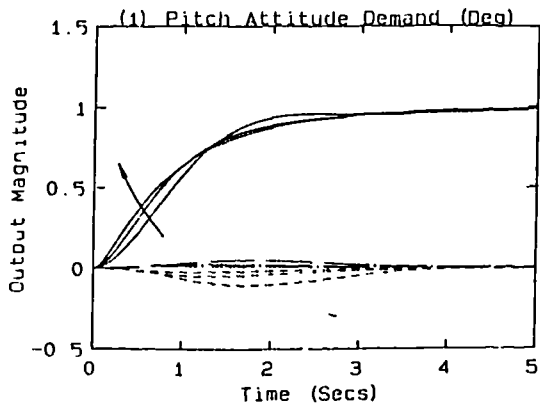


Key
 ——— Pitch Attitude (Deg)
 - - - Forward Speed (Kts)
 - · - Flight Path Angle (Deg)

Arrows represent increasing gain for gain = 2.5, 5.0, 10.0

Figure 5.8

Case 2.
 Frequency Response for Plant-1 System

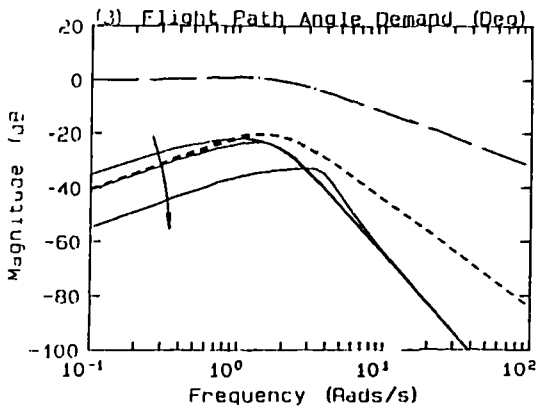
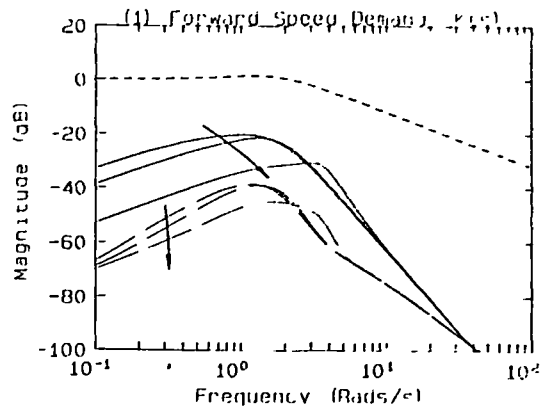
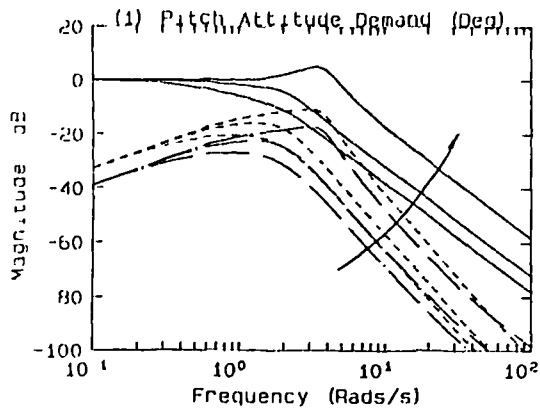


Key
 ——— Pitch Attitude (Deg)
 - - - Forward Speed (Kts)
 - · - Flight Path Angle (Deg)

Arrows represent increasing gain for gain = 2.5, 5.0, 10.0

Figure 5.9

Case 2.
 Step Response for Plant-1 System



key

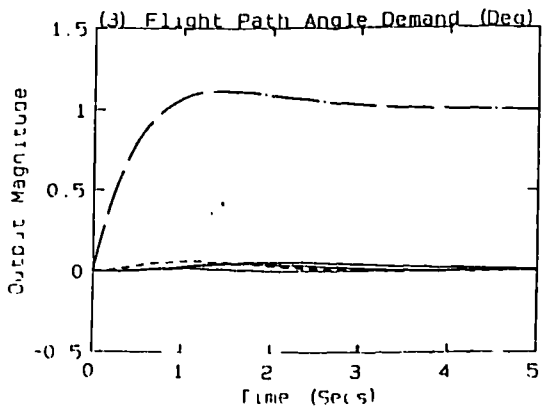
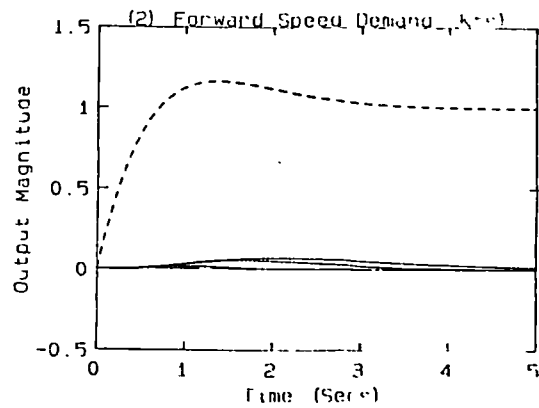
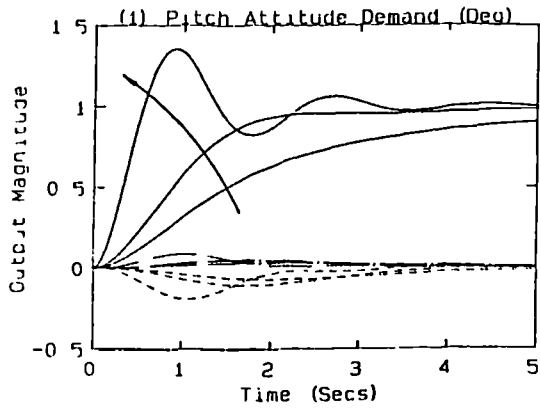
- Pitch Attitude (Deg)
- - - Forward Speed (Kts)
- - - Flight Path Angle (Deg)

Arrows represent decreasing extra measurement gain for $m = 2.0, 1.0, 0.2$ and for a gain of 2.5

Figure 5.10

Case 2.

Frequency Response for Plant-1 System



key

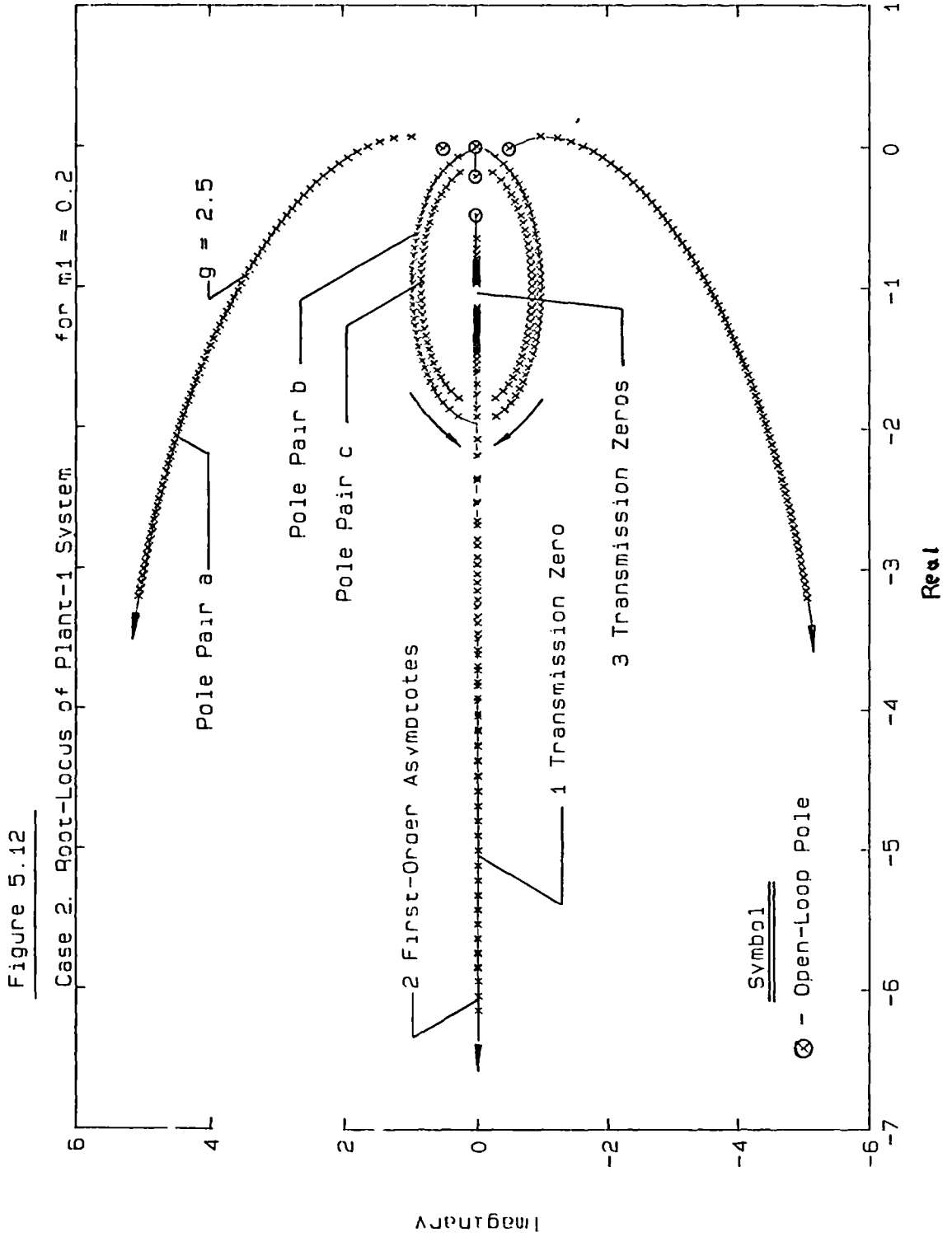
- Pitch Attitude (Deg)
- - - Forward Speed (Kts)
- - - Flight Path Angle (Deg)

Arrows represent decreasing extra measurement gain for $m = 2.0, 1.0, 0.2$ and for a gain of 5.0

Figure 5.11

Case 2

Step Response for Plant-1 System



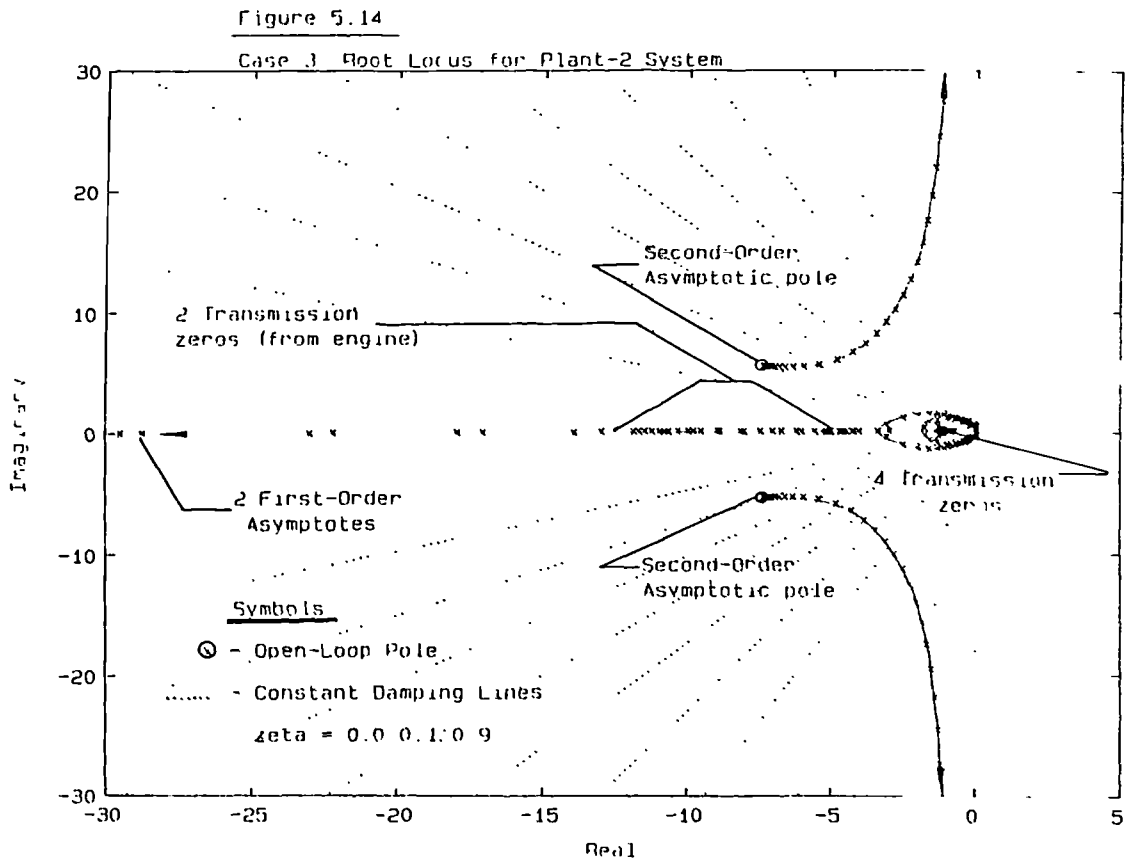
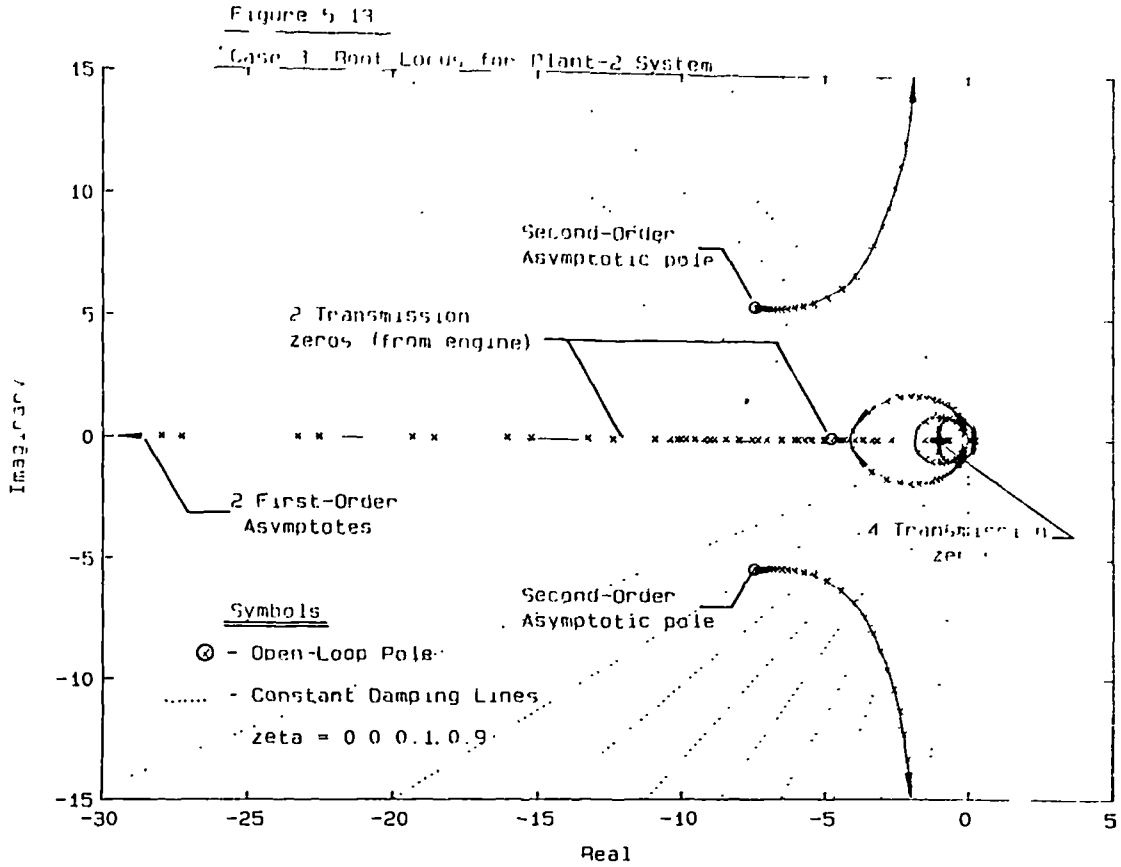
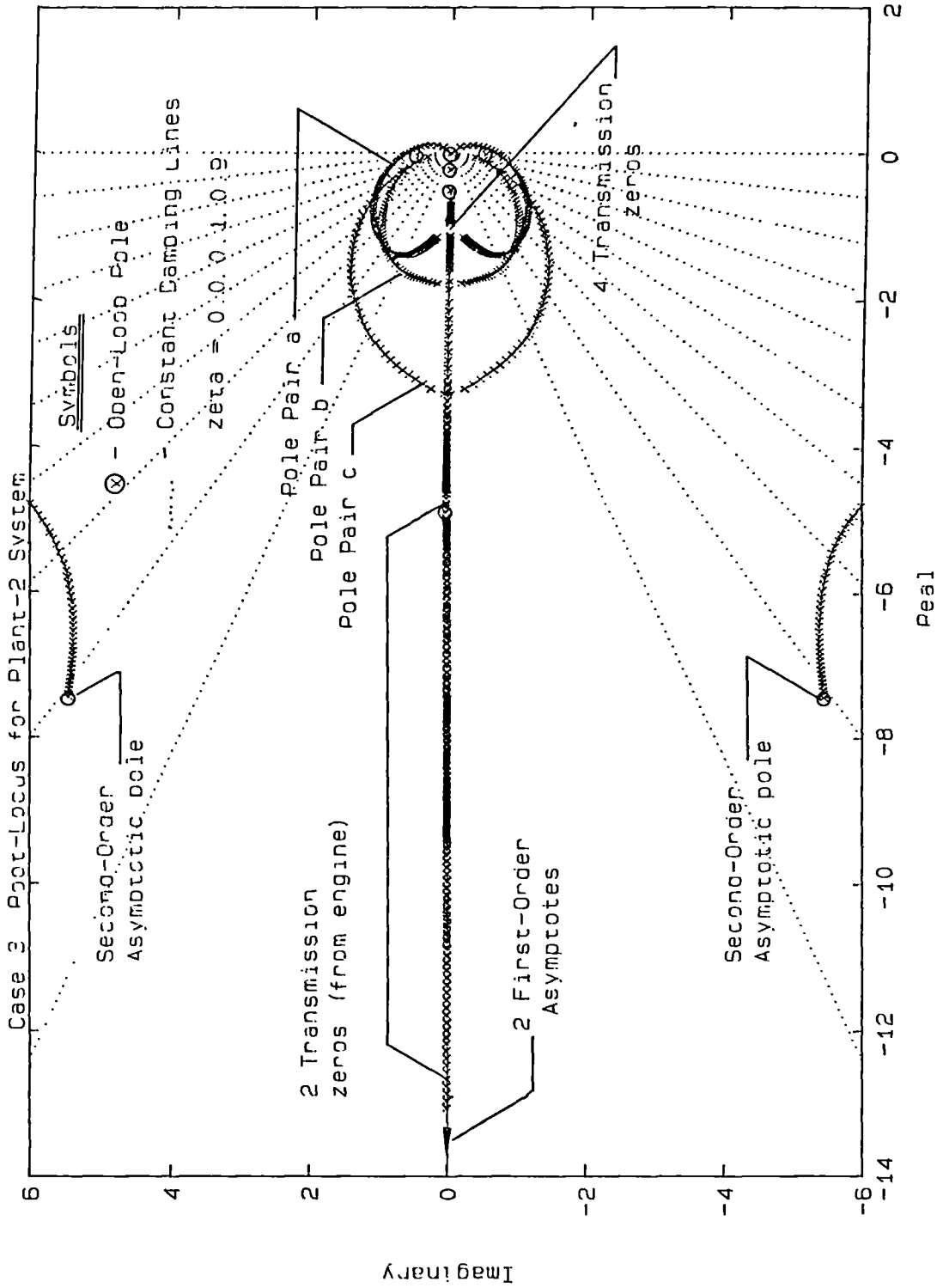
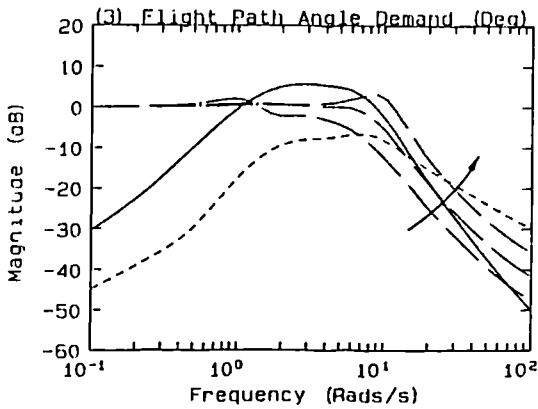
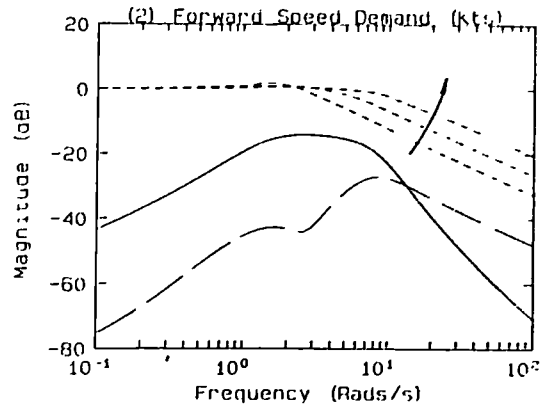
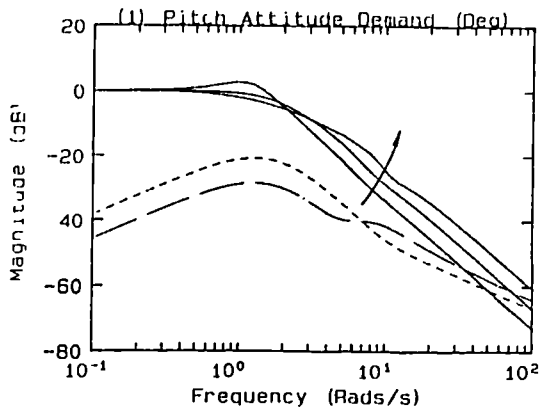


Figure 5.15





Key

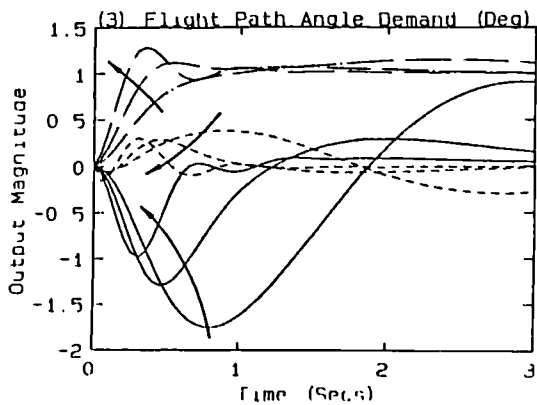
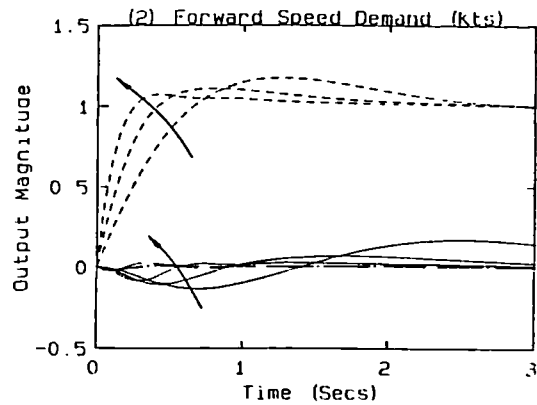
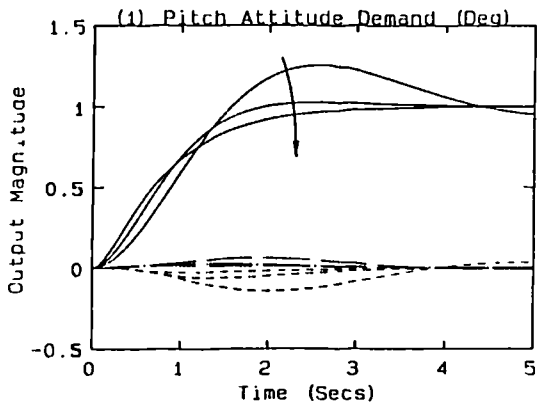
- - Pitch Attitude (Deg)
- - - Forward Speed (Kts)
- - - Flight Path Angle (Deg)

Arrows represent increasing gain for gain = 2.5, 5.0 and 10.0
Cross coupling for g=5.0 shown

Figure 5.16

Case 3.

Frequency Response for Plant-2 System



Key

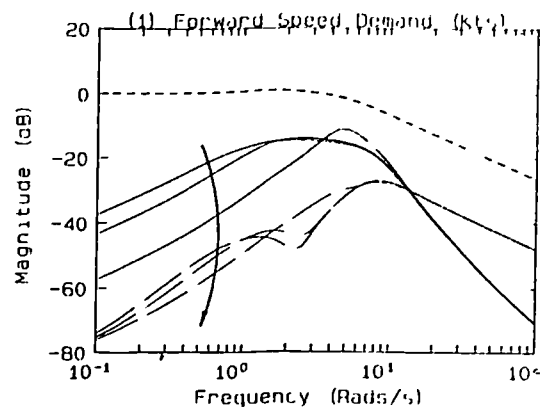
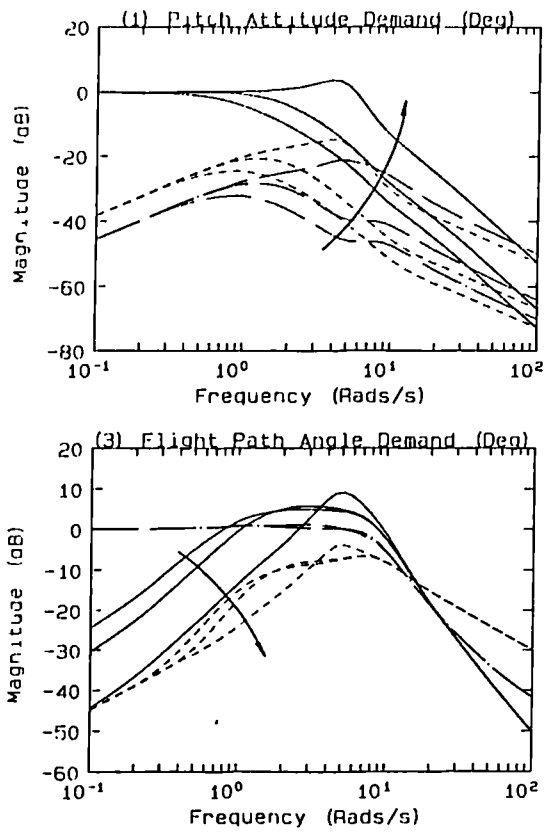
- - Pitch Attitude (Deg)
- - - Forward Speed (Kts)
- - - Flight Path Angle (Deg)

Arrows represent increasing gain for g = 2.5, 5.0 and 10.0

Figure 5.17

Case 3

Step Response for Plant 2 System

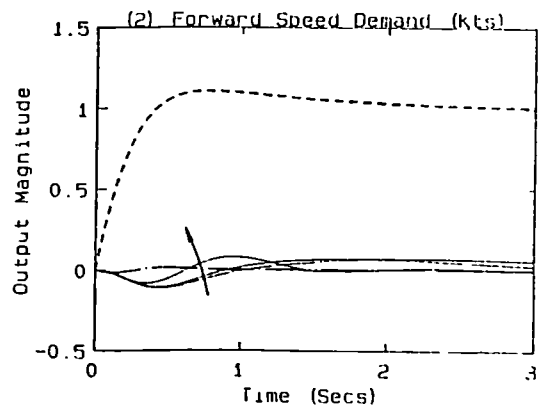
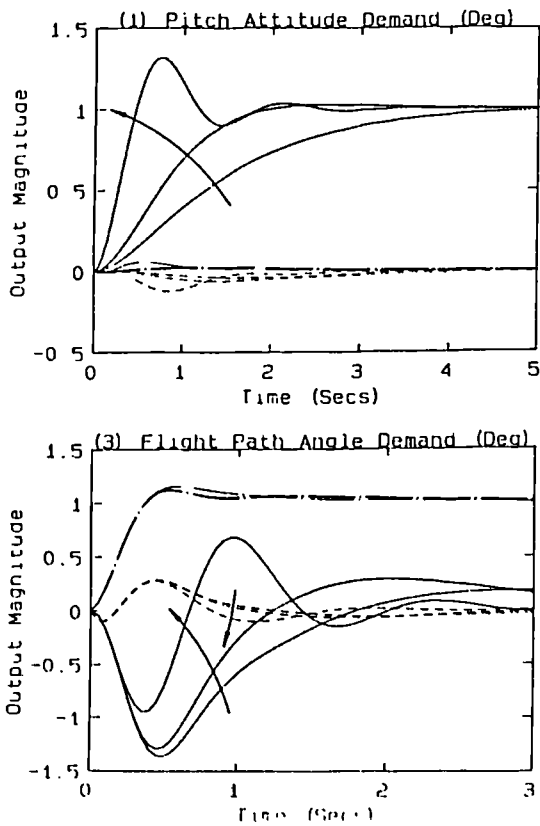


Key

- - Pitch Attitude (Deg)
- - - - Forward Speed (Kts)
- . - Flight Path Angle (Deg)

Arrows represent decreasing extra measurement gain for $m_1 = 2.0, 1.0$ and 0.2 and for a gain of 5.0

Figure 5.18
Case 3.
Frequency Response for Plant-2 System



Key

- - Pitch Attitude (Deg)
- - - - Forward Speed (Kts)
- . - Flight Path Angle (Deg)

Arrows represent decreasing extra measurement gain for $m_1 = 2.0, 1.0$ and 0.2 and for a gain of 5.0

Figure 5.19
Case 3.
Step Response for Plant-2 System

Figure 5.20

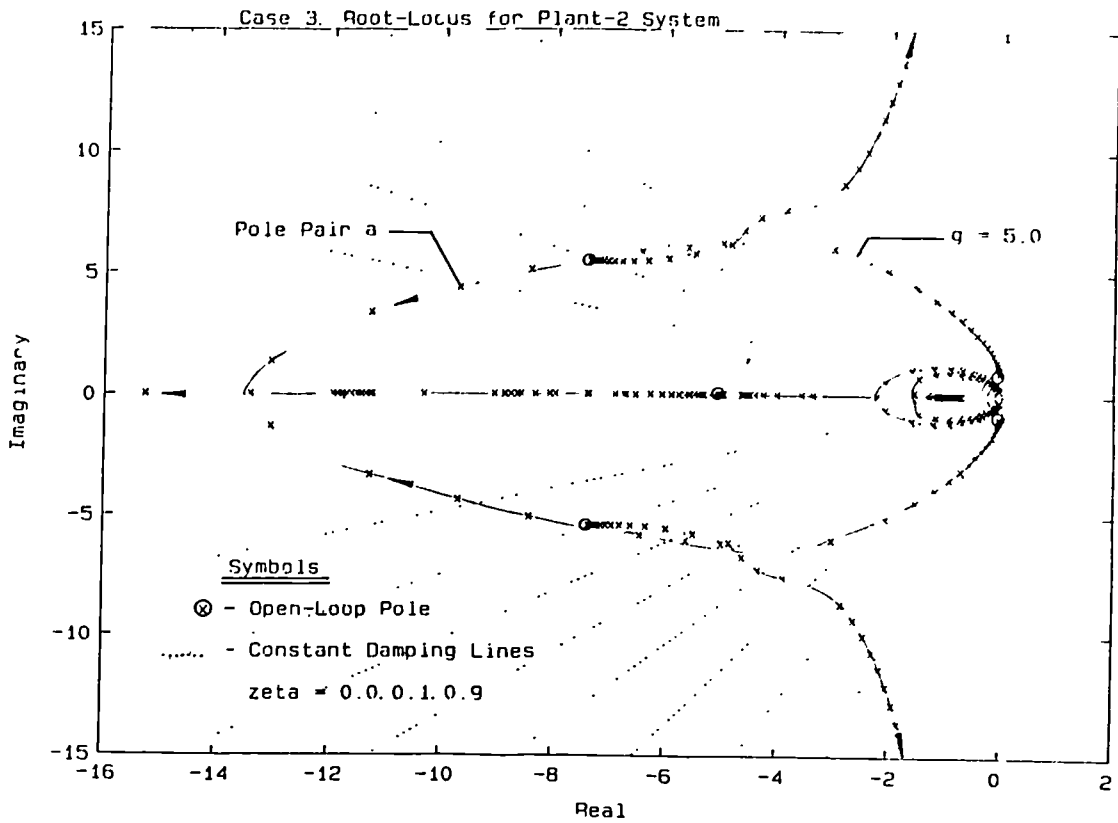
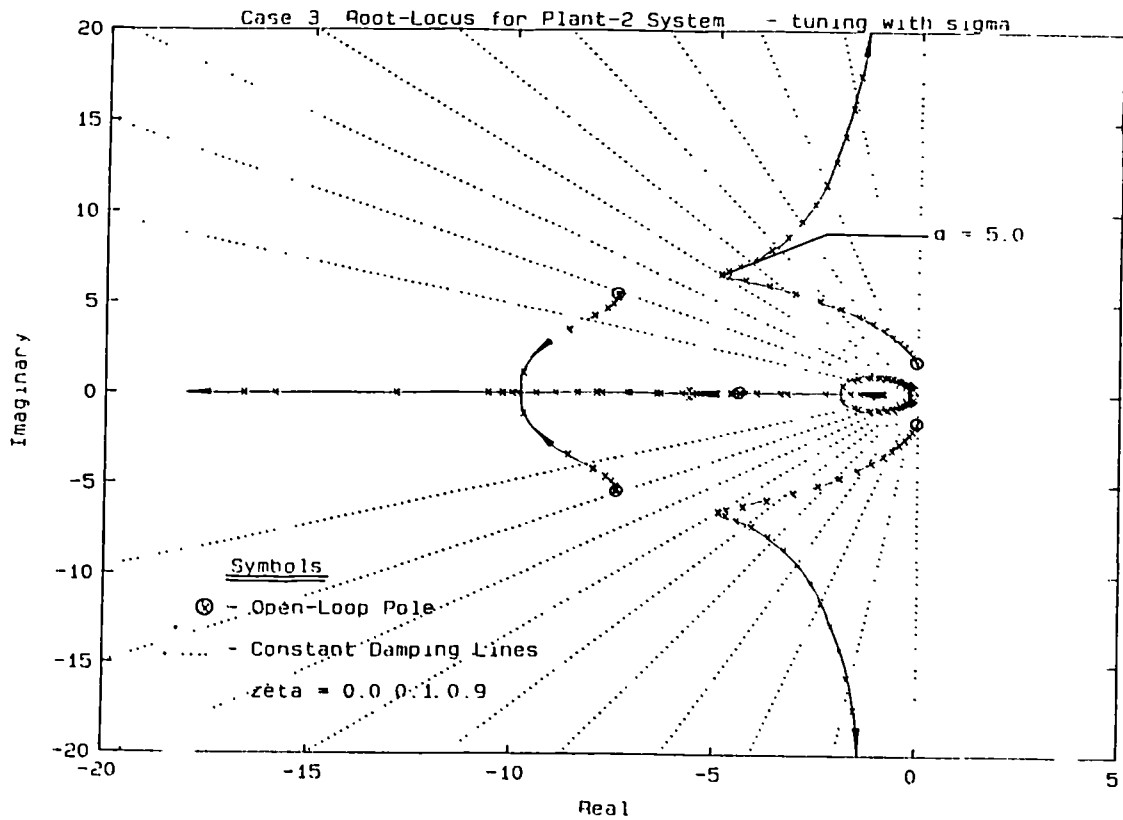
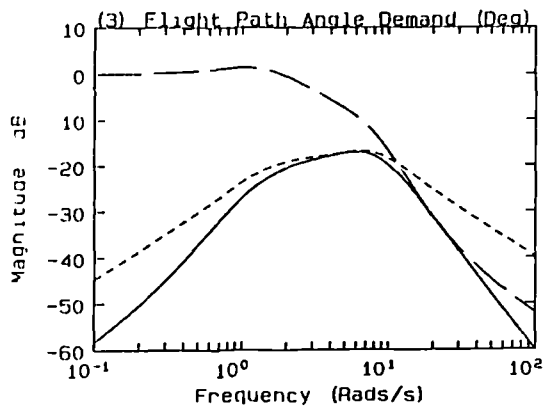
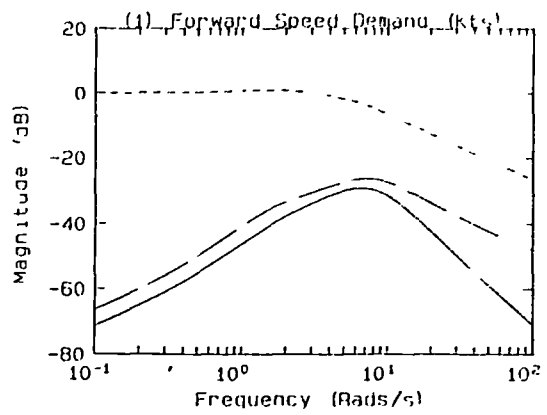
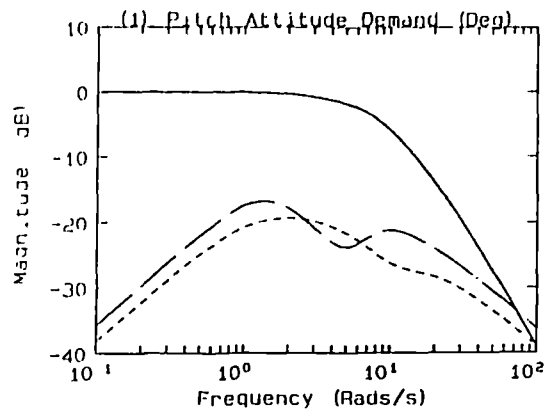


Figure 5.21

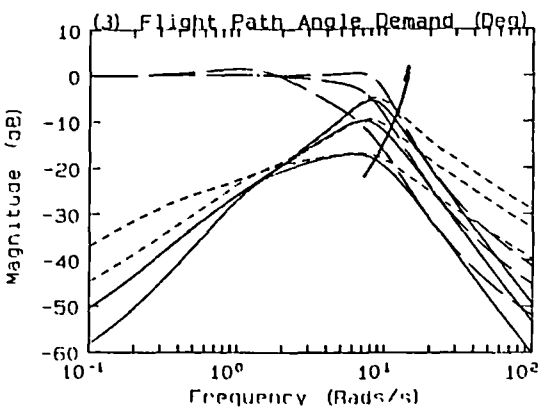
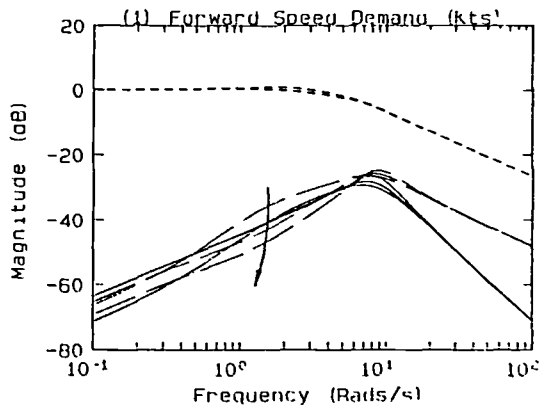
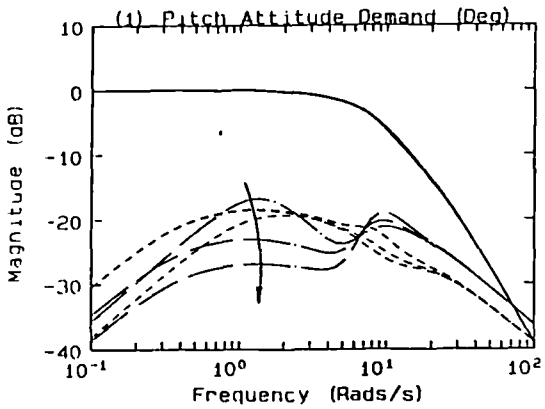




Key
 — Pitch Attitude (Deg)
 - - Forward Speed (kts)
 - . - Flight Path Angle (Deg)

System tuned with sigma to a damping ratio of 0.6 for the critical control-mode - flight path angle

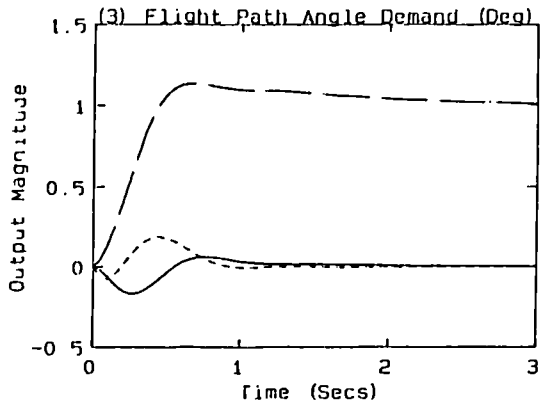
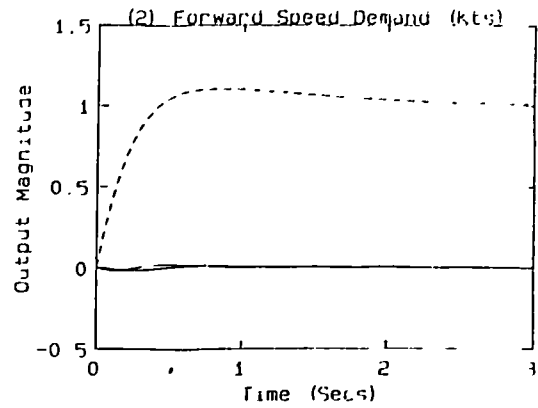
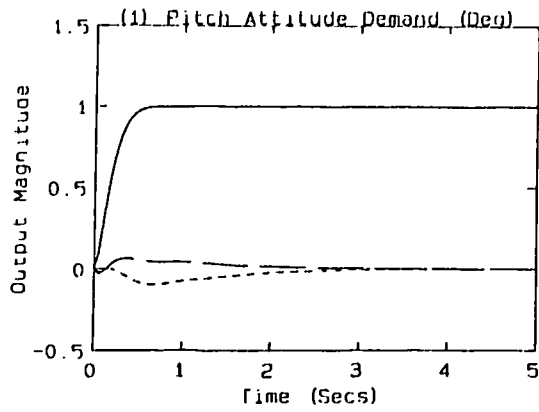
Figure 5.22
 Case 3.
 Frequency Response for Plant-2 System



Key
 — Pitch Attitude (Deg)
 - - Forward Speed (kts)
 - . - Flight Path Angle (Deg)

Tuned system showing the effects of varying sigma(3) on the flight path angle control-mode

Figure 5.23
 Case 3
 Frequency Response for Plant-1 System

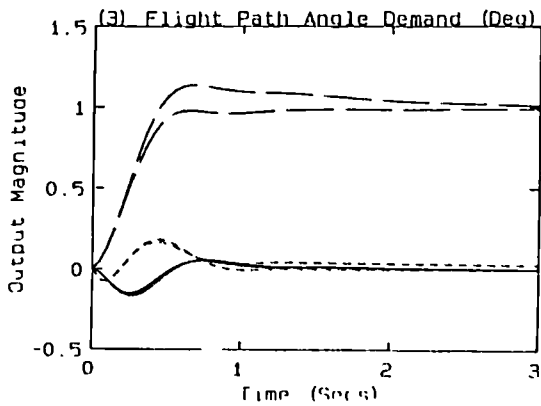
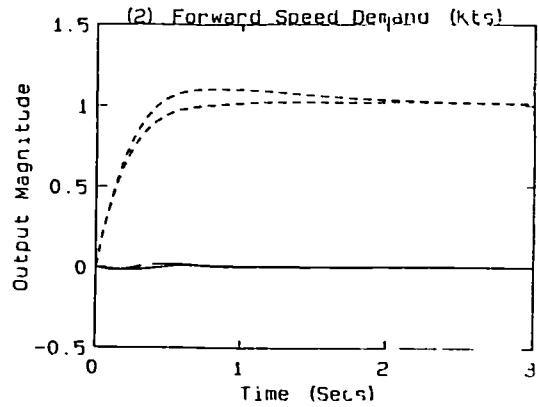
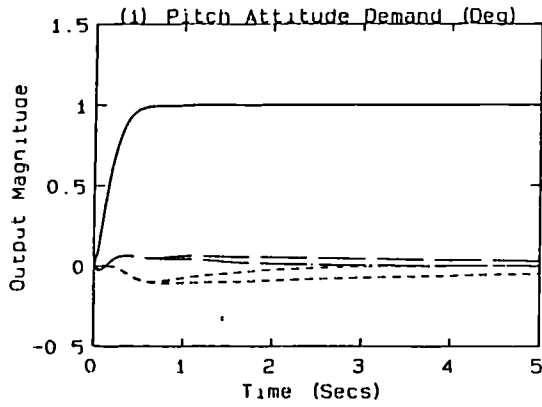


Key
 ——— - Pitch Attitude (Deg)
 - - - - Forward Speed (Kts)
 - · - Flight Path Angle (Deg)

System tuned with σ, α and ρ

Figure 5.24

Case 3.
 Step Response for Plant-2 System



Key
 ——— - Pitch Attitude (Deg)
 - - - - Forward Speed (Kts)
 - · - Flight Path Angle (Deg)

System tuned with σ, α, ρ
 and ρ - final design

Figure 5.25

Case 3.
 Step Response for Plant-2 System

Figure 5.26

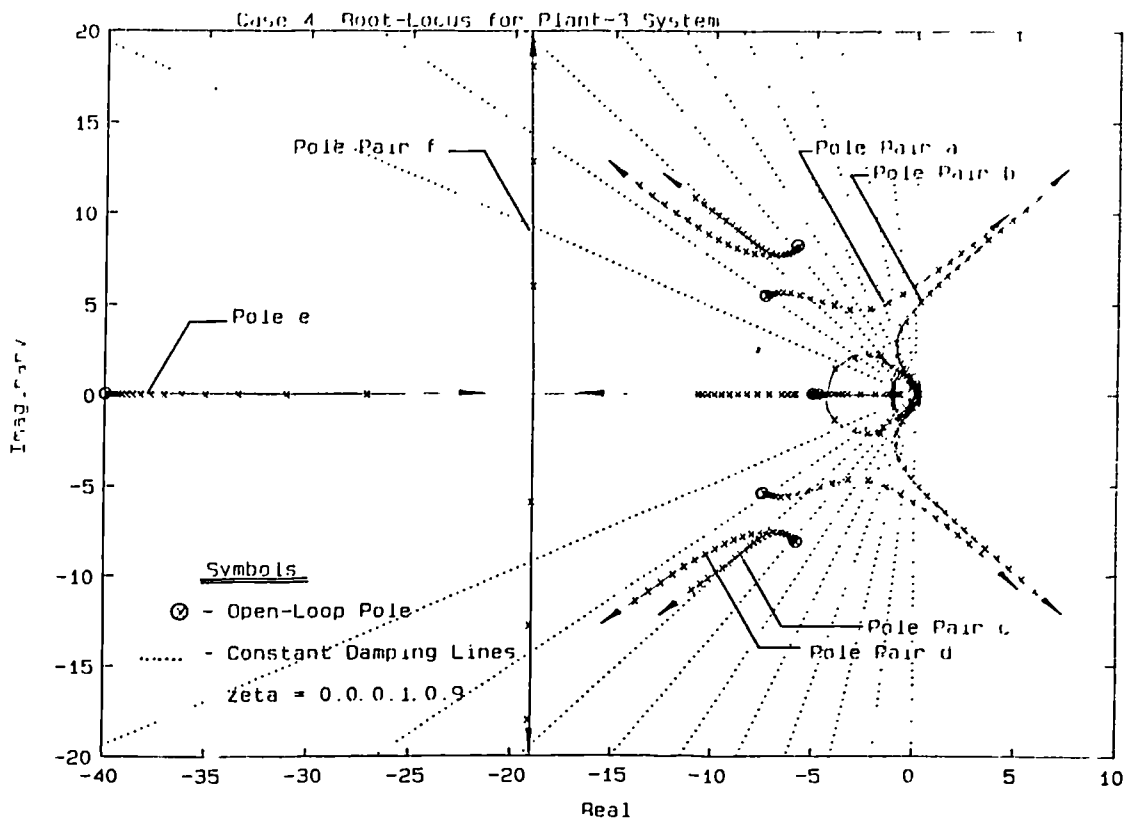


Figure 5.27

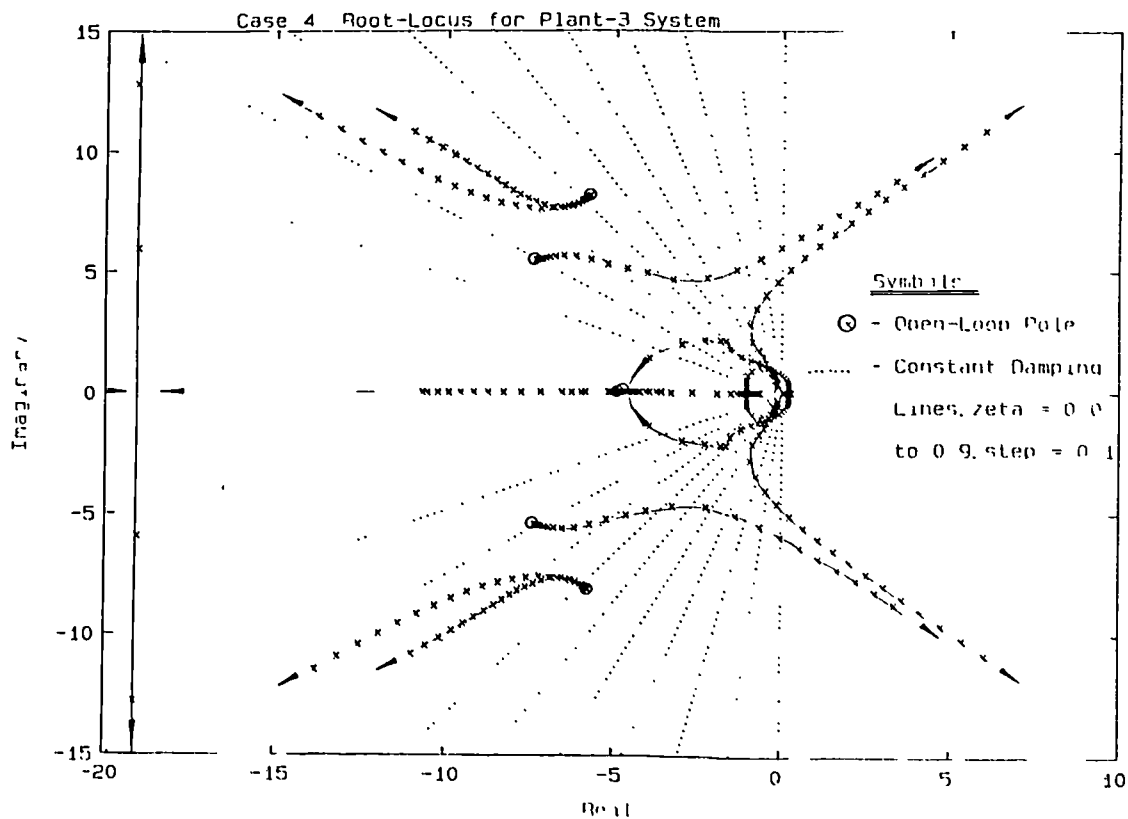
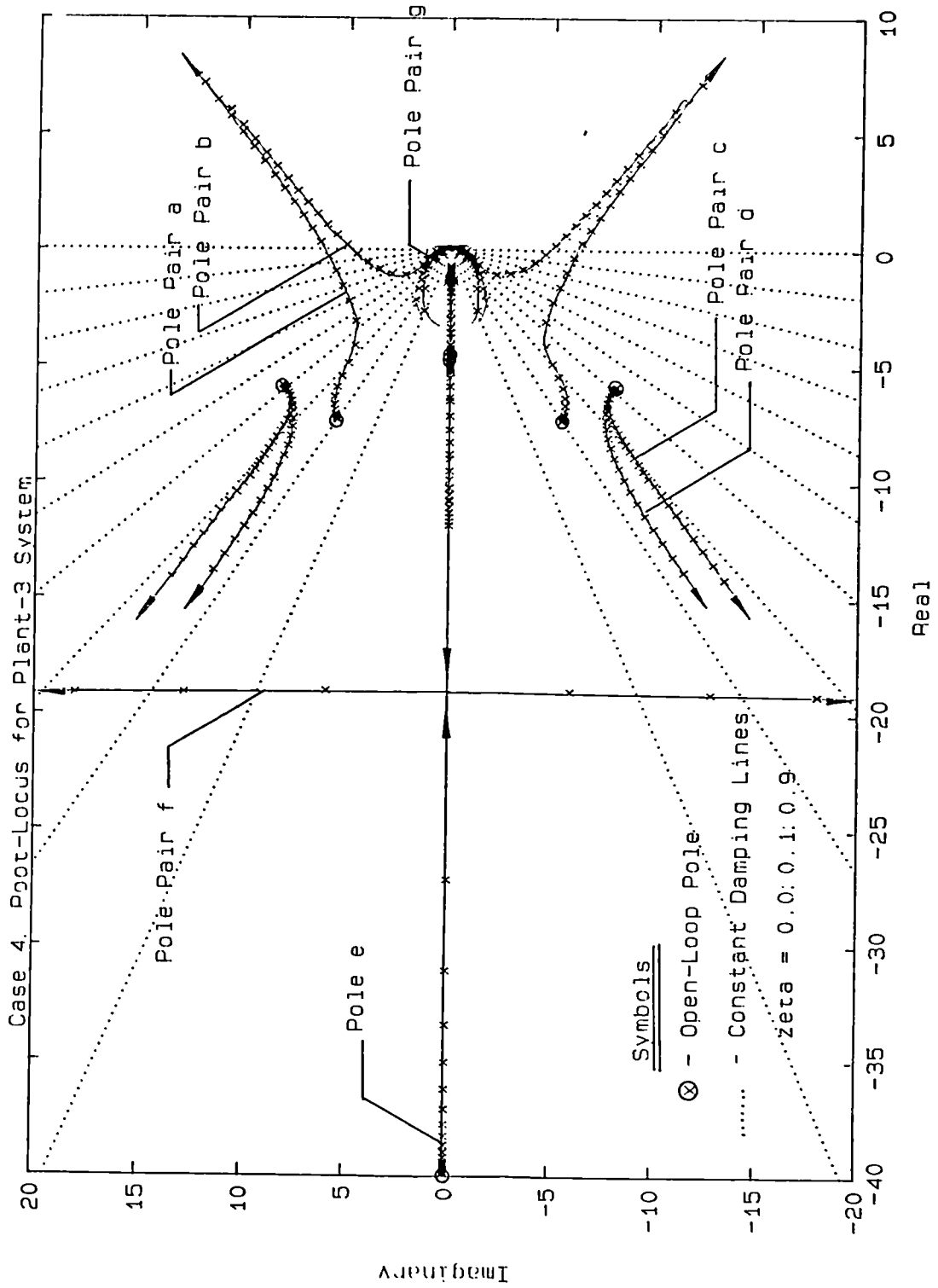
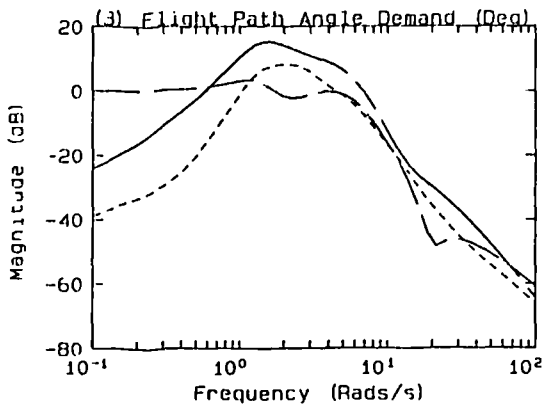
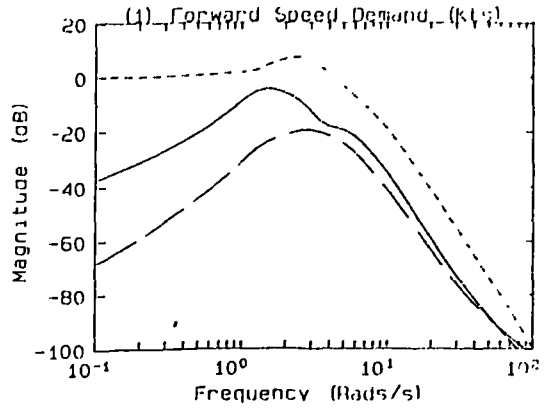
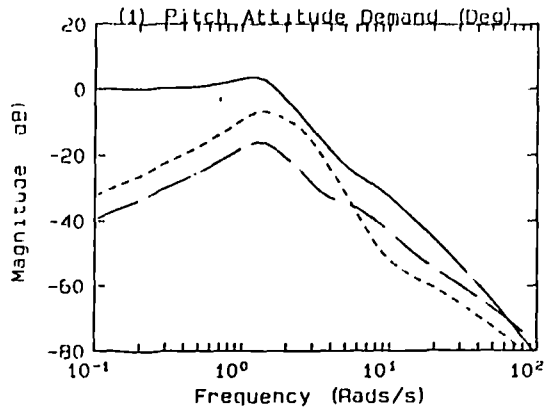


Figure 5.28





Key

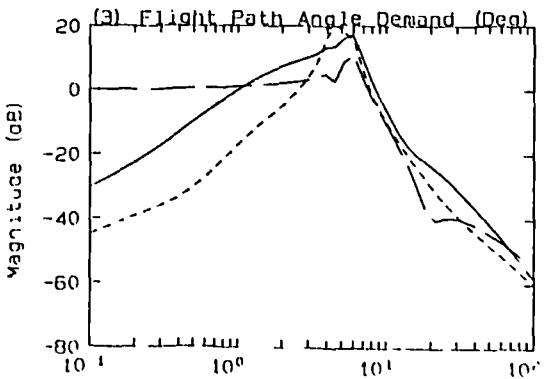
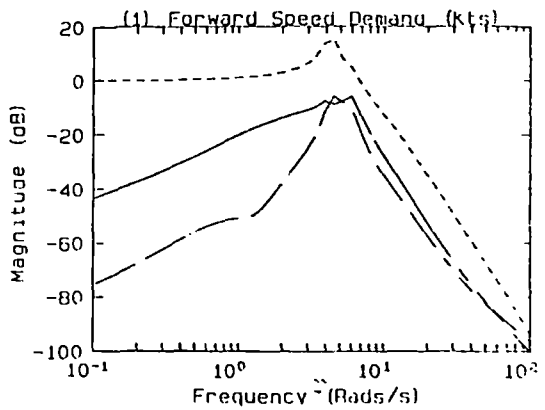
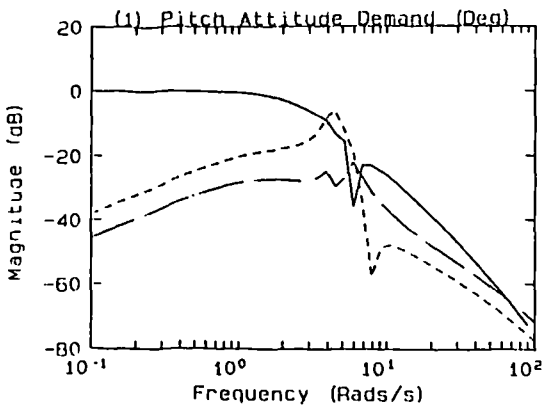
- - Pitch Attitude (Deg)
- - - - Forward Speed (Kts)
- · - Flight Path Angle (Deg)

The system gain is 5.0

Figure 5.29a

Case 4.

Frequency Response for Plant-3 System



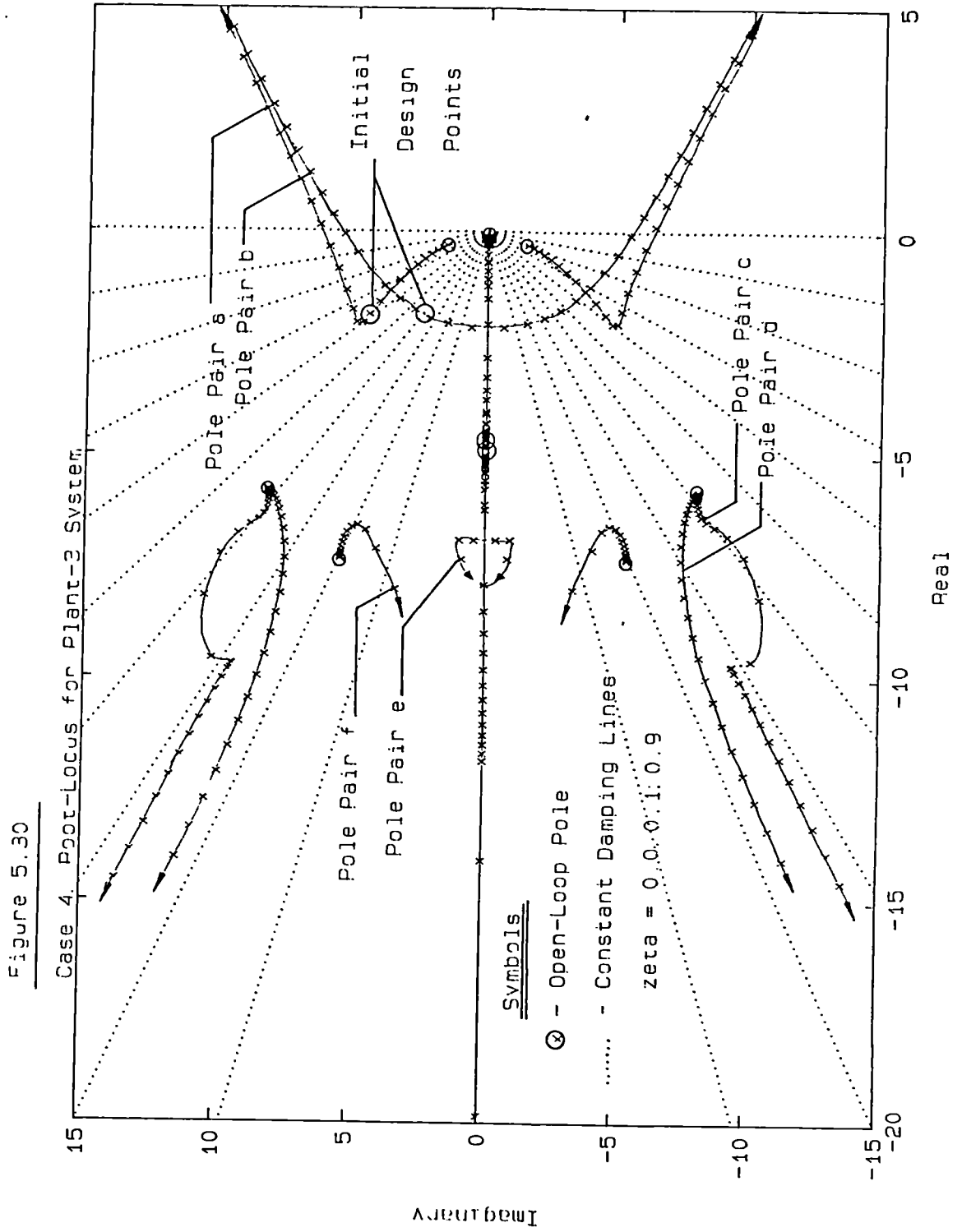
Key

- - Pitch Attitude (Deg)
- - - - Forward Speed (Kts)
- · - Flight Path Angle (Deg)

The system gain is 5.0

Figure 5.29b

Case 4



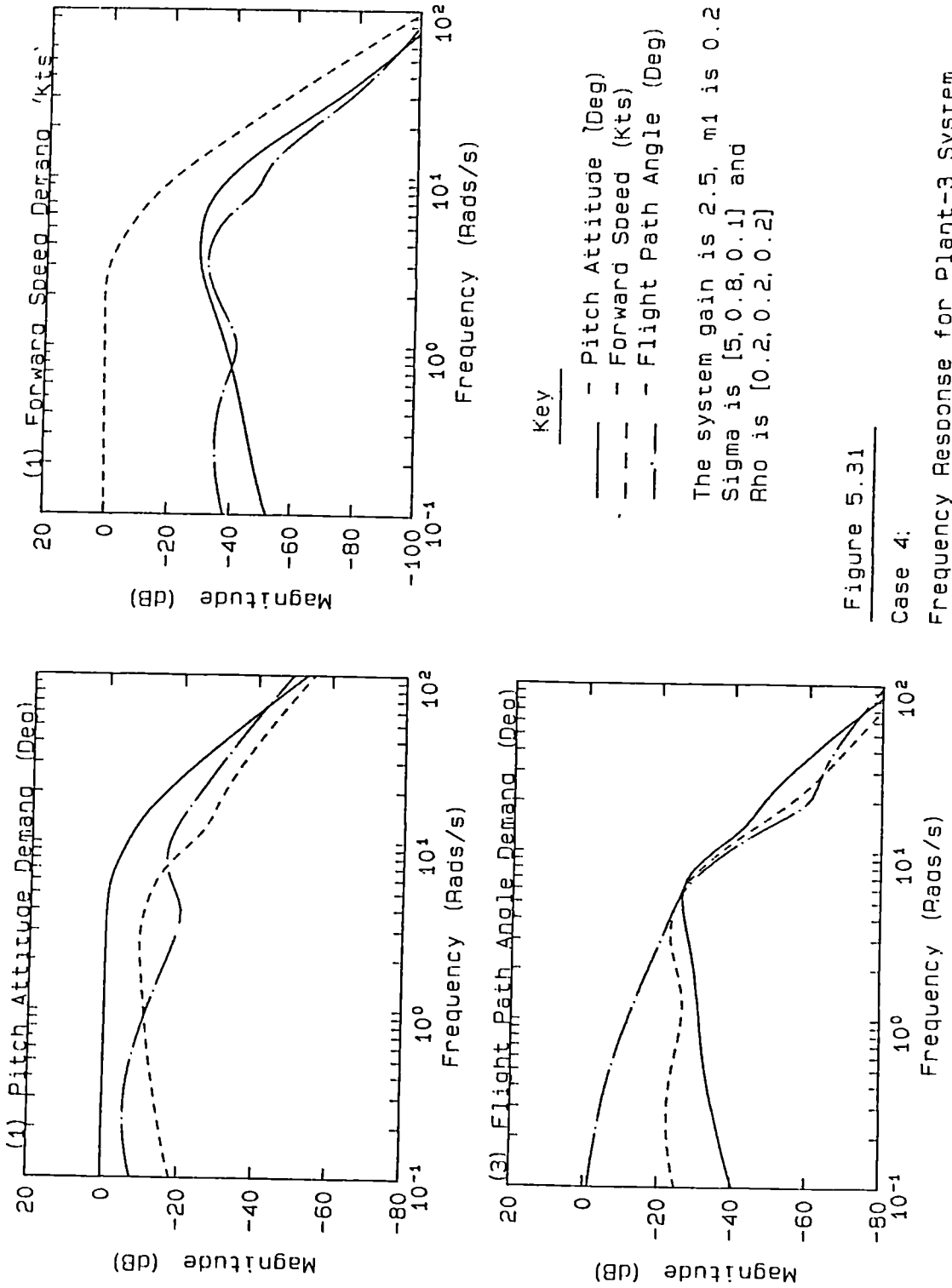
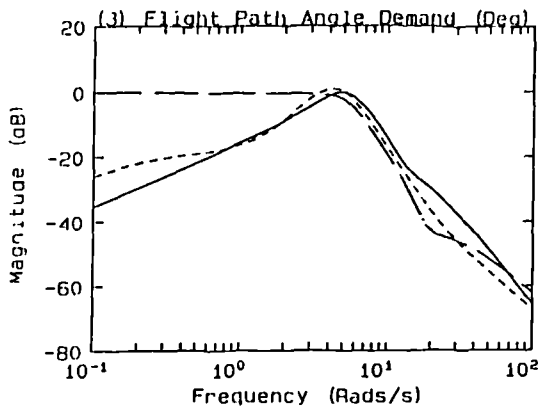
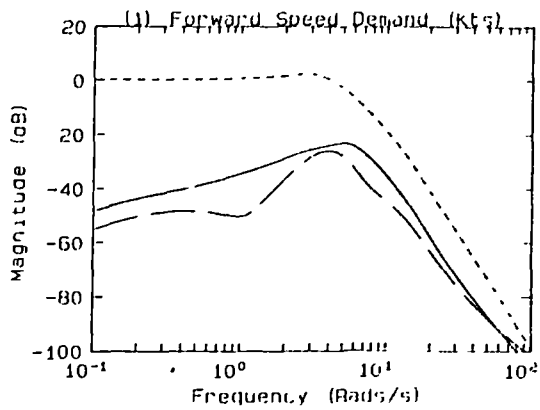
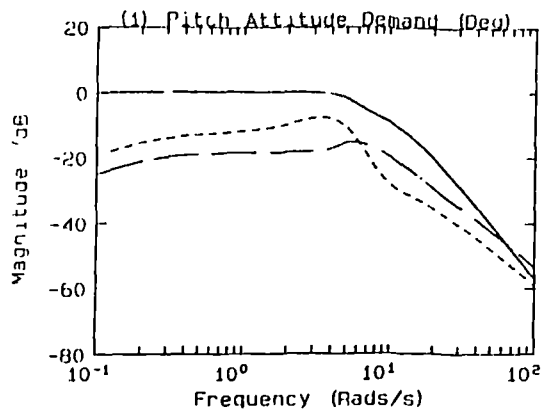


Figure 5.31

Case 4:

Frequency Response for Plant-3 System



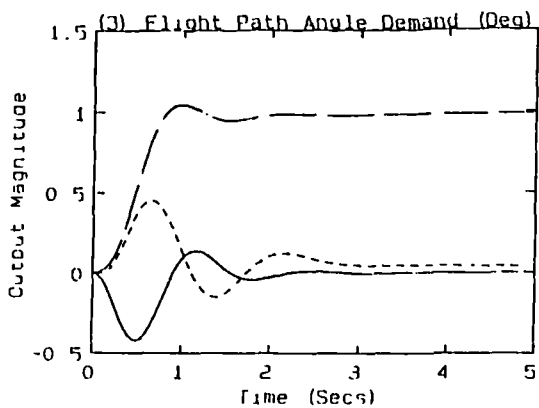
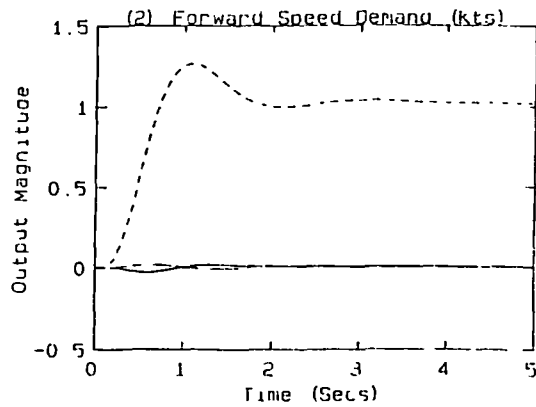
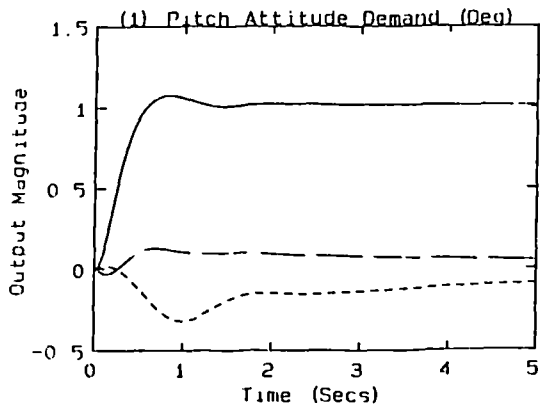
Key

- - Pitch Attitude (Deg)
- - - Forward Speed (kts)
- · - Flight Path Angle (Deg)

The system gain is 2.5, m_1 is 0.25
 Sigma is [4, 1.05, 0.85] and
 Rho is [0 2.0 2.0 2]

Figure 5.32

Case 4.
 Frequency Response for Plant-3 System



Key

- - Pitch Attitude (Deg)
- - - Forward Speed (kts)
- · - Flight Path Angle (Deg)

The system gain is 2.5, m_1 is 0.25
 Sigma is [4, 1.05, 0.85] and
 Rho is [0 2.0 2.0 2]

Figure 5.33

Case 4.
 Step Response for Plant-3 System

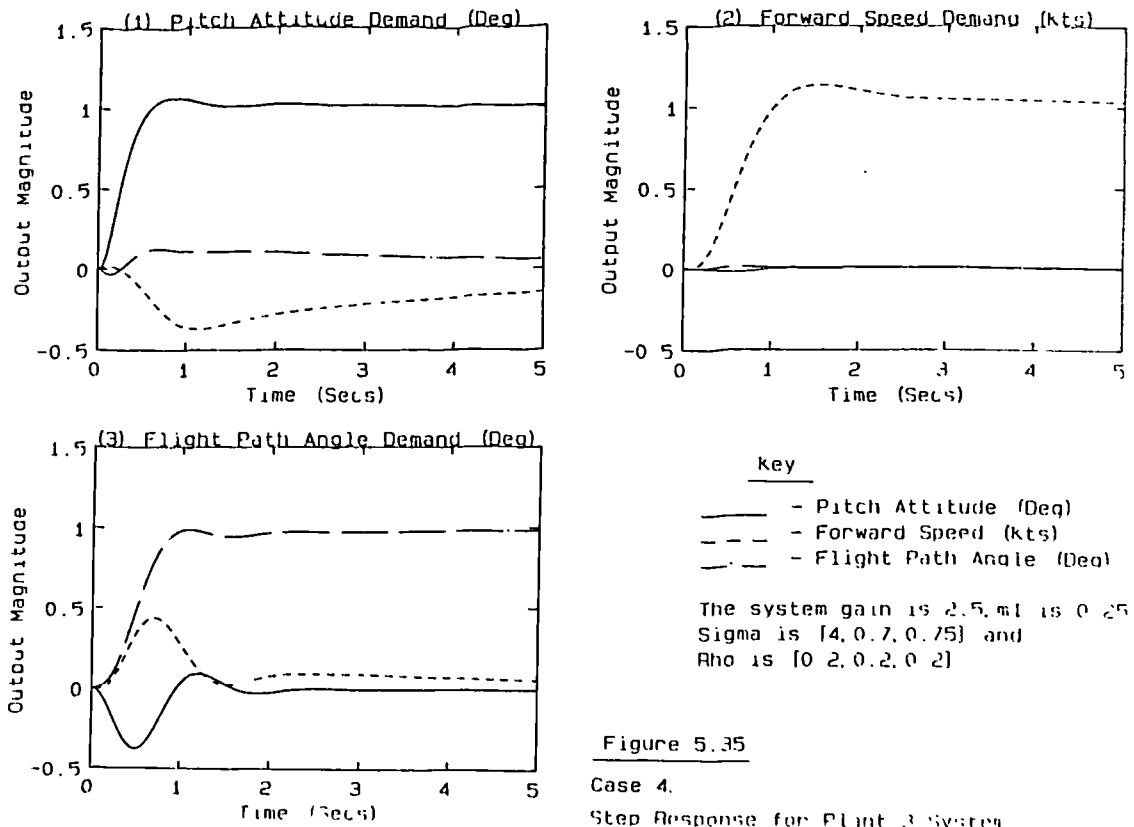
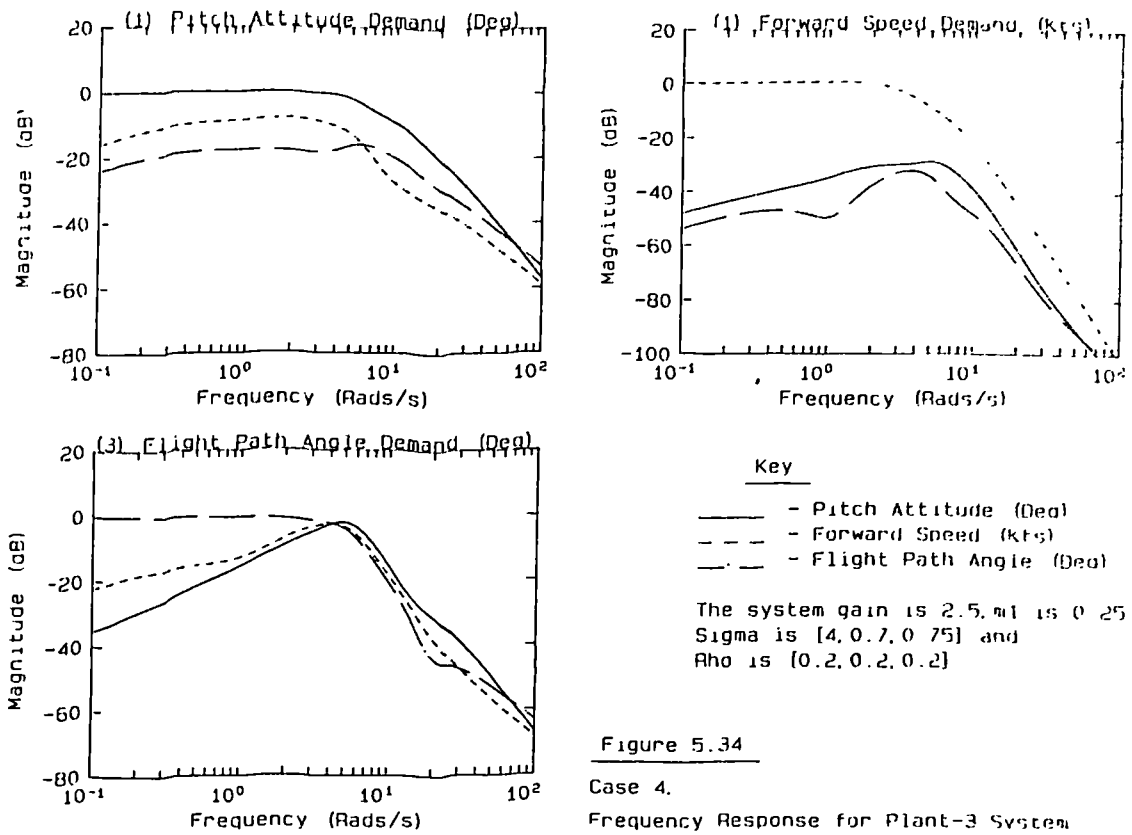
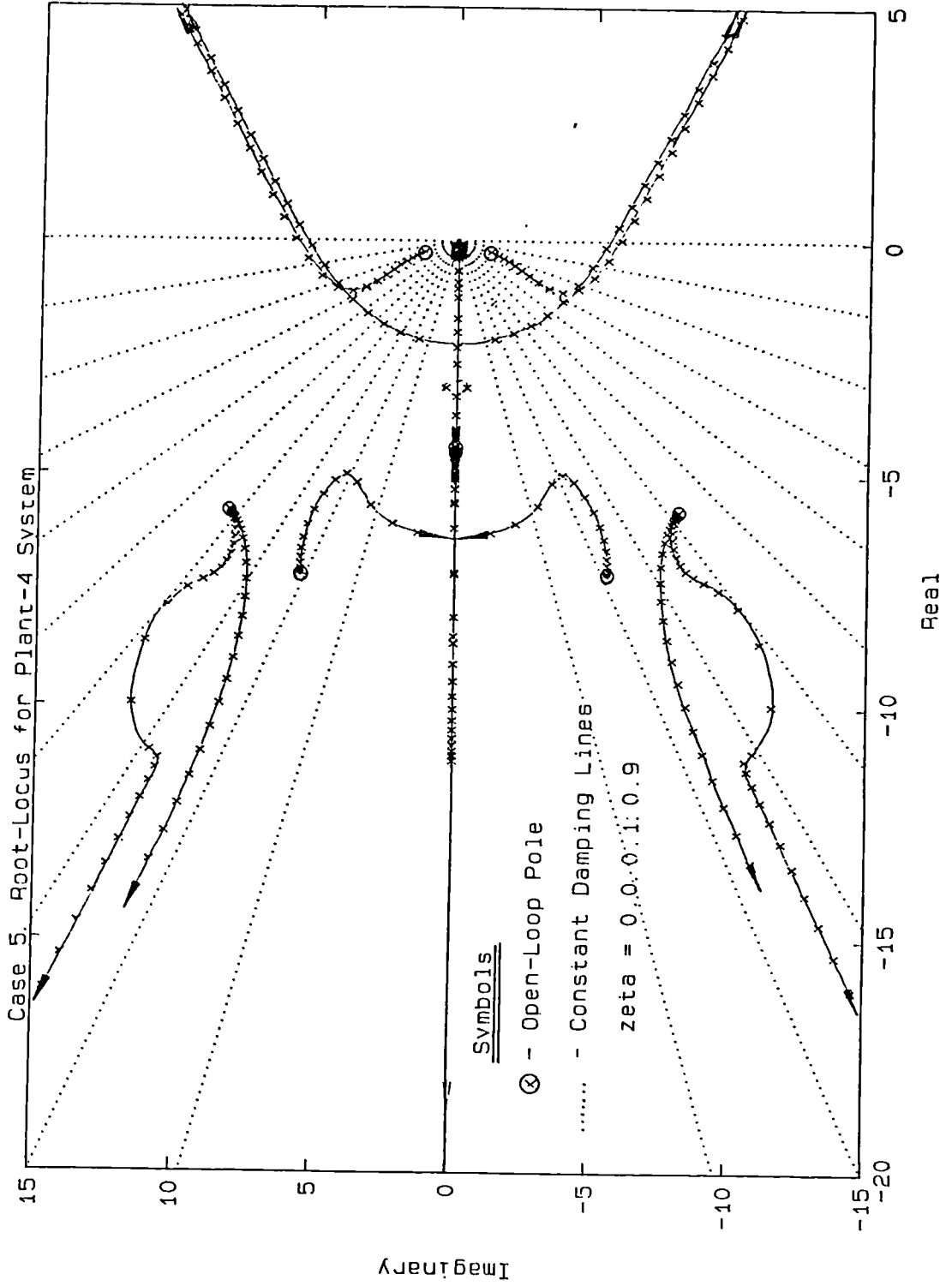
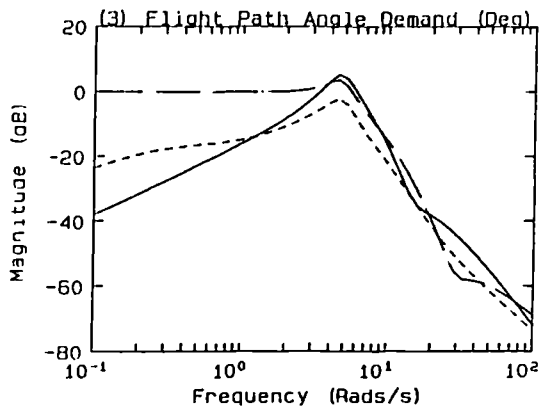
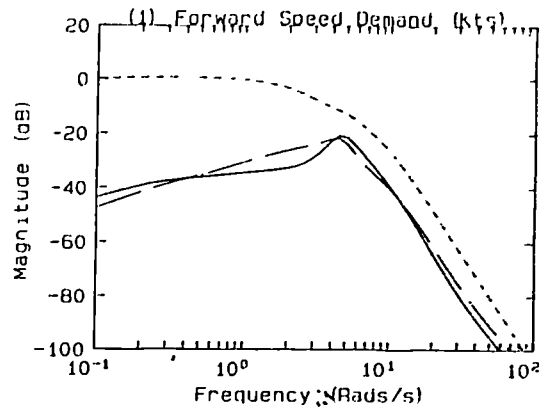
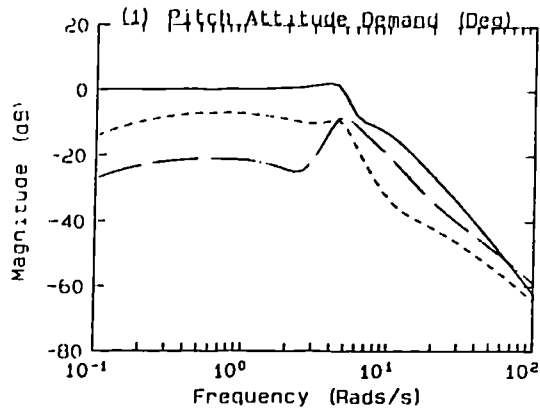


Figure 5.36



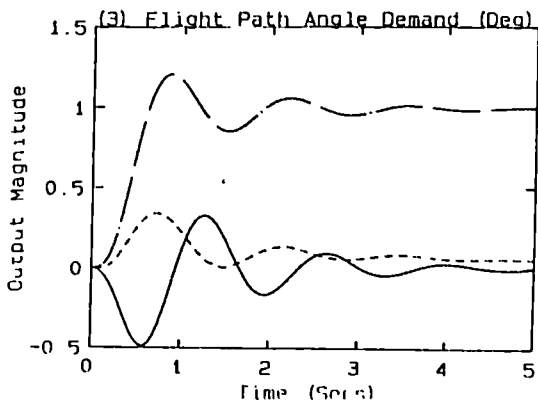
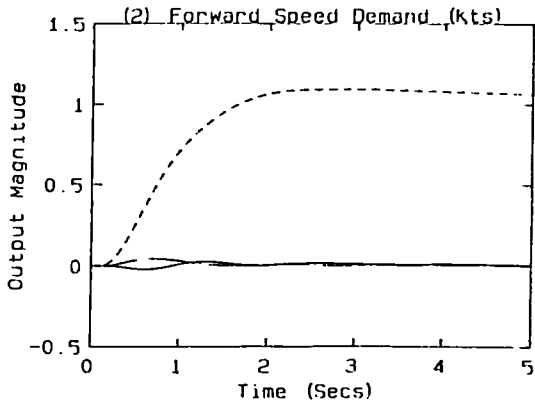
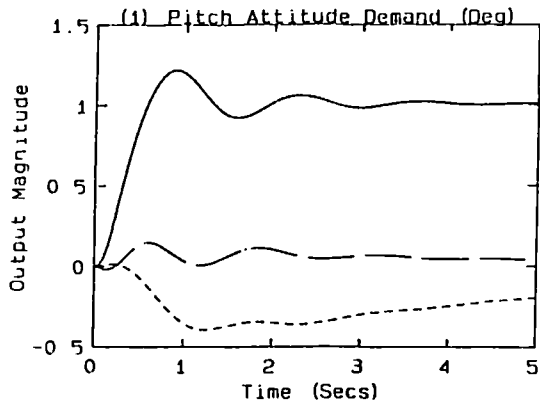


Key

- - Pitch Attitude (Deg)
- - - Forward Speed (Kts)
- · - Flight Path Angle (Deg)

The system gain is 2.5, m_1 is 0.2
 Sigma is [5, 0.8, 0.1] and
 Rho is [0.2, 0.2, 0.2]

Figure 5.37
 Case 5.
 Frequency Response for Plant-4 System



Key

- - Pitch Attitude (Deg)
- - - Forward Speed (Kts)
- · - Flight Path Angle (Deg)

The system gain is 2.5, m_1 is 0.25
 Sigma is [4, 0.7, 0.75] and
 Rho is [0.2, 0.2, 0.2]

Figure 5.38
 Case 5.
 Step Response for Plant-4 System

Figure 5.39

Case 6. Root Locus for Plant-5 System

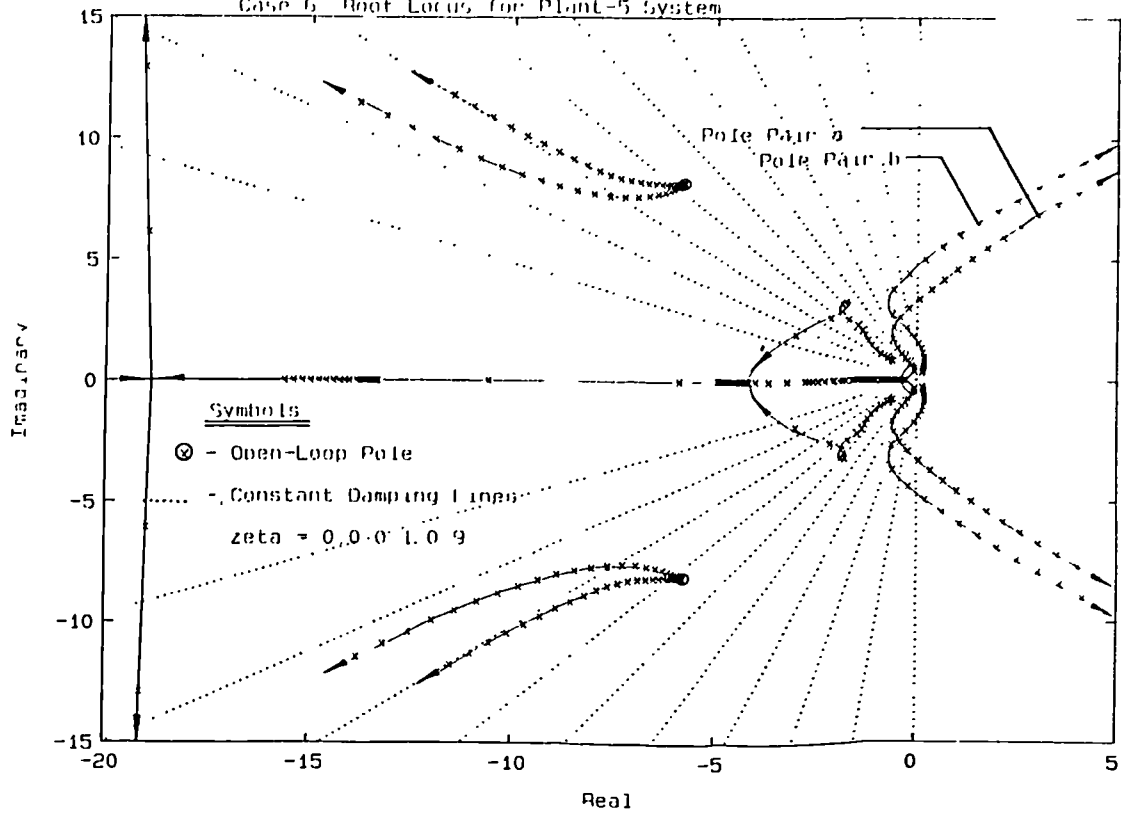
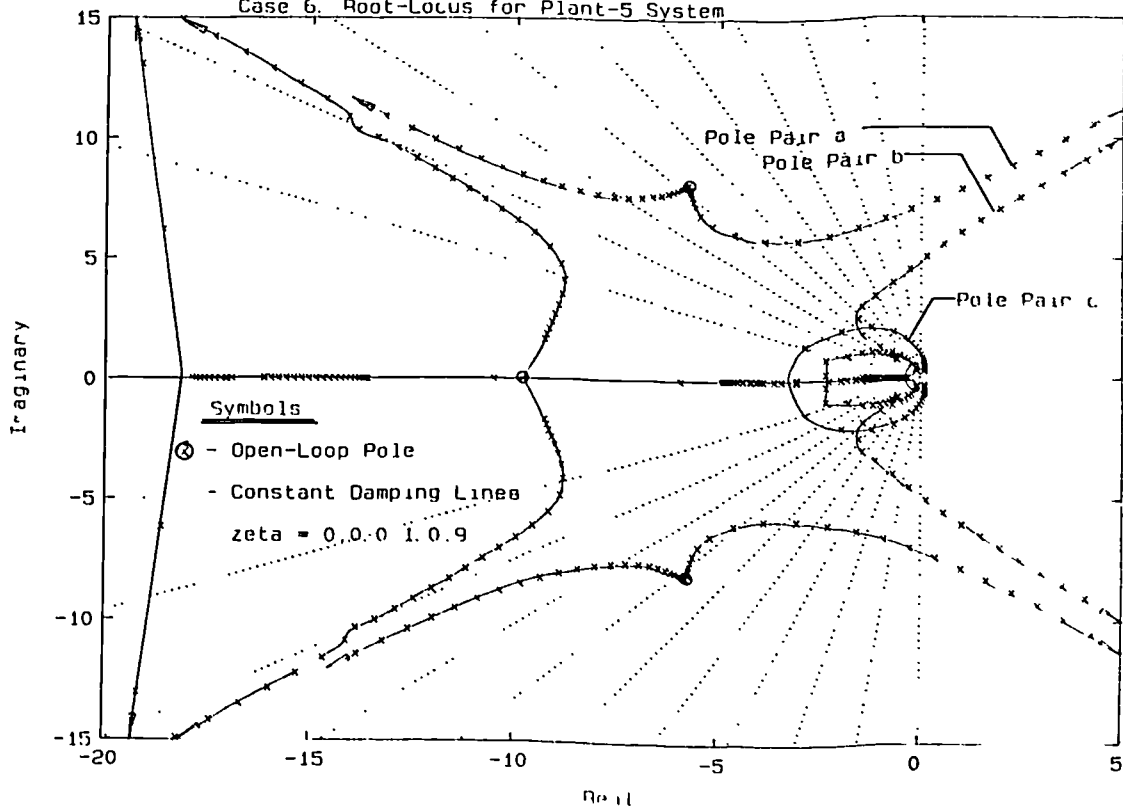
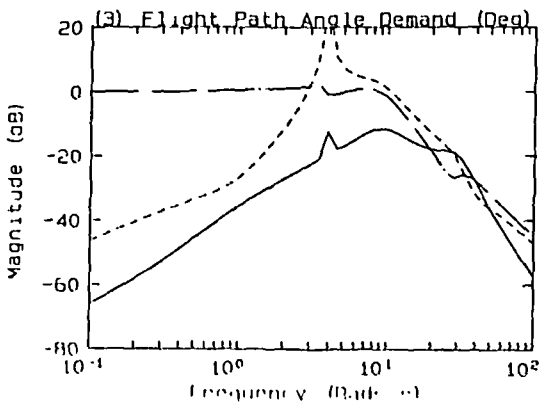
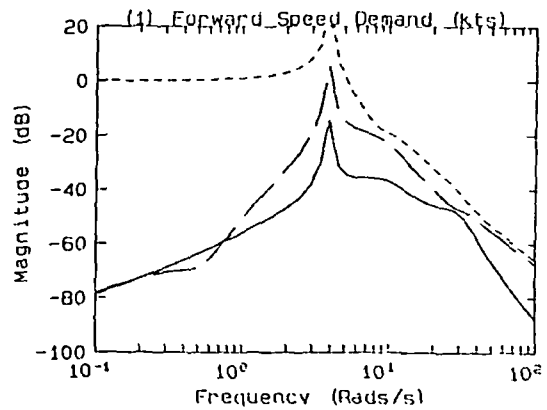
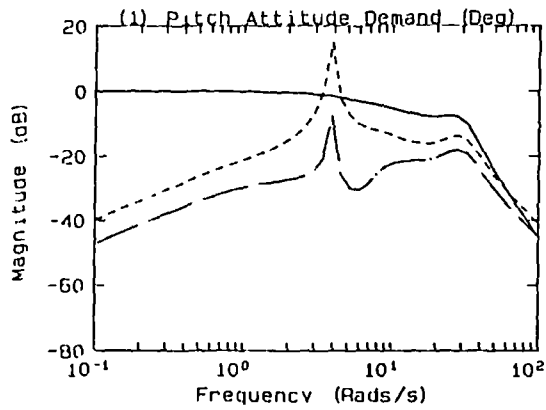
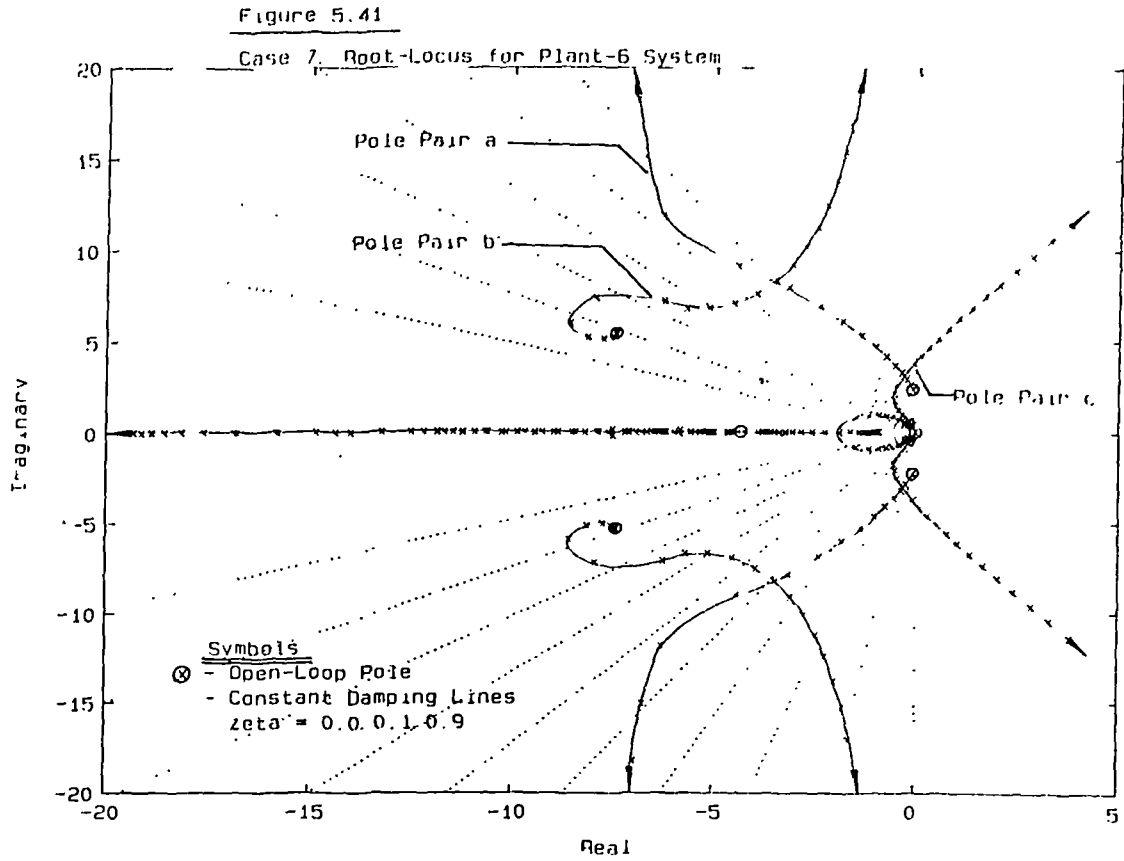


Figure 5.40

Case 6. Root-Locus for Plant-5 System





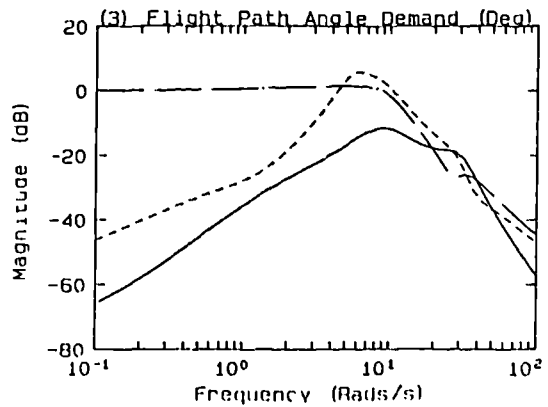
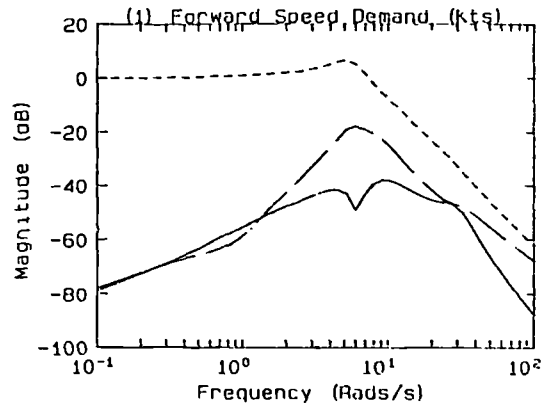
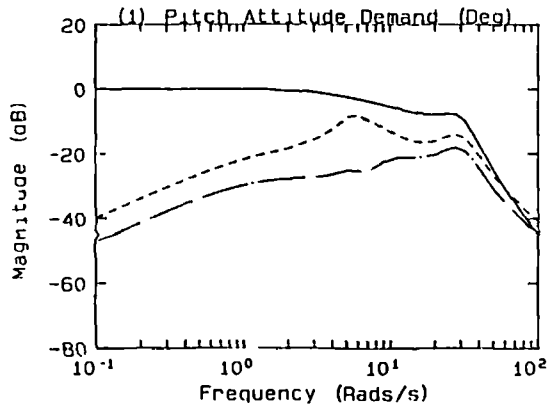
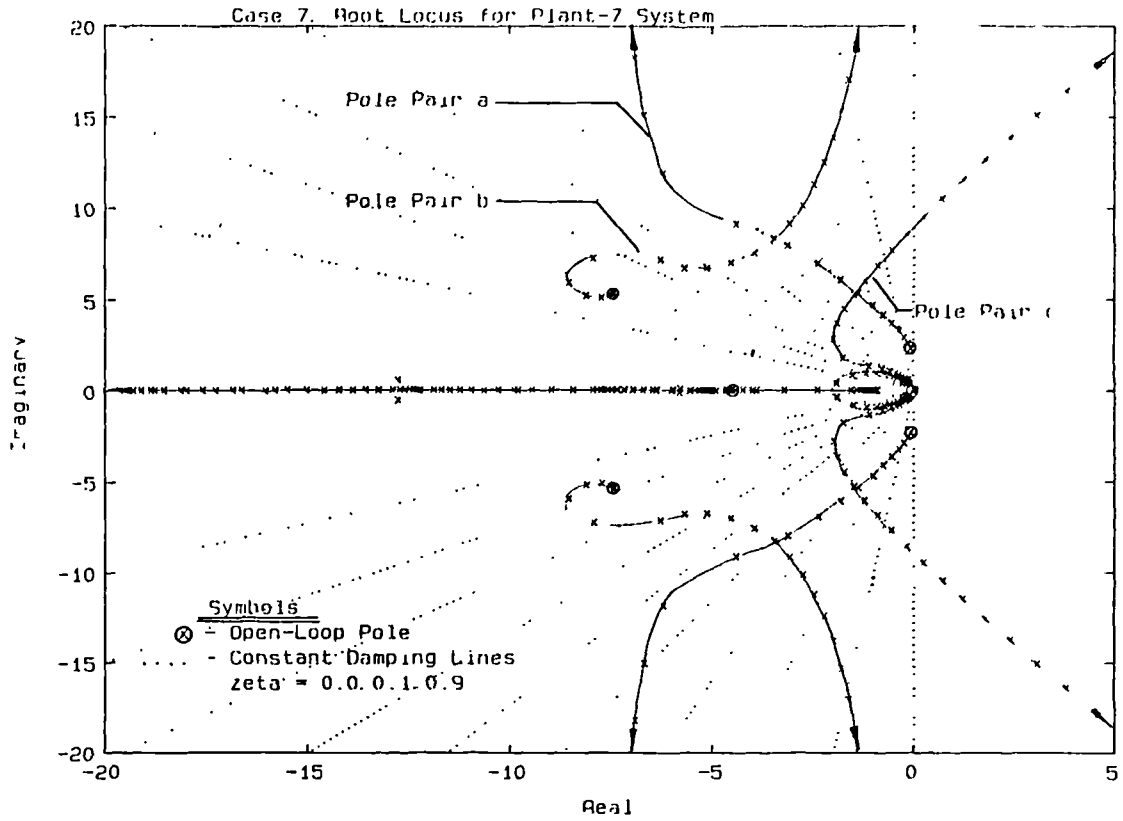
Key

- Pitch Attitude (Deg)
- - - Forward Speed (kts)
- · - Flight Path Angle (Deg)

The system gain is 6 0. m1 15 0 1
 Sigma is [10, 1, 1] and
 Rho is [1, 1, 1]

Figure 5.42
Case 7

Figure 5.43



Key

- - Pitch Attitude (Deg)
- - - Forward Speed (Kts)
- . - Flight Path Angle (Deg)

The system gain is 6 0. m1 is 0.1
Sigma is [10, 1, 1] and
Rho is [1, 1, 1]

Figure 5.44

Case 7.
Frequency Response for Plant 7 System.

CHAPTER 6

THE DESIGN BRIEF

THE DESIGN BRIEF

6.1 Introduction

Before describing the purpose and layout of this chapter, it is worth restating the two-fold main objective:

- 1) to develop and assess a MIMO controller design method to fulfil the criteria described earlier

and
- ii) to design a controller that reduces workload that is characteristic of V/STOL aircraft, using the GVAM87 as a representative application.

The best way to fulfil these two objectives is to define realistic design aims so that the high-gain method can be properly assessed whilst the second objective is pursued.

In this chapter suitable design aims are defined after current literature on the subject has been reviewed. It is intended to maintain a balance, in defining the design aims, between specific criteria and general principles. Specific criteria are of particular use in tuning the design and in assessing the design method, but there are instances where no criteria exist. In these instances general principles are developed for application to the design

problem. The final design will be assessed in Chapter 8 in the light of these general principles and the specific criteria. The results from this will then contribute to the future development of design aims for MIMO aircraft control, especially V/STOL aircraft in the transition region. Furthermore, these results will fulfil the secondary objectives of this report.

The design aims have been split into two areas and the resulting chapter layout is now described. Firstly, in section 6.2 there is a review of the subject Task Tailored Control (TTC), which has also been termed elsewhere Task Oriented Control (TOC). After this review a requirement is defined for the TTC design aims. Secondly, in section 6.3, there is a review of aircraft handling qualities which contributes to the definition of a requirement for the handling qualities design aims.

6.2 Task Tailored Control

In the past flight controllers have been compromised by requiring that one controller must accomplish many things throughout the flight envelope. This has often resulted in a controller that is always sufficient but never optimal. Now digital computers allow the controller to be tailored to suit the piloting task, especially as it involves only software changes and not hardware changes. In subsection 6.2.1 TTC considerations are reviewed and references are given. In subsection 6.2.2 the resulting TTC requirement is defined.

6.2.1 The Considerations

The modern fighter pilot is expected to fly a highly complex aircraft whilst managing the detection, weapons, communications and navigation systems. Furthermore, he is expected to maintain "head-up" flying (looking out rather than looking into the cockpit) and to accomplish it all with Hands On Throttle And Stick (HOTAS). The concept is admirable, but it is becoming increasingly difficult to implement. The shift to look-down Shoot-down systems with helmet mounted sights and the use of voice control, only serves to spread the overload to other pilot degrees of freedom and senses. It would seem that the only solution is to use Expert Systems to manage the complex aircraft systems and to give the pilot only that which he needs for each task. The first stage of this progression is the development of TTC.

The discussion of TTC is split into four areas : the vertical take-off and landing phase, the transition flight phase (including short take-off), the wing-borne flight phase and lastly a discussion of implementation considerations.

a) Vertical Take-Off and Landing

No TTC information could be found in the literature specifically for vertical take-offs, however information that concerns landing will be applicable. Clearly, reducing the three main control inputs to just two will help the pilot considerably as will decoupling the main flight variables. One study showed that pitch attitude hold is very beneficial, especially in poor visibility conditions, and that it

greatly reduces pilot workload [Bode et al]. The benefits are even greater in turbulence and cross-winds. Other systems using pitch rate command and pitch attitude hold have been reported favourably in similar studies [Merrick & Gerdes, Hindson & Hardy, Morales et al, Franklin & Hynes, Franklin]. With such a system it would be possible to set the pitch attitude for the landing conditions so that over-the-nose visibility and tail scrape angle are suitably handled [Wend].

If ground handling is a requirement then there needs to be switching logic between the ground based control laws and the airborne control laws. This switching is best accomplished with a "weight on wheels" sensor so that the pilot is not troubled with unnecessary button pushing. Such a sensor is used for the F/A-18 [Harschburger & Moomaw] to signal a TTC mode that improves its conventional take-off handling qualities.

Apart from attitude control the pilot may need to position the aircraft immediately before landing (or after take-off) and will need horizontal and vertical translation control. There are three specific hover translation modes, but only one is discussed in detail here as the other two are discussed in the next subsection.

The one discussed in detail here involves pitching and rolling the aircraft in order to perform translations in the horizontal plane [Stapleford, Radford & Andrisani II, Lee et al]. This "pitch to walk roll to crab" system had to be combined with a vertical translation controller which was thrust based, and therefore engine dependent. It was found that the aircraft pitch and roll dynamics seriously compromise the bandwidth of the translation command system

and that large commands produce excessive pitch and roll activity. Furthermore, turbulence gave rise to uncoordinated sensations which the pilots found disconcerting [Stapleford, Radford & Andrisani]. Another consideration, common to all thrust based V/STOL aircraft, is the use of the engine for vertical velocity control. It is found that the engine dynamics can dominate the control-mode and seriously limit the performance [Franklin]. An example of this is a V/STOL aircraft automatic ship landing system which has to track a moving deck [Bodson], where the engine can become saturated easily in high sea states.

The other two hover translation modes use : pitch attitude, vertical velocity and horizontal velocity, or, pitch attitude, flight path velocity and flight path angle. Consequently, these two modes are more suitable than the first because they are compatible with the usual transition control-modes. Each of these translation controllers can be used to position the aircraft for landing, automatic hover position hold control [Franklin, Donley] and may even be used in conjunction with a guidance beam for automatic landing or poor visibility aircraft recovery (to ships or land based dispersal sites). Such hover translation systems have been used for several studies [Franklin & Hynes, Morales & Merrick, Merrick & Gerdes] and it is accepted that decoupling the flight variables at low speed gives good results. [Franklin & Hynes, Morales & Merrick, Merrick & Gerdes, Clark & Goldstein].

Finally, to further the use of TTC at least two studies have investigated the possibility of having a control-mode for landing which is different to the transition control-mode. One is scheduled with speed [Bode et al] and the other is selected by the pilot just

before landing [Moralez & Merrick, Merrick & Gerdes].

b) Transition Flight

For transition flight it is still relevant to decouple the main flight variables and to reduce the number of control inputs. Hence, three control strategies can be defined for this flight phase, two of which were briefly referred to in the last subsection.

The first of these control strategies uses pitch rate command (pitch attitude hold), forward velocity or acceleration command and vertical velocity or acceleration command [Merrick & Gerdes]. The pilot sets an appropriate pitch attitude and the controller maintains this, leaving the pilot free to control the remaining two parameters with his two hands; left hand for vertical and right for horizontal in this case. An additional control on the right hand inceptor was used for changing the pitch attitude. This system was used for curved decelerating transitions and was well received by pilots.

The second of these control strategies uses pitch rate command (pitch attitude hold), flight path velocity or acceleration command and flight path angle command [Moralez & Merrick]. Once again the pilot sets his attitude and then controls the aircraft with the two remaining inputs. Pitch attitude may be adjusted using a button on the right hand inceptor. The right hand inceptor commands longitudinal acceleration (flight path acceleration); the left hand inceptor commanding flight path angle. This system was also well received by pilots.

The third of these control strategies uses a pitch rate command (pitch attitude hold) controller coupled with a speed stabiliser [Franklin & Hynes, Hindson & Hardy]. With this configuration two different control schemes are possible, termed "frontside" and "backside". The frontside scheme operates at the frontside of the drag curve and uses a nominally fixed throttle. The pitch attitude is controlled to give the correct flight path and the thrust is vectored automatically to maintain the trim speed. The backside scheme operates at the backside of the drag curve and uses a fixed pitch attitude. The throttle is then used to control the flight path and the trim speed is automatically maintained, again by thrust vectoring. The controller blends between frontside and backside control as it decelerates. The aircraft used for these studies was the QSRA which is quite different from the GVAM87, yet the two different schemes are possible using the GVAM87. Each of these studies were conducting decelerating landing approaches and both were accepted by pilots. Any of the three control strategies described could be suitable as each gives the pilot only two main control inputs which are decoupled. In this way, the transition task is made simpler. However, the deciding factor between the different strategies will be compatibility with the two extremes of the transition phase.

Additional considerations for this flight phase are carefree handling, secondary control presets and the short take-off. The inclusion of carefree handling relieves the pilot of the task of monitoring safety critical parameters. For example: the F1A-18 possesses a spin recovery mode [Harschburger & Moomaw], the AF11/F-16 possesses active structural limiting [Barfield] to prevent over stressing and it also has automatic collision avoidance protection

(ground and other aircraft). Furthermore, the AFTI/F-16 also makes use of angle of attack limiting to prevent stall [Anderson et al]. However, it should be noted that in a V/STOL transition, at low speed, the angle of attack becomes meaningless and theoretically a vertical landing has 90° of incidence. This makes such schemes difficult to implement with V/STOL aircraft

Secondary control presets refers to scheduling flaps with speed or putting the undercarriage up automatically. Such tasks should be automated where possible.

Finally, the short take-off ^{is considered} This will require careful controller handling so that the transition from ground control to airborne control is smooth. A "weight on wheels" sensor would be beneficial, indeed, a sensor giving the actual aircraft weight would be very useful. The aircraft weight could then be used by the controller to calculate the take-off speed, for a given length of runway, which could be shown on the HUD by a suitable symbol.

c) Wing-Borne Flight

This is a conventional flight phase which allows conventional TTC ideas to be applied. The most recent and comprehensive investigation into TTC has been the AFTI/F-16 project [Anderson et al, Barfield, Barfield & Swortzel, Bianco & Swortzel, Toles & Anderson]. This project has developed decoupling control laws which have been used to implement TTC modes. By selecting one of several options with a push button, the controller reconfigures the attack mode, the flight control mode, the weapons, the radar mode, the HUD

symbology and the sensor video [Barfield]. These changes enhance the pilot control for each task. For example, in air-to-surface bombing the aircraft velocity vector and the flight path are critical, consequently a fast normal acceleration response has been used with gust alleviation (at the expense of pitch rate overshoot). Conversely, for air to-air gun attacks the pitch response is dead beat to allow good tracking in pitch and gust response is not critical.

Indeed, the air-to-air gun attack mode has taken TTC even further [Barfield] by changing the mode according to the input level. Fast target acquisition is achieved using large inputs and fast flight path response (at the expense of pitch overshoot). Once the target is in sight, small inputs give a deadbeat pitch response for accurate tracking. This idea has also been suggested by Gill [Gill], who goes on to describe another type of command dependent control mode as follows: for no command inputs a low gain controller can be used to reduce sensor noise effects, then a high gain controller can be used for command following; the system gain being a function of the input level [Gill, Butler et al].

The actual flight variables given to the pilot for control are conventionally forward acceleration (left hand) and pitch rate or normal acceleration (right hand). As has been seen pitch rate control and normal acceleration control have different benefits to offer but pitch rate is more widely used. Pitch rate control for landing has been criticised however [Chalk] for conventional aircraft, but this is not expected to be a problem for this application as landing is highly unusual in the wing-borne flight phase.

An additional feature for V/STOL aircraft is Vectoring In Forward Flight (VIFF) which can be used to give instantaneous direct lift and a very large drag increase [Fozzard]. This may easily be performed with GVAM87 by vectoring the thrust. Indeed, putting the nozzles down will also switch the reaction controls on giving increased pitch, roll and yaw power. VIFF may also be used to alleviate the effects of a turn rate limit which is caused by the incidence limit imposed by stall considerations. Hence, VIFF used in a tight banking turn will give additional radial force and a tighter turning circle. Implementation of this is discussed in the next subsection. Carefree handling considerations in the previous subsection also apply here. In fact spin recovery, ground avoidance, collision avoidance, structural limiting, g limiting and stall prevention are all more likely to be needed in this flight phase. Lastly, the domination of the engine dynamics in all flight phases indicates that integration of the flight and engine controls could lead to improved TTC [Franklin].

d) Implementation Considerations

The use of TTC is only beneficial if it reduces pilot workload and improves efficiency. Consequently, the many TTC modes that can be supplied need to be managed so that the pilot is not overloaded [De Meis, Quinlivan]. The AFTI/F-16 uses a single button push to reconfigure six systems [Barfield] which is admirable, but it still requires the pilot to select a mode and to be aware of the flight mode he is in (because the inceptors take on different control characteristics). It is preferable to select TTC modes automatically and this could be

done using normal flight operations. For example:

selecting undercarriage down landing mode

arming the bombs air-to-surface bomb mode

removing the trigger guard - air-to-surface guns mode or air-to-air
gun mode (depending on altitude)

In the previous section VIFF was described for improving the turning circle. This could be implemented with a specific VIFF control but this increases the two inceptor systems to a three inceptor system. An alternative would be to use a stick breakout force. This is shown as Figure (6.1) and may be explained as follows. Banked over, the pilot would pull the right hand inceptor back to pitch the aircraft "up" and around the turn. Eventually the angle of attack limit would be reached and the turn rate would be maximum. This could be signalled to the pilot by feeding back a larger stick-force so that it appears that the right hand inceptor has reached its limit. However, if the pilot continues to pull back and overcome this extra stick-force, then the controller would bring the nozzles down and use VIFF to improve turn rate. In this way no extra controls are needed and the pilot signals the change in a natural way, simply by pulling back harder. Unfortunately this cannot be simulated or demonstrated in this application as there is no lateral control and no input "feel system".

The idea of bringing the nozzles down in wing-borne flight can cause problems as the controller changes from a two input/output system to a three input/output system (unknown to the pilot). Crossing boundaries such as this will cause implementation difficulties [Hunt] especially concerning the continuity of control signals and the integrators. Furthermore, detecting the "nozzles aft" condition at the end of a transition is not easy. Moreover, fixing the nozzles aft when they reach 0° could cause a problem if they are only at 0° to achieve a command mid-transition! Problems at boundaries can also occur if the control scheme is changed from high speed transition to low speed transition for landing.

Other problems can occur at boundaries when actuators become saturated [Morales & Merrick, Merrick & Gardes, Anderson et al]. This results in a higher pilot workload at least, and sometimes instability. Actuator saturation was avoided on the AFTI/F-16 [Anderson et al] by using command limit logic because it was found that decoupling purity was lost when saturation occurred. Another factor influencing decoupling purity was found to be the speed of response [Anderson et al]. It was discovered that a well decoupled system tended to be sluggish, whereas a faster response could be obtained by allowing some cross coupling. This reduction in response time gave a net reduction in pilot workload, despite the presence of some cross coupling. Another clear case of sound engineering judgement being required to perform sensible design trade-offs.

Finally, it should be noted that the pilot vehicle interface is critical as is the controls and displays integration. The AFTI/F-16 used multifunction displays and the cockpit was carefully designed to

give a "user friendly" environment [Barfield]. Many studies have commented upon the need for good controls and displays integration [Barfield, Barfield & Swortzel, Bode et al, Hindson & Hardy, Merrick & Gerdes] and one study actually varied the HUD time delay and measured pilot opinion [Garg & Schmidt]. The last study showed that even with "good" conventional aircraft dynamics, HUD time delay could result in poor pilot ratings. In addition to this, display content and presentation also affects the handling qualities.

6.2.2 The Requirements

Some of the considerations discussed in the previous section are not included in the requirement at this stage of the design but they were mentioned for completeness. The main theme of this work is concerned with MIMO control law design and V/STOL transition flight, consequently the following considerations are not included in the requirement: pilot display task tailoring, TTC modes for bombing and gun attacks in wing-borne flight, structural limiting, ground avoidance, collision avoidance, g-limiting and command dependant control modes. However, it should be noted that any (or all) of these TTC considerations could be incorporated at a later date. The requirements are defined in four subsections, in the same way that the TTC considerations were set out in the previous section, and they are summarised by Figure (6.2).

a) Vertical Take-Off and Landing

The controller will use a pitch attitude demand system and the pitch attitude will usually be set to a suitable value and left unchanged,

thereby reducing the number of main control inputs. The pilot will be able to change this setting, possibly using a button on the left hand inceptor. The pilot will also be given horizontal and vertical translation control in earth axes at low speed to enable airborne taxiing manoeuvres to be performed easily. The choice of earth axes reflects the fact that the pilot thinks in terms of horizontal and vertical relative to the earth at this stage. The right inceptor will command vertical translation height hold, and the left inceptor will command horizontal acceleration velocity hold.

A "weight on wheels" sensor will be used to signal take-off and landing conditions. This information will be used to help control integrators, which need careful handling at this boundary. The second boundary of this low speed region is before transition flight is reached. The controller TTC mode will be changed as the aircraft speed exceeds 60 ft/s (shown on Figure (6.2)).

b) Transition Flight

In this flight phase the right inceptor will give flight path angle rate of change commands, flight path hold, and the left inceptor will give acceleration commands along the flight path, flight path velocity hold. The third control input is a pitch attitude command, system, the same as the previous flight phase.

The alternatives to the control scheme described above use vertical and horizontal velocity or acceleration commands in either earth or body axes. However, although these decoupled modes have been found to

alleviate pilot workload, the pilot actually uses them to control his flight path direction and airspeed. Consequently, it was decided to give the pilot direct control of the flight path direction and airspeed. The "backside"/"frontside" control strategy [Franklin & Hynes, Hindson & Hardy] was discounted because it would not demonstrate the use of a multivariable controller sufficiently, however, the scheme chosen is actually a "backside" scheme. Piloted flight trials, or flight simulation trials, are needed to determine whether "backside" or "frontside" schemes are preferred. Although pilot opinion alone may not be the final deciding factor as "frontside" schemes are generally more energy efficient.

For this implementation of the controller, the undercarriage will be selected up or down automatically at 200 kts. The flaps will be selected in to 20° or out to 50° linearly between 200 kts and 300 kts, with flaps out for deceleration and in for acceleration. This relieves the pilot of managing these secondary controls and the different speed schedules may easily be changed, if necessary, in accordance with pilot comments in the future.

A "weight on wheels" switch will be used for the short take-off mode but the use of weight sensing for HUD task tailoring is beyond the scope of this controller implementation. A boundary also exists at the other extreme of this flight phase when the aircraft accelerates into wing-borne flight and the nozzles are fixed aft (0°). The true "nozzle aft" condition will be distinguished from a transient "nozzle aft" condition by a speed and angle of attack criterion.

For a given aircraft weight and angle of attack there is a particular speed at which the nozzles will be 0° in steady flight (assuming

height and ambient air conditions to be constant). This speed will vary though if the aircraft is performing any manoeuvre such as accelerating forwards. Consequently the boundary condition consists of a minimum speed (140 kts) above which the nozzles will be fixed aft if they are at 0° . The exception is if the angle of incidence is greater than 12° which will be explained in the next section which covers the reverse process; selecting nozzles down when decelerating across the boundary.

c) Wing Borne Flight

In this flight phase the left inceptor will command flight path acceleration, velocity hold; the right inceptor commanding pitch rate, pitch attitude hold. The strategy gives no boundary problems for the left inceptor, but requires flight path rate and pitch rate to be blended for the right inceptor. The change will be set by the "nozzle off" boundary described previously and there will be no boundary problems if there is no demand on the right inceptor when the boundary is being crossed. However, this scheme will give rise to pitching if there is a flight path angle demand when crossing the boundary, but this should not be excessive. Furthermore, at the higher speeds, it is normal to control flight path with the pitch attitude through pitch rate command inputs

When decelerating, the pilot will pitch up until a preset incidence limit is achieved (12°), where upon the nozzles are "unfrozen" and brought down. This mode is also invoked when maximum incidence is reached (12°) when the aircraft is not necessarily decelerating (i.e. tight turns), and is the equivalent of a VIFF mode.

d) Implementation Requirements

Some implementation requirements have been described in the three preceding subsections. The last remaining requirement concerns actuator saturation and decoupling purity during all flight phases. The philosophy here is that decoupling purity is the most important quantity and so commanded rates and commanded accelerations will usually be limited to keep all responses within actuator limits. However, these limits will be exceeded in some cases to show what effects this has and the controller will include integration wind-up protection to alleviate the affects of actuator saturation.

This completes the TTC requirements for the controller which are summarised by Figure (6.2).

6.3 Aircraft Handling Qualities

"Handling qualities are the closed-loop interactions between the pilot, the airplane, and the displays, while pursuing the execution of some task." [Twisdale]. It is essential that an aircraft has good handling qualities if the pilot task is to be physically possible; the handling qualities must be even better if pilot workload is to be minimised. However, despite many years of study, the definition and realisation of good handling qualities has proved to be an elusive goal [Twisdale]. It is widely acknowledged that there is a lack of information [A'Harrah et al, Cunningham & Pope, McRuer, Mooij & Van Gool, Moorehouse & Selegan] which is even worse for V/STOL aircraft [Clark and Goldstein].

In conjunction with this section, Appendix D has been provided as a glossary of terms for handling qualities criteria. The pilot rating schemes "aircraft type" and "flight phase classification" are also contained in Appendix D.

6.3.1 The Considerations

In the past, aircraft handling qualities have been defined in terms of typical aircraft dynamic modes, which are only modestly influenced by any stability augmentation system. This contrasts strongly with today's aircraft which have handling qualities that are dominated by the control system. Often the characteristic modes such as the short period oscillation and phugoid become unrecognisable in highly augmented aircraft. Because of this many people are working to define handling qualities suitable for future aircraft, and some of this work is reviewed here. The discussion of the handling qualities considerations has been divided into three parts. The first part contains the discussion of handling qualities for hover and transition flight, the second part for conventional wing-borne flight. The last part contains the discussion of general principles that should be applied. It should be noted that for this phase of the controller design, ground handling, take-off handling and landing handling are not considered.

a) Hover and Transition

Two early publications deal directly with V/STOL aircraft handling qualities, that is AGARD R 577 [AGARD] and MIL-F-83300 [United States^a]. Deficiencies in these two documents, especially with regard to Shipboard operations, have been noted and the results from them both have been summarised and extended, [Franklin, Franklin & Anderson]. The earlier two publications were both written with the first generation of V/STOL aircraft in mind and are therefore of limited applicability to this project. This is especially true concerning the acceleration margins which are of most use in the early stages of an aircraft design. However, assuming there are no fundamental deficiencies in the basic aircraft model used for this project, the closed-loop system should be able to satisfy the acceleration margin conditions. These acceleration margins are based upon giving the pilot sufficient control power to be able to control the aircraft satisfactorily and they are listed below:

- i) Sinking at 4 - 5 ft/s a vertical acceleration of 0.1g should be possible [United States^a]
- ii) A climb rate of 100 - 750 ft/s should be possible from straight and level flight [United States^a]
- iii) Vertical accelerations of $\pm 0.1g$ should be possible within 0.5 seconds for flight path control [AGARD]
- iv) A flight path angle of 6° or a climb rate of 600 ft min should be possible in less than 2 seconds [AGARD]

- v) Flight path control should allow $7^\circ \pm$ [Franklin]
- vi) Horizontal accelerations of 0.5g should be possible
[Franklin]
- vii) The thrust time constant should be less than 0.3 seconds
[United States^a, Franklin] or less than 0.5 seconds [AGARD]
- viii) Pitch acceleration should be in the right direction in 0.1
seconds and reach 63% in 0.2 seconds [AGARD]
- ix) Graphs of pitch angle, pitch rate and pitch acceleration
have been given for an abrupt step input [Franklin, Franklin
& Anderson] which may be used for comparison, see
Figure (6.3)

Handling qualities have also been defined in terms of the roots of characteristic modes. These are listed below:

- 1) All aperiodic roots should be stable and all oscillatory
roots with a natural frequency (ω) greater than 0.5 rad/s
should also be stable. Furthermore, for $\omega < 0.5$ rad/s the
damping (ζ) should be greater than -0.10 and for $\omega > 1.1$
rad/s then $\zeta > 0.3$ [AGARD].
- (11) Damping should be greater than 0.3 for the short period
oscillation and damping should keep the overshoot within 15%
[United States^a].

- (iii) A diagram relating to the frequency and damping of the short period oscillation has also been given [United States].

Handling qualities criteria have also been defined in terms of bandwidth for this flight phase. The bandwidth criteria are quite new but it is claimed that they encompass all other metrics and that they are the only possible way of dealing with multivariable cross-coupling and direct force control which are inherent in modern aircraft [Hon et al^{a,b}]. The general principles are explained below before actual criteria are given.

Ultimately, the pilot closes the loop in any aircraft system, even though there may be a "closed-loop" within this system such as that used for auto-stabilisers or a CCV full authority controller. Considering the aircraft as a complete system it is possible to examine the "open-loop" response, meaning the aircraft response as seen by the pilot. This "open-loop" response has been characterised for convention aircraft, but is of quite a different nature for the modern CCV. This has made it necessary to apply a new definition of bandwidth. Referring to Figure (6.4) it can be seen that there is a bandwidth based upon 6dB of gain margin (ω_{gm}) and a bandwidth based upon 45° of phase margin (ω_{pm}). The bandwidth of the system ω_{bw} is taken to be the smaller of the two. This figure also shows that it is possible to have the two bandwidths well separated for some systems which can cause misleading handling qualities results if bandwidth is used on its own. Consequently, an additional quantity that represents the rapid phase roll-off is defined as a pure time delay that may be estimated by

$$\tau_p = \frac{\phi_1 + 180^\circ}{57.3 \omega_1} \dots (6.1)$$

where τ_p is the time delay metric, and ϕ_1 is the phase at some frequency ω , much greater than the natural frequency ω_{180} (a typical value is $\omega_1 = 2*\omega_{180}$). These definitions may be obtained from the literature [Hoh et al^{a,b}].

It has already been proposed that bandwidth criteria could be useful for V/STOL aircraft handling qualities criteria [Clark & Goldstein]. Indeed a criteria of $\omega_{BW} > 1$ rad/s for pitch attitude has been proposed [Franklin & Anderson] and a criteria where $6.5 < \omega_{BW} < 3.5$ for level 1 handling qualities ω and $3.5 < \omega_{BW} < 2.5$ for level 2 handling qualities has also been proposed for category C flight phases [Moorhouse]. In fact, the same author [Moorhouse] suggests that $\omega_{BW} = 3.5$ rad/s is suitable for many cases and he reiterates this in a later paper [Moorhouse & Selegan]. Some of these references refer to figures which are included here as Figure (6.5) and Figure (6.6). They show the relationship between handling qualities, ω_{BW} and τ_p as defined previously with Figure (6.5) more relevant to this flight phase (category C). Before moving on to the next part of this discussion it should be mentioned that some current aircraft do not fit exactly onto the Figures (6.5) and (6.6) which shows that the bandwidth criteria possibly requires further development.

b) Conventional Flight

Considerably more information is available concerning this flight

phase but only the main points are discussed here at this flight phase is not the most important in this study. The most relevant publication for conventional aircraft handling qualities is MIL F 8785C [United States^b] which covers all aspects of flight for conventional aircraft in great detail. The information in this section is taken from other publications, some of which draw on MIL F 8785C for their information.

In the previous section, acceleration limits were the first criteria to be discussed and a similar criterion exists for pitch control for this flight phase. The ratio of pitch acceleration for steady pitch rate \dot{q}/q has been defined for level 1 handling qualities as $3.6 > (\dot{q}/q) > 0.28 \text{ rad/sec}^2/\text{g}$ [Gibson] which is similar to CAP (see later).

The roots of characteristic modes have been specified for pitch control in this flight phase also but there is a wide range of opinions as to the correct damping setting. The criteria are given below:

- i) Damping (ξ) for auto pilots should be $0.4 < \xi < 0.7$

[Bihrlé & Wantagh].

- ii) The minimum damping (ξ_{\min}) should be $\xi_{\min} = 0.35$

and generally $0.35 < \xi < 1.3$ [Bischoff].

- iii) Moorhouse states that $0.35 < \xi < 1.3$ is sufficient but

that $\xi > 0.5$ is recommended and so $0.5 < \xi < 1.1$ makes a better boundary with $0.7 < \xi < 0.8$ as an optimum

[Moorhouse & Morran].

- iv) Several figures exist showing the relationship between the short period oscillation frequency and damping, and the resultant handling qualities (e.g. [Moorhouse and Morran, Gibson, Lee et al]) but none are used specifically here.

The bandwidth criteria, discussed previously, also defines handling quality metrics appropriate to this flight phase. The figures described previously are still applicable (Figure (6.5) and Figure (6.6) but Figure (6.5) is more relevant to this flight phase as it covers category A flight phases [Hoh et al^{a,b}]. However, a lower limit to the upper bandwidth shown in Figure (6.5) has been suggested such that $\omega_{BW} < 9.42$ rad/s (1.5 Hz) [Gibson]. The bandwidth criteria of Figure (6.5) are used for a conventional aircraft [Moorhouse] and the criteria are suggested as a useful supplement to MIL-F-8785C.

The Neal Smith criteria are another set of frequency domain criteria [Neal & Smith] but they are not described in full here. However one particular criterion is worth noting, for a pilot compensation of 0° lead (or lag) the Neal-Smith criteria recommend a 3dB magnitude maximum which limits the resonance. Similarly, a "droop" limit is specified of -3dB where "droop" is a measure of how far the magnitude curve drops below 0 dB at frequencies lower than ω_{BW} .

The use of frequency domain and time domain criteria is advocated by Gibson [Gibson] who actually defines time response boundaries. A similar time response boundary has also been defined by McRuer [McRuer] and both are shown as Figure (6.7) and Figure (6.8).

Another factor that affects handling qualities criteria in highly augmented aircraft is the build up of the time delay caused by the inclusion of many filters (anti aliasing, structural notch and noise filters) and digital computer time delays (caused by computation, sampling and voting procedures). This time delay may be expressed as an apparent (or equivalent) time delay (T_e) and is specified as $T_e \leq 0.07$ preferably and $T_e < 0.1$ for Level 1, $T_e < 0.2$ for level 2 and $T_e < 0.25$ for level 3 [A'Harrah et al, Bischoff, Moorhouse & Morran, Smith and Bailey]. A simple test to calculate T_e is given here [Smith & Bailey] and it is illustrated by Figure (6.9). In this case the time response to a step input is shown and it is compared to an equivalent simple lag.

The final criterion described here is the Control Anticipation Parameter (CAP) which is defined as the pitch acceleration (\ddot{q}) divided by the normal acceleration n_{acc} . This is a measure of the dynamic cue that a pilot received when manoeuvring and is a measure of how precisely the pilot can control the flight path. Typically, $16^\circ S^2/g < CAP < 50^\circ S^2/g$ gives good handling qualities [Bihrie & Wantagh].

c) General Considerations

The use of handling qualities in this project is to help the assessment of the high-gain-method. Consequently, the achievement of good handling qualities is not the main objective. This leads to the decision that extra filters, for fine tuning the response handling qualities criteria should be omitted (such as notch filters, phase advance filters etc). This ensures that the performance of the high gain controller is not obscured. Furthermore, the fact that the

aircraft performance is fixed, but not completely known, requires that only the most vital handling qualities criteria are fixed in advance. Those criteria which are associated with performance should be left unspecified so that they are free to be optimised within the design limits. This will allow the interaction between design limits and handling qualities to be assessed and deficiencies caused by the controller can then be investigated.

The next subsection defines the measures of handling qualities that have been chosen as suitable for this project, but it is in chapter 8 that the actual handling qualities of the final system are demonstrated. In section 8.10 the actual handling qualities that have been achieved are discussed with respect to the criteria defined here, and the results from this fulfil the secondary objectives of this report.

6.3.2 The Requirements

The nature of the new coupled multivariable dynamic modes and the lack of suitable handling qualities criteria indicates that a new approach is required. Here, the main principle applied is that "Complexity should be sacrificed to simplicity every time", [Mooij & Van Gool]. From the wide variety of handling qualities metrics that have been described, the bandwidth criteria and associated frequency domain criteria have been chosen as the main handling qualities criteria. Their application is simple, yet they are suitable for the many different dynamic modes that occur in MIMO systems. In addition to these frequency domain criteria, two time domain criteria are also used: the minimum damping criterion and the effective time delay criterion. Together, these criteria form the handling qualities

requirements that are suitable for this project and it is suggested that they are also suitable for a wide variety of modern aircraft control applications.

The requirements are listed below and they are numbered (prefixed with R) for ease of reference through the text. Requirements for the transition flight are marked with (T) and requirements for wing-borne flight are marked with (W) (some requirements may have both markings. Important considerations relating to the handling qualities are listed below the requirements in the same way, numbered and prefixed with a C.

Requirements:

- R1 Bandwidth and effective time delay (as defined in sub section 6.3.1 a) and Figure (6.40) according to Figure (6.6) - (T)
- R2 Bandwidth and effective time delay (as for R1) according to Figure (6.5) - (W)
- R3 -- Magnitude curves should closely follow the 0dB line up to the bandwidth frequency and lie between -3dB and +3dB - (T) (W)
- R4 - Gain and Phase margins should be better than 6dB and 45° respectively - (T) (W)
- R5 Damping (ξ) should be $0.35 < \xi < 1.3$ with $0.5 < \xi \leq 0.8$ preferred - (T) (W)

- R6 - Effective time delay (T_e) as defined in subsection 6.3.1 b) should be $T_e \leq 0.1$ for level 1 and $T_e \leq 0.2$ for level 2 - (W)

Considerations

- C1 - Ensure all dynamic modes are stable, and as damped as possible - (T) (W)
- C2 - Achieve the largest bandwidth possible ensuring that $\omega_{BW} < 9.42$ (1.5Hz) - (T) (W)
- C3 - Achieve the minimum of cross-coupling with levels below 10%* (-20dB) - (T) (W)

* Care should be taken when examining cross-coupling levels as the model is dimensional. Consequently at a forward speed of 200 ft/s the cross-coupling could be 10 ft s of forward speed perturbations per radian of pitch pointing. This would give a level of cross-coupling of +20dB and would indicate high cross-coupling, whereas the level of cross-coupling is actually low in real terms (0.5% per radian of pitch pointing which is 57° of pitch pointing!).

This list of handling qualities criteria, together with the TTC modes defined in subsection 6.2.2, constitute the design brief for the controller.

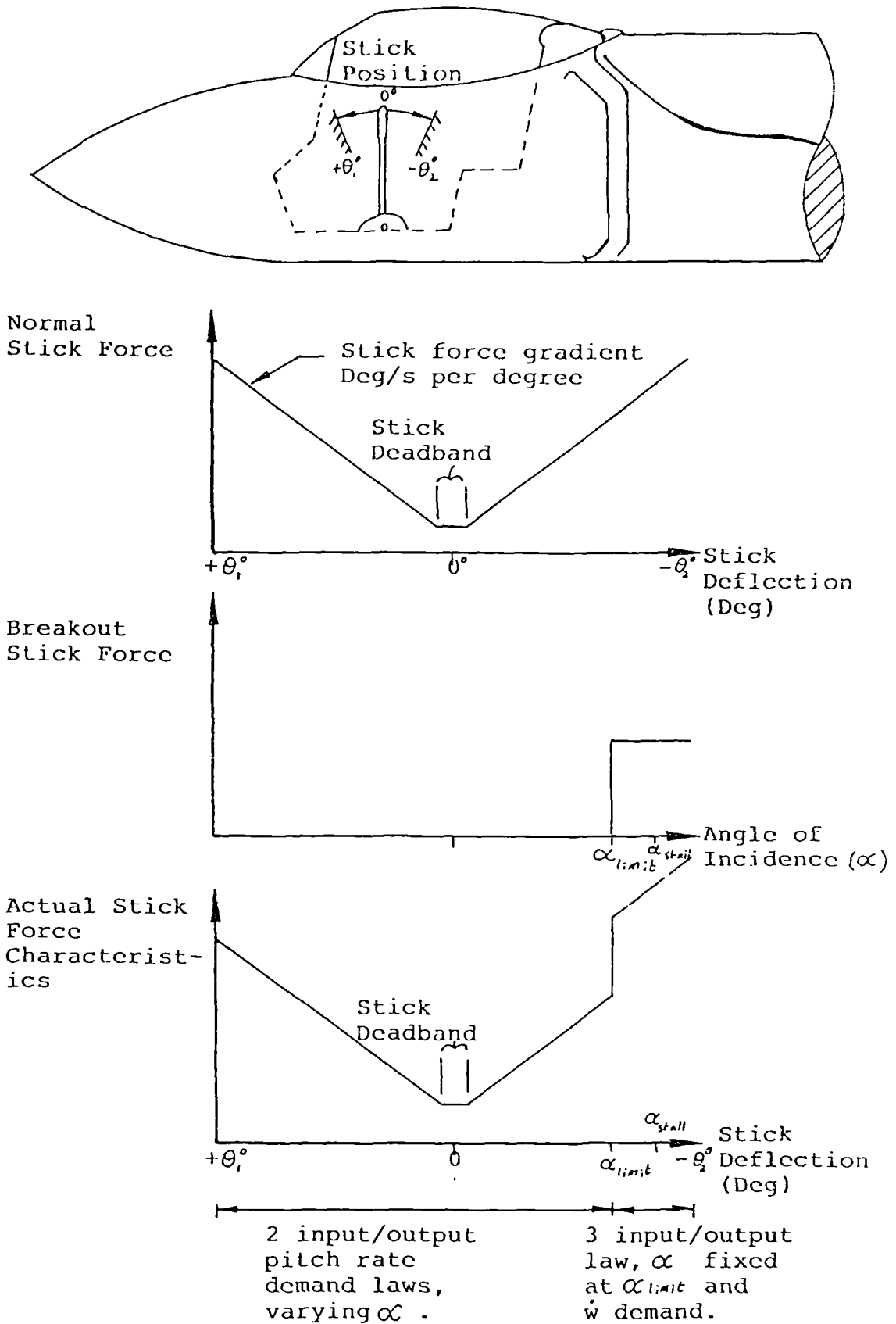


Figure (6.1) Illustration of Stick Breakout Force

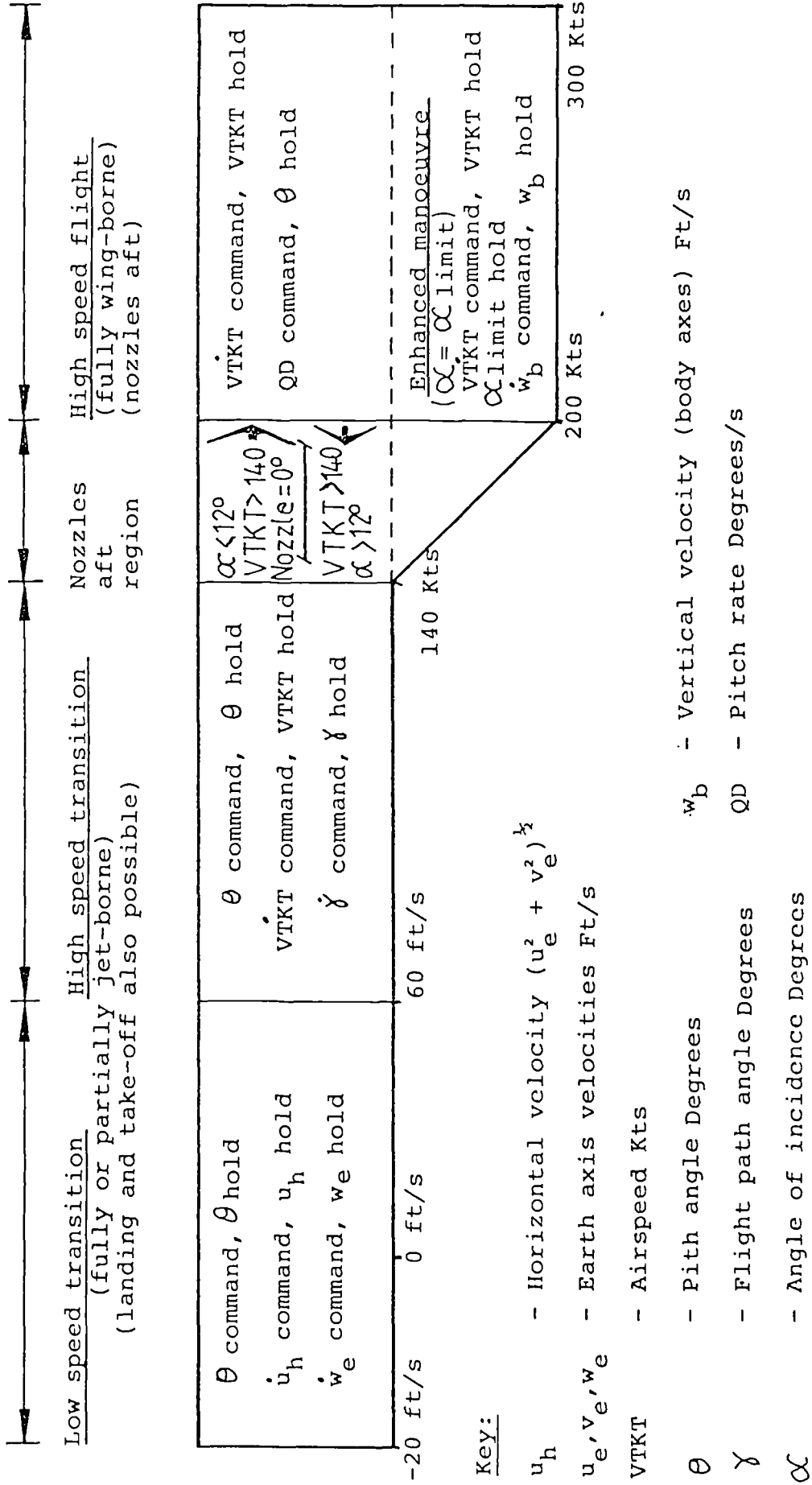


Figure (6.2) Schematic Diagram of the Control Scheme

Flying Qualities Requirement	AGARD 577		MIL-f-83300
	$\dot{\theta}_{max}$ rad/s ²	$\theta(1)$ Deg	$\theta(1)$ Deg
Level 1 Satisfactory without improvement	0.1-0.3	2 - 4	3
Level 2 Adequate improvement warranted			2

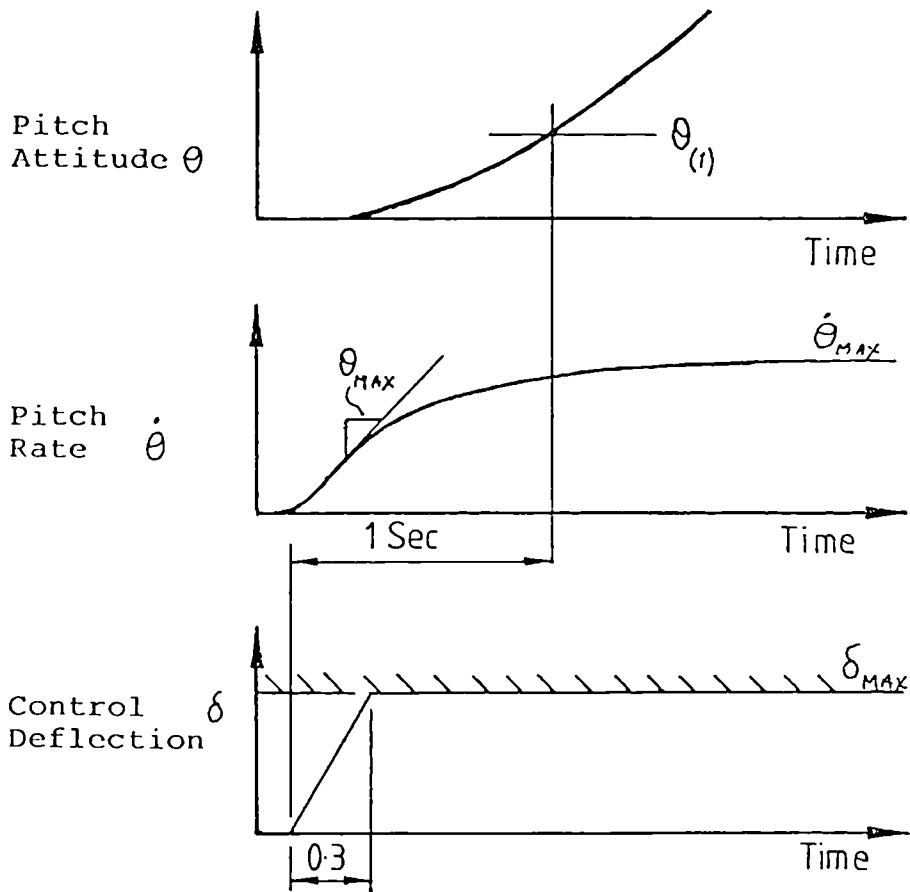


Figure (6.3) Pitch Response to Abrupt Input

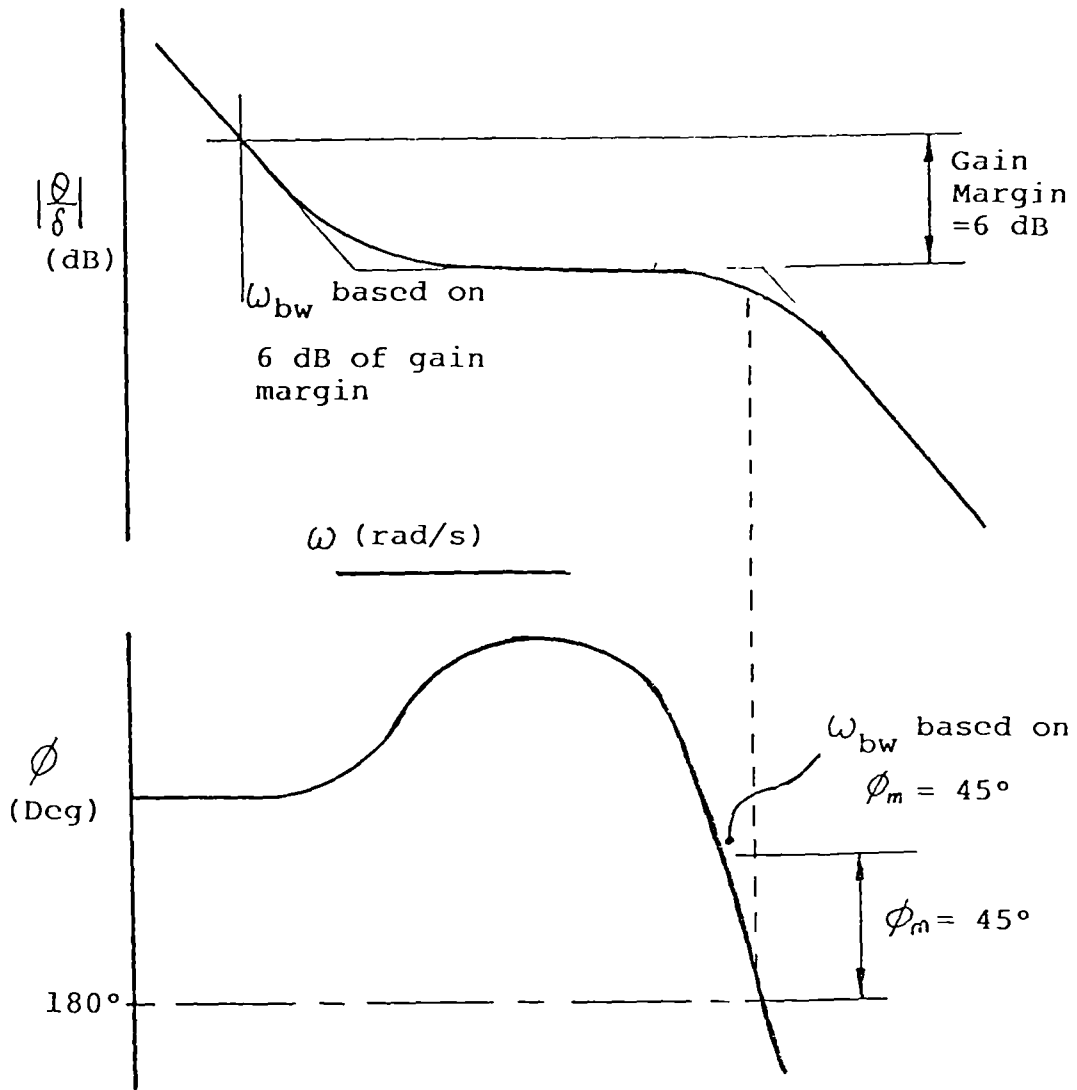


Figure (6-4) Handling Qualities Bandwidth Definition

Figure (6.5) Bandwidth HQ Criteria -

(for up and away flight)

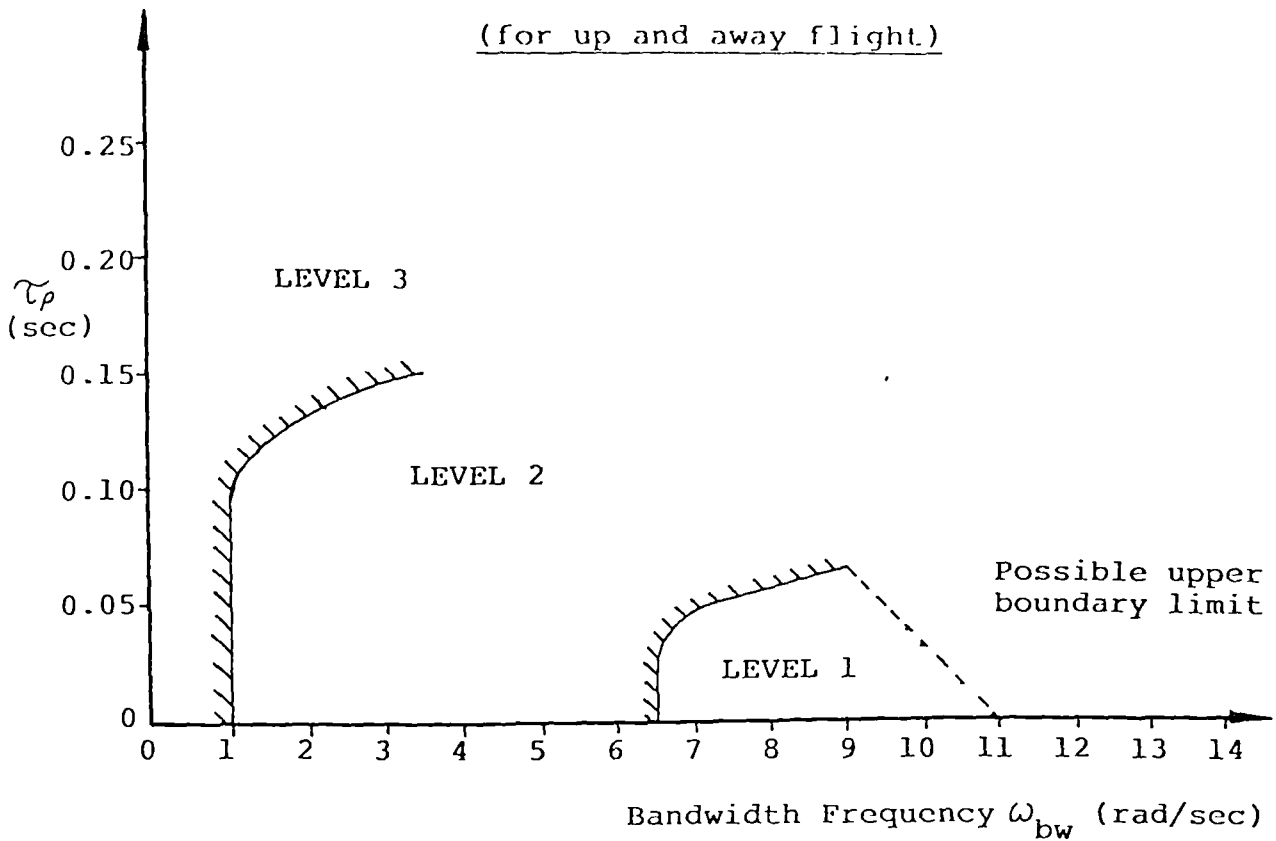
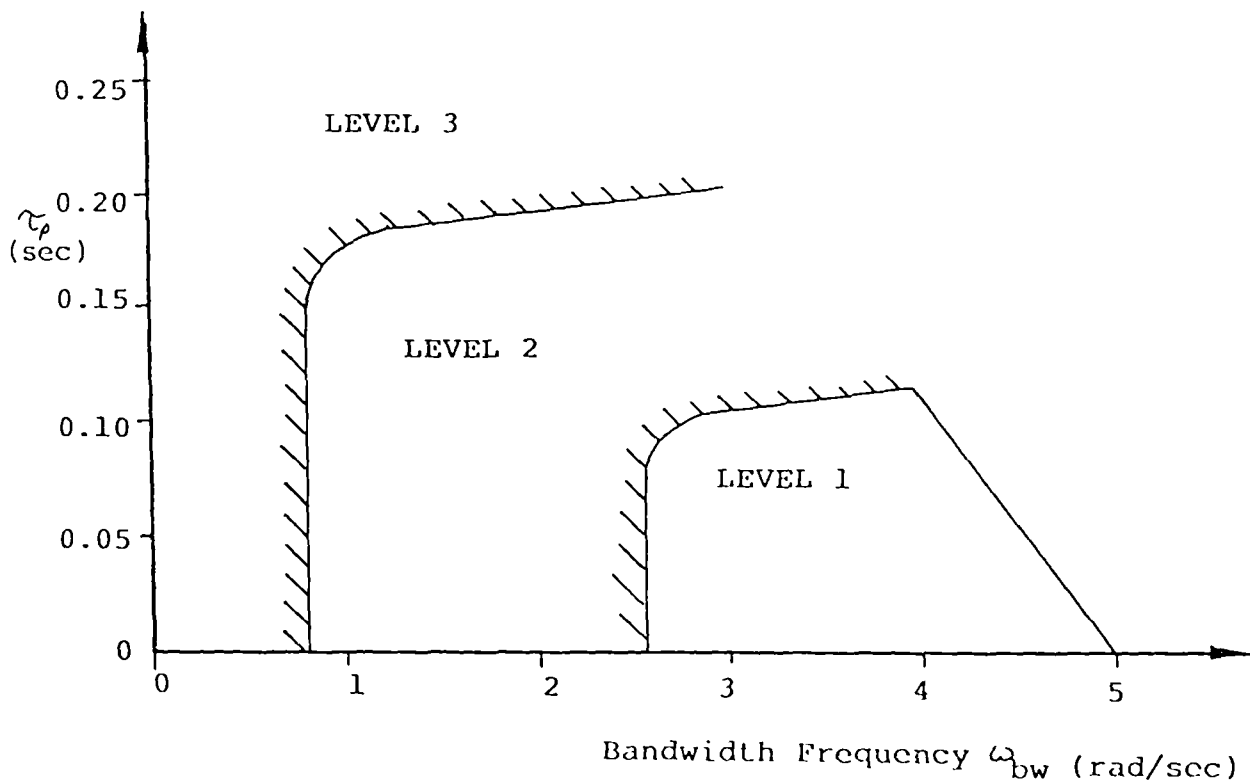
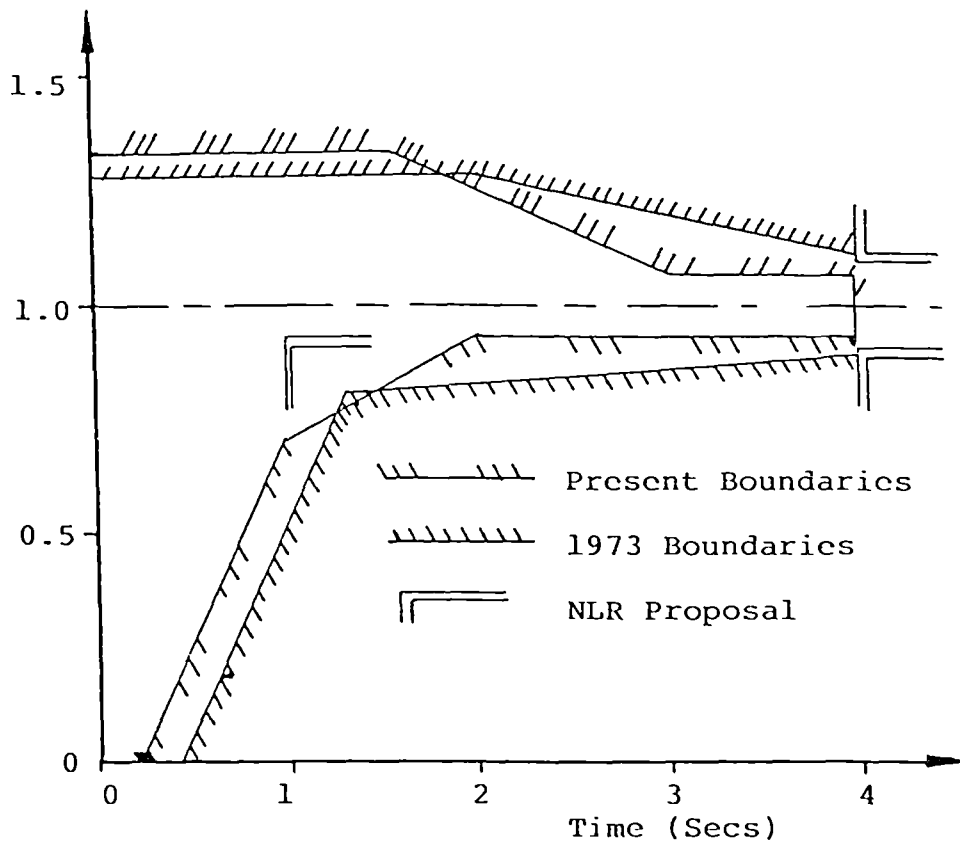
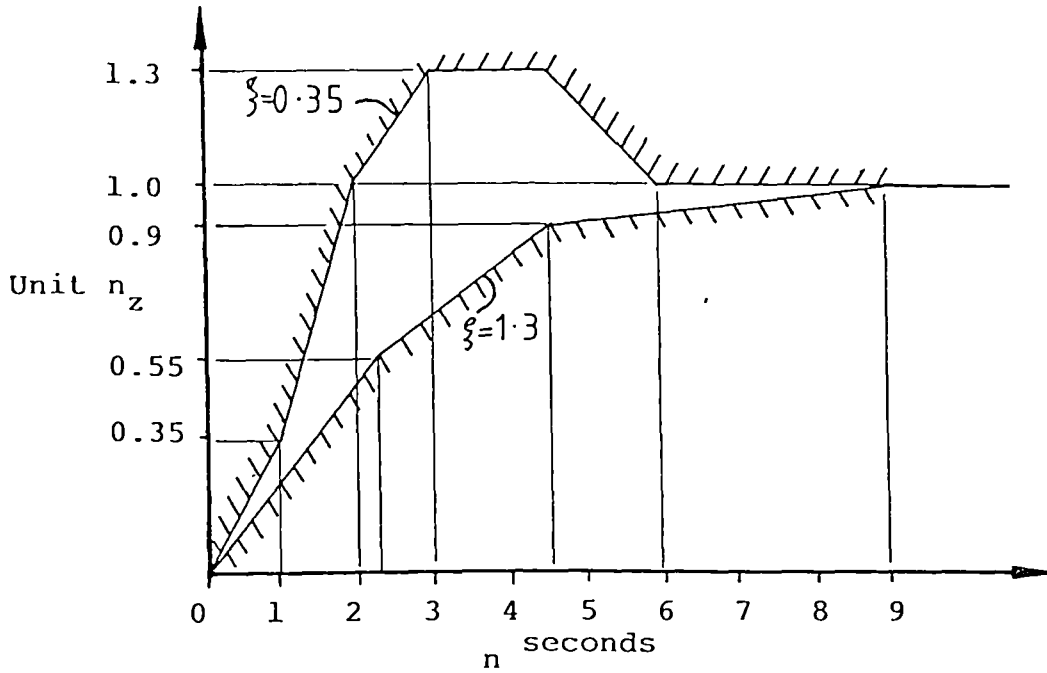
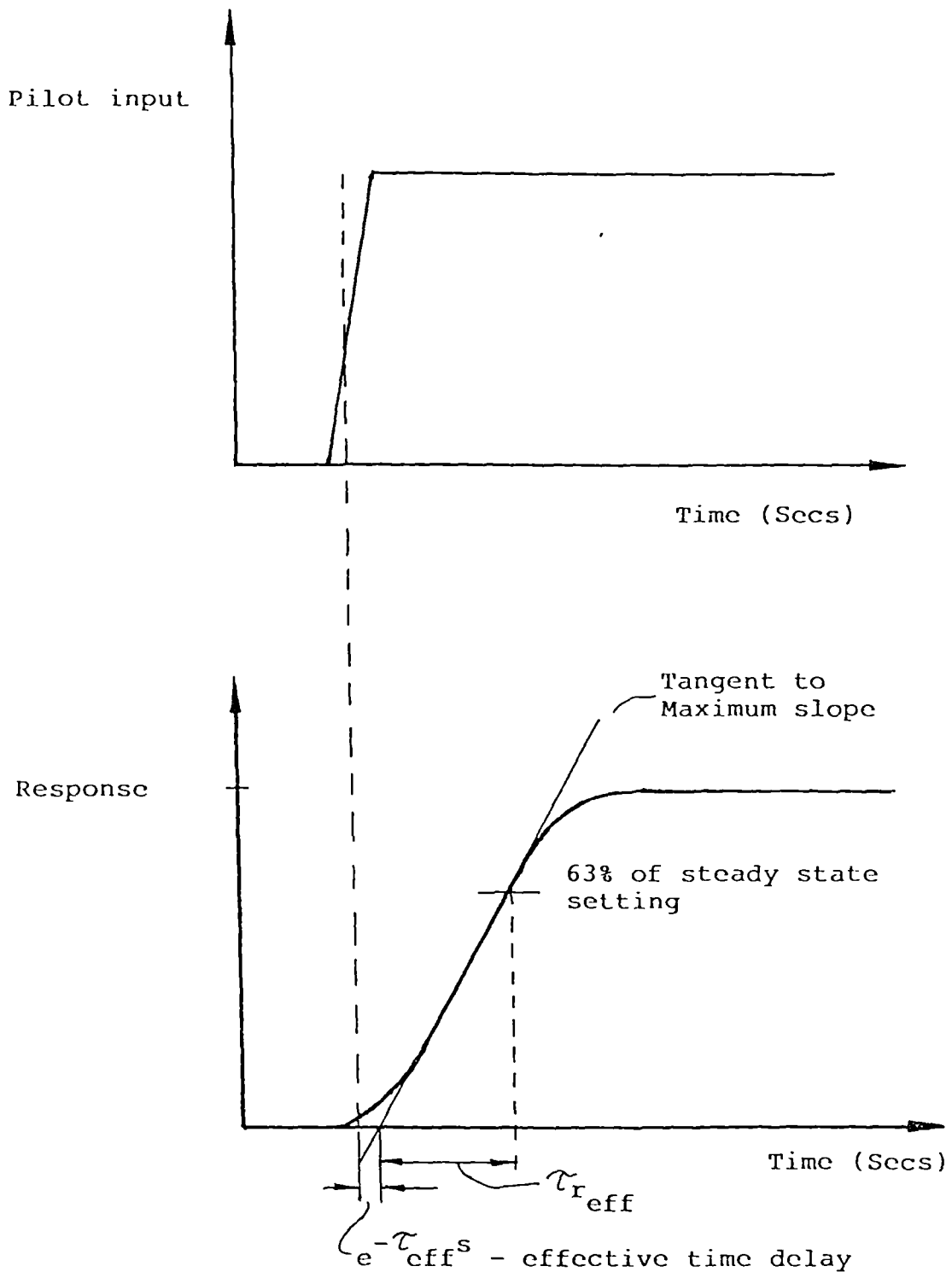


Figure (6.6) Bandwidth HQ Criteria -

(for approach and landing)







($\tau_{r\text{eff}}$ - effective time constant)

Figure (6.9) Effective Time Delay and Time Constant

CHAPTER 7

THE CONTROLLER DESIGN

THE CONTROLLER DESIGN

7.1 Introduction

This chapter describes the controller which has been developed for the GVAM87, in the flight envelope 0 300 Kts, (in fact it is -20ft/s to 500 ft/s) to satisfy the design specification defined in chapter 6. The design specification is realistic and comprehensive and so it imposes severe constraints on the controller design. Furthermore, the flight envelope provides many complex and challenging control problems including time varying dynamics and non-linearities. These factors combined have necessitated a controller which is made up of several fully integrated parts.

These different parts are described in general terms in section 7.2 where the overall controller structure is defined. Some of the individual parts are then discussed in more detail grouped under four headings, one for each of the remaining sections of this chapter. The way in which the controller has been interfaced to the GVAM87 is described in section 7.3. Section 7.4 contains a description of the basic control laws and the gain scheduling that has been used for this application. Section 7.5 contains a description of the integrator wind-up protection and finally, the implementation of intitialisation and TTC mode changes is described in section 7.6.

The actual FORTRAN 77 code of the controller subroutine is not given here as a detailed description of its functioning would be too laborious. Likewise, the many different development ideas and the

evolution of the controller are not specifically listed here. It should be noted also that the design is, in one sense, still under development as further tuning and refinements to the code are needed. However, the controller is sufficient for the aims of this project.

7.2 Overview of the Controller Structure

The structure of the controller is given by Figure (7.1). From this figure it can be seen that there are ten basic sub-units, six of which are contained within the "controller management" block (block (11)). The controller management block is responsible for detecting and setting the TTC modes and for initialising/reinitialising the controller at boundary conditions. These boundary conditions represent the start of a simulation, or the act of crossing from one TTC mode to another. The six sub-units placed within the controller management block are still affected in some way by boundary conditions and are placed within block (11) for this reason. Here it will be assumed that the controller is fixed in one TTC mode and that it has already been initialised so that the controller management block is redundant allowing the function of the ten sub-units to be examined.

Sub-unit (1) collects flight data from GVAM87 and calculates other unmeasurable signals from this flight data. This data is the source of all input to the controller and it consists of the main flight variables, some other derived variables, plus the engine fan speed. All the input data is normally measurable on a standard instrumented fast jet aircraft ensuring that implementation of the controller is practical.

Sub-unit (2) picks up and remembers the actual actuator settings and flight variable settings that exist whenever a boundary condition is crossed. These settings are used to interface the input and outputs of the controller to the GVAM87. These "off-set" signals are the difference between the GVAM87's absolute variables and the controllers perturbation variables.

Sub-unit (3) takes the "raw" pilot stick inputs and calculates the actual commands that they represent, according to the current TTC mode.

Sub-unit (4) conditions the basic flight variable input signals according to the current TTC mode.

Sub-unit (5) takes the off-set information from sub-unit (2), the pilot commands from sub-unit (3) and the actual flight variables from sub-unit (4) in order to calculate the error signals. These error signals must be appropriate to the current TTC mode.

Sub-unit (6) integrates the error signals which are received from sub-unit (5). Sub unit (6) also receives information from sub-unit (9) concerning the state of the actuators, saturated or not. On the basis of this actuator saturation information sub-unit (6) implements integrator wind-up protection where necessary.

Sub-unit (7) performs the gain scheduling, both two-dimensional (transition flight) and one-dimensional (wing borne flight). It receives information concerning the scheduling parameters from sub-unit (1) and its operation depends upon the TTC mode.

Sub unit (8) is the core of the controller and it contains the basic control equation represented by (3.4). The error signals come from sub unit (5), the integral of error signals come from sub unit (6) and the gain matrices and tuning parameters come from sub-unit (7). Sub unit (8) calculates the actuator perturbation demands that will achieve the desired response.

Sub-unit (9) receives the actuator perturbation demands from sub-units (8) and the off-set signals from sub-unit (2) before calculating the absolute actuator signals. These signals are further conditioned to interface with the GVAM87 and the signals are also bounded to lie within the acceptable maximum and minimum actuator limits.

Sub-unit (10) receives the absolute unbounded actuator signals and generates actuator saturation flags which are passed to sub-unit (6) for action in the next time frame.

This completes the overview of the controller structure.

7.3 Interfacing the Controller to the GVAM87

(Sub-units (1), (2), (3), (4), and (9))

This interfacing at the outside simply consists of matching the correct numbers with the correct variables so that the relevant data is passed successfully between subroutines. However, two differences between the controller's internal variables and the model's internal variables makes signal conditioning necessary.

The first difference is that the GVAM87 uses absolute variables whereas the controller uses perturbation variables. This is because the controller is derived from linear control theory using linear small perturbation models and so the basic controller inputs and outputs are all perturbations about a nominal condition. This is handled here by using off-set signals which "remember" the nominal condition. The off-sets are subtracted from absolute variables input from the GVAM87 to the controller and are later added to the perturbation variables output from the controller to the GVAM87.

A second difference is that the range and off-set of the variables is not always the same between the GVAM87 and the controller. This is corrected with simple scaling and off-set signal conditioning.

A further type of signal conditioning is applied in the controller to alleviate some of the engine non-linear effects. If the engine is allowed to wind-down to a low speed it can take a considerable time for it to wind-up again to a high speed which could leave the aircraft without the necessary power during a critical manoeuvre. Furthermore, the engine governor switches off for throttle settings below 0.6 giving rise to large dynamic changes which should be avoided where possible. The signal conditioning applied sets a minimum throttle limit which varies with flight condition. It is designed to approximately follow the steady state trim settings of the throttle whilst allowing a margin for manoeuvre control. This limit is a function of airspeed and it is shown as Figure (7.2).

Finally, there is an interface between the TTC mode command inputs from the pilot and the internal controller variables. The controller actually controls the forward speed, vertical speed and pilot

attitude in the transition flight phase. Consequently, pilot commands involving rates of change of these internal controller variables need to be integrated. Hence, the forward acceleration commands are integrated to give the actual forward speed and flight path angle rate of change is integrated and converted to a vertical speed equivalent. These are effectively moving targets for the controller and so the controller will experience steady state errors when attempting to track these ramped input commands. However, this is transparent to the pilot because the pilot will obtain the correct response, in the correct direction, moving at a rate that is proportional to his stick deflection. Forward acceleration in the high speed mode is also implemented in this way. All of these integrators used like this are handled by the controller management block.

7.4 The Basic Control-laws and Gain Scheduling

(Sub-units (7) and (8))

The core of the controller is the basic control equation given by (3.4) which links the errors (and the integral of the errors) for each control feedback signal to the actuators. Equation (3.4) shows that link is entirely dependent upon the controller matrices K_p and K_I and the feedback gain g , which are designed for each flight case as shown in chapter 5.

It has already been shown that the matrices K_p and K_I depend upon the input and feedback matrices (equations (3.29) and (3.30)), the former changing with flight condition and the latter changing with both flight condition and the TTC modes. Consequently there is a need to

schedule the controller gains as a function of flight condition and TTC mode.

To simplify this task the similarity between the low speed and high speed transition TTC modes has been exploited. Subsection 6.2.2. and Figure (6.3) define the TTC modes as follows:

Low Speed Transition:

Pitch attitude	(THETD)	[Deg]
Horizontal acceleration	(VELHOR)*	[Ft/s]
Vertical velocity	(VKD)	[Ft/s]

* $VELHOR = (VKN^2 + VKE^2)^{1/2}$

High Speed Transition:

Pitch attitude	(THETD)	[Deg]
Flight Path acceleration	(VTKT)	[Kts/s]
Flight path angle	(GAMMAD)	[Deg]

Clearly, the simple geometric/dynamic relationships between VELHOR and VTKT, and also VKD and GAMMAD, enables the control laws to be simplified. Hence, the control matrices can be generated in terms of the low speed transition variables and conversion factors can be used when the high speed transition TTC mode is required. The conversion factors used for nominally straight and level flight are

$$VELHOR = VTKT * KTOF \quad \dots (7.1)$$

and

$$VKD = \frac{GAMMAD * VTKT * KTOF}{RTOD} \quad \dots (7.2)$$

where KTOF is the knots to feet per second conversion factor and RTOD is the radians to degrees conversion factor.

This change is handled by the controller management block removing the need to schedule the controller gains as a function of TTC mode in the transition region. There is, however, a different set of controller gains used for high speed flight and one reason for this is explained below.

The GVAM87 in the transition region used the engine (thrust magnitude) the nozzles (thrust direction) and the tail plane for longitudinal control. The nozzles are fixed aft for fully wing-borne flight (high speed flight) by definition which reduces the number of inputs by one resulting in a two input/output system. This is a significant change which requires a complimentary input/output controller. The high speed flight controller therefore uses two control matrices which are two-by-two instead of the three-by-three control matrices used for transition flight.

The method of gain scheduling used here is the well tried and tested method of linear interpolation. Controllers have been designed to operate at different spot points (flight conditions) which are placed strategically through the flight envelope. It is assumed that all gradients between spot points are approximately constant and so an off-design gain may be calculated using linear interpolation. The other assumptions inherent in gain scheduling are that the control laws are sufficiently robust to give satisfactory off-design performance and that the rate of change of the scheduling parameter is sufficiently slow so as to make the controller appear quasi-static.

The robustness assumption has in fact been proven in section 5.7 which suggests scheduling with airspeed at a design interval of 40

Kts through the transition flight phase. Other tests suggested an interval of 50 Kts for the high speed flight phase with one exception: where the transition and high speed flight meet an interval of just 20 Kts should be used. However, early tests in the transition flight phase showed that there could be large changes in engine dynamics which significantly affect the closed-loop system performance. This required that the controller gains should also be scheduled as a function of engine state. The effect of not changing the controller, when the engine dynamics change considerably, was demonstrated in part by section 5.8.

This has resulted in a two-dimensional gain matrix look-up table in which the gain matrix changes as a function of the airspeed and the engine low pressure fan speed in order to remain compatible with the aircraft dynamics. The scheduling parameters used for both the transition flight phase and the high speed flight phase are given below in Table (7.1).

Table (7.1)

<u>2-Dimensional table - transition flight</u>						
VTKT	0	40	80	120	160	200
and						
FNP	0.5018	0.7993	0.8691	0.8791	0.9354	0.9938
(equivalent throttle settings)	41%	56%	59%	63%	78%	93%

Table (7.1) (continued)

1 Dimensional table - high speed flight						
VTKT	140	160	180	200	250	300

Several parameters need to be scheduled for each controller (not just the basic gain matrices) and the shortest method of doing this is to store K_0 , Σ , Ξ , g and m_1 , where K_0 is given by

$$K_0 = (C_2 B_2)^{-1} \text{ or } (F_2 B_2)^{-1} \quad \dots (7.3)$$

That K_p and K_I may be given by

$$K_p = K_0 \Sigma \quad \dots (7.4)$$

and

$$K_I = K_0 \Sigma \Xi \quad \dots (7.5)$$

Furthermore, the result given in subsection 5.4.2 (step 8) may be applied to simplify the definition of the controller still further using (5.51) and (5.52).

The standard three-by-three gain matrix was expanded to a three-by-six gain matrix (K_{GS3}) for gain scheduling purposes where the three-by-six matrix had the following components:

$$K_{GS3} = \begin{bmatrix} K_0(1,1), K_0(1,2), K_0(1,3), \sigma_1, \rho_1, g \\ K_0(2,1), K_0(2,2), K_0(2,3), \sigma_2, \rho_2, m_1 \\ K_0(3,1), K_0(3,2), K_0(3,3), \sigma_3, \rho_3, 1.0 \end{bmatrix} \quad \dots (7.6)$$

and $K_{GS3}(3,6)$ is unused. The high speed two-by-two gain matrix was similarly expanded to a two by five gain matrix (K_{GS2}) for gain scheduling purposes where the two-by five matrix had the following components:

$$K_{GS2} = \begin{bmatrix} K_0(1,1), K_0(1,2), \sigma_1, \rho_1, g \\ K_0(2,1), K_0(2,2), \sigma_2, \rho_2, 1.0 \end{bmatrix} \quad \dots (7.7)$$

and $K_{GS2}(2,5)$ is unused.

Once, each controller for each design flight case has been tuned, it is put into the form of either (7.6) or (7.7) so that the minimum of space is used for storing the gain look-up table. The actual gain scheduling is then performed by a function. This is illustrated for a transition flight phase with the aid of Figure (7.3). This figure shows how each element of the matrix K_{GS3} is calculated. A similar procedure would be used for K_{GS2} , except that it is scheduled only one-dimensionally making the equations simpler. Once the gain matrix has been calculated by the function it is "unpacked" by the controller routine and implemented in the basic control laws of sub-unit (8).

7.5 Integrator Wind-Up Protection

(sub units (6) and (10))

The purpose of the integrators in the high-gain controller is to remove steady state errors. This is achieved by the integrators driving the actuators to a new steady state condition after a

disturbance or a commanded manoeuvre. If the disturbance or the command is very large it will produce large errors which will most likely saturate the actuators. This can result in the large errors being evident for some time causing the integrators to wind-up to a much larger value than that which will be required for the new steady state. The integrators will only then unwind (or wind down) if the errors change sign which is only possible if the system overshoots the new steady state. Thus, integrator wind-up can cause large overshoot and severe oscillations, both of which reduce the overall system performance.

The cause and effect of integrator wind-up is well understood in SISO systems where a particular actuator is usually associated with a particular integrator. In this case one solution is simply to freeze the integrator output when the associated actuator reaches a limit and becomes saturated. Unfortunately, this understanding is not well defined for MIMO systems. Indeed, the cause and effect of wind-up is more complex in MIMO systems incorporating integrator action as will be shown for a high-gain system.

In a typical high-gain controller every integrator is linked to each actuator, to varying degrees, by the matrix K_I . Thus the effect of one integrator winding-up could be felt by each actuator. Conversely, any actuator which saturates could promote integrator wind-up for any or all of the integrators. However, methods for conditioning integrators in MIMO systems are beginning to appear in the literature and one general technique for anti-wind-up and bumpless transfer [Hanus et al] is being applied to high-gain controllers by researchers at Lancaster University (working under Professor Bradshaw).

Such methods were not used for this project though as it was possible to exploit the structure of the aircraft to enable a simple method of wind up protection to be used. The structure of the GVAM87 is such that the longitudinal controls can be placed into two groups. The first group contains the engine and nozzles which control the thrust magnitude and direction. These are the main motivators affecting forward and vertical planar motion. The second group contains the tailplane (and reaction controls) which controls the pitch moment. This is the main motivator affecting all pitching motion. Although there is some interaction between each group they are largely separate in their affects. This separation allows each group to be treated individually for wind-up protection.

The scheme used is essentially the same as that described for SISO wind-up protection. For group 2, if the tailplane becomes saturated the pitch integrator is frozen (pitch rate or pitch attitude, depending upon the TTC mode). Alternatively, for group 1, if either the nozzles or the engine becomes saturated then both the integrators associated with forward and vertical planar motion are frozen. This group 1 scheme is for transition TTC modes; the high speed flight phase makes the scheme even easier as only forward motion and the engine are involved making it identical to the equivalent SISO case.

Treating the nozzle and engine together with the forward and vertical planar motion is essential as the different quantities are very closely linked throughout the transition. However, treating the tailplane and pitch motion separately is also essential for the following two reasons. Firstly, in the transition flight phase it is very important to maintain tight control of the pitch attitude. If

the pitch integrator were frozen because the engine was saturated then the pitch attitude would drift away from its correct value making the problem worse and possibly leading to instability.

Secondly, the tailplane has a very high authority and it seldom becomes saturated in normal transition flight phase manoeuvres. Consequently it is sensible to separate the pitching motion group from the planar motion group which saturate more easily.

The integrator wind-up protection scheme that is used in this controller is summarised below in Table (7.2).

Table (7.2)

Saturated actuator:	Engine	Nozzles	Tailplane
Low Speed Transition:			
Forward speed integrator	Frozen	Frozen	Free
Vertical speed integrator	Frozen	Frozen	Free
Pitch attitude integrator	Free	Free	Frozen
High Speed Transition:			
Forward speed integrator	Frozen	Frozen	Free
Flight path angle integrator	Frozen	Frozen	Free
Pitch attitude integrator	Free	Free	Frozen
High Speed Flight:			
Forward speed integrator	Frozen	-	Free
Pitch rate integrator	Free	-	Frozen

7.6 Controller Management

(Sub units (3),(4),(5),(6) and (7))

As the name suggests, the controller management block manages the functioning of the controller, in particular the six sub-units (2),(3),(4),(5),(6) and (7). This block is responsible for detecting boundary conditions and taking the appropriate action. The boundary condition can be the first initialisation (at time = 0) or the act of crossing from one TTC mode to another. The "appropriate action" means a whole variety of tasks which will be described in the following subsections. The initialisation procedure is described in subsection 7.6.1, the TTC mode sensing is described in subsection 7.6.2. and TTC mode changes are described in subsection 7.6.3.

7.6.1 Controller Initialisation

Before any simulation or analysis work is undertaken, the GVAM87 must be prepared for running within TSIM. This involves a period of data input from files which initialise certain key model variables. This stage is also used to initialise certain key controller variables such as: time constants for input signal filters, dead band filter characteristics for the pilot's inputs, pilot input scaling factors, parameters which define the TTC modes and also the gain matrix look-up tables. After this "pre-initialising" stage the GVAM87 may be taken to any part of the design flight envelope, in or out of trim. From this point the controller initialises itself.

Firstly, the controller performs a simple test to discover the flight conditions and hence which TTC mode should be in operation. This information is then used to initialise the TTC mode dependent variables such as pilot input scaling factors and error scaling factors (for VKD to GAMMAD conversion). This information is also used to select TTC mode dependent equations which define the input variables, the error scaling factors, the command inputs and the actual error signals. Secondly, the controller initialises the remaining variables which are not necessarily TTC mode dependent such as: the input and output signal off-sets, the dead band filter variables, the integrator initial conditions, the blending variables (used to blend between TTC modes) and the various logic flags which are used for controller management.

All this activity results in a controller which is ready to run and is aware of its mode of operation. Starting from an untrimmed flight condition the controller will quickly compensate and stabilise the system; starting from a trimmed flight condition nothing at all will happen, showing that the GVAM87 and the controller are in harmony.

7.6.2 Task Tailored Control-Mode Sensing

The TTC mode design specification is given in subsection 6.2.2. These criteria are applied directly in the controller and their actual operation is described here.

When accelerating, the high speed flight phase is defined as nozzles fully aft at speeds greater than 140 kts when the angle of incidence is less than 12° (the GVAM87 is usually flown at 8° angle of

incidence). This allows the aircraft to be manoeuvred freely up to 140 kts without fear of a sudden mode change; speeds beyond this are usually achieved only in accelerating transitions to wing borne flight which requires a TTC mode change anyway. The angle of incidence criterion excludes the high speed flight phase at high angles of incidence so that the decelerating TTC mode change can be sensed and enhanced manoeuvres can be performed. For example, when decelerating from a high speed flight phase the aircraft will begin to lose height which the pilot compensates for by increasing the angle of incidence until the maximum (12°) is reached, thereby changing the TTC mode to high speed transition.

The low speed transition flight phase is defined simply as being all speeds less than 60 ft/s which is easily detected. The high speed transition flight phase is in between the foregoing two flight phases and here it is not sensed at all. Rather, if the flight phase is not highspeed and it is not low speed transition, then it must be high speed transition. This use of redundant logic saves time and complications in the controller management block.

The landing mode (or take-off mode) is simply a TTC mode in which the integral action is suspended leaving the pilot with proportional control action. This prevents the integrators becoming unstable when the aircraft is on the ground. The landing mode is simply defined by an internal model variable which represents the "weight on wheels" sensor. When the "weight on wheels" reaches 25% of the aircraft gross weight it is considered to be in landing mode.

Once a TTC mode has been sensed particular logic flags are set. These logic flags have "old" and "new" versions so that the "old" (or

previous) TTC mode can be compared to the "new" (or current) TTC mode. Thus, by examining the "old" and "new" flags the controller management block can detect TTC mode boundary conditions. The management of these boundary conditions is discussed in the next subsection.

7.6.3 Task Tailored Control Mode-Changing

There are four main TTC mode changes possible in this controller but most of the operations are common for each of these changes. Indeed much of the change is implemented by "re-initialising" some of the controller sub-units. This is made possible by the use of perturbation equations within the controller which allows the offset variables to be re-initialised maintaining absolute input/output consistency. In addition to this, perturbation variables may generally be set to zero. Hence all of the TTC mode dependant variables and equations initialised in subsection 7.6.1. are reinitialised during these four TTC mode changes. Any additional operations that these four mode changes require are described below under the appropriate headings. The effect of TTC mode changing is also described in each case from the pilots perspective.

Low speed transition to highspeed transition:

No additional operations are required. The TTC mode change occurs as the speed rises above 60 ft/s and the forward acceleration rate is maintained despite the change of control variable from ft/s to Kts. Any pilot inputs concerning pitch attitude are unaffected by the TTC mode change, however pilot inputs using the right hand inceptor will

have the following effects.

A climb rate command during the TTC mode change will become a "flight path angle increase" command and so the pilot will need to return the inceptor to the centre zero position to maintain a constant flight path angle. Conversely, a descent rate command during the TTC mode change will become a "flight path angle decrease" command and the pilot should still return the inceptor to the centre zero position. In both cases the pilot action is natural, simple and non-hazardous.

High speed transition to low speed transitions

The additional operation here is a flight path to height rate blend which also acts as a carefree handling feature. The TTC mode change occurs as the speed falls below 60 ft/s and once again acceleration rates and pitch attitude commands are unaffected by the change. However, a downwards flight path with the inceptor at zero, is smoothly levelled out without further pilot input. This blends the two different TTC modes together and acts as a safety feature requiring the pilot to actively select a descent rate to continue the descent. A similar blend occurs if the aircraft is climbing as the TTC mode changes, but this scenario is unlikely. In the unlikely event that the pilot actually maintains a flight path angle increase/decrease command when the TTC mode changes then this is blended into a height rate command resulting in a flight path angle gradient change which is both natural and unobtrusive.

High speed transition to high speed flight (wing-borne)

There are two additional operations here. The first operation reconfigures the right hand inceptor for pitch rate command inputs as well as zeroing the nozzles and canceling residual flight path commands. The second operation changes the gain scheduling so that it uses the high speed look-up table and one-dimensional gain scheduling. This final operation also changes the three input/output basic control equation into a two input/output control equation.

The forward speed commands are unaffected by the TTC mode change and the pitch attitude commands are disabled. The flight path angle commands are also disabled and replaced by pitch rate commands on the same inceptor. This means that a residual flight path angle increase/decrease command during the TTC mode change will command a pitch rate. This results in consistent flight path angle changes being produced which are natural to the pilot.

Hightspeed flight (wing-borne) to high speed transition

There are three additional operations here two of which are the reverse of those described for the previous TTC mode change. Firstly, the right hand inceptor is configured for flight path angle changes and pitch attitude commands are reinstated. Secondly, the gain scheduling ceases to be one-dimensional using the high speed look-up table and becomes two-dimensional using the transition look-up table. In this operation the basic control laws revert from two input/output form into three input/output form allowing the nozzles to "unfreeze".

The final operation reinstates the pitch attitude trim setting to 8° , unless the pilot commands a different level. The pitch attitude is then brought to this setting from its previous setting in a smooth blended way.

The pitch attitude is reinstated as described above and the forward speed commands are unaffected by the TTC mode change. The remaining command inputs also blend in smoothly as pitch rate commands become flight path angle commands. Crossing this boundary in a VIFF mode would be similar but VJFF mode could not be fully implemented in the time available and so it is not described here. Once again, all boundary crossing effects appear natural to the pilot.

This completes the description of the four main TTC mode changes and one of the carefree handling features. There are three other carefree handling features to be described and a general TTC mode change. These descriptions are given below under the appropriate headings.

Landing mode

The landing (or take off) mode can ^{be} engaged or disengaged from any of the three flight phases. However, the controller management functions which make it possible are the same for each flight phase and so it

is counted as one TTC mode. The two operations that take place when this mode is entered are as follows: firstly the controller integral action is suspended and these integrators are frozen, secondly the engine speed is allowed to reduce to its minimum level (however the minimum engine speed is usually limited to a setting greater than the idle speed). These two operations are reversed when this mode is left and so the main integrators are then unfrozen.

When landing or taking off, in any flight phase, the pilot will experience a negligible change in response due to the loss of the integral action. Some slight activity in pitch attitude is to be expected though as the aircraft will find its own natural pitch attitude when sitting on its wheels. Likewise, after take-off, the pitch attitude will head for the value set by the pilot once the integrators are working again.

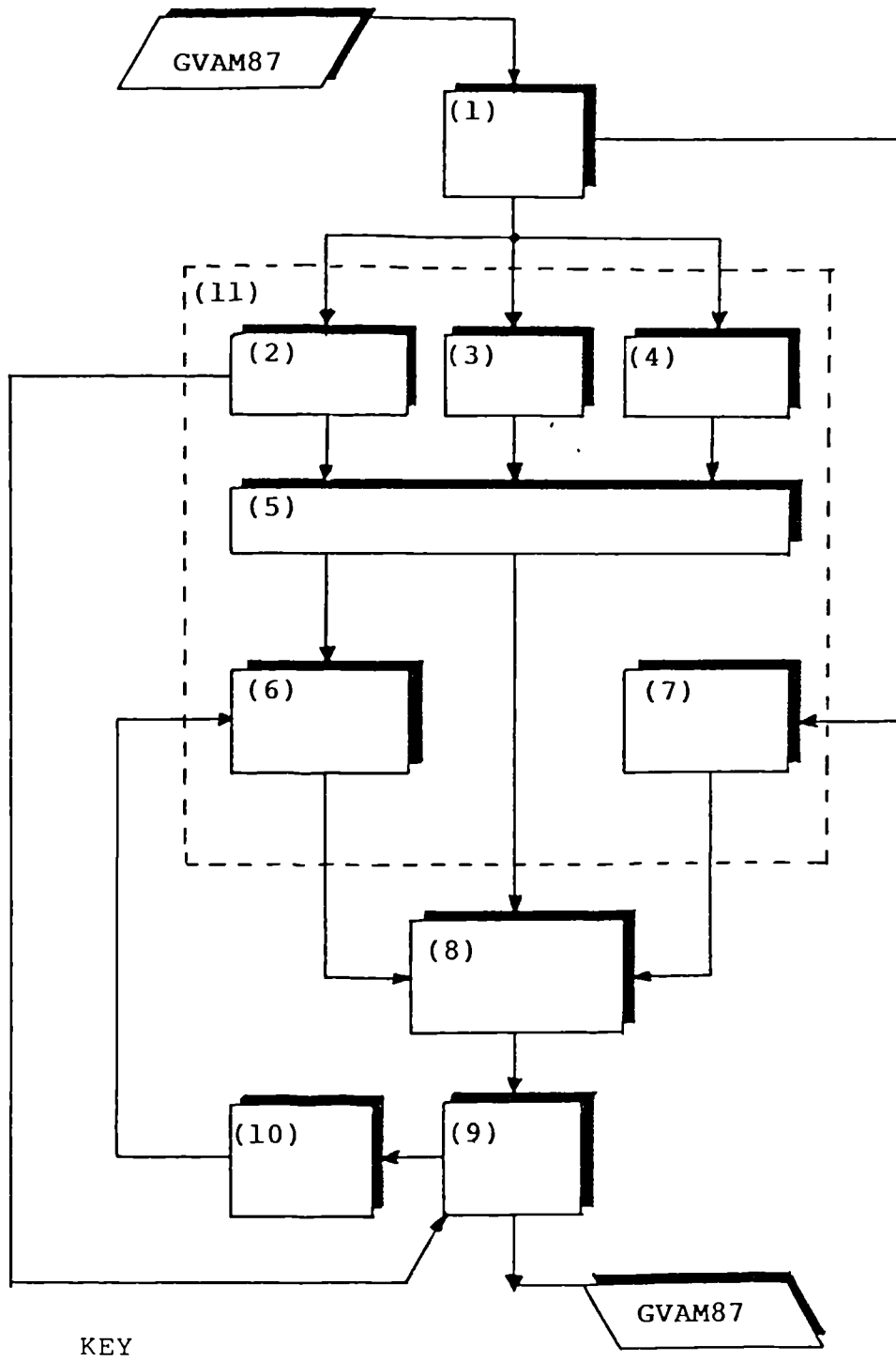
Carefree handling

In the low speed transition TTC mode it is possible to fly backwards, but the GVAM87 becomes unstable if the speed becomes too large. Hence a carefree handling feature is introduced which limits the backwards speed to 20ft/s which is adequate for taxiing manoeuvres. The forward speed command integrator is also reinitialised when this carefree handling mode is invoked

In accordance with the recommendations of chapter 6, the flaps and undercarriage are scheduled with airspeed. Normally the pilot would select these secondary items well in advance so that the main piloting tasks are not compromised. The pilot also needs to ensure

that flaps and undercarriage are not extended beyond certain speeds but also that the undercarriage is extended before landing!. Thus automatic selection of these items at the correct speeds can improve flight efficiency in addition to the obvious advantages of a reduction in pilot workload and improved carefree handling.

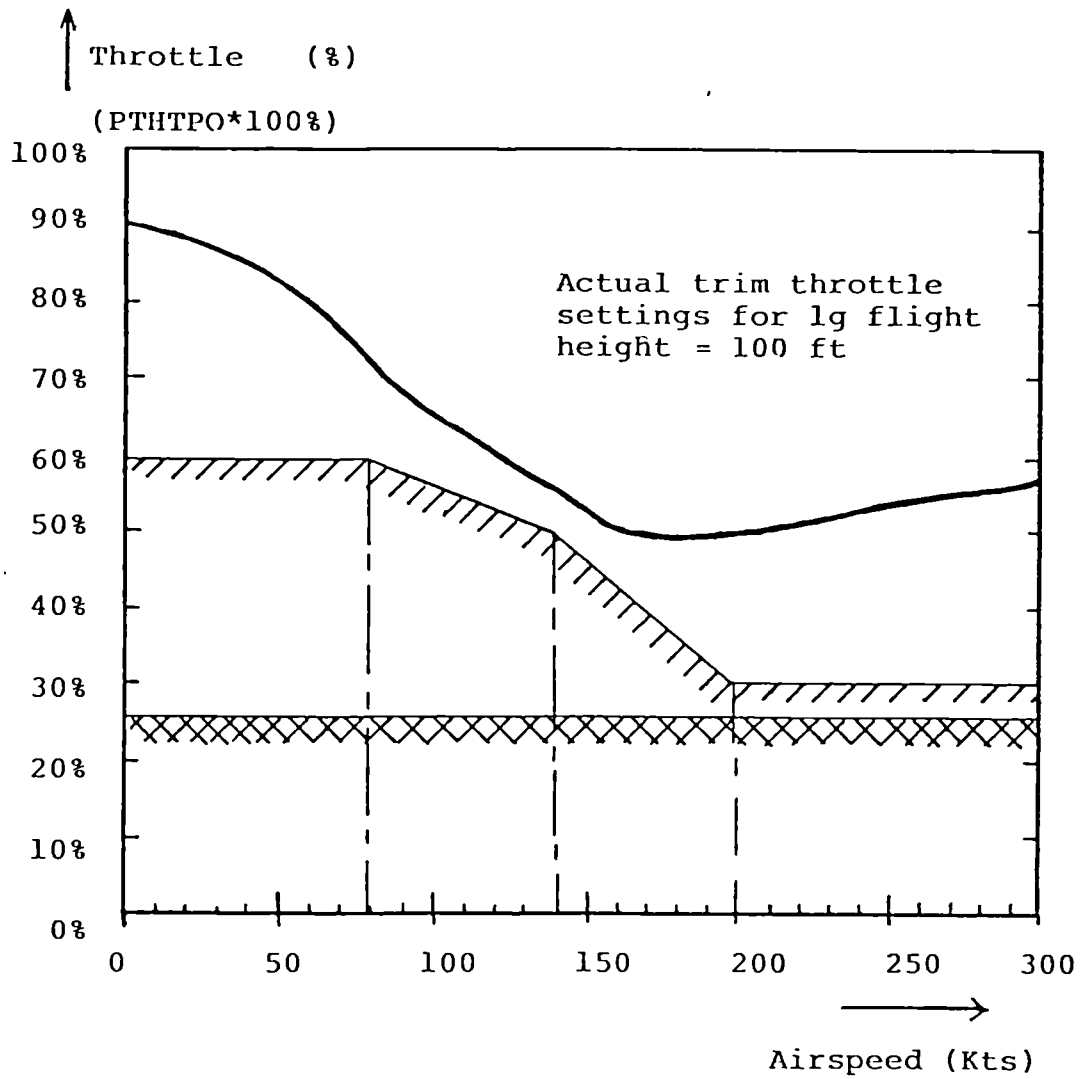
It has been shown that the management block largely consists of FORTRAN IF...THEN...ELSE statements which form a logic safety net within which the six sub-units function. Only three distinct TTC modes and two carefree handling modes are implemented and yet the management block has become a large proportion of the whole controller. Any increase in TTC modes or carefree handling modes will greatly increase the size and complexity of this block. And yet there is little, if any, formal guidance on the design of this critical feature. There is little point proving the robustness of a multivariable controller when flawed controller management can switch the engine off in a landing mode! It is hoped that such large errors will not be made, but the conclusion is that this area of controller design needs considerable further development. The emerging disciplines of Artificial Intelligence and Intelligent Knowledge Based Systems could be beneficial methods of approach.



KEY

- (1) Flight data collection/calculation.
- (2) Signal off-set monitoring.
- (3) Pilot input signal conditioning.
- (4) Feedback signal conditioning.
- (5) Error signal calculations.
- (6) Integral of error calculations and wind-up protection.
- (7) Gain scheduling, both one and two dimensional.
- (8) Controller core, the basic control equations.
- (9) Output signal conditioning.
- (10) Actuator saturation control.
- (11) Controller management block.

Figure (7.1) Block Diagram of Controller Structure.



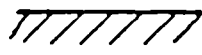
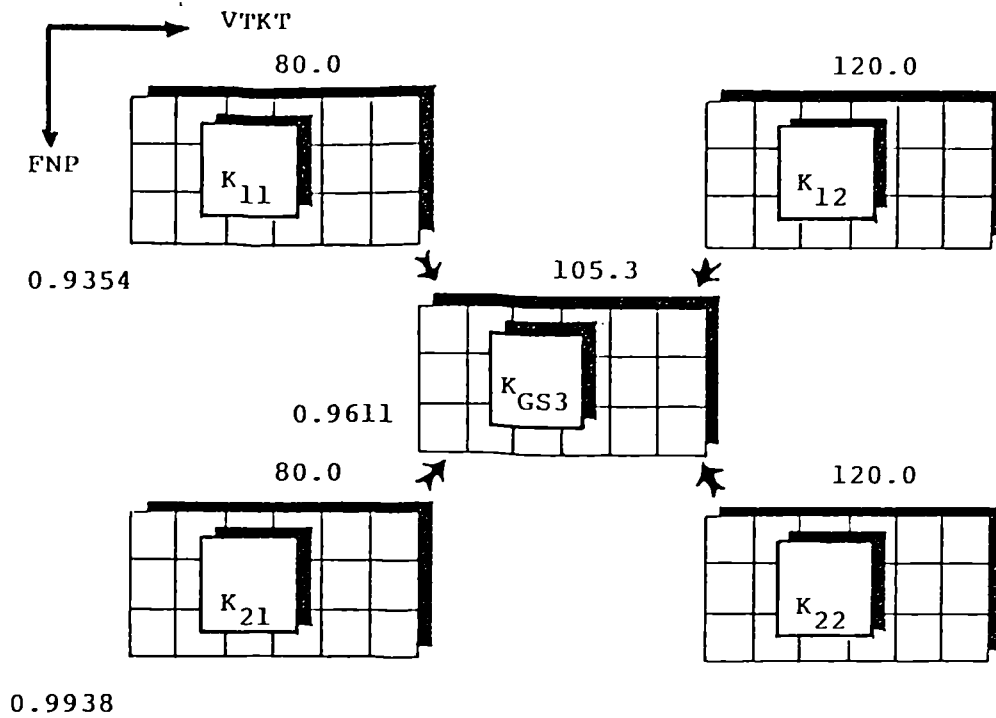
-  - Speed scheduled lower throttle limit used by the controller.
-  - Absolute lower limit or engine-idle throttle setting (26%)

Figure (7.2) Diagram of Scheduled Throttle Lower Limit



$$\Delta X = \frac{105.3 - 80.0}{120.0 - 80.0} = 0.6325$$

$$\Delta Y = \frac{0.9611 - 0.9354}{0.9938 - 0.9354} = 0.4401$$

$$\text{temp1} = K_{11}(i, j) + [K_{12}(i, j) - K_{11}(i, j)] \Delta X$$

$$\text{temp2} = K_{21}(i, j) + [K_{22}(i, j) - K_{21}(i, j)] \Delta X$$

$$K_{GS3}(i, j) = \text{temp1} + [\text{temp2} - \text{temp1}] \Delta Y$$

for $(i = 1, 2, 3)$ and for $(j = 1, 2, \dots, 6)$

Figure (7.3) Illustration of 2-D Gain Scheduling.

The matrices K_{11} , K_{12} , K_{21} and K_{22} represent four on design flight conditions in the gain matrix look-up table at speeds of 80 kts and 120 kts and for FNP at 0.9354 and 0.9938. K_{GS3} represents the current flight condition.

CHAPTER 8

DEMONSTRATION OF THE CONTROLLER DESIGN

DEMONSTRATION OF THE CONTROLLER DESIGN

8.1 Introduction

This chapter demonstrates the controller design which was described in the previous chapter. The design covers a wide flight envelope which can be represented by the valid speed range -20 ft/s to 507 ft/s (300 Kts). In various parts of this flight envelope there are large plant dynamic changes, non-linear effects, control-mode changes and blends, carefree handling features and dynamic problems. In order to demonstrate such a complex multi-mode system fully a great number of simulations would normally be required which is more easily and effectively accomplished with a piloted real-time flight simulation. A piloted simulation is also the only way in which the handling qualities can be properly assessed*. Despite these limitations the controller is demonstrated here using a few select simulations to illustrate particular features, but principally four realistic flying tasks are used to demonstrate the overall functionality of the controller.

* These facts are mentioned here because this controller has taken part in a piloted simulation trial at the RAE, Bedford, and this work is the subject of a separate report [Hopper] funded by a separate contract.

The demonstration is split into eight sections as follows. Section 8.2 contains a demonstration of the controller's standard control modes at four different flight conditions. The first of the realistic flying tasks consists of a vertical take off followed by an accelerating transition to wing-borne flight and is described in section 8.3. The second flying task is described in section 8.4 and consists of a short take off, a horizontal acceleration and deceleration in the transition region followed by a Rolling Vertical Landing (RVL). The third flying task involves a decelerating transition from wing-borne flight followed by a vertical landing and is described in section 8.5. The final flying task is described in section 8.6 and consists of a deceleration from the highspeed transition region to backwards flight and then a forwards RVL. These flying tasks are followed by three demonstration sections (sections 8.7, 8.8 and 8.9) which illustrate the integrator wind-up protection, the turbulence and gust response and the possibilities of automatic landing aids respectively. The last section, section 8.10, discusses the handling qualities aspects of the controller.

It should be noted that one flying mode mentioned in Chapter 6 is not demonstrated here, that is the VIFF mode. Without lateral control it was found to be impossible to actually invoke this mode in the way that was intended. Furthermore, it is anticipated that a change in the controller management would also be required to distinguish between the high speed transition TTC mode and the VIFF TTC mode. Inexact VIFFing manoeuvres can be performed by setting the nozzles down during high speed flight, however, in the time available this manoeuvre could not be incorporated into the control scheme. Before describing the first manoeuvre demonstrations, the way in which the flying tasks were performed is described.

Usually the job of flying a V/STOL aircraft falls to just a few highly trained and experienced adaptive multivariable controllers, namely RAF pilots. These pilots continuously update their control inputs to maintain the desired flight path whilst obtaining information from their instruments, the outside view, the vestibular system (the inner ear) and the proprioceptive and somatic systems (the "seat of the pants"). However, each flying task shown here has been "flown" by an untrained "pilot" (the author) who issues discrete commands via a computer keyboard using the plots shown in the figures as the only source of flight information. Despite this limitation the different tasks have been flown adequately if somewhat imprecisely. This is a testament to the controller and not the "pilot"!

The tasks could have been made easier for desktop flying by modifying the inputs but this was avoided as the controller needed to be ready for piloted real-time flight simulation trials. Furthermore, this would not exercise the whole control scheme. The result was that the controlled aircraft was almost unflyable in the high speed region. This is because the flight path is usually controlled by the angle of incidence which is normally controlled by the pilot using pitch rate inputs. In an accelerating or decelerating transition this would require constant retrimming inputs to maintain constant height, something which was beyond the "pilot"/keyboard arrangement used here. The solution was to incorporate a simple height hold autopilot which commands pitch rate whilst monitoring the vertical speed (VKD). The autopilot was a PID control loop as given by

$$Q_{com} = K_p e + K_I z + K_D \dot{e} \quad \dots (8.1)$$

$$\dot{z} = e \quad \dots (8.2)$$

and

$$e = R - VKD \quad \dots (8.3)$$

for $R = 0$, where K_p, K_I and K_D are scalar gains, e is the error signal, \dot{e} is the error rate of change, z is the integral of the error and where Q_{COM} is the pitch rate command which was given to the high-gain control system to implement. This is effectively a very simplistic pilot model which was approximately tuned on-line. It has been used for simulation in two instances and these are pointed out in the text.

An additional simple pilot model is also used because a pilot does not usually perform abrupt discrete command inputs or step inputs, instead the commands are smoother. This is represented here by shaping the discrete keyboard inputs to the controller so that they conform to cubic ramps, as shown by Figure (8.1). The time constant T is varied but it will be given, where relevant, within the text. The exception to this stick input shaping is the forward acceleration commands which are usually passed through a simple lag with a time constant of 0.2.

It should be noted that some explanations given here for the cause of dynamic effects are described as "probable" causes. This is because the highly complex aircraft model does not always allow the exact cause of a dynamic effect to be discovered. This is compounded by the interrelationships between the controller and the GVAM87.

Finally, Table (8.1) below gives a description of each variable which appears in subsequent plots shown in this chapter. The list of variables is in alphabetical order and each actuator variable is post fixed with an "0" indicating it is an output variable and so it is the actual actuator position (after any dynamics, rate limits or position limits which may affect it).

Table_(8.1)

Variable	Description	Units
AIRBRO	Airbrake position	%/100
ALFAD	- Angle of incidence	Deg
ETADO	- Tailplane angle	Deg
FLAPDO	- Flap angle	Deg
FNP	- Low pressure fan speed	%/100
GAMMAD	- Flight path angle	Deg
H	Height	Ft
HNP	- High pressure fan speed	%/100
MYSTK1	- Left hand inceptor	Ft/s ² & Kts/s
MYSTK2	- Right hand inceptor	Ft/s & Deg/s
MYSTK3	Button on left hand inceptor	Deg
PTHTPO	- Throttle setting	%/100
QD	- Pitch rate	Deg
QEF	- Fuel flow rate	Gall/Hour
THDFPO	Nozzle angle	Deg
THETD	- Pitch attitude	Deg
UCO	- Under carriage position	%/100
VKD	- Vertical speed down	Ft/s
VKN	- Horizontal speed north	Ft/s
VTKT	- Airspeed	Kts
VWD	- Wind speed down	Ft/s
VWN	- Wind speed north	Ft/s

8.2 Demonstration of Standard Control-Modes

For this demonstration the GVAM87 was trimmed at four different flight conditions where each of the standard control-modes was operated. This is described for each flight condition in the following subsections.

8.2.1 Low Speed Transition - The Hover

The aircraft was trimmed for flight at the hover at a height of 100ft, pitched up at 8° relative to the earth. The control trim settings for this were 91% throttle setting, 81° nozzle angle and $+1.1^{\circ}$ tailplane angle. The following manoeuvres are shown in Figure (8.2). The first manoeuvres demonstrated the forward speed control mode. It consisted of an acceleration command (MYSTK1) at 15ft/s^2 forwards up to 40ft/s , followed by a deceleration at -15ft/s^2 until the carefree handling feature prevented backwards flight faster than 20ft/s . It should be noted that despite the fact that the pilot input remained at -15ft/s^2 , the speed was held at -20ft/s . Finally, the aircraft was returned to the hover with a brief forwards acceleration of 15ft/s^2 .

The next manoeuvre demonstrated the pitch pointing control-mode (MYSTK3) and the aircraft was pitched up and down by $\pm 5^{\circ}$ with a cubic ramp time constant of 2 seconds. The third and final manoeuvre demonstrated the height-rate control-mode (MYSTK2) and the pilot demand was $\pm 10\text{ft/s}$ with a cubic ramp time constant of 4 seconds.

The descent phase was maintained slightly longer than the climb phase and so the aircraft finished lower than the original 100 ft.

Clearly, each control-mode required only one input from the pilot whilst the controller managed all three actuators to achieve the desired response. Cross coupling was evident but small, and the manoeuvres were all executed crisply. The forward acceleration control-mode required some pilot anticipation to reach the desired values of forward speed accurately. This was due to the phase lags inherent in the command integration system.

The high command levels caused the nozzles to saturate once (at A) and the throttle to saturate three times (at B,C and D). This caused no problems as it was handled by the i.e. controller's anti-wind-up protection. The last feature to note is the small cycle that appeared and was most evident on the nozzles (at E). This cycle coincided with the steady climb and sink rates and it was probably caused by the controller acting at an off-design condition. The air speed VTKT does not have a direction and so it was always positive, as shown by Figure (8.2). Consequently it reached + 6 Kts for both vertical manoeuvres and the gains were scheduled with this VTKT value, despite the fact that the aircraft was still at the hover. The same cycle was evident on the VKN, QD and ETADO responses but ETADO and QD were the controller reacting against the nozzle cycle and VKN was the final result of this activity. Clearly, the response, as seen by the pilot, was negligible but the presence of a cycle was undesirable.

8.2.2 High Speed Transition - 80 Kts (135 ft/s)

The aircraft was trimmed for flight at a height of 100ft, pitched up at 8° relative to the earth flying straight and level. The control trim settings for this were 73% throttle setting, 68° nozzle angle and $+2.9^{\circ}$ tailplane angle. The following manoeuvres are shown in Figure (8.3).

The first manoeuvre demonstrated the forward speed control-mode. It consisted of an acceleration at 15 ft/s^2 to 185 ft/s, a deceleration at -15 ft/s^2 to 85 ft/s and then a final acceleration at 15 ft/s^2 back to 135 ft/s, all using just MYSTK1 as input.

The next manoeuvre demonstrated the pitch pointing control-mode (MYSTK3) and the aircraft was pitched up and down by $\pm 5^{\circ}$ with a cubic ramp time constant of 2 seconds. The third and final manoeuvre demonstrated the flight path angle control-mode (MYSTK2). The pilot demand was $+2 \text{ deg/s}$ flight path rise to 3° followed by a -2 deg/s flight path fall to -3° , pausing at 0° (straight and level flight), before returning once again to straight and level flight. This resulted in the aircraft climbing to 150 ft, holding height and then returning to 100ft.

Once again, each control-mode required only one input from the pilot, cross coupling was negligible and all manoeuvres were executed crisply. Both the forward acceleration and the flight path angle control-modes required some pilot anticipation for accurate speed/flight path achievement, due again to the phase lags inherent in the command integration system.

Only the nozzles saturated here (at A) during a deceleration and this caused no problems, as before. The throttle command was quite oscillatory here (at B) and it produced an oscillatory engine response which is undesirable. However, it should be remembered that all oscillations appear to be at high frequencies due to the long time scale used (80 seconds); this is true for all the manoeuvres featured in this chapter. Another cycle appeared which was most evident on the throttle (at C) and this produced the small cycle on VKD (at D); once again ETADO and QD were the controller reacting against the cycle. The reason for this cycle was that the acceleration to 185 ft/s brought the flight condition close to a very difficult dynamic region which will be described in the next sub-section. The oscillatory nature of the engine occurred most during flight path changes and was probably due to the apparent aircraft dynamics differing from the controller's design condition. This indicated that the controller needs retuning and careful attention to prevent oscillatory modes, or even another scheduling dimension to handle flight path or angle of attack changes.

8.2.3. High Speed Transition - 120 Kts (≈ 200 ft/s)

The aircraft was trimmed for flight at a height of 100ft, pitched up at 8° relative to the earth and flying straight and level. The control trim settings were 61% throttle setting, 57° nozzle angle and $+4.3^\circ$ tailplane angle. The first manoeuvre is shown by Figure (8.4) and it demonstrated the forward acceleration control-mode. It consisted of an acceleration of 10 ft/s^2 followed by a deceleration at 10 ft/s^2 to 160 ft/s and finally an acceleration back to 200 ft/s

¹²⁰
(~~7~~ Kts). The actual manoeuvre was performed well, but inspection of VKD, THETD and QD shows that the pilot would experience an uncomfortable ride!

The large number of very lightly damped oscillations at this flight condition were directly or indirectly caused by the engine non-linearities. Indeed, the gain matrix was scheduled with engine state as well as airspeed as an attempt to alleviate worse problems that had arisen due to the gross dynamic changes that occur within the engine (see Figures (4.8) and (4.9)). Consequently, without this feature the system would either be unstable, or would be using a very low bandwidth controller. However, this feature also brought the problem that fast engine state changes produced fast gain scheduling changes which effectively increased the dynamic order of the system and contravened earlier gain scheduling assumptions (section 7.4).

It was also possible that dynamic modes, other than the three control-modes, were lightly damped and became apparent as oscillations. This can happen when a particular control mode is dominated by a pole on the real axis which allows the gain to be increased further. This gain increase may improve the control-mode dynamics but make another dynamic mode become lightly damped, such as an actuator mode. These trade-offs should be monitored by the control law designer.

Detuning the controller could have reduced these oscillatory effects and a different gain scheduling scheme or more design points near this difficult region could also have helped. However, the GVAM87 engine dynamics were designed for human open-loop operation and are not ideal for closed-loop automatic control. This is an important

observation which should be acknowledged in future ASTOVL aircraft designs whenever a CCV is the desired end product.

No further manoeuvres are shown for the flight condition as they are executed adequately, but have severe oscillations superimposed upon each response and nothing further can be learnt from examining them.

8.2.4 High Speed Flight (Fully Wing-Borne) - 250 Kts

The aircraft was trimmed for flight at 100 ft, pitched up at 0° flying straight and level (ALFAD = 0°). The control trim settings for this were 53% throttle setting 0° nozzle angle (nozzles aft) and 0.4° tailplane angle. The following manoeuvres are shown in Figure (8.5). The first manoeuvre demonstrated the pitch rate control-mode using MYSTK2 which was scaled in radians/s in the figure. The manoeuvre consisted of pitching up at 5 deg/s to 15° , pitching down at -5 deg/s to -15° and then levelling out once again at approximately 0° pitch attitude to fly straight and level. This implemented a climbing manoeuvre and the aircraft rose to over 1000ft before diving and levelling out at about 500ft. Although climbing sharply and increasing its potential energy the aircraft did not lose any kinetic energy and the speed remained almost constant. This was achieved by the controller which increased the engine power to maintain speed automatically. GAMMAD, the flight path angle, shows that $\pm 15^\circ$ flight path angle was achieved and the angle of incidence (ALFAD) lay within $\pm 8^\circ$ throughout.

The second manoeuvre demonstrated the forward acceleration control mode (MYSTK1). The aircraft was accelerated at 10 ft/s^2 to 280 Kts (an increase of over 50 ft/s) and was then decelerated at 10 ft/s^2 to 230 Kts before returning to 250 Kts. This manoeuvre highlighted the problem of "desktop flying" in the high speed version. The speed increase caused the aircraft to climb and the decrease caused it to descend because the pitch rate was held at zero and so the pitch attitude/angle of incidence was not used to control the height. Indeed, the height fell to just 200 ft and a "pitch up" command was given (at A) to prevent a "crash landing".

This manoeuvre also showed some overshoot in the decelerating phase (at B). This was caused by the engine winding down to a low speed for deceleration and then taking a long while to wind back up to a high level to stop the deceleration. This was a demonstration of the effect that non-linearities can have and also a good example of the reason why the controller has a minimum throttle limit that varies with speed. Clearly, a command which sets the engine very low, close to a landing task, could jeopardise the landing if the engine is unable to regain speed and power fast enough. The minimum throttle level prevents this happening at low speeds.

Apart from the above criticisms, each control-mode operated in a crisp way, cross coupling was minimised and control inputs were simple. Control in this region is satisfactory, but not ideal.

These demonstrations have shown how the controller functioned in different areas of the flight envelope and how it generally gave good control with simple inputs, reducing the pilot work load. The exception to this was of course the region around the 120 Kts flight condition which was unsatisfactory. The poor closed loop response, in this region especially, needs further work. Any flying task that passes by this region is degraded by the poor closed-loop response as will be seen in some of the following figures.

8.3 Accelerating Transition to Wing-Borne Flight-Task 1

For this demonstration (shown as Figure (8.6)) the GVAM87 was initialised at 6.9 ft, 0 Kts sitting on the runway. The height (6.9 ft) represents the height of the centre of gravity above the runway and it was slightly higher than the "dead weight" height of 5.5 ft. This was due to the thrust lift which was caused by the throttle being at the low speed flight minimum of 60%. The weight on wheels switch was obviously active making this a landing mode and the aircraft was at rest, though only just, as the engine and reaction controls were active.

The first command was for a vertical take-off and a climb at 10 ft/s^2 (MYSTK2). Whilst the aircraft was climbing a forwards acceleration of 5 ft/s^2 was initiated to begin the transition. As a height of 100ft was approached the climb rate was set to zero (or height hold) (MYSTK2) and the forwards acceleration was increased to 15 ft/s^2 . Also at this time, the controller moved from the low speed transition TTC mode to the high speed transition TTC mode (at A). It can be seen

that the flaps were at 50° (fully out) and the undercarriage was extended also, causing the air brake to be at its middle position (0.4). Throughout this early part of the transition the pitch attitude remained constant at a value set during the controller initialisation. The pilot did not need to adjust the pitch attitude and so MYSTK3 was at zero throughout and is not shown.

As the aircraft accelerated VTKT exceeded 140 Kts (at B) the transition lower speed limit, and soon after this the nozzles went to zero and were fixed aft (at C). At this point the controller moved into the high speed flight (wing-borne) TTC mode. At this moment the height hold auto pilot also became active and began to eliminate the vertical speed residuals shown by VKD (at D). Accelerating with no autopilot would cause the aircraft to climb, but the auto pilot progressively lowered the aircraft's nose (see E), reducing the angle of attack and maintained a constant height of 120 ft. The pitch rate activity (from F onwards) was mainly the autopilot "control action" which the controller implemented through the tailplane.

The next feature to note is the undercarriage being selected up at 200 Kts automatically with no pilot action required (see G); the undercarriage also set the airbrake to be in (see H). The flaps also began to retract to 20° at 200 Kts as they are scheduled linearly with speed up to 300 Kts (see I). The last pilot action (excluding the autopilot) was to remove the acceleration command as VTKT approached 300 Kts. The speed overshoot and then undershoot as the engine was slow to respond (see J) and the undershoot caused the flaps to extend and retract slightly (see K).

The take off TTC mode to low speed transition TTC mode blend was undetectable, as was the low speed transition to high speed transition blend. The high speed transition to high speed flight blend was a little "bumpy" due to the need to sense the nozzles aft condition so close to the difficult 120 Kts region. However, the 120 Kts region did not have a large effect in this manoeuvre as it was passed through quite quickly. The throttle showed a few oscillations though (at L) which produced the VKD oscillations (near D).

This manoeuvre was executed easily and with the minimum of pilot input. A human pilot alone could not have performed the same manoeuvre as all three actuators were moved in harmony until wing-borne flight was reached. The use of only two pilot inputs rather than three has clearly led to a reduction in pilot workload.

8.4 Low Speed Manoeuvring - Task 2

For this demonstration (shown as Figure (8.7)) the GVAM87 was again initialised at 6.9 ft, 0 Kts sitting on the runway. The first command was for a forwards acceleration, along the runway, at 10 ft/s^2 (MYSTK1). Then at 50 Kts ($\approx 80 \text{ ft/s}$) a flight path increase command of 2 deg s was given (MYSTK2) and a standard short take-off was executed. During the acceleration along the runway the controller was changed from the low speed transition TTC mode to the high speed transition TTC mode automatically, the landing mode also being active in both cases. As VTKT approached 60 Kts ($\approx 100 \text{ ft/s}$) the forwards acceleration was set to zero and a steady 60 Kts was maintained whilst climbing.

As a flight path angle of 6° was reached (corresponding to -10 ft/s at this speed) the flight path increase command was set to zero (MYSTK2) and that flight path was maintained. As the height of 100 ft was approached the flight path was reduced to zero (using MYSTK2) before being reduced further to 6° to make a landing approach. As the height dropped below 50 ft the downwards flight path was levelled out so that at 12 ft the aircraft was once again flying straight and level at 60 Kts.

Finally, the flight path was inclined down at -1° for the final landing phase and a deceleration of 10 ft/s^2 was also commanded. This resulted in a Rolling Vertical Landing (RVL) which is a common feature of V/STOL operations. The actual point of landing is marked on the VKD and H plots (by A) and the sharp VKD gradient change shows it clearly. The aircraft actually lands at approximately 50 Kts before slowing down to 12 Kts (20 ft/s) which was maintained as if taxiing on the runway.

The two blends to and from low speed transition flight occurred on the ground in this manoeuvre and are not detectable. The nozzle was saturated during the final deceleration (at B) but this did not affect performance. Clearly, this low speed flying task has been executed easily and with the minimum of pilot input. The usually complex manoeuvres of short take off, climb, height hold and RVL were all performed using keyboard inputs only. Once again the pitch attitude did not need to be controlled by the pilot at all and MYSTK3 was zero throughout the task. This task also shows that pilot workload has been reduced.

8.5 Decelerating Transition from Wing-Borne Flight - Task 3

For this demonstration (shown as Figure (8.8)) the GVAM87 was initialised at 300ft, 308 Kts (520 ft/s) and 1.1° pitch attitude flying straight and level with the undercarriage up, the airbrake in and the flaps at 20° . The autopilot was engaged to maintain height through the wing-borne phase of the deceleration. The first command was for a deceleration of -10 ft/s forward speed (MYSTK1) and to help the aircraft to slow down, the air brake was also deployed by the "pilot". As the airspeed fell below 300 Kts the flaps began to move out to 50° , scheduled by speed (sec A). As 200 Kts was reached the flaps had reached 50° and here the undercarriage was automatically selected down (at B) which also selected the airbrake to be at the middle position (at C). Whilst the aircraft was slowing down the autopilot was bringing the nose of the aircraft up, increasing the angle of incidence (and hence the lift) to maintain the height.

It should be noted that the throttle minimum level was increasing (at D) as the speed decreased and this reduced the deceleration rate. In fact the situation can arise whereby the aircraft will not cross into the high speed transition TTC mode as the speed cannot fall below 140 Kts and the angle of incidence will not rise above 14° . This showed one flaw in the boundary condition logic which has been fixed for this particular case by resetting the transition speed limit from 140 Kts to 180 Kts. Hence at 180 Kts (see E) the controller changed to the highspeed transition TTC mode and soon after this the nozzles came forwards (see F).

After crossing the TTC mode boundary the large deceleration command received no response from the aircraft initially and it grew, eventually forcing the nozzles fully forwards and increasing the thrust. This violent control action set up several severe oscillations on VKD, THETD, QD, PTHTPD, THDFPD and ETADO (labelled by F). If left alone these oscillations would have continued for some time aided by the oscillatory dynamics in the 120 Kts region. Clearly the high speed to high speed transition boundary logic and boundary management was unsatisfactory. There is a need for an earlier nozzles forward maximum deceleration mode and a clearer definition of this boundary.

Despite these problems the flying task was continued and the oscillations were "flown through". To do this a descend command was given using MYSTK2 as seen on the VKD plot (at G). The command was for a -2 deg s flight path reduction reaching -7° . Soon after this the speed deceleration was reduced from -10 ft/s^2 to -5 ft/s^2 (at H). As the speed then fell below 60 ft/s (at I) the TTC mode changed to become the low speed transition TTC mode and the carefree handling feature reduced the downwards flight path (from J) to zero. Thus the aircraft began flying straight and level at 50 ft (see K). Meanwhile the deceleration command was set to zero as the speed reached 0 Kts , the hover. Finally, MYSTK2 was used to demand a descent rate of -4 ft/s which landed the aircraft vertically.

This manoeuvre has shown the controller to be capable of a decelerating transition and a vertical landing. Clearly, the high speed to high speed transition TTC mode change needs further development as described previously. However, despite this drawback the controller has still only required two inputs to perform the

flying task and this indicates a reduction in pilot workload.

8.6 Decelerating Transition from the Jet-Borne Flight - Task 4

This demonstration (shown as Figure 8.9) shows a deceleration from 120 Kts and an RVL. It represents some aspects of the previous flight task but shows them more clearly. The GVAM87 was initialised at 300 ft, 200 ft/s (\approx 120 Kts) and pitched up at 8° flying straight and level. The first command was a decrease in flight path angle at -2 deg/s (MYSTK2) to -3° (corresponding to 11 ft/s VKD). Whilst the flight path was being lowered the command to decelerate at -10 ft/s² was given (MYSTK1). As the speed passed through 60 ft/s (see A) the carefree handling feature reduced the rate of decent to zero (see B), levelling off the aircraft at 90 ft (see C).

The deceleration command was maintained even as the speed passed zero and the aircraft began to fly backwards. Another carefree handling feature prevented the backwards speed exceeding -20 ft/s with no further pilot input. Then a brief acceleration command was given (MYSTK1) to put the aircraft back into the hover. Finally, a descent rate of 10 ft/s was commanded (MYSTK2) until the height reached 45 ft whereupon the descent rate was reduced to 5 ft/s until the height reached 15 ft where the descent rate was again reduced to 2 ft/s. The sharp gradient change on the VKD plot (at D) shows that the landing occurred at 3 ft/s.

The aircraft experienced some oscillations (at E) close to the oscillatory 120 Kts region which has been explained before. Another

feature to note is that the throttle and nozzle saturated (at F and G respectively) during the levelling off carefree handling manoeuvre. Once again, this caused no problems due to the anti-wind-up protection in the controller.

This manoeuvre has shown more clearly the low speed phase of a decelerating transition and vertical landing. All the pilot commands were simple and only two inputs were required; MYSTK3 controlling pitch attitude was not used at all. Once more, a reduction in pilot workload has been demonstrated.

8.7 Demonstration of Integrator Wind-Up Protection

For this demonstration (shown as Figure (8.10)) the GVAM87 was initialised at 100 ft, 200 ft/s (\approx 120 Kts) pitched up at 8° flying straight and level. In order to saturate both the throttle and the nozzle two large simultaneous commands were given for a flight path increase at 5 deg/s and a deceleration at -20 ft/s^2 (see MYSTK2 and MYSTK1 respectively). Both commands were removed at the same time in order to give a forward speed of approximately 100 ft/s and a flight path angle of approximately 15° . This manoeuvre was performed twice, identically, with the integrator wind-up protection on and then off. Curves labelled "1" have integrator wind-up protection whilst curves labelled "0" do not have integrator wind-up protection.

It can be seen from the plots for throttle and nozzle that both became unsaturated at A with wind-up protection whilst they do not become unsaturated until B without wind up protection. The result of these actuators being saturated longer, and the integrators being

allowed to wind-up, can be seen in plots of VKN, VKD, ALFAD and GAMMAD. In each case the system without wind-up protection overshoots. The effect of throttle saturation can also be observed in the FNP, HNP and QEF plots.

The final feature to note is that THETD tracking 8° was maintained as the pitch integrator was not frozen because the tailplane was not saturated. Maintaining pitch attitude tracking is vital as it can completely destabilise a saturated system if it is allowed to wander. This demonstration clearly shows the effectiveness of the integrator wind up protection.

8.8 Demonstration of Disturbance Rejection

The characteristic of the controller which is demonstrated here is the ability to reject unmeasured disturbances. These disturbances will be provided using wind gusts and turbulence which have been described in section 4.8. The tests are described in separate subsections below.

8.8.1. Wind Gust Disturbance Rejection

For this demonstration the aircraft is initialised at 100 ft, 135 ft/s (≈ 80 Kts) at a pitch attitude of 8° flying straight and level. The wind gust test used here consists of 60 ft/s 1 - cosine type gusts in the longitudinal plane, each lasting 4 seconds. The first gust was a horizontal tailwind heading north like the aircraft, the second gust was a horizontal headwind heading south against the

aircraft, the third gust was a vertical updraft and the fourth gust was a vertical downdraft.

These gusts are shown by VWN and VWD in Figure (8.11). In this figure the scales have been greatly magnified to show the deviations from trim of each parameter because the deviations were small, despite the size of the gusts. It was not possible to compare these to the response of the uncontrolled aircraft as the uncontrolled aircraft goes completely unstable due to large pitch deviations. However, it is possible to see each of the three actuators moving in harmony to keep the aircraft steady in pitch and the maintain speed and flight path. Only the vertical down draft gust actually saturated any actuators (the engine) but this did not have any serious effect; it simply produced a larger deviation in vertical speed (at A). The amount of actuator movement shows the level of disturbance that is being counteracted.

Despite the serious nature of these "once in a lifetime" type gusts, the aircraft deviated very little from its chosen flight path as each plot shows. Furthermore, this was achieved with no pilot input whatsoever. Clearly, this is an example of reduced pilot workload.

8.8.2 Turbulent Air Disturbance Rejection

For this demonstration the aircraft was initialised at the same flight condition as that used in the previous subsection. As described in section 4.8, the levels of turbulence in each of three perpendicular directions can be varied by changing the three RMS levels. For this test the forward and vertical turbulence is used

together (USIG and WSIG respectively) at three different RMS levels as follows: 3.0 (moderate turbulence), 6.0 (moderate to high turbulence) and 9.0 (high turbulence). The response to turbulence is shown in Figure (8.12) and the turbulence is switched on in three different sections, one for each RMS level.

Hence from A to B, $USIG = WSIG - 3.0$,

from B to C, $USIG = WSIG - 6.0$ and

from C to D, $USIG = WSIG - 9.0$

From the figure it is clear that the higher turbulence levels cause greater fluctuations in the flight variables, but these fluctuations are very small and the controller still maintains the original trim settings. Once again, it is not possible to compare these to the response of an uncontrolled aircraft as the uncontrolled aircraft goes unstable. The cost involved here is clearly that increased turbulence levels exert quite high frequency inputs on each actuator which would reduce actuator life, especially for the engine.

The amount of turbulence that the pilot actually experiences would be a direct measure of pilot ride comfort and this could be balanced against the cost of preventing it (actuator life, control power etc) and the likelihood of high turbulence levels being encountered. This particular balance is obviously beyond the scope of this study but the controller could clearly be used for turbulence rejection and related studies.

If the actuator signal high frequency content caused concern then the relevant signals could be filtered to remove this, allowing the controller to concentrate upon maintaining the altitude, speed and flight path against larger, slower disturbances. Finally, it is interesting to note that after each phase of turbulence, causing high frequency actuator movements, the turbulence was set to zero and the actuator movements returned to their trim settings. This shows that the controller can recover from turbulent disturbances and settle back into controlled steady flight after high frequency excitation.

The turbulence was rejected by the control system automatically, even when the turbulence was at a high level. This was performed with no pilot inputs once again, showing a decrease in pilot workload.

In each of the preceding tests the gusts or turbulent disturbances were not measured or known in advance by the controller. And yet in each case the controller rejected these disturbances and maintained steady controlled flight. This shows the benefits of using an error actuated multivariable PI controller to reduce pilot workload. Another example of this disturbance rejection has been given by Figure (8.6) and Figure (8.8) where disturbances caused by the deployment of flap and airbrake do not prevent the aircraft from tracking the pilot commands. Once again, no compensatory pilot input was needed.

8.9 Automatic Ship Landing Systems - A Demonstration of the possibilities

Once an aircraft has been fitted with a control system other ways of reducing the pilot workload become possible. Indeed, some piloting tasks which were previously impossible may now become feasible. One such task is landing V/STOL aircraft on ships in rough seas and in poor visibility.

A very simple autopilot has already been demonstrated in previous high speed flight phases. A similar autopilot could easily be made to follow a flight path other than horizontal. This would make it possible to fly a ship approach in bad weather by tracking along a guidance beam automatically, for example. This could include curved decelerating approaches (such as those used in a separate study [Merrick & Gerdes]).

However, once the aircraft has located the ship other problems can arise. To track a moving ship requires precise speed control and good disturbance rejection. This is because gusts and turbulence are to be expected, both because of the weather generally and also because of wind being disturbed by the forward motion of the ship and its irregular superstructure. This could be achieved by the controller used in this study as its accurate tracking and disturbance rejection has already been proven. The final problem with ship landing is the deck movement which could lead to the undercarriage rates being exceeded in high sea states.

Such problems have been investigated elsewhere [Bodson and Athans, McMuldloch et al] and from one of these references an approximate ship model has been obtained [Bodson and Athans]. Deck movement depends upon wave height, wave frequency, ship speed, ship heading, ship size and deck position. For a particular ship model in sea state 5 (quite rough weather) the ship deck moves approximately ± 4 ft vertically at a frequency of 0.114 Hz. (The ship model was a stochastic process whose power spectrum was a narrow band, usually single peaked, spectrum concentrated around 0.2 - 2.0 rad/s; the model frequency was 0.72 rad/s). The deck also moves in five other degrees of freedom but only heave is used here.

For this final demonstration, the controller is made to track a moving deck vertically whilst flying horizontally at 20 Kts (≈ 34 ft/s) pitched up at 8° beginning at a height of 60 ft. The deck moves sinusoidally at 0.114 Hz and the amplitude of this sinusoid is increased until the aircraft can no longer track it accurately. This was achieved by feeding a sinusoid into MYSTK2 as shown on Figure (8.12). This figure shows the maximum amplitude that the controller can accurately track at this frequency. A higher amplitude would result in the throttle saturating which would clip each peak on the throttle response. This in turn would result in the aircraft having a nett downwards flight path with the sinusoid superimposed on top.

The maximum achievable vertical speed command amplitude at 0.114 Hz was ± 4 ft/s resulting in a height variation of ± 5.9 ft (the actual height response was 53.64 ± 5.885 ft). This was actually a greater height variation than that needed by the above reference in sea state 5 (± 4 ft) indicating that this aircraft plus controller is capable of landing on the ship modelled in the above reference. It

should also be noticed that whilst performing this demanding manoeuvre the forward speed remained steady at 20 Kts and the pitch attitude deviated very little from 8° .

With this particular manoeuvre it was also possible to vary the deck amplitude and frequency to investigate the key relationships. The throttle margin is crucial in determining the control power available and it can be shown that lower frequency sinusoids may be tracked with larger amplitudes, and vice versa. Clearly, such studies could be used to indicate the suitability of particular ships to particular V/STOL aircraft in certain sea states.

Whilst this demonstration has been quite simplistic, it has shown the potential and possibilities that this controller has for further reductions in pilot workload. Indeed, once a satisfactory wide envelope controller has been developed for a CCV aircraft it can be attached to the navigation and guidance systems giving a fully integrated aircraft system which is capable of all the above tasks as well as three-dimensional terrain following, obstacle avoidance and automatic route plan following.

8.10 Handling Qualities of the Controller

It has already been suggested that the handling qualities can only really be examined using a piloted real-time flight simulation (Section 8.1) and that this is the subject of a separate report [Hopper]. Despite this it is possible to discuss some aspects of the handling qualities as they have been demonstrated in previous sections.

The handling qualities listed in subsection 6.3.2. were applied, to a degree, at each flight condition. However, the large number of flight conditions and the complexity of the different trade-offs involved made it impossible to seek an "optimal" solution manually. The main criteria applied were R5, R3, and bandwidth/overshoot criteria in both the frequency and the time domains. The considerations C1, C2 and C3 were applied throughout. The requirements R1, R2, R4 and R6 have proven useful and applicable to this problem and the high-gain method but the large number of flight cases precluded their use for the main wide-envelope controller.

However, the following observations can be made regarding handling qualities from the simulations that have been performed. General control is crisp and non-interactive making flying tasks easy to perform. Standard realistic manoeuvres were flown including vertical take-off and landing, short take-off, RVL's, accelerating and decelerating transitions. There are some problems however, notably: oscillations when climbing or descending at some speeds, some very lightly damped marginally stable dynamic modes near 120 Kts and a bad TTC boundary cross over from high speed to high speed transition flight.

Further observations concern the control scheme. The way in which forward acceleration or flight path changes were implemented required the pilot to anticipate the aircraft response. This was due to the large phase lags inherent in the integrators and filters that were used. Other schemes should therefore be considered, such as direct acceleration control. In addition to this, the provision of a maximum deceleration manoeuvre in the high speed flight phase is desirable as

this would bring the nozzles down to achieve a higher deceleration rate. It would also solve some of the boundary crossing problems that occur in a decelerating transition.

The simulations performed do not make it possible to make specific observations regarding the control input scaling, the speed of response or the general handling. Only a trained test pilot could currently assess these things (in real-time) until handling qualities metrics are improved. This also applies to the suitability of the TTC modes that were chosen; although the author found them easy to use, a test pilot can have other ideas (see [Hopper]).

In conclusion, it should be noted that the author could not fly the basic GVAM87 in a real-time flight simulation using joysticks as control inputs; and yet the author can fly the GVAM87-plus-controller using only keyboard inputs, which is far more difficult than real-time joystick control. This indicates that handling qualities have definitely been improved and that pilot workload has been reduced.

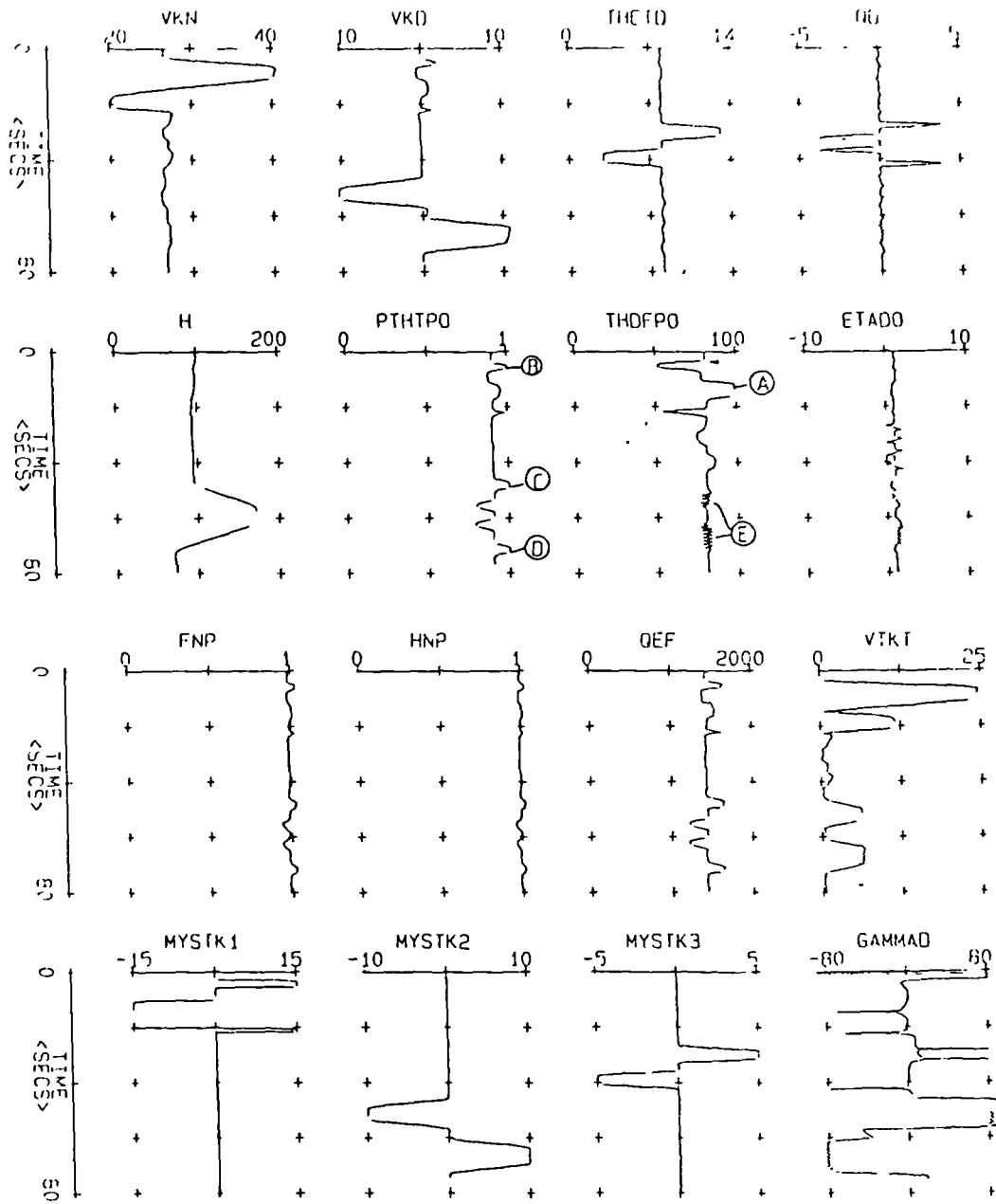


Figure (8.2) Basic Manoeuvre at the Hover

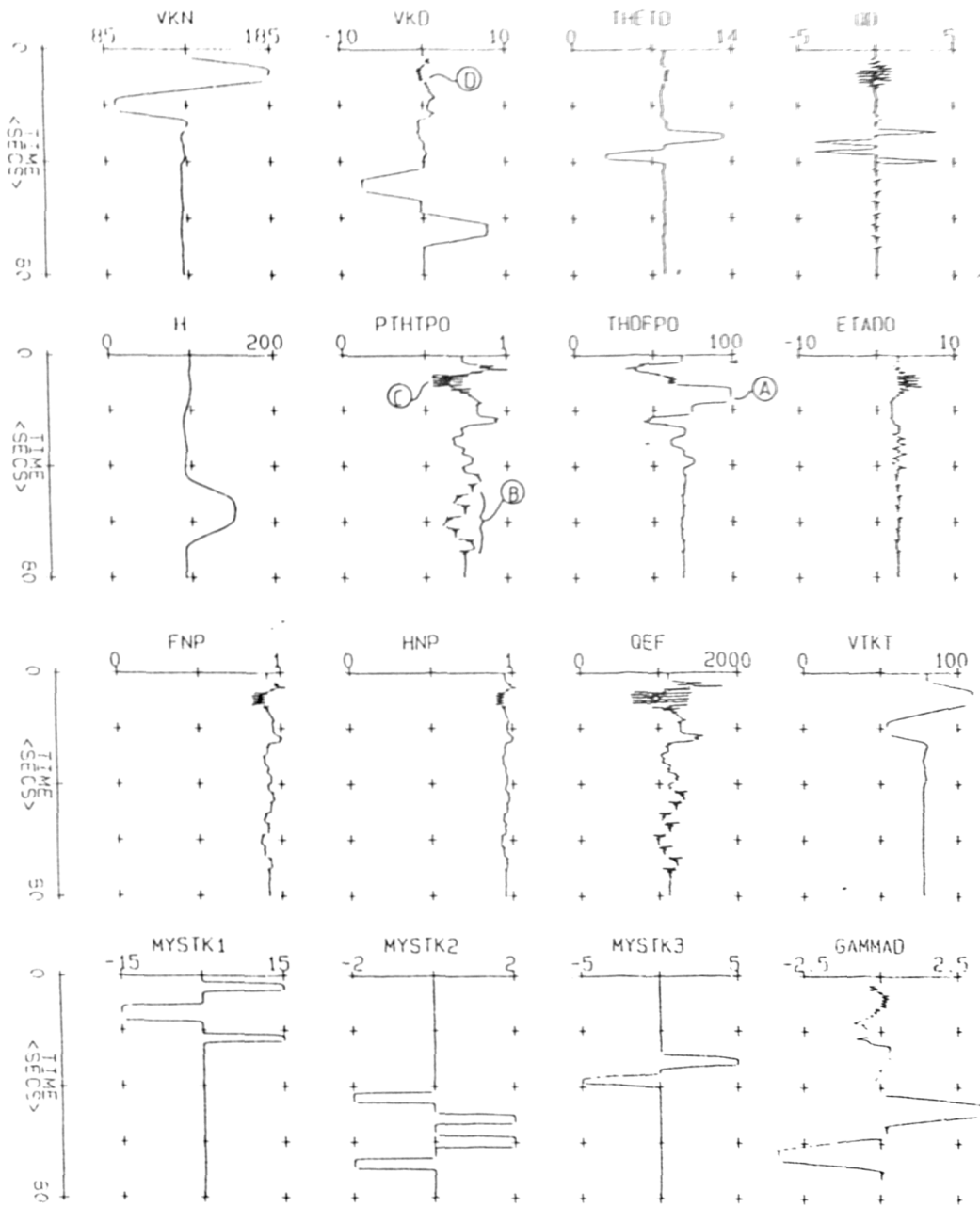


Figure (8.3) Basic Manoeuvres at 80 Kts

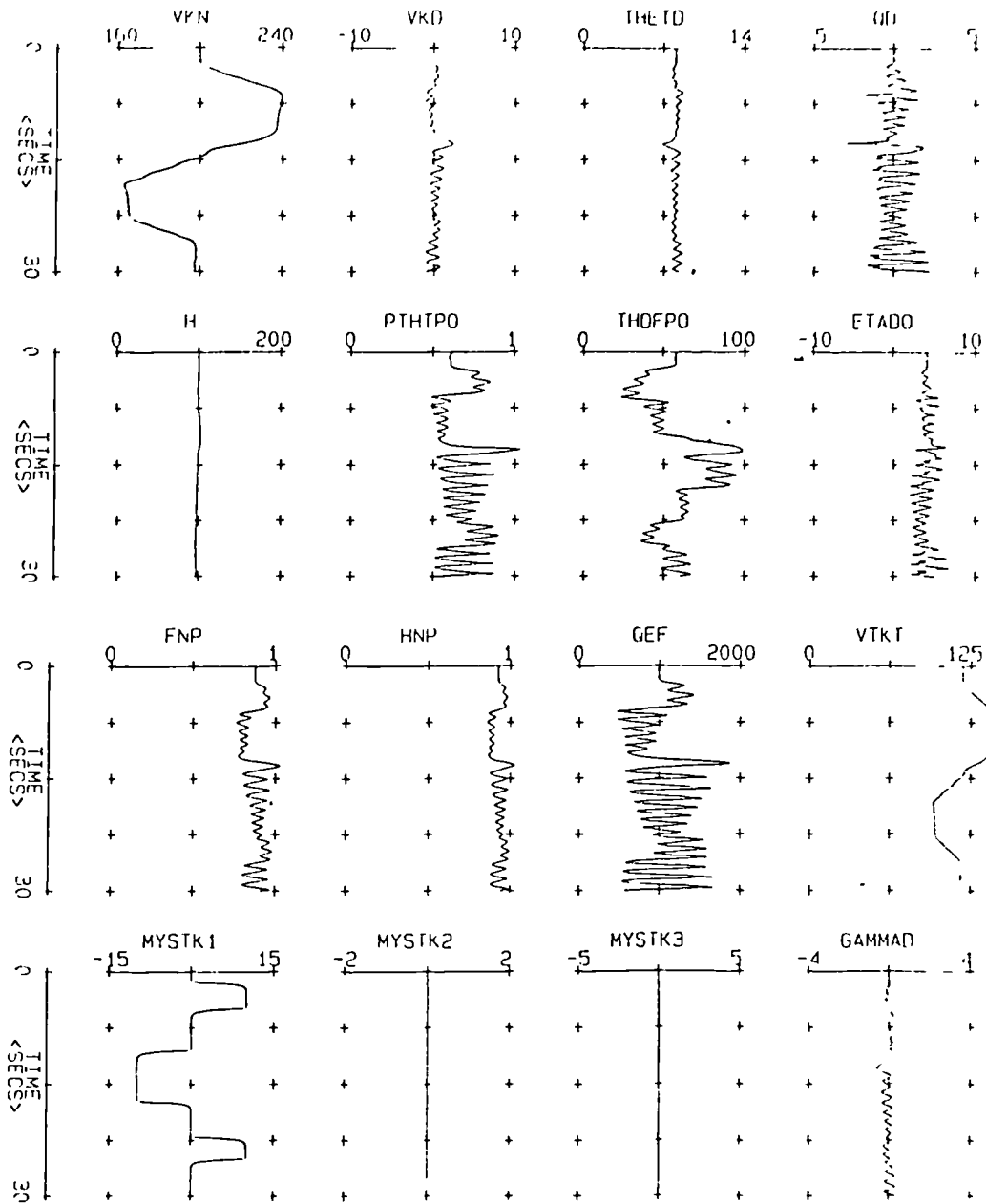


Figure (8.4) Basic Manoeuvre at 120 Kts

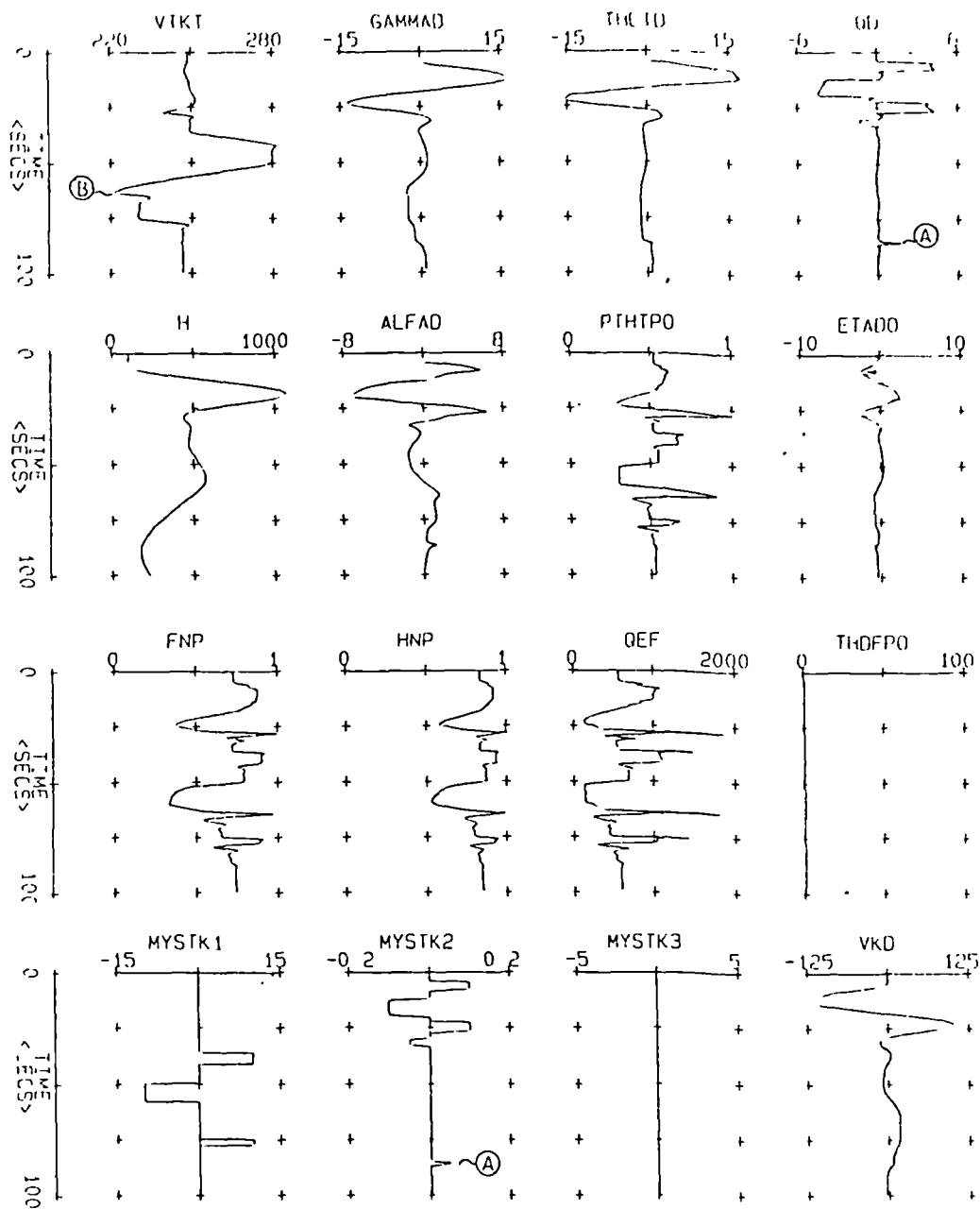


Figure (8.5) Basic Manoeuvres at 250 Kts

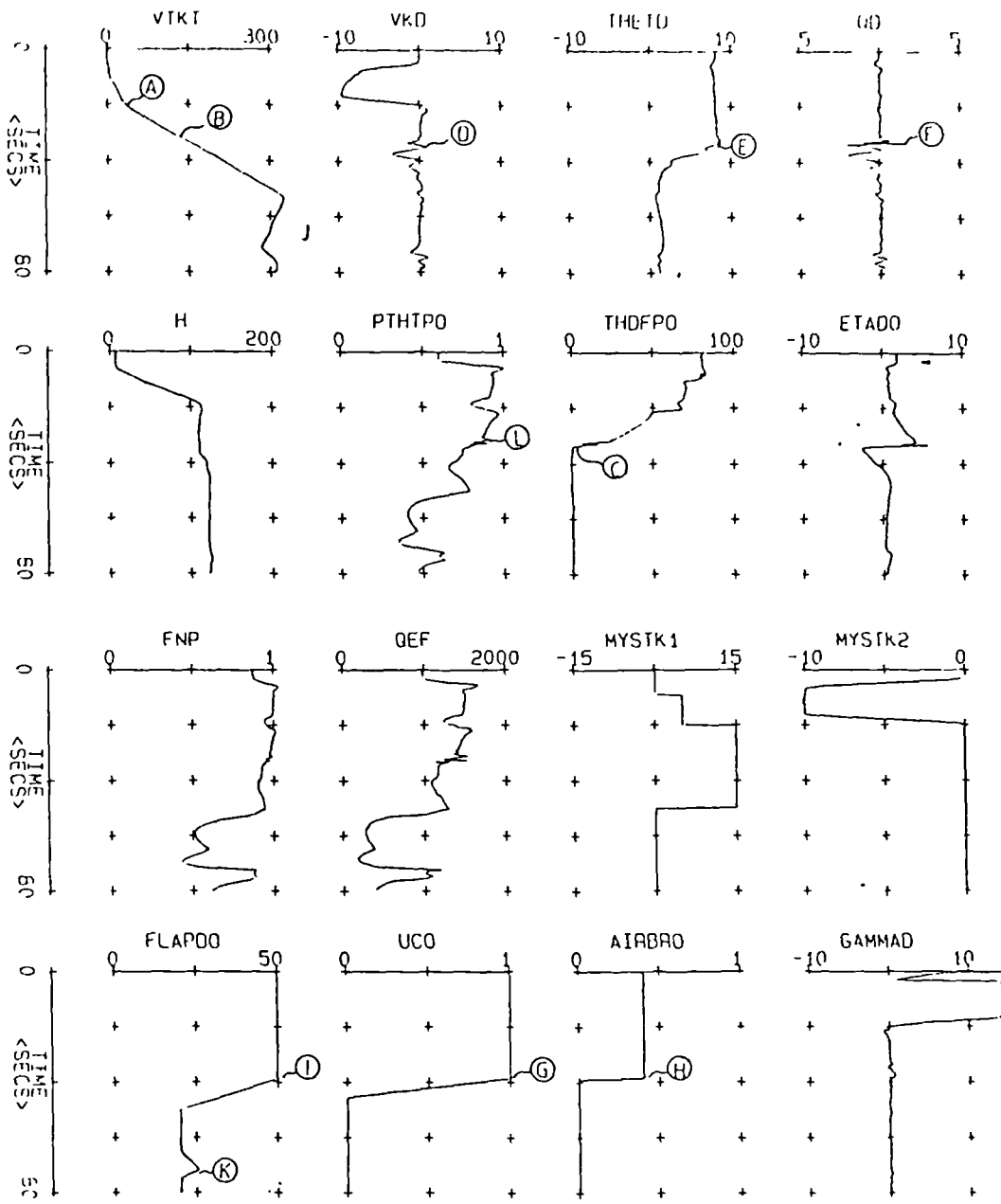


Figure (8.6) Task 1 - Forwards Accelerating Transition

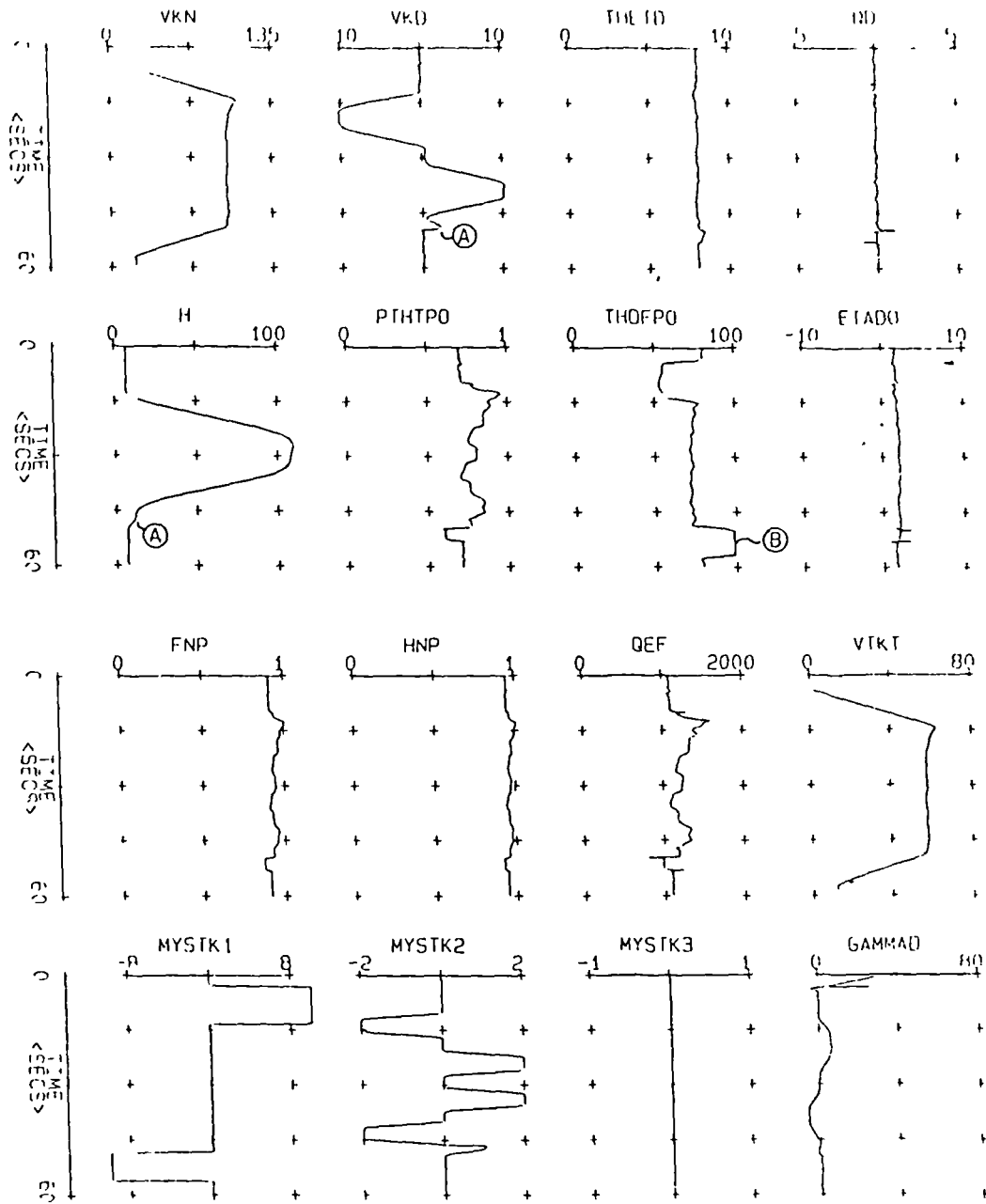


Figure (8.7) Task2- Low Speed Manoeuvres

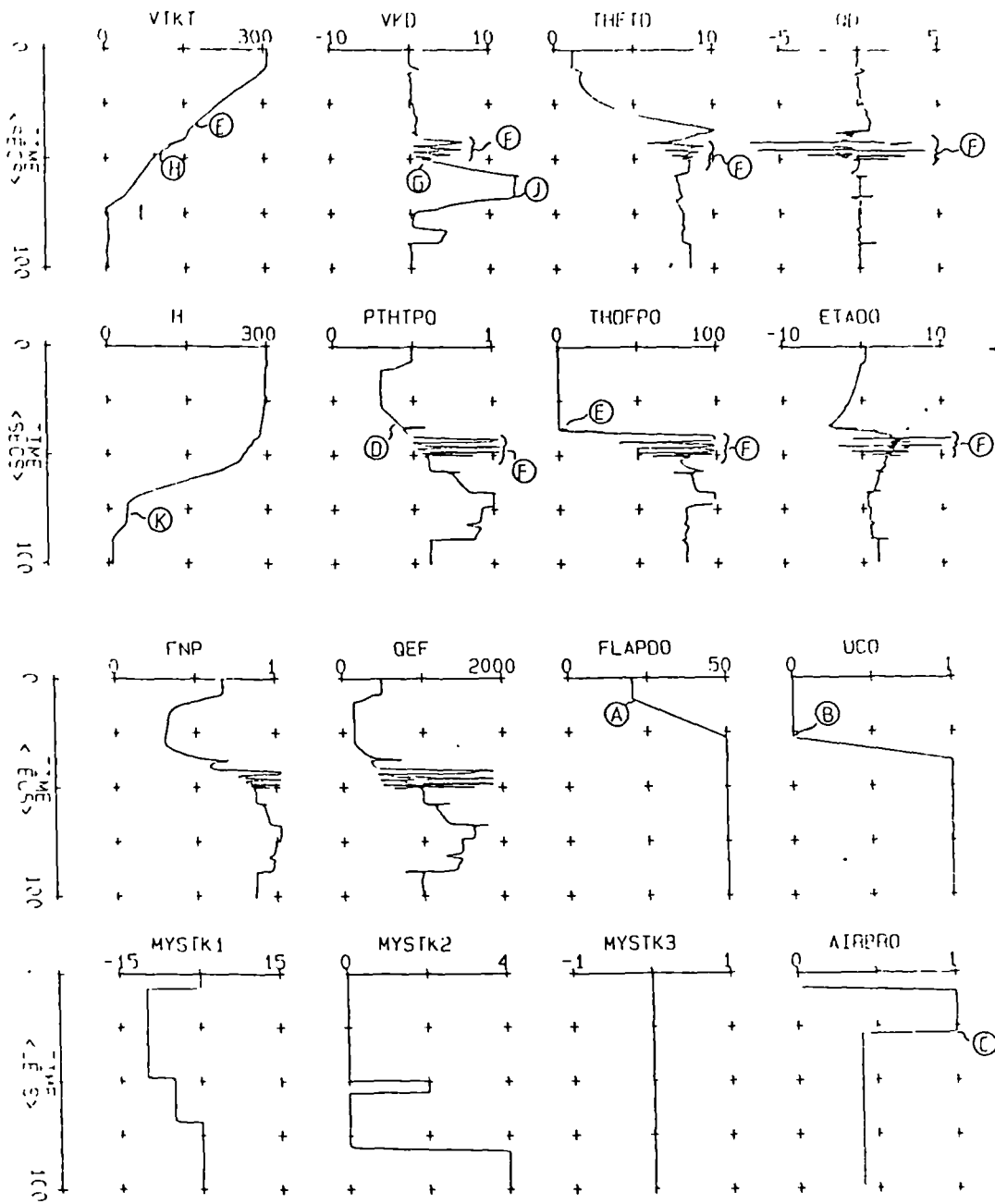


Figure (8.8) Task 3 - Forwards Decelerating Transition

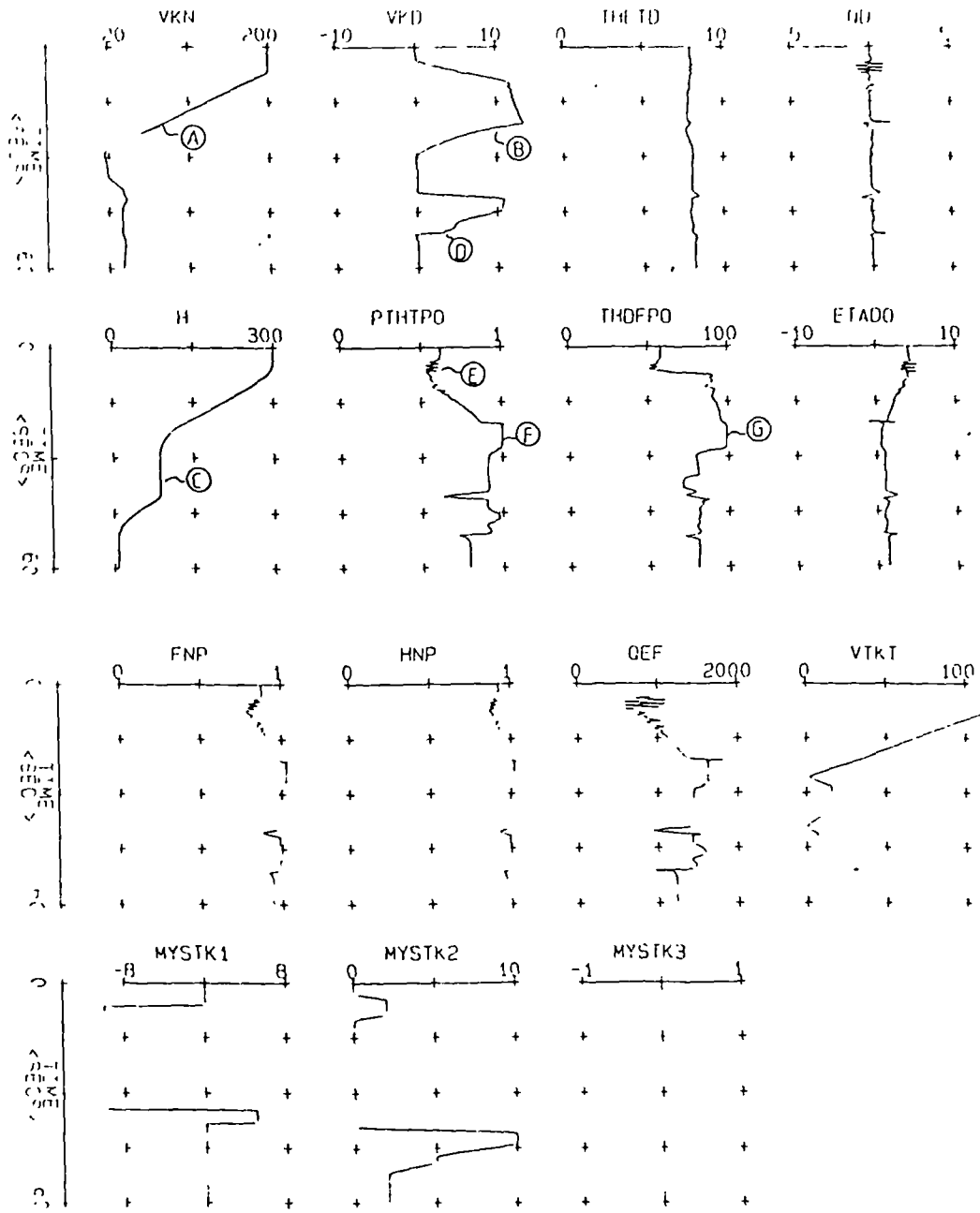


Figure (8.9) Task4- Low Speed End of Transition

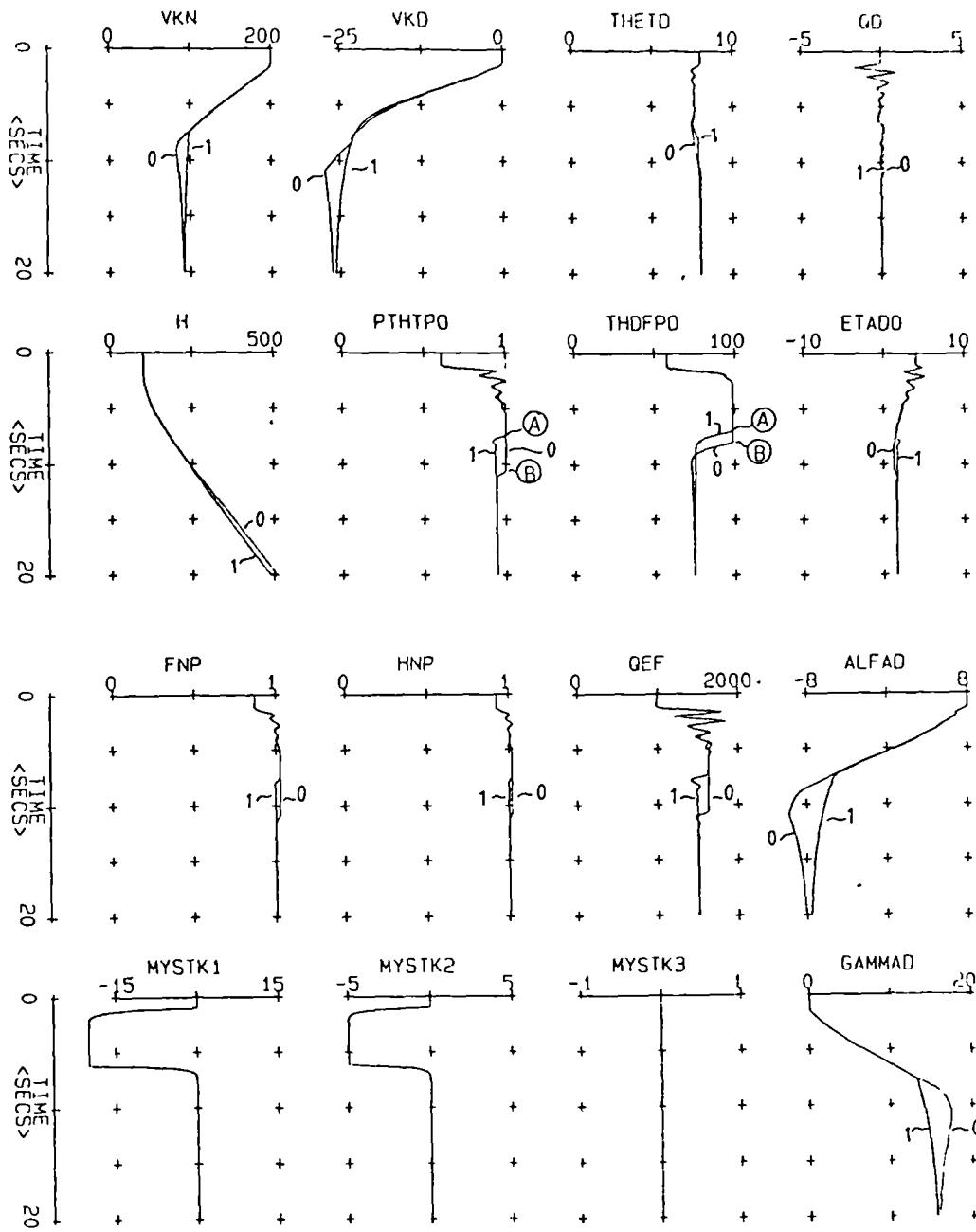


Figure (8.10) Demonstration of Wind-Up Protection

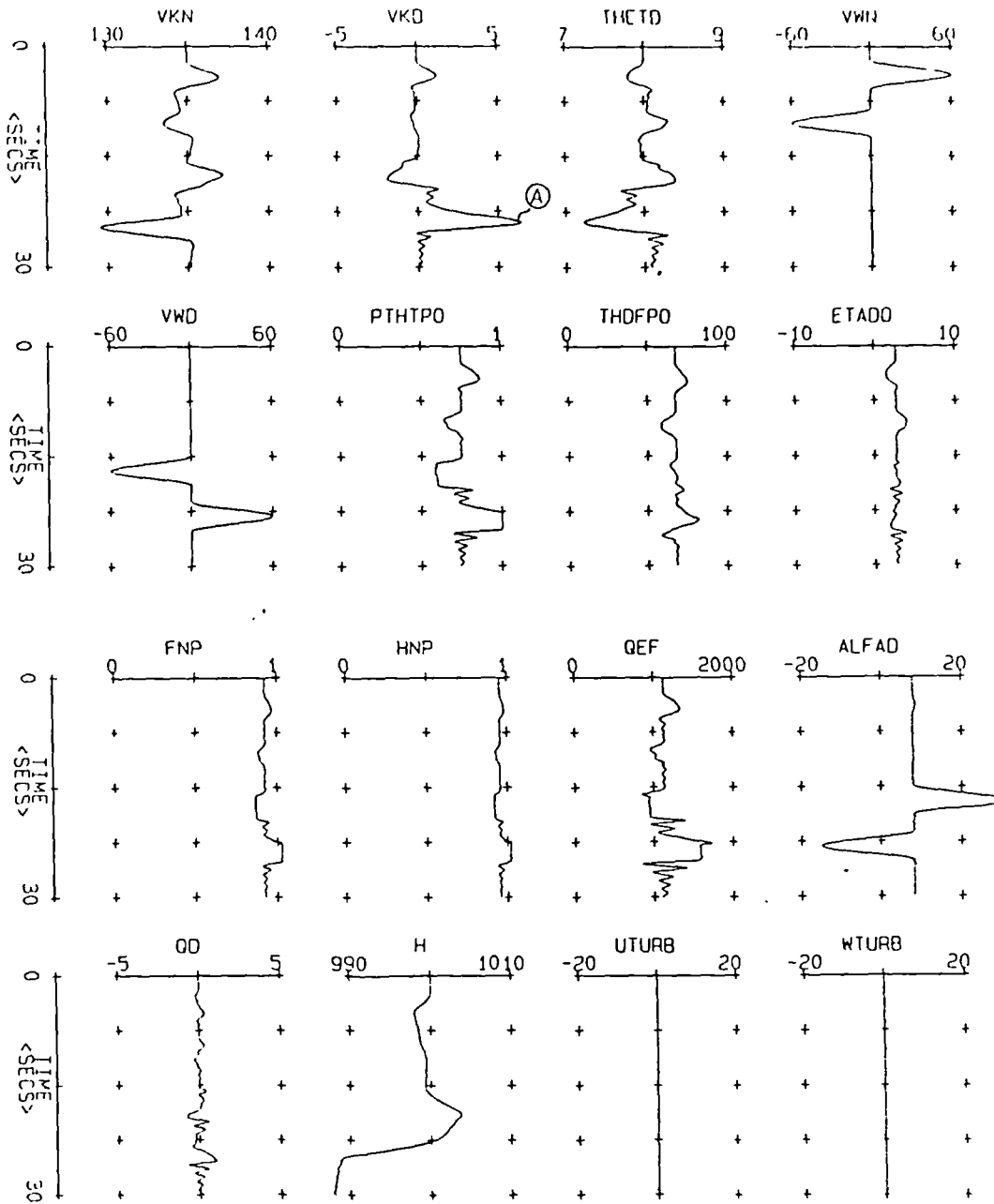


Figure (8.11) Demonstration of Gust Rejection

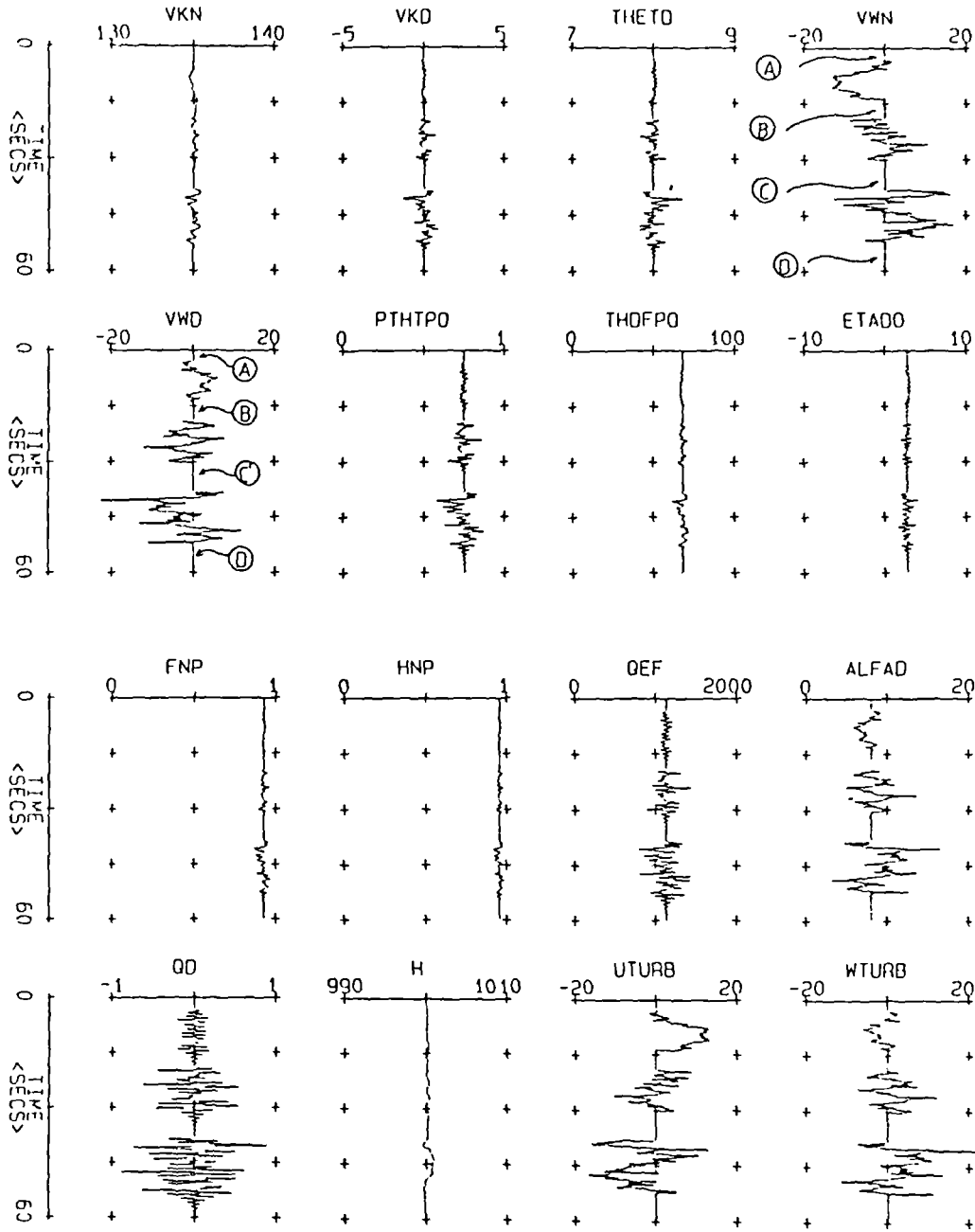


Figure (8.12) Demonstration of Turbulence Rejection

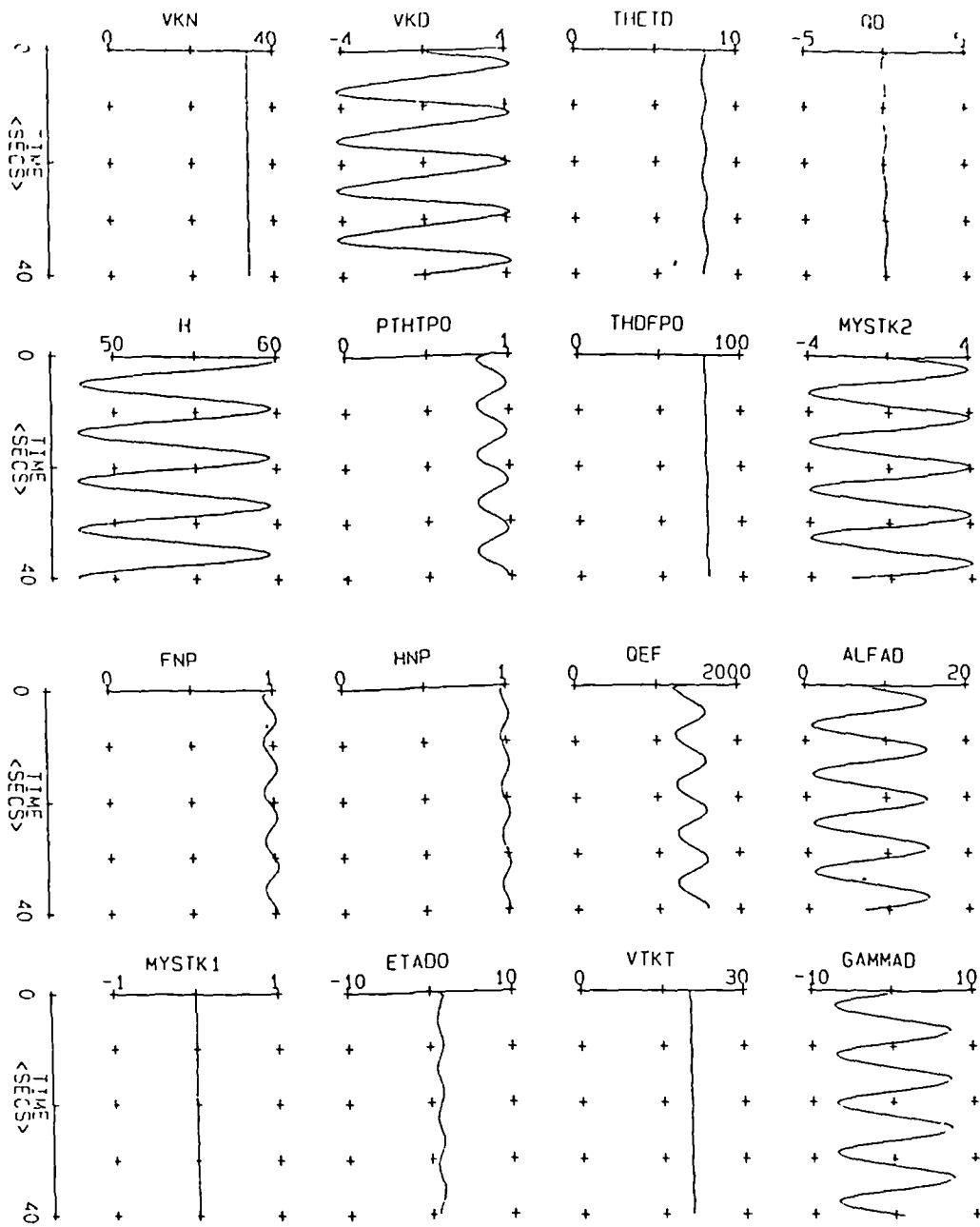


Figure (8.13) Demonstration of Ship Landing Potential

CHAPTER 9

CONCLUSIONS AND RECOMMENDATIONS

CONCLUSIONS AND RECOMMENDATIONS

9.1 Conclusions

There are two main objectives which permeate this report: the development of a controller design method which fulfills the criteria described in previous chapters, and the design of a controller that reduces the pilot workload which is characteristic of V/STOL aircraft. A secondary objective concerns the specification of task tailored control modes and handling qualities criteria for V/STOL aircraft. These three themes are discussed separately below.

9.1.1 Development of a Suitable Controller Design Method

The inadequacy of current controller design techniques was described in general terms before the most relevant classical and modern techniques were discussed in detail. This survey discovered many beneficial characteristics among other methods, but also many detrimental characteristics. This resulted in a specification for a suitable controller design method.

The high-gain technique was subsequently chosen as having the basis of a suitable controller design technique and its roots were then traced from its earliest inception to its recent developments. However, the high-gain technique still lacked three essential characteristics:

- (i) It could not be used to "work backwards" enabling it to be used in the fully integrated design of a CCV aircraft.
- (ii) Slow, high order and dynamically complex parasitics could not be incorporated into the design.
- (iii) It did not completely encapsulate the simplicity and insight that classical SISO techniques give to a designer.

Despite these drawbacks the high-gain technique does simplify multivariable dynamic systems by exposing the underlying dynamic structure. This property has been combined here with results drawn from fundamental research concerning multivariable root-loci. Together these have resulted in new developments to the high-gain technique which overcome the above drawbacks. The whole has been presented as a step-by-step method termed the high-gain method. This high-gain method has been used throughout this project and the following observations may be made concerning its characteristics.

The high-gain method is a graphically based method which allows it to be fully iterative with the designer. It uses time response, frequency response and root-locus plots to analyse systems, enabling users, to apply skills based upon SISO classical design experience and to receive similar insights into system behaviour. Even so, this method is not based upon any particular CAD package, requiring extensive hands-on experience, and so it allows the designer to apply the method using familiar software tools.

The design complexity is built up in stages as the designer gains knowledge of the system. In this way engineering trade-offs and "weak links" in the design are made apparent allowing the designer to make informed decisions concerning the progress of the solution. Even slow, high order, dynamically complex parasitics can now be incorporated into the design. Furthermore, phase compensation may be added, where necessary, using simple classical SISO techniques. These same new developments also allow the designer to "work backwards" and to specify hardware requirements, given specific performance criteria.

The end result is a robust multivariable PI controller which tracks constant inputs and rejects unmeasured disturbances using only measurable outputs for feedback. Moreover, the simple controller structure is ideally suited to use at different flight conditions and with gain scheduling. Freedom in the choice of the control variables allows task tailored control modes to be implemented and there is also considerable freedom in the selection and application of handling qualities criteria. For example, root-loci, frequency and time responses are all utilised in the design. These freedoms are facilitated by the simple tuning parameters which have real meaning and known effects on the design

Finally, it should be remembered that the "high-gain" controller has a "fast-sampling" discrete-time equivalent which makes conversion to digital control a simple process. Indeed, discrete-time controllers compensating for one or more sample periods delay are possible and they have been proven in reality elsewhere.

The conclusion is that the high gain method satisfied the specification for a suitable control law design method. It was not enough, however, that it satisfied this specification, it also had to be shown to be applicable to real problems and that it really can produce practical and functional multivariable controllers. This aspect of the conclusions is concerned with the second main objective which is discussed next.

9.1.2 Design of an Active Flight Controller for a V/STOL Aircraft

The need for active flight control to alleviate pilot workload in V/STOL aircraft was described at the start of this report when it was also suggested that a suitable design method did not currently exist. A brief description of the Royal Aerospace Establishment's VAAC Programme put this problem into its wider perspective. As a small part of the VAAC Programme this project has sought to develop and assess one particular method. The medium for this has been a lifelike non-linear Generic V/STOL Aircraft Model (GVAM87). Consequently, the design of a realistic controller for the GVAM87 is both a way of assessing the high gain method, and a worthwhile goal in itself.

Before the controller was presented the GVAM87 was described in detail to emphasise the reality of the task and also to highlight certain features that later caused dynamic problems. A controller design specification was then defined and this ensured that the final solution would undergo a realistic assessment. The actual controller design was then presented and its function was described. This was followed by a series of flight simulations which illustrated various good and bad features of the final controller design. From this,

several observations may be made.

The various task tailored control modes, which were defined in the controller design specification, were easily implemented using the high gain method. Moreover, the resulting control laws decoupled the highly coupled aircraft dynamics producing diagonally dominant systems, whatever the control scheme. The simple structure of each control law enabled the different task tailored control modes to be integrated into one controller. This structural simplicity also made gain scheduling a relatively easy process.

Unfortunately, the final controller did exhibit two particular problems, namely, lightly damped modes in some regions of the flight envelope, and no "nozzle forwards" logic during decelerations in wing-borne flight. This last problem also caused difficulties during the boundary cross over from wing-borne into jet-borne flight. However, aside from these two difficulties the controller performed well, fulfilling its design specification and, more importantly, reducing pilot workload. Whether the task was gust and turbulence rejection, a simple manoeuvre at one flight condition, or a complicated series of manoeuvres spanning several flight conditions, the controller gave crisp non-interactive control. The ability to fly the GVAM87 from a keyboard was, in itself, a measure of the "controllability" and the accompanying reduction in pilot workload was always evident.

Although every control mode was essentially an enhanced manoeuvre, the VIFF enhanced manoeuvre, though possible, could not be implemented in the time available. However, other enhanced modes of operation were made possible by the high-gain controller and these

were discussed and demonstrated. These modes of operation concerned automatic landing systems, autopilots, terrain following/avoidance and navigation systems.

The conclusion is that an active controller was designed for a realistic V/STOL aircraft which did alleviate pilot workload during the transition from jet-borne to fully wing-borne flight (and vice versa), and which could provide enhanced manoeuvres in otherwise conventional flight phases. This conclusion, being positive, completes the previous conclusion concerning the applicability of the high-gain method.

9.1.3. The Specification of Task Tailored Control Modes and Handling Qualities for V/STOL Aircraft

Chapter 6 contained a detailed literature survey (though not fully comprehensive) concerning task tailored control and handling qualities for V/STOL aircraft. This simply illustrated the lack of useful information that exists, especially with respect to multivariable systems and transition flight phases. Despite this, the relevant information was discussed and brought together with general principles which should be applied. Finally this mixture of specific criteria and general principles were used to define the design specification used in this project.

The task tailored control modes selected appear to be well suited to V/STOL aircraft in transition flight. However, it has already been noted that only a trained test pilot can really pass judgement on this issue and a subsequent report should be consulted for a further

discussion of this [Hopper]. A similar situation arises with respect to the handling qualities criteria, but the following two points can be made.

Firstly, most current handling qualities criteria were concerned with traditional aircraft dynamic modes which do not exist in highly augmented aircraft. Multivariable systems with task tailored control modes were barely touched upon by conventional criteria and acceptable cross coupling limits were not mentioned at all! Only the emerging bandwidth criteria [Hoh] holds promise for these important considerations. Secondly, no one type of criterion is likely to satisfy every need. A mixture was suggested in the final requirements and this appears to be the best policy. The high-gain method uses information from root-locus plots, frequency responses and time responses and it is usual to change the design a little at each stage. A designer cannot afford to throw away candles when stumbling around in the dark!

In conclusion, it is hoped that the task tailored control modes and handling qualities criteria suggested here will help to clarify the available options for aircraft multivariable control system designers.

N.B. The the most important areas of further research relating to this subsection were given at the end of chapter 6. Hence, this subject matter is not contained in the following recommendations.

9.2 Recommendations

This work has covered many different areas and there are several recommendations to be made. Consequently, these are divided into subject headings and they appear in the subsections below.

9.2.1 The Controller Design Method

Non linear actuator dynamics have been used in this project but their non-linear effects need further investigation. Their effects have been considered previously in conjunction with high-gain systems [Porter^C] but this work does not deal with the practical issues. It can be shown that severe non linearities can produce limit cycles in MIMO systems just as they do in SISO systems. Furthermore, it is believed that extensions to the high-gain method could make it possible to predict such occurrences and could suggest solutions to the problem.

Integrator wind-up and bumpless transfer has been handled here in a simple way that was sufficient for the problem. More complex MIMO systems may not be dealt with so easily. Consequently, a method of dealing with these problems in a truly multivariable way needs to be developed. Indeed, such research is already underway at Lancaster University attempting to apply the work of Hanus [Hanus et al] to high-gain systems.

This is the first implementation of a gain scheduling multivariable high-gain controller and clearly further developments are required.

The gain scheduling scheme chosen sometimes led to fast gain changes which clearly contravenes the quasi static assumption. An investigation into the effects of gain rate-of-change needs to be performed as it is believed that these effects raise the effective order of the system and could produce significant damping and frequency changes.

It has been shown that the tuning parameters possess real meaning and have known effects upon the system enabling knowledgeable tuning to take place. Furthermore, a large variety of design constraints and design objectives may be applied with the "best" solution lying somewhere between. The high-gain method allows the designer to obtain insight into the relevant engineering trade-offs and to approach an "optimal design" but a great deal of work may be involved in finding the "ideal" solution. However, once the above learning stage has taken place, the final tuning of the system could be automated, to a degree, whilst still allowing the designer to guide the optimisation process. Such a method exists in multi-objective optimisation [Grace & Fleming, Fleming & Pashkevich] and it is suggested as the next major stage in developing the high-gain method.

Conventional robustness measures have been used for this project and this is believed to be satisfactory as the final system is diagonally dominant. However, truly multivariable robustness measures are desirable and if a suitable technique is developed it would be a useful addition to the high gain method. Such robustness measures are being developed (for example [Doyle^a, Safonov et al]) but it is believed that this work needs further development before it can be usefully applied to real problems.

Finally, it should be remembered that a large part of the controller was the controller management block which was critical to its performance and yet there was no guidance for its design. Furthermore, any additional task tailored control-modes or carefree handling features would greatly increase the size of this block. Clearly, whatever method is used to design the actual control laws, this block would remain essentially the same. Therefore standard flight safe controller management functions could be designed as a framework into which control laws could slot. Furthermore, the use of artificial intelligence and expert system technology could help to alleviate the complex programming problems.

9.2.2. The Controller Design

The controller code needs to be refined and some further development is needed, as has been described in Chapter 8. In addition to this, the actual controller tuning parameters need to be re-examined at some flight cases to ensure that all lightly damped modes are eliminated. This work is essential if the controller is to progress beyond the recent piloted simulation trial [Hopper]. Other recommendations concerning the detailed development of the controller and the pilot's opinion of the handling qualities and the task tailored control-modes are also contained in the above reference.

9.2.3 The Design Environment

In this project the model was simulated using the package TSIM and another package Pro-Matlab was used for linear analysis. This, together with a programme developed for this project, constituted a simple design, analysis and simulation environment. This was extremely useful in developing the controller but it could be enhanced with the use of a data base to keep track of code changes, model changes and data changes during the development work. Such environments are being developed and one example is ECSTASY [Munro]. However, care should be taken that such environments do not restrict the control engineer but merely provide a helpful management facility.

One strength of the high-gain method is that it is not tied to a particular CAD package. However Pro-Matlab is now widely used by control engineers and would provide an ideal medium for development of a software toolbox for the high gain method. Many of the necessary tools already exist, but it is hoped that a complete toolbox could be produced in the future. This would greatly enhance the design environment and help to disseminate the high-gain method.

9.2.4. Design Trade-Offs

During the course of this project several design trade offs became apparent but two of them are fundamental to the full understanding of the design problem. The first is the trade-off between decoupling purity and speed of response. This has also been observed during the AFTI/F-16 work [Anderson et al] where pilots found that a decoupled response was desirable, but not at the expense of control bandwidth. A very similar trade-off was also exhibited here, speed of response versus quality of response. The impact of these factors on handling qualities criteria needs further study.

The second is the trade-off between performance and robustness. It was shown that more highly tuned (high performance) controllers were less robust to plant parameter changes. This also meant that highly tuned controllers would require more design points through the flight envelope in order to retain that high performance between on-design flight conditions. The balance here is between level of performance and cost of production. This balance could also benefit from further study.

REFERENCES

REFERENCES

AGARD

AGARD
"VSTOL Handling Qualities Criteria:
Part 1 - Criteria and Discussion
Part 11 - Documentation".
AGARD R-577, June 1973

A'Harrah et al

A'Harrah R C , Lamanna W J and Hodgkinson J
"Are Today's Specifications Appropriate for Tomorrow's Airplanes?".
AGARD CP-260: Stability and Control, May 1979, Paper 23.

Anderson et al

Anderson D C, Smith K L and Watson J M
"AFTI/F-16 Advanced Multimode Flight Control Systems Development
Concepts and Design".
AIAA Paper No:82-1571. Presented at "Guidance and Control
Conference", AIAA San Diego, California, August 1982.

Andry et al

Andry A N, Shapiro E Y and Chung
"Eigenstructure Assignment for Linear Systems".
IEEE Transaction on Aerospace and Electronic Systems,
Vol AES-19 No:5, pp 711-728.

Barfield

Barfield A F
"A View of the Future with the AFTI/F-16".
Royal Aeronautical Society, "ACT - Experience and Prospects".
14-19 May 1987.

Barfield & Swortzel

Barfield A F and Swortzel F R
"Integration and Automation on AFTI/F-16".
AIAA/AHS/ASEG "Aircraft Design Systems and Operations Meeting".
14-16 October 1985, Colorado Springs, Colorado.

Bellman^a

Bellman R
"Dynamic Programming".
Princeton, NJ, Princeton Univ Press 1957.

Bellman^b

Bellman R
"On the Application of the Theory of Dynamic Programming to the
Study of Control Processes".
Proceedings of the symposium on Non-Linear Circuit Analysis.
New York: Polytechnic Institute of Brooklyn Press 1956, pp 199-213.

Bianco & Swortzel

Bianco A J and Swortzel F R
"AFTI/F-16 - An Integrated Systems Approach to Combat Automation".
IEEE Paper 2.3.1 of Proc of IEEE/AIAA 5th Digital Avionics System
Conference, 1983, USA.

Birhle & Wantagh

Birhle W I and Wantagh N Y
"Handling Qualities Theory for Precise Flight Path Control".
Air Force Flight Dynamics Laboratory - Technical Report, 1966.
AFFDL-TR-65-189.

Bischoff

Bischoff D E
"A Comparison of Proposed MIL-Handbook Dynamic Longitudinal
Flying Qualities Criteria".
Presented at: "Design Criteria for the Future of Flight Controls",
Workshop for the Wright Patterson Air Force Base, Ohio, 2-5 March
1982.

Blight & Gangaas

Blight J D and Gangaas D
"Classical and Modern Control Design of a speed-hold System for a
STOL airplane".
AIAA Paper 81-0017, Aerospace Sciences Meeting 19th, St Louis, MO,
12-15 January 1981.

Blakelock

Blakelock J H
"Automatic Control of Aircraft and Missiles".
New York, London, Wiley, 1965.

Bode

Bode H W
"Network Analysis and Feedback Amplifier Design".
Princeton NJ, Van Nostrand, 1945.

Bode et al

Bode W E, Kendrick R A and Jane E J
"Simulation and Study of VSTOL Landing Aids for USMC AV-8 Aircraft".
AGARD CP-255: The Guidance and Control of Helicopters and V/STOL
Aircraft at Night and in Poor Visibility, May 1979, Paper 23,
pp 1-16.

Bodson & Athans

Bodson M and Athans M
"Multivariable Control of VTOL Aircraft for Shipboard Landing".
AIAA Paper 85-1928, AIAA Guidance, Navigation and Control
Conference, Snowmass, CO, 19-21 August 1985, pp 473-481.

Bradshaw^a

Bradshaw A

"The Evaluation of Pole Assignment Methods for the Design of Servo Controls".

Collected Lectures from the SERC Vacation School, "Deterministic Control 1", held at UMIST, Manchester, on 6-11 April 1986.

Bradshaw^b

Bradshaw A

"Notes on the Design of High Performance Active Control Systems for Helicopter Longitudinal Motion".

Internal report, Department of Aeronautical and Mechanical Engineering, The University of Salford.

Bradshaw & Counsell

Bradshaw A and Counsell J

" "

Royal Aeronautical Society Symposium on Guidance and Control 1988.

Bradshaw & Davis

Bradshaw A and Davis A T

"Design of an Active Flight Control System for a VSTOL Aircraft".

Internal report, Department of Aeronautical and Mechanical Engineering, The University of Salford.

Bradshaw & Porter^a

"Singular Perturbation Methods in the Design of Tracking Systems incorporating Fast Sampling Error-Actuated Controllers".

International Journal of Systems Science; Vol 12 No:10, 1981, pp 1181-1191.

Bradshaw & Porter^b

"Singular Perturbation Methods in the Design of Tracking Systems incorporating Inner-Loop Compensator and Fast-Sampling Error-Actuated Controllers".

International Journal of Systems Science; Vol 12 No:10, 1981, pp 1207-1220.

Bradshaw et al

Bradshaw A, Davis A T and Woodhead M A

"Digital Flight Control of Longitudinally Unstable Aircraft".

AIAA/AHS/ASEG Aircraft Design Systems and Operations Conference, Colorado Springs, USA, October 1984.

Bradshaw & Woodhead

Bradshaw A and Woodhead M A

"Time Delay Compensation in Active Control Algorithms"

The Aeronautical Journal; Vol 89 No:886, pp 219-226.

Burge

Burge S E
"Design of Multi-Functional Flight Controller for Structural Load Alleviation".
PhD Thesis, University of Salford 1984.

Butler et al

Butler G F, Corbin M S, Mepham S, Seewart J F and Larson R R
"NASA/RAE Collaboration on Non-Linear Control using the F-8c Digital Fly-by-Wire Aircraft".
AGARD CP-321: Advances in Guidance and Control Systems, June 1983, Paper 21.

Calderbank

Calderbank J A
"Control of the Longitudinal Dynamics of Vehicle system using Fast-Sampling Techniques".
PhD Thesis, University of Salford 1981.

Cambridge Control

Cambridge Control Ltd.
"TSIM User Guide".
Cambridge Control Ltd, High Cross, Madingley Rd, Cambridge, CB3 0HB. Issue 1 for TSIM 2.2a, 1986

Chalk

Chalk C R
'Flying Qualities of Pitch Rate Command/Attitude Hold Control Systems for Landing".
Journal of Guidance, Control and Dynamics; Vol 9, Part 5, 1986, pp 541-545.

Clark & Goldstien

Clark J W and Goldstein K W
"Status of VTOL and VSTOL Flying Qualities Criteria Development: Where are we and where are we going?".
AGARD CP-333: Criteria for the Handling Qualities of Military Aircraft, 1982, Paper 2.

Cowling

Cowling D
"The Design of Control System for an Unstable Canard Aircraft using Eigenstructure Assignment".
Transactions of the Institute of Measurement & Control, October 1987.

Cunningham & Pope

Cunningham T B and Pope R E
"Advanced Flight Control Design Techniques and Handling Quality Requirements".
AGARD CP-321: Advances in Guidance and Control of Systems, June 1983.

D'Azzo

D'Azzo J J
"Synthesis of Linear Multivariable Sampled Data Feedback Control Systems by Entire Eigenstructure Assignment".
PhD Thesis, University of Salford 1978.

Demeis

Demeis R
"Fighter Manoeuvrability".
Aerospace America; Vol 22 May 1984, pp 80-83.

Donley

Donley S T
"Evaluation of Several Control/Display Concepts for VSTOL Shipboard Landings".
SAE Paper 801205, October 1980.

Doyle^a

Doyle J C
"Robustness of Multiloop Linear Feedback Systems".
Proc: 17th Conf on Decision & Control, San Diego 1978, WA1-10:45, pp 12-18.

Doyle^b

Doyle J C
"Guaranteed Margins for LQG Regulators".
IEEE Transactions on Automatic Control, AC-23, NO:4, pp 756-757, Aug 1978.

Doyle & Stein

Doyle J C and Stein G
"Multivariable Feedback Design: Concepts for a Classical/Modern Synthesis".
IEEE Transactions on Automatic Control, Vol AC-26, No:1, 1981.

Edmunds

Edmunds J M
"Cambridge Linear Analysis and Design Package".
3rd Version, July 1981.

Etkin

Etkin B
"Dynamics of Flight, Stability and Control".
New York, Chichester, Wiley, 1982.

Evans

Evans W R
"Graphical Analysis of Control Systems".
Transactions of the AIEE 1984, No:67 pp 547-551.

Falb & Wolovich

Falb P L and Wolovich W A
"Decoupling in the Design and Synthesis of Multivariable Control Systems".
IEEE Transactions on Automatic Control, December 1967, Vol AC12, No:6, pp 651-659.

Fleming & Pashkevich

Fleming P J and Pashkevich A P
"Computer Aided Control Systems Design using a Multiobjective Optimisation Approach".
Control 85, IEEE Conference, pp 174-179.

Fletcher et al

Fletcher L R, Kautsky J, Kolka G K L and Nichols N K
"Some Necessary and Sufficient Conditions for Eigenstructure Assignments".
International Journal of Control; Vol 42, No:6, 1985, pp 1457-1468.

Flight International^a

"RAE Studies Advanced Digital VSTOL".
17th August 1985, pp 15.

Flight International^b

"VAAC Harrier Begins Work".
19th July 1986, pp 11.

Fontain

Fontain J K
"A Study on Active Control Including a Linear Aircraft Dynamic Simulation".
MSc Dissertation, University of Salford 1986.

Fozard

Fozard J W
"The Jet VSTOL Harrier - An Evolutionary Revolution in Tactical Air Power".
AIAA Professional Study Series. British Aerospace Aircraft Group Kingston-Brough Division, Richmond Rd, Kingston Upon Thames, Surrey.

Franklin et al

Franklin G F, Powell J D and Emami-Naini A
"Feedback Control of Dynamic Systems".
Addison-Wesley Publishing Company 1986.

Franklin

Franklin J A
"Control of VSTOL Aircraft".
Aeronautical Journal, August 1986 Vol 90 No:895, pp 157-173.

Franklin & Anderson

Franklin J A and Anderson S B
"VSTOL Maneuverability and Control".
AGARD R-710: Special Course on on VSTOL Aerodynamics, pp 8-47.

Franklin & Hynes

Franklin J a and Hynes C S
"Flight Evaluation of Augmented Controls for Approach and Landing
of Powered-Lift Aircraft".
AIAA Paper 85-1944, AIAA Guidance, Navigation and Control
Conference, Snowmass, CO, 19-21 August 1985.

Gangsaas et al

Gangsaas D, Bruce K R, Blight J D and Ly U
"Application of Modern Synthesis to Aircraft Control: Three case
Studies".
IEEE Transactions on Automatic Control; Vol AC31, No:11, November
1987, pp 995-1013.

Garg & Schmidt

Garg S and Schmidt D K
"Cooperative Synthesis of Control and Display Augmentation for
STOL Aircraft in the Approach and Landing Task".
Guidance, Navigation and Control Conference, Minneapolis, Minnesota,
15-17 August 1988. AIAA Paper 88-4182-CP,
pp 1071-1082.

Garis

Garis A
"Fast Sampling Direct Digital Flight Mode Control System".
PhD Thesis, University of Salford 1981.

Gibson

Gibson J C
"Piloted Handling Qualities Design Criteria for High Order Flight
Control Systems".
AGARD CP-333: Criteria for Handling Qualities of Military Aircraft,
1982, Paper 4.

Gill

Gill F R
"Engineering of Control Systems and Implications on Control Law
Design".
AGARD LS-89: Task Oriented Flight Control Systems, May 1977, Paper
3.

Grace & Fleming

Grace A C W and Fleming P J
"Use of Multiobjective Optimisation in CACSD".
IEE Coloquium on Computer Aided Control Systems Design Environment
and Methods. Digest No:108, UK London 30th November 1987.

Grubel & Kreisselmeier

Grubel G and Kreisselmeier G
"Systematic Computer Aided Control Design".
AGARD CP-321: Advances in Guidance and Control Systems, June 1983,
Paper 6.

Harschburger & Moomaw

Harschburger H E and Moomaw R F
"Experience with the F/A-18 Digital Flight Control System".
Paper 6.1.1, Proceedings of the IEEE/AIAA 5th Digital Avionics
Systems Conference.

Hanus et al

Hanus R, Kinnaorti M and Henrotte J L
"Conditioning Technique, A General Anti-Windup and Bumpless
Transfer Method".
Automatica; Vol 23, No:6, pp 729-739, 1987.

Hemami

Hemami A
"Design of High Gain Controllers for Linear Multivariable Systems".
PhD Thesis, University of Salford 1980.

Hikita et al

Hikita H, Kubota Y and Yamashita M
"Design of Variable Structure Servo Mechanisms".
Control 88, IEEE Conference, pp 30-34.

Hindson & Hardy

Hindson W and Hardy
"Flight Experience with Advanced Controls and Displays During
Piloted Curved Decelerating Approaches in a Powered Lift STOL
Aircraft".
AGARD CP-260: Stability and Control, May 1979, Paper27, pp 1-12.

Hoh et al^a

Hoh R H, Myers T and Ashkenas I L
"Development of Flying Qualities Criterion for Control Configured
Vehicles".
Analysis and Flight Tests.

Hoh et al^b

Hoh R H, Mitchell D G and Hodgkinson J
"Bandwidth - A Criterion for Highly Augmented Airplanes".
AGARD CP-333: Criteria for Handling Qualities of Military Aircraft,
1982, paper 9.

Hopper

Hopper D J F
"Active Control of VSTOL Aircraft - A Piloted Flight Simulation Trial".
RAE Report for Agreement No: 2101/66/RAE(B) (Further Work).

Horowitz

Horowitz I
"Quantative Synthesis of Uncertain Multiple Input - Multiple Output Feedback System".
International Journal of Control; Vol 30, No:1, 1979, pp 81-106.

Hunt

Hunt G H
"Introduction and Overview"
AGARD LS-89: Task-Oriented Flight Control Systems, May 1977,
Paper 1.

Jackson

Jackson W H
"An Evaluation of High Performance Decoupling Flight Control Systems".
Final year project, Department of Aeronautical and Mechanical Engineering, The University of Salford 1983.

Kalman^a

Kalman R E
"Contributions to the Theory of Optimal Control"
Bol. Soc. Mexico; Vol 5, pp 102-119, 1960.

Kalman^b

Kalman R E
"The Theory of Optimal Control and the Calculus of Variations".
In "Mathematical Optimisation Techniques", Edited by R Bellman.
Berkley CA; Univ. of Calif. Press, 1963.

Kaul et al

Kaul H J, Sella F and Walker M J
"The Flight Control System for the Experimental Aircraft Program (EAP) Demonstration Aircraft".
AGARD CP-384: Active Control Systems - Review, Evaluation and Projections, March 1985, Paper 24.

Kautsky et al

Kautsky J, Nichols N K and VanDooran P
"Robust Pole Assignment in Linear State Feedback".
International Journal of Control; Vol 41 No:5, pp 1129-1155.

Kokotovic

Kokotovic P V

"A Ricatta Equation for Block Diagonalisation of Ill Conditioned Systems".

IEEE Transactions on Automatic Control; Vol AC-10, P 812, 1975.

Kouvaritakis

Kouvaritakis B

"Gain Margins and Root-Locus Asymptotic Behaviour in Multivariable Design".

Part I: The properties of the Markov Parameters and High Feedback Gain.

International Journal of Control; Vol 27, No:5, 1987, pp 705-725.

Part II: A Critical Appraisal of Frequency Response and a Root-Locus Point of View.

International Journal of Control; Vol 27, No:5 1987, pp 725-751.

Kouvaritakis & Edmunds

Kouvaritakis B and Edmunds J M

"Multivariable Root Loci: A Unified Approach to Finite and Infinite Zeros".

Part I: Square Systems.

Part II: Non-Square Systems

International Journal of Control 1979; Vol 29, No:3, pp 393-428.

Kouvaritakis et al

Kouvaritakis B, Murray W and MacFarlane A G J

"Characteristic Frequency-Gain Design Study of an Automatic Flight Control System".

International Journal of Control; Vol 29, 1979, pp 325-358.

Kouvaritakis & Shaked

Kouvaritakis B and Shaked U

"Asymptotic Behaviour of Root-Loci of Linear Multivariable Systems".

International Journal of Control; Vol 23, No:3, 1976, pp 297-340.

Lee et al

Lee H P, Youssef H M and Hanel R P

"Application of Eigenstructure Assignment to the Design of STOVL Flight Control System".

AIAA Guidance, Navigation and Control Conference, Minneapolis, 15-17 August 1988. AIAA paper 88-4140-CP, p 736-748.

Lehtomaki et al

Lehtomaki N A, Sandell N and Athans M

"Robustness Results in Linear-Quadratic Gaussian Based Multivariable Control Designs"

IEEE transactions on Automatic Control; Vol AC-26, No:1, pp 75-93.

MacFarlane^a

MacFarlane A G J

"Complex Variable Methods for Linear Multivariable Feedback Systems"
Taylor and Francis, London, 1978.

MacFarlane^b

MacFarlane A G J

"Return-Difference and Return-Ratio Matrices and their uses in
Analysis and Design of Multivariable Feedback Control Systems".
Proceedings of the IEE; October 1970, Vol 117, No:10, pp 2037-2049.

MacFarlane & Belletrutti

MacFarlane A G J and Belletrutti J J

"The Characteristic Locus Design Method".
Automatica; Vol 9, pp 575-588.

MacFarlane & Karcanias

MacFarlane A G J and Karcanias N

"Poles and Zeros of Linear Multivariable Systems: A Survey of the
Algebraic, Geometric and Complex-Variable Theory".
International Journal of Control; Vol 24, No:1, 1976, pp 33-74

MacFarlane & Kouvaritakis

MacFarlane A G J and Kouvaritakis B

"A Design Technique for Linear Multivariable Feedback Systems".
International Journal of Control; Vol 25, No:6, 1977, pp 837-874.

McMuldroy et al

McMuldroy G C, Stein G and Athans M

"VTOL Control for Shipboard Landing in High Sea States".

IEEE: Conference on Decision and Control and Symposium on Adaptive
Processes, 18th. Fort Lauderdale, Florida, 12-14 December 1979.

McRuer

McRuer D

"Progress and Pitfalls in Advanced Flight Control Systems".

AGARD CP-321: Advances in Guidance and Control Systems, June 1983,
Paper K.

Mathworks

The MathWorks Inc.

"Pro-Matlab: User's Guide"

The MathWorks, Inc. 20 North Main St, Suite 250, Sherborne,
MA 01770, USA. Version 3.1-VMS.

Merrick & Gerdes

Merrick V K and Gerdes R M

"VTOL Controls for Shipboard Operation."

Proceedings of the Aerospace Congress and Exposition, Longbeach,
CA, 3-6 October 1983, "Powered Lift Systems Plus an Overview of the
JVX Programme", pp33-48. SEA paper No: 831428.

Meyer & Cicolami

Meyer G and Cicolami L.
"Application of Non-Linear Systems Inverses to Automatic Flight Control Design-System Concepts and Flight Evaluation".
AGARD AG-251; Theory and Application of Optimum Control in Aerospace Systems.

Mooij & VanGool

Mooij H A and Van Gool M F C
"Handling Qualities of Transports with Advanced Flight Control Systems".
AGARD-CP-333: Criteria for Handling Qualities of Military Aircraft, 1982, paper 7.

Moomaw & Lowry

Moomaw R F and Lowry D J
"Application of Multivariable Control to the STOL and Manoeuvre Technology Demonstrator".
AIAA Guidance, Navigation and Control Conference, Monterey, CA; Vol II, pp 773-7863, 17-19 August 1987. AIAA paper 86-2403.

Moore

Moore B C
"On the Flexibility Offered by State Feedback in Multivariable Systems Beyond Closed-Loop Eigenvalue Assignment".
IEEE Transactions on Automatic Control; Vol 21, pp 689-692.

Moorhouse

Moorhouse D J
"STOL Flying Qualities and the Impact of Control Integration".
Proceedings of the IEEE, NAECON 1983; Vol 12, pp 1410-1419.

Moorhouse & Morran

Moorhouse D J and Morran W A
"Flying Qualities Design Criteria for Highly Augmented Systems".
Proceedings of the IEEE, NAECON 1985: Vol 2, pp 1536-1545.

Moorhouse & Selegan

Moorhouse D J and Selegan D R
"The STOL and Manoeuvre Technology Programme Integrated Control System Development".
AGARD CP-384: Active Control Systems: Review, Evaluation and Projections, March 1985.

Morales et al

Morales E, Merrick V K and Schroeder J A
"Simulation Evaluation of the Advanced Control Concept for the NASA VSTOL research Aircraft (VSRA)".
AIAA Guidance, Navigation and Control Conference, Monterey, CA, 17-19 August 1987, pp 1273-1294. AIAA paper 87-2535.

Morran

Morran W A

"Operational and Developmental Experience with the F/A-18A
Digital Flight Control System".

AGARD CP-384: Active Control Systems: Review, Evaluation and,
Projections, March 1985, Paper 12a.

Muir & Kellett

Muir E A M and Kellett M G

"The RAe Generic VSTOL Aircraft Model: GVAM87 - User Guide".

RAe Internal Report (draft version).

Munro

Munro N

"FOSTASY - A Control System CAD Environment".

Control 88, IEEE Conference, pp 76-80.

Neal & Smith

Neal T P and Smith R E

"An In-Flight Investigation to Develop Control Systems Design
Criteria for Fighter Airplanes".

Air Force Flight Dynamics Laboratory - Technical Report,
AFFDL-TR-70-74, December 1970.

Nelson & Smith

Nelson T P and Smith R E

"Improved Combat Performance using Relaxed Static Stability and a
Spin Prevention System".

AGARD CP-409: Improvements on Combat Performance for Existing and
Future Aircraft, pp 31-39.

Nyquist

Nyquist H

"Regeneration Theory".

Bell Systems Technical Journal, No:11, 1932, pp126-147.

Owens^a

Owens D H

"Dynamic Transformations and the Root-Loci of Linear
Multivariable Systems".

International Journal of Control; Vol 28, 1978, pp 333-343.

Owens^b

Owens D H

"A Note on Compensation of Multivariable Root-Loci".

International Journal of Control; Vol 29, 1979, pp 387-391.

Owens^c

Owens D H

"Multivariable Root-Loci and the Inverse Transfer Function Matrix".

International Journal of Control; Vol 28, 1978, pp 345-351.

Owens^d

Owens D H

"On Structural Invariants and the Root-Loci of Multivariable Systems".

International Journal of Control; Vol 28, 1987, pp 187-196.

Owen

Owen K

"Beyond Harrier".

Aerospace America, January 1987, pp 14.

Patel & Munro

Patel R V and Munro N

"Multivariable Systems Theory and Design".

International Series on Systems and Control; Vol 14, Pergamon Press, 1982.

Pautzke et al

Pautzke F, Heister M and Nou Reldin H A

"A Constructive Solution of the Decoupling Problem for Computer Aided Control System Design".

Control 88, IEEE Conference, pp 230-235.

Porter^a

Porter B

"Design of Tunable set-point Tracking Controllers for Linear Multivariable Plants".

International Journal of Control; Vol 35, No:6, 1982, pp 1107-1115.

Porter^b

Porter B

"Design of Digital Flight Mode Control Systems for Helicopters with Non-Linear Actuators".

Aeronautical Journal, June/July 1985, pp 213-218.

Porter^c

Porter B

"High Gain Tracking Systems incorporating Lur'e Plants with Multiple Non-Linearities".

International Journal of Control; Vol 34, pp 333-344.

Porter^d

Porter B

"High Gain Error-Actuated Controllers for Linear Multivariable Plants with Explicit Actuator Dynamics".

Proceedings of the IFAC, CAD of Multivariable Technological Systems, West Lafayette, USA, 15-17 September 1982.

Porter & Bradshaw^a

Porter B and Bradshaw A

"Asymptotic Properties of Linear Multivariable Continuous-Time Tracking Systems incorporating High-Gain Error-Actuated Controllers".

International Journal of Systems Science; Vol 10, No: 12, 1979, pp 1433-444.

Porter & Bradshaw^b

Porter B and Bradshaw A

"Singular Perturbation Methods in the Design of Tracking Systems incorporating High-Gain Error-Actuated Controllers".

International Journal of Systems Science; Vol 12, No:10, 1981, pp 1169-1179.

Porter & Bradshaw^c

Porter B and Bradshaw A

"Singular Perturbation Methods in the Design of Tracking Systems incorporating Inner-Loop Compensator and High-Gain Error-Actuated Controllers".

International Journal of Systems Science; Vol 12, No:10, 1981, pp 1193-205.

Porter & Bradshaw¹

Porter B and Bradshaw A

"Design of Direct Digital Adaptive Flight-Mode Control System for High Performance Aircraft".

Proceedings of the IEEE, NAECON 1982, pp818-824.

Porter & Manganas^a

Porter B and Manganas A

"Recursive Real-Time Identification of Step-Response Matrices of High Performance Aircraft for Adaptive Digital Flight Control".

AIAA Atmospheric Flight Mechanics Conference, Williamsburg VA, Aug 1986. AIAA paper 86-2017.

Porter & Manganas^b

Porter B and Manganas A

"Design of Robust Digital Controllers for Gas Turbines with Explicit Actuator and Sensor Dynamics".

AIAA/SAG/ASME; 20th Joint Propulsion Conference, 11-13 June 1984, Cincinnati, Ohio.

Porter & Crossley

Porter B and Crossley T R
"Modal Control Theory and Application".
London, Taylor and Francis, 1972.

Postlethwaite et al^a

Postlethwaite I, O'Young S D and Gu D W
"H^{*} Control System Design: A critical Assesment".
IFAC World Congress, Munich, 1987.

Postlethwaite et al^b

Postlethwaite I, O'Young S D and Gu D W
"Stable-H User Guide".
University of Oxford, Department of Engineering Science Report OUEL
1687/87.

Pontryagin et al

Pontryagin L S, Boltyanskii V G, Gmakrelidze R V and Mischensko Y F
"The Mathematical Theory of Optimal Process".
London, New York, Wiley-Interscience, 1963.

Powers

Powers B G
'Active Control Technology Experience with the Space Shuttle
in the Landing Regime".
AGARD CP-384: Active Control Systems: Review, Evaluation and,
Projecions, March 1985, Paper 16.

Pugh

Pugh A C
'Transmission and Systems Zeros".
International Journal of Control; Vol 26, No:2, pp 315-324.

Quinlivan

Quinlivan R P
"The Need for Task-Oriented Control-Laws".
AGARD LS-89: Task-Orientated Flight Control Systems, 1977.

Radford & Andrisani

Radford R C and Andrisani D
"An Experimental Investigation of VSTOL Flying Quality
Requirements in Shipboard Landings".
Journal of Aircraft; Vol 21, June 1984, pp 371-379.

Richards

Richards R J
"An Introduction to Dynamics and Control"
London, New York, Longman, 1979.

Rosenbrock^a

Rosenbrock H H
"Computer Aided Control System Design".
London, Academic Press, 1974.

Rosenbrock^b

Rosenbrock H H
"Inverse Nyquist Array Design Method".
Modern Approach to Control System Design; Editor: N Munro,
Chapter 5, pp 66-81.

Rosenbrock^c

Rosenbrock H H
"Distinctive Problems of Process Control"
Chemical Engineering Progress; Vol 58, No:9, pp 43.

Rosenbrock^d

Rosenbrock H H
"State Space and Multivariable Theory".
London, Nelson, 1970.

Safonov et al

Safonov M G, Laub A and Hartmann G L.
"Feedback Properties of Multivariable Systems: The Role and Use
of the Return Difference Matrix".
IEEE Transactions on Automatic Control; Vol AC-26, No:1,
pp 47-65.

Sangola

Sangola B A
"Singular Perturbation Methods of Asymptotic Closed-Loop
Eigenstructure Assignment in the Design of Feedback Control
Systems".
PhD Thesis; University of Salford, 1980.

Shaked^a

Shaked U
"Design Techniques for High Feedback Gain Stability".
International Journal of Control; Vol 24, No:1, 1976, pp 137-144.

Shaked^b

Shaked U
"The Intersection of Root-Loci of Multivariable Systems with the
Imaginary Axis".
International Journal of Control; Vol 25, No:4, 1977, pp 603-607.

Shenton

Shenton A T
"Asymptotic Modal Control of Singularly-Perturbed Dynamical
Systems".
PhD Thesis; University of Salford, 1977.

Smith T D et al

Smith T D, Yeo C J and Marshall R E W
"Ground and Flight Testing on the FBW Jaguar Equipped with a
Fulltime Quadruplex FCS".
AGARD CP-321: Advances in Guidance and Control Systems, June 1983,
Paper 23.

Sobel & Lallman

Sobell K and Lallman F J
"Eigenstructure Assignment for a Thrust Vected High Angle of
Attack Aircraft".
AIAA Guidance, Navigation and Control Conference, Minneapolis,
Minnesota, 15-17 August 1988, pp 408-413; AIAA paper 88-4101 CP

Sobel & Shapiro

Sobel K M and Shapiro E Y
"Application of Eigenstructure Assignment to Flight Control
Design: Some Extensions".
Journal of Guidance, Control and Dynamics; Vol 10, 1987, pp 73-81.

Stapleford

Stapleford R L
"Velocity Command/Position Hold - A New Flight Control Concept
for Hovering Vtol Aircraft".
Aerospace Congress and Exposition, Los Angeles, 14-16 October 1980.
SAE paper 801206.

Taylor

Taylor J H
"A Study on Active Control including a Longitudinal Aircraft
Dynamics Simulation".
MSc. Dissertation, University of Salford, 1986.

Toles & Anderson

Toles R D and Anderson D C
"AFTI/F-16 DFCS Development Summary - A Report to Industry
Multimode Control Law Design".
IEEE Proceedings: NAECON 1983 , pp 1212-1219.

Tomlinson

Tomlinson B N
"SESAME - A System of Equations for the Simulation of
Aircraft in a Modular Environment".
RAE(B) MoD, Technical Report, 1979.

Tsingas

Tsingas A
"Singular Perturbation Methods in the Design of Controllers for
Linear Multivariable Plants with Slow and Fast Modes".
PhD Thesis; University of Salford, 1978.

Smith P R

Smith P R

"A Graphical Method for Improved Eigenstructure Assignment Design".
AIAA Guidance, Navigation and Control Conference, Minnesota, 15-17
August 1988, pp 421-429. AIAA, Paper 88-4103 CP.

Smith & Bailey

Smith R E and Bailey R E

"Effects of Control System Time Delays on Fighter Flying Qualities".
AGARD CP-333: Criteria for Handling Qualities for Military Aircraft,
1982.

Smith & Meyer^a

Smith G R and Mryer G

"Total Aircraft Flight-Control System-Balanced Open and
Closed-Loop Control with Dynamic Trim Maps".
IEEE: Challenge of the 80's. 3rd Digital Avionics Systems
Conference, Fort Worth, Texas, 6-8 November 1979, pp 215-223.

Smith & Meyer^b

Smith G A and Meyer G

"Application of the Concept of Dynamic Trim Control and
Non-Linear System Inverses to Automatic Control of a Vertical
Attitude Take Off and Landing Aircraft".
AIAA Digital Avionics Systems Conference, 4th St Louis, MO, 17-19
November 1981, pp 102-115. AIAA paper 81-2238.

Smith G A et al

Smith G A, Meyer G and Nordstrom M

"Aircraft Automatic-Flight-Control System with Inversion of the
Model in the Feed-Forward Path using a Newton-Raphson Technique
for the Inversion".
National Aeronautics and Space Agency - Technical Memo,
NASA-TM-88209.

Smith K L et al

Smith K L, Kerr W B, Hartmann G L and Skira C

"Aircraft Control Integration - Methodology and Performance Impact".
AIAA, Paper 85-1424, Joint Propulsion Conference, Monterey, CA,
8-10 July 1985.

Smith P R et al

Smith P R, Hopper D J F and Bradshaw A

"Comparison of Eigenstructure Assignment and the Salford Singular
Perturbation Methods in VSTOL Aircraft Controller Design".
AIAA Guidance, Navigation and Control Conference, 14-16 August 1989.

Twisdale

Twisdale T R
"A User Friendly Introduction to Handling Qualities".
IEEE Conference, NAECON 1984, 21-25 May, pp 457-463.

United States

US Department of Defence
"Flying Qualities of Piloted VSTOL Aircraft"
Washington (DC), DoD 1980. MIL-F-83300

United States

US Department of Defence
"Flying Qualities of Piloted Airplanes"
Washington (DC), DoD 1970. MIL-F- 8785C

Van De Vegte

Van De Vegte J
"Feedback Control Systems"
London, Prentice Hall International, 1986.

Walker

Walker K
"VSTOL Comes of Age".
Flight International, 19 July 1986, pp 22-25.

Wendl

Wendl M J
"Additional Degrees of Freedom".
AGARD LS-89: Task Oriented Flight Control Systems, Paper 7, May
1977.

Winter et al

Winter J S, Corbin M J and Lesley M M
"Description of TSIM2: A Software Package for Computer Aided
Design of Flight Control Systems".
RAE Technical Report 83007.

Wonham and Morse

Wonham W M and Morse A S
"Decoupling and Pole Assignment in Linear Multivariable Systems:
A Geometric Approach".
SIAM Journal of Control and Optimisation, No:8, 1970, pp 1-18.

Yue

Yue A
"Design of Robust Multivariable Helicopter Control Laws for
Handling Qualities Enhancement".
Control 88, IEEE Conference, pp 689-694.

APPENDIX A

BLOCK DIAGONALISATION OF A SINGULARLY

PERTURBED SYSTEM

APPENDIX A

Block Diagonalisation of a Singularly Perturbed System

This appendix contains the mathematical description of the block diagonalisation theory for singularly perturbed systems [Kokotovic] in part one. In part two this theory is applied to the state and output equations of the closed-loop singularly perturbed system given by (3.16) and (3.17) to derive the closed-loop block diagonalised asymptotic form.

A1.1 Block Diagonalisation Theory

A linear multivariable time-invariant system with n_1 "slow" modes and n_2 "fast" modes may be described by the state and output equations

$$\begin{bmatrix} \dot{x}_{n1}(t) \\ \dot{x}_{n2}(t) \end{bmatrix} = \begin{bmatrix} A_1 & A_2 \\ A_3 & A_4 \end{bmatrix} \begin{bmatrix} x_{n1}(t) \\ x_{n2}(t) \end{bmatrix} + \begin{bmatrix} B_{n1} \\ B_{n2} \end{bmatrix} u(t) \quad \dots (A1)$$

and

$$y(t) = \begin{bmatrix} C_{n1} & C_{n2} \end{bmatrix} \begin{bmatrix} x_{n1}(t) \\ x_{n2}(t) \end{bmatrix} \quad \dots (A2)$$

respectively, where $x_{n1} \in \mathbb{R}^{n_1}$, $x_{n2} \in \mathbb{R}^{n_2}$, $A_1 \in \mathbb{R}^{n_1 \times n_1}$, $A_2 \in \mathbb{R}^{n_1 \times n_2}$, $A_3 \in \mathbb{R}^{n_2 \times n_1}$, $A_4 \in \mathbb{R}^{n_2 \times n_2}$, $B_{n1} \in \mathbb{R}^{n_1 \times \ell}$, $B_{n2} \in \mathbb{R}^{n_2 \times \ell}$, $u(t) \in \mathbb{R}^{\ell}$, $y(t) \in \mathbb{R}^{\ell}$, $C_{n1} \in \mathbb{R}^{\ell \times n_1}$ and $C_{n2} \in \mathbb{R}^{\ell \times n_2}$. There exists a linear transformation of state variables

$$\begin{bmatrix} x_{n1}(t) \\ x_{n2}(t) \end{bmatrix} = \begin{bmatrix} I_{n1} & M \\ -L & I_{n2-LM} \end{bmatrix} \begin{bmatrix} z_{n1} \\ z_{n2} \end{bmatrix} \quad \dots (A3)$$

and its explicit inverse

$$\begin{bmatrix} z_{n1}(t) \\ z_{n2}(t) \end{bmatrix} = \begin{bmatrix} I_{n1}^{-ML} & -M \\ L & I_{n2} \end{bmatrix} \begin{bmatrix} x_{n1} \\ x_{n2} \end{bmatrix} \quad \dots (A4)$$

where $Z_{n1} \in \mathbb{R}^{n1}$, $Z_{n2} \in \mathbb{R}^{n2}$, $M \in \mathbb{R}^{n1 \times n2}$ and $L \in \mathbb{R}^{n2 \times n1}$, such that the state equations (A1) may be expressed in block diagonal form

$$\begin{bmatrix} \dot{Z}_{n1}(t) \\ \dot{Z}_{n2}(t) \end{bmatrix} = \begin{bmatrix} F_{n1} & 0 \\ 0 & F_{n2} \end{bmatrix} \begin{bmatrix} Z_{n1}(t) \\ Z_{n2}(t) \end{bmatrix} + \begin{bmatrix} G_{n1} \\ G_{n2} \end{bmatrix} u(t) \quad \dots (A5)$$

and the output equation (A2) assumes the form

$$y(t) = [H_{n1} \ H_{n2}] \begin{bmatrix} Z_{n1}(t) \\ Z_{n2}(t) \end{bmatrix} \quad \dots (A6)$$

where

$$F_{n1} = (A_1 - A_2L) \quad \dots (A7)$$

$$F_{n2} = (A_4 + LA_2) \quad \dots (A8)$$

$$G_{n1} = (I_{n1} - ML) B_{n1} - MB_{n2} \quad \dots (A9)$$

$$G_{n2} = LB_{n1} + B_{n2} \quad \dots (A10)$$

$$H_{n1} = C_{n1} - LC_{n2} \quad \dots (A11)$$

and

$$H_{n2} = MC_{n1} + (I_{n2} - LM) C_{n2} \quad \dots (A12)$$

provided that the matrix Riccati equations

$$A_2 + (A_1 + A_2L) M - M (A_4 - LA_2) = 0 \quad \dots (A13)$$

and

$$LA_1 + A_3 - LA_2L - A_4L = 0 \quad \dots (A14)$$

can be satisfied by L and M.

In general, the solutions to these Riccati equations can be obtained [Kokotovic] by the iterative schemes

$$L_{k+1} = A_4^{-1} (I_k A_1 + A_3 - L_k A_2 L_k) \quad \dots (A15)$$

and

$$M_{k+1} = (A_2 + (A_1 - A_2L) M_k - M_k LA_2) A_4^{-1} \quad \dots (A16)$$

with the starting values.

$$L_0 = A_4^{-1} A_3 \quad \dots (A17)$$

and

$$M_0 = A_2 A_4^{-1} \quad \dots \text{ (A18)}$$

If the assumption of n_1 "slow" modes and n_2 "fast" modes is valid then the eigenvalues of A_1 and A_4 will be well separated. This situation gives rise to the rapid convergence of (A15) and (A16) which allows the approximate but sufficient solution of

$$L \approx L_0 = A_4^{-1} A_3 \quad \dots \text{ (A19)}$$

and

$$M \approx M_0 = A_2 A_4^{-1} \quad \dots \text{ (A20)}$$

to be used in many cases. Such a case occurs when high-gain error actuated feedback control is applied to a plant and $g \rightarrow \infty$. Clearly, in these circumstances, block diagonalisation will be achieved and the state and output equations (A5) and (A6) will result in a transfer function matrix of the form

$$G(s) = G_s(s) + G_f(s) \quad \dots \text{ (A21)}$$

where the "slow" transfer function matrix is given by

$$G_s(s) = H_{n1} (sI_{n1} - F_{n1})^{-1} G_{n1} \quad \dots \text{ (A22)}$$

and the "fast" transfer function matrix is given by

$$G_f(s) = H_{n2} (sI_{n2} - F_{n2})^{-1} G_{n2} \quad \dots \text{ (A23)}$$

A1.2 Application of Block Diagonalisation Theory

The state and output equations of the closed loop singularly perturbed system (3.16) and (3.17) are given by

$$\begin{bmatrix} \dot{Z}(t) \\ \dot{x}_1(t) \\ \dot{x}_2(t) \end{bmatrix} = \begin{bmatrix} 0 & -F_1 & -F_2 \\ 0 & A_{11} & A_{12} \\ gB_2K_I & A_{21}-gB_2K_pF_1 & A_{22}-gB_2K_pF_2 \end{bmatrix} \begin{bmatrix} Z(t) \\ x_1(t) \\ x_2(t) \end{bmatrix} + \begin{bmatrix} I_m \\ 0 \\ gB_2K_p \end{bmatrix} v(t) \quad \dots (A24)$$

and

$$y(t) = \begin{bmatrix} 0 & C_1 & C_2 \end{bmatrix} \begin{bmatrix} Z(t) \\ x_1(t) \\ x_2(t) \end{bmatrix} \quad \dots (A25)$$

In this case $x_{n1}(t) = [Z(t) \ x_1(t)]^T$ and $x_{n2} = [x_2(t)]$

and so clearly

$$A_1 = \begin{bmatrix} 0 & -F_1 \\ 0 & A_{11} \end{bmatrix} \quad \dots (A26)$$

$$A_2 = \begin{bmatrix} -F_2 \\ A_{12} \end{bmatrix} \quad \dots (A27)$$

$$A_3 = [gB_2K_I \ A_{21}-gB_2K_pF_1] \quad \dots (A28)$$

$$A_4 = [A_{22} \ gB_2K_pF_2] \quad \dots (A29)$$

$$B_{n1} = \begin{bmatrix} I_m \\ 0 \end{bmatrix} \quad \dots (A30)$$

$$B_{n2} = [gB_2K_p] \quad \dots (A31)$$

$$C_{n1} = [0 \ C_1] \quad \dots (A32)$$

and

$$C_{n2} = [C_2] \quad \dots (A33)$$

Substituting from (A28) and (A29) into (A19) gives

$$L = [A_{22} \ gB_2K_pF_2]^{-1} [gB_2K_I \ A_{21}-gB_2K_pF_1] \quad \dots (A34)$$

which may be rearranged to give

$$L = (-gB_2K_pF_2)^{-1} [I_2 - 1/g A_{22} (B_2K_pF_2)^{-1}]^{-1} [gB_2K_I A_{21} - gB_2K_pF_1] \dots (A35)$$

The middle bracketed expression of (A35) may be expanded using the binomial expansion to a first order approximation, as all higher-order terms become insignificant as $g \rightarrow \infty$. ($1/g$ is the singular perturbation in this singular perturbation analysis).

This yields

$$L = -1/g (B_2K_pF_2)^{-1} [I_2 - 1/g A_{22}(B_2K_pF_2)^{-1}][gB_2K_I A_{21} - gB_2K_pF_1] \dots (A36)$$

which may be multiplied out and then simplified by ignoring terms with $1/g^2$ which become negligible as $g \rightarrow \infty$. This gives

$$L = [-F_2^{-1} K_p^{-1} K_I F_2^{-1} F_1] \dots (A37)$$

substituting from (A27) and (A29) into (A20) gives

$$M = \begin{bmatrix} -F_2 \\ A_{12} \end{bmatrix} [A_{22} - gB_2K_pF_2]^{-1} \dots (A38)$$

which may be rearranged and then simplified using the binomial expansion to a first order approximation, as used above, to give

$$M = \begin{bmatrix} F_2 \\ A_{12} \end{bmatrix} [I_2 \quad 1/g \quad A_{22} \quad (B_2 K_p F_2)^{-1}] (g) (B_2 K_p F_2)^{-1} \quad \dots \quad (A39)$$

which again may be multiplied out and then simplified by ignoring insignificant terms as $g \rightarrow \infty$ to give

$$M = \frac{1}{g} \begin{bmatrix} K_p^{-1} B_2^{-1} \\ -A_{12} F_2^{-1} K_p^{-1} B_2^{-1} \end{bmatrix} \quad \dots \quad (A40)$$

The result (A37) may be substituted into (A7) with (A26) and (A27) and multiplied out to yield.

$$F_{n1} = \begin{bmatrix} K_p^{-1} K_I & 0 \\ A_{12} F_2^{-1} K_p^{-1} K_I & A_{11} - A_{12} F_2^{-1} F_1 \end{bmatrix} \quad \dots \quad (A41)$$

The result (A37) may also be substituted into (A8) with (A29) and (A27) to yield

$$F_{n2} = [-g \quad B_2 K_p F_2] \quad \dots \quad (A42)$$

The result (A37) and (A40) may be substituted into (A9) with (A30) and (A31) to yield

$$G_{n1} = \begin{bmatrix} 0 \\ A_{12} F_2^{-1} \end{bmatrix} \quad \dots \quad (A43)$$

The results (A37) may be substituted into (A10) with (A30) and (A31) to yield

$$G_{n2} = [g R_2 K_p] \quad \dots \quad (A44)$$

The result (A37) may be substituted into (A11) with (A32) and (A33) to yield

$$H_{n1} = [C_2 F_2^{-1} K_p^{-1} K_I \quad C_1 \quad C_2 F_2^{-1} F_1] \quad \dots \text{ (A45)}$$

Finally, both the results (A37) and (A40) may be substituted into (A12) with (A32) and (A33) to yield

$$H_{n2} = [C_2] \quad \dots \text{ (A46)}$$

The results (A41), (A42), (A43), (A44), (A45) and (A46) may be substituted into (A5) and (A6) to give the final asymptotic block diagonalised form of the closed-loop plant which was described by (3.16) and (3.17), in the form of the state equation

$$\begin{bmatrix} \bar{z}(t) \\ \bar{x}_1(t) \\ \bar{x}_2(t) \end{bmatrix} \begin{bmatrix} -K_p^{-1} K_I & 0 & 0 \\ A_{12} F_2^{-1} K_p^{-1} K_I & A_{11} - A_{12} F_2^{-1} F_1 & 0 \\ 0 & 0 & -g B_2 K_p F_2 \end{bmatrix} \begin{bmatrix} \bar{z}(t) \\ \bar{x}_1(t) \\ \bar{x}_2(t) \end{bmatrix} + \begin{bmatrix} 0 \\ A_{12} F_2^{-1} \\ g B_2 K_p \end{bmatrix} v(t) \quad \dots \text{ (A47)}$$

and the output equation

$$y(t) = [C_2 F_2^{-1} K_p^{-1} K_I \quad C_1 - C_2 F_2^{-1} F_1 \quad C_2] \begin{bmatrix} \bar{z}(t) \\ \bar{x}_1(t) \\ \bar{x}_2(t) \end{bmatrix} \quad \dots \text{ (A48)}$$

where the new asymptotic state (after linear state transformation of (A3) and (A4) is $[\bar{z}(t) \quad \bar{x}_1(t) \quad \bar{x}_2(t)]^T$.

From the results (A41), (A42), (A43), (A44), (A45) and (A46) together with the equations (A22) and (A23) the 'slow' and 'fast' transfer function matrices may also be defined.

APPENDIX B

EXAMPLE 3.2

APPENDIX B

Example 3.2:

This appendix contains the worked example from subsection 3.4.2. The example was calculated using Pro-Matlab and the "DIARY" function was used to save the results of each step. However, to help the reader follow the example, the raw output has been edited and some text has been added. The fine detail of the calculation is contained here, but the discussion of the results is contained in section 3.4.2 under the heading "Example 3.2".

The state and output equations of the example plant are given by

$$\begin{aligned} \dot{X}_p &= \underbrace{\begin{bmatrix} -5.6107e-02 & -5.5741e-02 & 2.5394e-02 & -3.9686e+01 \\ -6.5479e-02 & -2.0975e-01 & -1.1412e+00 & -2.8338e+01 \\ 2.2894e-03 & -7.3745e-04 & -4.7622e-01 & -9.9674e-02 \\ 0 & 0 & 1.0000e+00 & 0 \end{bmatrix}}_{A_p} \underbrace{\begin{bmatrix} x_1 \\ x_2 \\ x_3 \\ x_4 \end{bmatrix}}_{X_p} \\ &+ \underbrace{\begin{bmatrix} 6.6096e+00 & -4.6762e-01 & -8.6850e-02 \\ -5.4489e+01 & -8.1062e-02 & -2.2621e-01 \\ 1.0215e+00 & 7.7141e-04 & -1.1808e-01 \\ 0 & 0 & 0 & 0 \end{bmatrix}}_{B_p} \underbrace{\begin{bmatrix} u_1 \\ u_2 \\ u_3 \\ 0 \end{bmatrix}}_{U_p} \\ &\dots (B1) \end{aligned}$$

and

$$\begin{aligned} Y_p &= \underbrace{\begin{bmatrix} 1 & 0 & 0 & 0 \\ 0 & 1 & 0 & 0 \\ 0 & 0 & 1 & 1 \end{bmatrix}}_{C_p} \underbrace{\begin{bmatrix} x_1 \\ x_2 \\ x_3 \\ x_4 \end{bmatrix}}_{X_p} + \underbrace{\begin{bmatrix} 0 & 0 & 0 \\ 0 & 0 & 0 \\ 0 & 0 & 0 \end{bmatrix}}_{D_p} \underbrace{\begin{bmatrix} u_1 \\ u_2 \\ u_3 \end{bmatrix}}_{U_p} \\ &\dots (B2) \end{aligned}$$

where $C_p(3,3)$ represents the extra measurement to augment y_3 and make $C_p \cdot B_p$ full rank.

The poles (P_{ac}), zeros (Z_{ac}) and constants (K_{ac}) of the actuator dynamics are given by

$$\begin{aligned} \text{Actuator 1:} \quad & P_{ac1} = [] \\ & Z_{ac1} = [] \\ & K_{ac1} = [1] \\ \\ \text{Actuator 2:} \quad & P_{ac2} = [-5] \\ & Z_{ac2} = [Inf] \\ & K_{ac2} = [5] \\ \\ \text{Actuator 3:} \quad & P_{ac3} = [-6, -8+6*j, -8-6*j] \\ & Z_{ac3} = [-4] \\ & K_{ac3} = [150] \end{aligned}$$

where the transfer function is given by

$$G_{ac}(s) = K_{ac} \cdot \frac{Z_{ac}(s)}{P_{ac}(s)} \quad \dots \text{ (B3)}$$

and $G(s)$ for $s \rightarrow 0$ is 1.

The resultant state and output equations are given by

Actuator 1:

$$y_{a1} = 0 \cdot x_{a1} + 1 \cdot u_{a1} \quad \dots \text{ (B4)}$$

Actuator 2:

$$x_{a2} = -5 \cdot x_{a2} + 1 \cdot u_{a2} \quad \dots \text{ (B5)}$$

and

$$y_{a2} = 5 \cdot x_{a2} + 0 \cdot u_{a2} \quad \dots \text{ (B6)}$$

Actuator 3:

$$\begin{bmatrix} x_{a31} \\ x_{a32} \\ x_{a33} \end{bmatrix} = \begin{bmatrix} -22 & -196 & -600 \\ 1 & 0 & 0 \\ 0 & 1 & 0 \end{bmatrix} \cdot \begin{bmatrix} x_{a31} \\ x_{a32} \\ x_{a33} \end{bmatrix} + \begin{bmatrix} 1 \\ 0 \\ 0 \end{bmatrix} \cdot u_{a3} \quad \dots \text{ (B7)}$$

and

$$y_{a3} = \begin{bmatrix} 0 & 150 & 600 \end{bmatrix} \cdot \begin{bmatrix} x_{a31} \\ x_{a32} \\ x_{a33} \end{bmatrix} + \begin{bmatrix} 0 \end{bmatrix} \cdot u_{a3} \quad \dots \text{ (B8)}$$

It may be shown that the error actuated high gain controller is defined by

$$\begin{aligned}
 u(t) = & \underbrace{g \cdot \begin{bmatrix} 3.0672e-03 & -1.7398e-02 & 3.1074e-02 \\ -2.0975e+00 & -2.1769e-01 & 1.9598e+00 \\ 1.2831e-02 & -1.5193e-01 & -8.1873e+00 \end{bmatrix}}_{K_p} \cdot e(t) + \\
 & \underbrace{g \cdot \begin{bmatrix} 3.0672e-03 & -1.7398e-02 & 3.1074e-02 \\ -2.0975e+00 & -2.1769e-01 & 1.9598e+00 \\ 1.2831e-02 & -1.5193e-01 & -8.1873e+00 \end{bmatrix}}_{K_i} \cdot \frac{e(t)}{s} \\
 & \dots(B12)
 \end{aligned}$$

when the diagonal tuning matrices (see equations (3.29) and (3,30)) are $\Sigma = \Xi = \text{diag}(1,1,1)$.

Connecting this controller in series with the plant and actuators when $g=1$ gives the correct form of open-loop high-gain system from which the root-locus asymptote characteristics may be found. The resulting composite system is given by

$$\dot{X}_{hg} = A_{hg} \cdot X_{hg} + B_{hg} \cdot U_{hg} \quad \dots (B13)$$

and

$$Y_{hg} = C_{hg} \cdot X_{hg} + D_{hg} \cdot U_{hg} \quad \dots (B14)$$

where $\begin{bmatrix} A_{hg}(11,11) & , & B_{hg}(11,3) \\ C_{hg}(3,11) & , & D_{hg}(3,3) \end{bmatrix}$ is given by

Columns 1 through 4

0	0	0	0
0	0	0	0
0	0	0	0
-2.0975e+00	-2.1769e-01	1.9598e+00	-5.0000e+00
1.2831e-02	-1.5193e-01	-8.1873e+00	0
0	0	0	0
0	0	0	0
2.0273e-02	-1.1499e-01	2.0538e-01	-2.3381e+00
-1.6713e-01	9.4799e-01	-1.6932e+00	-4.0531e-01
3.1331e-03	-1.7771e-02	3.1741e-02	3.8570e-03
0	0	0	0
0	0	0	0
0	0	0	0
0	0	0	0

Columns 5 through 8

0	0	0	0
0	0	0	0
0	0	0	0
0	0	0	0
-2.2000e+01	-1.9600e+02	-6.0000e+02	0
1.0000e+00	0	0	0
0	1.0000e+00	0	0
0	-1.3028e+01	-5.2110e+01	-5.6107e-02
0	-3.3932e+01	-1.3573e+02	-6.5479e-02
0	-1.7712e+01	-7.0847e+01	2.2894e-03
0	0	0	0
0	0	0	1.0000e+00
0	0	0	0
0	0	0	0

Columns 9 through 12

0	0	0	1.0000e+00
0	0	0	0
0	0	0	0
0	0	0	-2.0975e+00
0	0	0	1.2831e-02
0	0	0	0
0	0	0	0
-5.5741e-02	2.5394e-02	-3.9686e+01	2.0273e-02
-2.0975e-01	-1.1412e+00	-2.8338e+01	-1.6713e-01
-7.3745e-04	-4.7622e-01	-9.9674e-02	3.1331e-03
0	1.0000e+00	0	0
0	0	0	0
1.0000e+00	0	0	0
0	1.00000e+00	0	0

Columns 13 through 14

0	0
1.0000e+00	0
0	1.0000e+00
-2.1769e-01	1.9598e+00
-1.5193e-01	-8.1873e+00
0	0
0	0
-1.1499e-01	2.0538e-01
9.4799e-01	-1.6932e+00
-1.7771e-02	3.1741e-02
0	0
0	0
0	0
0	0

... (B15)

The Markov parameters are constructed from the matrices Ahg, Bhg and Chg (as given by (B13), (B14) and (B15)) according to equation (3.46). The first 6 Markov parameters and their rank are given overleaf in table B1.

Table B1

No	Markov parameters	Rank	Rank defect
1	2.0273e-02 -1.1499e-01 2.0538e-01	1	2
	-1.6713e-01 9.4799e-01 -1.6932e+00		
	3.1331e-03 -1.7771e-02 3.1741e-02		
2	4.9327e+00 3.4715e-01 -4.2932e+00	2	1
	7.1318e-01 8.6519e-01 -2.1821e+00		
	-3.1465e-03 -2.8882e-02 5.7645e-02		
3	-2.0225e+01 5.8061e-01 1.2409e+02	3	0
	-4.3902e+00 5.1143e+00 2.8080e+02		
	-1.8773e-01 2.6904e+00 1.4498e+02		
4	1.0255e+02 -2.3276e+01 -1.9248e+03	3	0
	2.7034e+01 -8.9752e+01 -4.9718e+03		
	3.5640e+00 -4.4349e+01 -2.3891e+03		
5	-5.2081e+02 2.0723e+02 1.4438e+04	3	0
	-1.7577e+02 9.2690e+02 5.0594e+04		
	-3.8356e+01 4.6493e+02 2.5049e+04		
6	2.5540e+03 -4.4618e+02 -4.0329e+04	3	0
	9.9174e+02 -5.9722e+03 -3.2500e+05		
	2.6153e+02 -3.1506e+03 -1.6976e+05		

This table may be used as to calculate the order and direction of the root-locus asymptotes as shown by example 3.1. Clearly, there are 5 finite zeros and 6 infinite zeros.

The 5 finite zeros are: 3 due to the integrators,
1 due to the third-order actuator,
1 due to the transmission zero of
the basic plant.

The 6 infinite zeros are : 1 first-order ,
2 second-order and
3 third-order.

The asymptote patterns of each set correspond to the respective patterns given by figure 3.4, as the high-gain theory always results in asymptotes corresponding to pattern A.

The pivot-points of each asymptote set may be calculated by following the 5 steps given in subsection 3.4.2. Clearly, only the first 4 Markov parameters are needed as the 3rd Markov parameter is full rank.

Step 1

Step 1 of the pivot-point calculation is to define M_1 which is given by the first 4 Markov parameters

M1 =

Columns 1 through 3

2.0273e-02	-1.1499e-01	2.0538e-01
-1.6713e-01	9.4799e-01	-1.6932e+00
3.1331e-03	-1.7771e-02	3.1741e-02

Columns 4 through 6

4.9327e+00	3.4715e-01	-4.2932e+00
7.1318e-01	8.6519e-01	-2.1821e+00
-3.1465e-03	-2.8882e-02	5.7645e-02

Columns 7 through 9

-2.0225e+01	5.8061e-01	1.2409e+02
-4.3902e+00	5.1143e+00	2.8080e+02
-1.8773e-01	2.6904e+00	1.4498e+02

Columns 10 through 12

1.0255e+02	-2.3276e+01	-1.9248e+03
2.7034e+01	-8.9752e+01	-4.9718e+03
3.5640e+00	-4.4349e+01	-2.3891e+03

... (B16)

Step 2

Step 2 of the pivot-point calculation is to perform the unimodular transformation which gives M1bar

M1bar =

Columns 1 through 3

0	0	0
0	1.0000e+00	0
0	0	0

Columns 4 through 6

4.9828e+00	-2.6394e-02	3.7421e+00
0	8.5557e-01	0
2.2838e-02	-4.0536e-02	1.7151e-02

Columns 7 through 9

-1.9790e+01	7.3148e-01	-1.2751e+02
-4.3027e-01	2.5282e-01	-3.2313e-01
-7.8473e-01	6.7746e-03	1.4941e+02

Columns 10 through 12

9.3189e+01	3.5522e-01	1.8926e+03	
2.5214e+00	9.3344e-02	-1.1873e+02	
1.1852e+01	2.5177e-02	-2.4695e+03	... (B17)

Clearly the (3x3) block (Mlbar(1:3,1:3)) is now in the correct form and the only non-zero eigenvalue is in the middle.

Step 3

Step 3 of the pivot-point calculation requires row and column operations to obtain the correct block structure. In this case the correct block structure is given by

$$\begin{bmatrix} a & 0 & b \\ 0 & c & 0 \\ d & 0 & e \end{bmatrix} \quad \dots \text{ (B18)}$$

where a, b, c, d and e are not touched by the row column operations, but the other terms are reduced to zero as shown by (B18).

Assuming that Mlbar = [m1 m2 m3 m4], where each mi (i=1,2,3,4) is a (3x3) matrix, then the first 3 row operations are

$$\begin{aligned} m2(\text{row1}) &= m2(\text{row1}) - m1(\text{row2}) * (Mlbar(1,5) / Mlbar(2,2)) \\ m3(\text{row1}) &= m3(\text{row1}) - m1(\text{row2}) * (Mlbar(1,8) / Mlbar(2,2)) \\ m4(\text{row1}) &= m4(\text{row1}) - m1(\text{row2}) * (Mlbar(1,11) / Mlbar(2,2)) \end{aligned} \quad \dots \text{ (B19)}$$

which gives

Mlbar =

Columns 1 through 3

0	0	0
0	1.0000e+00	0
0	0	0

Columns 4 through 6

4.9828e+00	0	3.7421e+00
0	8.5557e-01	0
2.2838e-02	-4.0536e-02	1.7151e-02

Columns 7 through 9

-1.9790e+01	0	-1.2751e+02
-4.3027e-01	2.5282e-01	-3.2313e-01
-7.8473e-01	6.7746e-03	1.4941e+02

Columns 10 through 12

9.3189e+01	0	1.8926e+03	
2.5214e+00	9.3344e-02	-1.1873e+02	
1.1852e+01	2.5177e-02	-2.4695e+03	... (B20)

The next 3 row operations are

m2(row3)=m2(row1) - m1(row2)*(Mlbar(3,5)/Mlbar(2,2))
m3(row3)=m3(row1) - m1(row2)*(Mlbar(3,8)/Mlbar(2,2))
m4(row3)=m4(row1) - m1(row2)*(Mlbar(3,11)/Mlbar(2,2))
... (B21)

which gives

Mlbar =

Columns 1 through 3

0	0	0
0	1.0000e+00	0
0	0	0

Columns 4 through 6

4.9828e+00	0	3.7421e+00
0	8.5557e-01	0
2.2838e-02	0	1.7151e-02

Columns 7 through 9

-1.9790e+01	0	-1.2751e+02
-4.3027e-01	2.5282e-01	-3.2313e-01
-7.8473e-01	0	1.4941e+02

Columns 10 through 12

9.3189e+01	0	1.8926e+03	
2.5214e+00	9.3344e-02	-1.1873e+02	
1.1852e+01	0	-2.4695e+03	... (B22)

Four column operations finish off this step of the calculation as follows:

$$\begin{aligned} m3(\text{col1}) &= m3(\text{col1}) - m1(\text{col2}) * (\text{Mlbar}(2,7) / \text{Mlbar}(2,2)) \\ m3(\text{col3}) &= m3(\text{col3}) - m1(\text{col2}) * (\text{Mlbar}(2,9) / \text{Mlbar}(2,2)) \\ m4(\text{col1}) &= m4(\text{col1}) - m1(\text{col2}) * (\text{Mlbar}(2,10) / \text{Mlbar}(2,2)) \\ m4(\text{col3}) &= m4(\text{col3}) - m1(\text{col2}) * (\text{Mlbar}(2,12) / \text{Mlbar}(2,2)) \end{aligned}$$

... (B23)

giving

Mlbar =

Columns 1 through 3

0	0	0
0	1.0000e+00	0
0	0	0

Columns 4 through 6

4.9828e+00	0	3.7421e+00
0	8.5557e-01	0
2.2838e-02	0	1.7151e-02

Columns 7 through 9

-1.9790e+01	0	-1.2751e+02
0	2.5282e-01	0
-7.8473e-01	0	1.4941e+02

Columns 10 through 12

9.3189e+01	0	1.8926e+03	
0	9.3344e-02	0	
1.1852e+01	0	-2.4695e+03	... (B24)

Clearly M1bar is now in the correct block structured form.

Step 4

Step 4 calculates the pivot-point for this asymptote set. In this case there is only one first-order asymptote set and equation (3.54) defines its pivot-point as

$$p1=(m1bar(2,5)/m1bar(2,2))/1 = 8.5557e-01 \dots (B25)$$

Step 5

Step 5 requires that as $d1 \neq 0$ (ie there are still pivot-points to be found) then M2 must be formed. This is formed by extracting 3 (2x2) submatrices from m2, m3 and m4 such that the elements extracted correspond to the elements a, b, d and e from equation (B18). This yeilds

M2 =

Columns 1 through 4

4.9828e+00	3.7421e+00	-1.9790e+01	-1.2751e+02
2.2838e-02	1.7151e-02	-7.8473e-01	1.4941e+02

Columns 5 and 6

9.3189e+01	1.8926e+03	
1.1852e+01	-2.4695e+03	... (B26)

The algorithm now returns to step 2.

Step 2

Step 2 once again performs the unimodular transformation to give M2bar

M2bar =

Columns 1 through 4

$$\begin{array}{cccc}
 5.0000e+00 & 0 & -2.0380e+01 & 0 \\
 0 & 0 & -6.5152e-03 & 1.5000e+02
 \end{array}$$

Columns 5 and 6

$$\begin{array}{cc}
 1.0191e+02 & -3.8548e+01 \\
 6.6050e-02 & -2.4783e+03
 \end{array}
 \dots \text{ (B27)}$$

Step 3

In this case the correct block structure is

$$\begin{bmatrix} f & 0 \\ 0 & g \end{bmatrix}
 \dots \text{ (B28)}$$

where f and g are not touched by the row and column operations, but the other elements are reduced to zero as shown by (B28).

Assuming that M2bar = [m1 m2 m3] where each mi (i=1,2,3) is a (2x2) matrix, then the following 3 row and column operations are required

$$\begin{aligned}
 m2(\text{row}2) &= m2(\text{row}2) - m1(\text{row}1) * (M2bar(2,3) / M1bar(1,1)) \\
 m3(\text{row}2) &= m3(\text{row}2) - m1(\text{row}1) * (M2bar(2,5) / M1bar(1,1)) \\
 m3(\text{col}2) &= m3(\text{col}2) - m1(\text{col}1) * (M2bar(1,6) / M1bar(1,1))
 \end{aligned}
 \dots \text{ (B29)}$$

to yield the desired form of M2bar

M2bar =

Columns 1 through 4

$$\begin{matrix} 5.0000e+00 & 0 & -2.0380e+01 & 0 \\ & 0 & & 1.5000e+02 \end{matrix}$$

Columns 5 and 6

$$\begin{matrix} 1.0191e+02 & 0 \\ & -2.4783e+03 \end{matrix} \quad \dots \text{ (B30)}$$

Step 4

Step 4 calculates the pivot-point for this asymptote set. In this case there is only one second-order asymptote set and equation (3.54) defines its pivot-point as

$$p_2 = (M2bar(1,3)/M1bar(1,1))/2 = -2.0380e+00 \quad \dots \text{ (B31)}$$

Step 5

Step 5 requires that as $d_2 \neq 0$ (ie there are still pivot-points to be found) then M3 must be formed. This is formed by extracting 2 (1x1) submatrices from m3 and m4 such that the elements extracted correspond to the element g from equation (B28). This yeilds

M3 =

$$\begin{matrix} 1.5000e+02 & -2.4783e+03 \end{matrix} \quad \dots \text{ (B32)}$$

Clearly, M3 is already in the required form and the calculation may advance to step 4 where $M3bar = M3$.

Step 4

Step 4 calculates the pivot-point for this asymptote set. In this case there is only one third-order asymptote set and equation (3.54) defines its pivot-point as

$$p_3 = (M_{3\bar{1},1} / M_{3\bar{1},2}) / 3 = -5.5072e+00 \dots (B33)$$

Summary

The asymptote pivot-points have been calculated and are tabulated below

Table B2

Asymptote order	Pivot-point
1st	8.5557e-01
2nd	-2.0380e+00
3rd	-5.5072e+00

This particular example also shows how the calculation is performed when the block structure is of a different form to that shown in equation (3.52), such as the structure given by (B18)

APPENDIX C

HEADER LISTINGS OF THE PRO-MATLAB FUNCTIONS

APPENDIX C

This appendix contains a listing of the "HELP" banners for some of the more important Pro-Matlab m-files that were used for this project. Many other M-files were used for specific calculation and plotting functions but these are not given here. The format of each "HELP" banner shown here has been altered slightly to fit the general format of this report. The M-files are listed in alphabetical order below and the complete listing also follows this order.

M-files listed:

ADAPTLOCUS
ASYMPTOTES
BLOCKSLCT
BLOCKSWOP
CLOSELOOP
DAMPER
GMAG
HGCLBLD
HGCONT
HGLOCUS
MARKOV
NULLER
ROOT_IMDAT
ROOT_INDEX
ROOT_PP
ROOT_SORT
SPD
TUNER

ADAPTLOCUS

[GAINS,ROOTS, RG, MX] = ADAPTLOCUS(A, B, C, D, KO,
GMIN, GMAX, SIG, RHO, TOL)

This calculates the root-locus of a system using a variable gain step. The algorithm sorts the roots so that the distance between any pair of roots on 1 root locus branch is minimised and orders them so that plotting a ROW of the ROOTS matrix gives ONE branch of the locus. The distance between roots is calculated and if the largest distance is more than the tolerance allowed, the gain is decreased; otherwise the gain step is increased slightly to "take up the slack".

<Continued overleaf>

INPUTS: A,B,C,D - The open-loop plant matrices.
 KO,SIG,RHO - The controller matrix, sigma and
 rho tuning parameters from the
 high gain theory.
 GMIN,GMAX - The starting and finishing gains
 of the root-locus.
 TOL - The maximum distance between roots
 on a branch.

OUTPUTS: GAINS - The actual gains used to produce
 the locus.
 ROOTS - The matrix of roots, each collumn
 is a different rootlocus branch.
 RG - All the gains that were tried.
 MX - The largest root distances for
 each gain.

This function also calls HGCONT, CLOSELOOP, ROOT_SORT and ROOT_PP.

ASYMPTOTES

[ASYMPT] = ASYMPTOTES(A,B,C,D,KO,SIG,RHO,dispflg)

This calculates the order and position of multivariable root-locus asymptotes for a high-gain system. It uses $g=1$ to get the high-gain system into the right form (see PhD thesis, D Hopper, chapter 3).

The method of calculation follows that of Owens, Int. J. Control 1980, Vol.

INPUTS:

 A,B,C,D - The open-loop state space matrices.
 KO - The high-gain controller matrix.
 SIG,RHO - The diagonal tuning parameters.
 DISPFLG - If 1, the answer is displayed in a
 table, if 0 or omitted the answer is
 not displayed.

OUTPUTS:

 ASYMPT - A vector containing the order and
 position of the asymptotes.

This also calls MARKOV, SPD, HGCONT and CLOSELOOP.

BLOCKSLCT

[ABSL,BBSL,CBSL,DBSL] = BLOCKSLCT(A,B,C,D,S1
;F1,S2,F2)

This takes a subset of state space matrices out of a large state space system.

INPUTS:

A,B,C,D - are the original state space system.
S1,F1 - are the start and finish of the
first sub-state.
S2,F2 - are the start and finish of the
second sub-state.

OUTPUTS:

*BSL - are the output state space matrices
of the subsystem.

The arguments supplied (ie ABSL.. etc.) will then contain the state space system of the sub-states.

BLOCKSWOP

[ABSW,BBSW,CBSW,DBSW] = BLOCKSWOP(A,B,C,D,l)

This changes the order of two subsets of states from the state space system A,B,C,D. The input l is the number of state variables on the top of the state vector which are being put to the bottom.

The output arguments supplied (ie ABSW.. etc.) will then contain the state space system with the state variables in a different order.

CLOSELOOP - CLOSE LOOP

Purpose

Closes the loop around a system with state space realization (a,b,c,d). The option is available to include a constant feedback matrix.

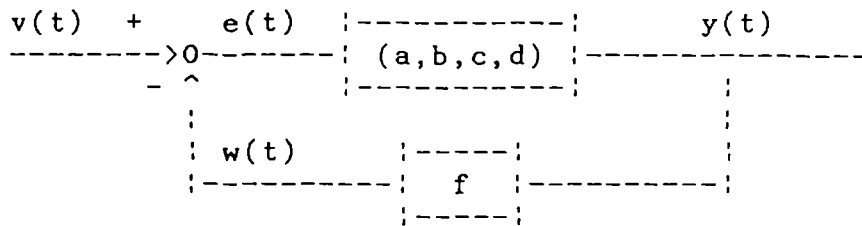
Synopsis

[ac,bc,cc,dc]=closeloop(a,b,c,d) '
[ac,bc,cc,dc]=closeloop(a,b,c,d,f)

Description

A system having a state space realization (ac,bc,cc,dc) is formed by placing a unity negative feedback loop around the system (a,b,c,d). A constant feedback matrix f is incorporated if it is specified in the argument list.

The diagram below shows this;



The closed loop system thus has state and output equations;

$$\dot{x}(t) = ac*x(t) + bc*v(t)$$

$$y(t) = cc*x(t) + dc*v(t)$$

Diagnostics

If the system given by (a,b,c,d) does not have the same number of inputs and outputs and no f matrix is specified:

Number of inputs does not equal number of outputs

If f is specified and its dimensions are not compatible with the remainder of the system then:

F matrix is not of compatible size

DAMPER

[DAMP] = DAMPER(RTS)

This calculates the damping of a vector of roots. The answer is a NAN if the root is at the origin, 0 if the root is on the imaginary axis, positive if the root is stable and negative if the root is unstable.

GMAG

[Z] = GMAG(POLES,ZEROS,SPOTS)

This returns the gain magnitude Ka for a system described as follows:

$$G(s) = Ka * \frac{s^m + b(m-1)s^{m-1} + \dots + b(2)s^2 + b(1)s + b(0)}{s^n + a(n-1)s^{n-1} + \dots + a(2)s^2 + a(1)s + a(0)}$$

Where Ka represents the overall gain and the poles and zeros are described by the equations a(s) and b(s) which are both monic.

NB [Monic means that the highest power of s has the coefficient 1]

The spot point is a point, or a vector of points, on the locus at a particular gain. This function calculates the distances from the spot point(s) to each pole and to each zero and the gain magnitude is the product of the pole distances divided by the product of the zero distances.

It can be used to analyse a set of roots which are associated with a MIMO root locus 'layer' created using the high-gain method. This function also forms the basis of the actuator compatibility test.

HGCLBLD

HGCLBLD is a script file that takes the open loop plant state space matrices (including actuator and/or sensor dynamics) and the controller matrices and builds the open loop high gain state space matrices.

It assumes the following naming convention:

- *ol - The open-loop state space matrices.
- *hg - The open-loop high-gain system state space matrices.
- *cl - The closed-loop state space matrices.

HGCONT

[ac,bc,cc,dc]=hgcont(a,b,c,d,k0,g,rho,sigma)

This connects a high gain controller in series with a system having state space realization (a,b,c,d), as follows:

INPUTS: A,B,C,D - The open-loop plant matrices.
G,K0 - The scalar gain and the controller matrix.
SIGMA,RHO - The sigma and rho tuning parameters.
OUTPUTS: *C - The closed-loop state-space matrices.

The controller equation is:

$$\dot{z}(t) = e(t)$$

$$u(t) = g*k0*sigma*\{ e(t) + rho*z(t)\}$$

HGLOCUS

HGLOCUS is a script file that generates a root locus from an open-loop system in series with a high-gain controller. The following naming convention is used:

*ol - open-loop state space matrices.
*hg - open-loop high-gain state space matrices.
*cl - closed-loop state space matrices

MARKOV

[RANKS,CHAIN] = MARKOV(A,B,C,l)

This generates the Markov chain for proper systems using the A, B and C matrices. It either generates the chain up to the first full rank Markov parameter plus one (for l=1) or it generates the chain for 'n' terms where 'n' is the number of states (if l=1 or l is absent).

NULLER

[X]=NULLER(X,TOL)

This takes a matrix and sets each element which is smaller than 'tol' to zero. It operates on the absolute values. If a value for tol is not given then 1.0e-12 is used.

It is used in ASYMPTOTES by SPD to remove rounding errors.

ROOT_IMDAT
[BREAK_POINTS] = ROOT_IMDAT(RTS)

This returns a matrix containing the location of break and joining points. If there are x break and joining points then the matrix will be a two-by-x matrix. The top row contains the array locations of the break or joining points. The element below each array location of a break or joining point is plus or minus one to say which is which.

-1 means one less imaginary part - a joining point.
+1 means one more imaginary part - a break point.

This is called from ROOT_PP.
See also ADAPTLOCUS, ROOT_SORT and ROOT_INDEX.

ROOT_INDEX
[RTINDX1,RTINDX2] = ROOT_INDEX(V1,V2,K)

This takes two column vectors containing the roots either side of a break or joining point (V1 & V2), and an integer K. The integer K is -1 if there is a joining point or +1 if there is a break point. It returns the locations of the roots which are going complex or joining the axis.

This is called from ROOT_PP
See also ADAPTLOCUS, ROOT_SORT and ROOT_IMDAT.

ROOT_PP
[RTS] = ROOT_PP(RTS)

This is a Post Processor for the routine ADAPTLOCUS.M which generates a root locus with a variable size gain step. This routine alters the order of the roots in the root_locus to conform to a particular convention. This ensures that any root locus which joins-to and breaks-from the real axis more than once is still reproduced correctly when drawn one branch at a time. Convention: "Fast" roots go "up" (+ve imaginary part) and "up" roots go "fast"

INPUTS:

RTS - Contains the input root_locus matrix with each column containing roots for a different gain, and each row containing an assumed single branch of the locus.

<Continued overleaf>

OUTPUTS:

RTS - Contains the output root_locus matrix with each column containing roots for a different gain, and each row containing the corrected single branch of the locus.

This calls ROOT_IMDAT and ROOT_INDEX.
See also ADAPTLOCUS and ROOT_SORT.

ROOT_SORT

ROOT_SORT(RTSOLD,RTSNEW)

This returns a set of roots (RTSNEW) that have been sorted to minimise the vector magnitude between RTSOLD(i) and RTSNEW(i).

The return arguments are:

RTSNEW - containing the sorted rtsnew set of roots
DIST - containing the vector magnitudes (or distances between the roots.

The original can be created by ADAPTLOCUS.

This function is called from ADAPTLOCUS.
See also ROOT_IMDAT,ROOT_INDEX,ROOT_PP.

SPD

[MOUT]=SPD(MIN,NZMP)

This performs a spectral decomposition on a Markov chain. The first square matrix is decomposed and the others are transformed by the same transformation matrix.

TUNER

COST=TUNER(VECT)

This is a function that tunes a high gain controller to give a minimum damping for each response. VECT contains the guess vector and cost returns the cost associated with

that guess. The M file NELDER is used in conjunction with this function. The A,B,C and D matrices ONLY should be saved to 'temp' before the NELDER function is called.

APPENDIX D

GLOSSARY OF TERMS FOR HANDLING QUALITIES

APPENDIX D

Glossary of Terms for Handling Qualities Criteria

D1 AIRCRAFT CLASSIFICATION

Class I

Small light aircraft such as:

Light utility
Primary trainer
Light observation

Class II

Medium Weight, low-to-medium manoeuvrability aircraft such as:

Utility
Search and rescue
Medium transport/cargo/tanker
Early warning/electronic countermeasures/airborne
command, control, or communications relay.
Antisubmarine
Assault transport
Reconnaissance
Tactical bomber
Heavy attack
Trainer for Class II

Class III

Large, heavy, low-to-medium manoeuvrability aircraft such as:

Heavy transport/cargo/tanker
Heavy bomber
Patrol / early warning / electronic countermeasures /
airborne command, control, or communications relay.
Heavy search and rescue
Trainer for class III

Class IV High-maneuvrability aircraft such as:

Fighter/interceptor
Attack
Tactical reconnaissance
Observation
Combat search and rescue
Trainer for class IV

D2 FLIGHT PHASES

D2.1 Nonterminal Flight Phases:

Category A - Those nonterminal flight phases that require rapid manoeuvring, precision tracking, or precise flightpath control. Included in this category are:

- a) - Air-to-ground combat (CO)
- b) - Ground attack (GA)
- c) - Weapon delivery/launch (WD)
- d) - Aerial recovery (AR)
- e) - Reconnaissance (RC)
- f) - In flight refueling (receiver) (RR)
- g) - Terrain following (TF)
- h) - Antisubmarine search (AS)
- i) - Close formation flying (FF)
- j) - Precision hover (PH)

Category B - Those nonterminal flight phases that are normally accomplished using gradual manoeuvres and without precision tracking, although accurate flight-path control may be required. Included in this category are:

- a) - Climb (CL)
- b) - Cruise (CR)
- c) - Loiter (LO)
- d) - In flight refueling (tanker) (RT)
- e) - Descent (D)
- f) - Emergency descent (ED)
- g) - Emergency deceleration (DE)
- h) - Aerial delivery (AD)
- i) - Hover (H)
- j) - Nonterminal transition (NT)

D2.2 Terminal Flight Phases:

Category C - Terminal flight phases that are normally accomplished using gradual manoeuvres and usually require accurate flight-path control. Included in this category are:

- a) - Vertical take-off (VT)
- b) - Short take-off (ST)
- c) - Approach (PA)
- d) - Wave-off/go-around (WO)
- e) - Vertical landing (VL)
- f) - Short landing (SL)
- g) - Terminal transition (TT)

When necessary, recategorization or addition of flight phases or delineation of requirements for special situations will be accomplished by the procuring activity.

D3 HANDLING QUALITIES RATINGS

Level 1: Flying qualities are clearly adequate for the mission flight phase.

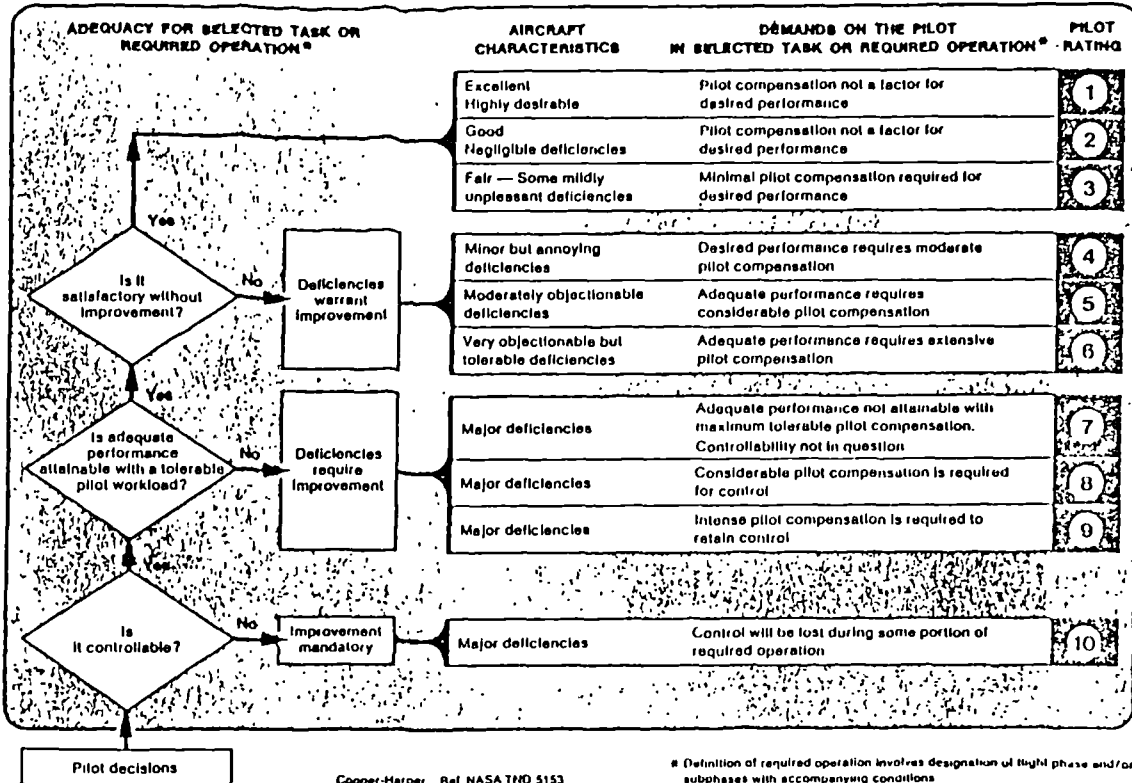
Level 2: Flying qualities are adequate to accomplish the mission flight phase, but some increase in pilot workload or degradation in mission effectiveness, or both, exists.

Level 3: Flying qualities are such that the aircraft can be controlled safely, but pilot workload is excessive or mission effectiveness is inadequate, or both. Category B and C flight phases can be completed.

NB:

A complementary ratings scheme exists which allows a more detailed assessment to be made. This is known as the Cooper-Harper rating scheme and the figure overleaf gives an illustration of how the scheme is applied. The first nine Cooper-Harper ratings, in groups of three, correspond directly to the the three rating levels given

HANDLING QUALITIES RATING SCALE



DEFINITIONS FROM TN D-5153

<p>COMPENSATION</p> <p>The measure of additional pilot effort and attention required to maintain a given level of performance in the face of deficient vehicle characteristics</p>	<p>PERFORMANCE</p> <p>The precision of control with respect to aircraft movement that a pilot is able to achieve in performing a task. (Pilot-vehicle performance is a measure of handling performance. Pilot performance is a measure of the manner or efficiency with which a pilot moves the principal controls in performing a task.)</p>
<p>HANDLING QUALITIES</p> <p>Those qualities or characteristics of an aircraft that govern the ease and precision with which a pilot is able to perform the tasks required in support of an aircraft role</p>	<p>ROLE</p> <p>The function or purpose that defines the primary use of an aircraft.</p>
<p>MISSION</p> <p>The composite of pilot-vehicle functions that must be performed to fulfill operational requirements. May be specified for a role, complete flight, flight phase, or flight subphase.</p>	<p>TASK</p> <p>The actual work assigned a pilot to be performed in completion of or as representative of a designated flight segment.</p>
<p>WORKLOAD</p> <p>The integrated physical and mental effort required to perform a specified piloting task.</p>	